APPLICATIONS OF CAPILLARY ELECTROPHORESIS AND MASS SPECTROMETRY FOR THE ANALYSIS OF THIOSALTS

by

© Michael Pappoe

A Thesis submitted to the

School of Graduate Studies

in partial fulfillment of the requirements for the degree of

Doctor of Philosophy

Department of Chemistry, Faculty of Science

Memorial University of Newfoundland

November, 2014

St. John's Newfoundland

ABSTRACT

Thiosalt species are unstable, partially oxidized sulfur oxyanions formed in sulfur-rich environments but also during the flotation and milling of sulfidic minerals especially those containing pyrite (FeS_2) and pyrrhotite ($Fe_{(1-x)}S$, x = 0 to 0.2). Detecting and quantifying the major thiosalt species such as sulfate (SO_4^{2-}), thiosulfate ($S_2O_3^{2-}$), trithionate ($S_3O_6^{2-}$), tetrathionate ($S_4O_6^{2-}$) and higher polythionates ($S_xO_6^{2-}$, where $3 \leq x \leq 10$) in the milling process and in the treated tailings is important to understand how thiosalts are generated and provides insight into potential treatment. As these species are unstable, a fast and reliable analytical technique is required for their analysis. Three capillary zone electrophoresis (CZE) methods using indirect UV-vis detection were developed for the simultaneous separation and determination of five thiosalt anions: SO_4^{2-}, $S_2O_3^{2-}$, $S_3O_6^{2-}$, $S_4O_6^{2-}$ and $S_5O_6^{2-}$. Both univariate and multivariate experimental design approaches were used to optimize the most critical factors (background electrolyte (BGE) and instrumental conditions) to achieve fast separation and quantitative analysis of the thiosalt species. The mathematically predicted responses for the multivariate experiments were in good agreement with the experimental results. Limits of detection (LODs) (S/N = 3) for the methods were between 0.09 and 0.34 µg/mL without a sample stacking technique and nearly four-fold increase in LODs with the application of field-amplified sample stacking. As direct analysis of thiosalts by mass spectrometry (MS) is limited by their low m/z values and detection in negative mode electrospray ionization (ESI), which is typically less sensitive than positive ESI, imidazolium-based (IP-L-Imid

and IP-T-Imid) and phosphonium-based (IP-T-Phos) tricationic ion-pairing reagents were used to form stable high mass ions non-covalent +1 ion-pairs with these species for ESI-MS analysis and the association constants (K_{assoc}) determined for these ion-pairs. K_{assoc} values were between 6.85×10^2 M^{-1} and 3.56×10^5 M^{-1} with the linear IP-L-Imid; 1.89×10^3 M^{-1} and 1.05×10^5 M^{-1} with the trigonal IP-T-Imid ion-pairs; and 7.51×10^2 M^{-1} and 4.91×10^4 M^{-1} with the trigonal IP-T-Phos ion-pairs. The highest formation constants were obtained for $S_3O_6^{2-}$ and the imidazolium-based linear ion-pairing reagent (IP-L-Imid), whereas the lowest were for IP-L-Imid: SO_4^{2-} ion-pair.

ACKNOWLEDGMENTS

I thank my supervisor Dr. Christina S. Bottaro and my supervisory committee members Dr. Fran Kerton and Dr. Bob Davis for their direction and guidance in helping me successfully complete my work.

I am grateful to my office colleagues Ali Modir and Dr. Geert van Biesen of for their help and especially for their suggestions in troubleshooting the capillary electrophoresis (CE) and CE-ESI-MS instrumentation. My appreciation also goes to Linda Windsor and Dr. Celine Schneider in C-CART for training me to use the various instruments in C-CART and Dr. Louise Dawe for analyzing my synthesized single crystals. I also appreciate the help and encouragement from my office colleagues. I would not have come this far in this research without everyone's help.

Finally, I thank my wife Michaelina for her love and overwhelming support without which I would not have come this far.

Table of Contents

List of Tables

List of Figures

List of Abbreviations

AC	alternating current
ACN	acetonitrile
AMD	acid mine drainage
BBD	Box-Behnken design
BGE	background electrolyte
CCRS	central composite response surface
CD	conductivity detection
C4D	capacitively coupled contactless conductivity detection
CE	capillary electrophoresis
CEC	capillary electrochromatography
CGE	capillary gel electrophoresis
CHES	2[N-cyclohexylamino]ethane-sulfonic acid
CID	collision-induced dissociation
CIEF	capillary isoelectric focusing
CMC	critical micelle concentration
CIP	compact ion-pair
CITP	capillary isotachophoresis
CRM	charge residue model
CTAB	cetyltrimethylammonium bromide
CTAC	cetyltrimethylammonium chloride
CZE	capillary zone electrophoresis
DCM	dichloromethane

DETA	diethylenetriamine (dien)
DOE	design of experiment
E	electric field
EA	ethylamine
EKC	electrokinetic chromatography
EOF	electroosmotic flow
EPC	electrochemical preconcentration
ESI	electrospray ionization
FIA	flow injection analysis
FF	fractional factorial
GFF	general fractional factorial
HDM	hexadimethrine
HMBr	hexamethonium bromide
HMOH	hexamethonium hydroxide
HPLC	high performance liquid chromatography
IEC	ion-exchange chromatography
IC	ion chromatography
id	internal diameter
IP	ion-pair
IP-L-Imid	1,3-bis[6-(3-benzyl-1-imidazolio)-hexyl]imidazolium
IP-T-Imid	1,3,5-tris[(3-butyl-imidazolium)methyl]-2,4,6-trimethylbenzene
IP-T-Phos	1,3,5-tris[(tripropylphosphonium)methyl]benzene
IPR	ion-pair reagent
KRF	Kohlrausch's regulating function

LDI	laser desorption ionization
LOD	limit of detection
MCE	microchip capillary electrophoresis
MEKC	micellar electrokinetic chromatography
MES	2-(N-morpholino)ethanesulfonic acid
MS	mass spectrometry
MRM	multiple reaction monitoring
OFM	osmotic flow modifier
ODS	octadecylsilica
PB	Plackett-Burman
PDCA	2,6-pyridinedicarboxylic acid
PAH	polycyclic aromatic hydrocarbon
PDMS	poly(dimethylsiloxane)
PFOA	perfluorooctanoic acid
PMA	pyromellitic acid
PMMA	poly(methylmethacrylate)
psi	pounds-per-square inch
SDS	sodium dodecyl sulfate
SIM	selected ion monitoring
SIP	solvent-shared ion-pair
SSIP	solvent-separated ion-pair
STM	scanning tunnelling microscopy
SULSAL	5-sulfosalicylic acid
μTAS	micro total analysis systems

TBA	tetrabutylammonium
TMC	trimethyl carbonate
TOF	time-of-flight
TR	transfer ratio
TS	thiosalt
TTAOH	tetradecyltrimethylammonium hydroxide
UPS	ultraviolet photoelectron spectroscopy
UV	ultraviolet
UV-vis	ultraviolet-visible
V	applied voltage (volts)
V_{cap}	capillary voltage
RF OCT 1Vpp	radiofrequency voltage (peak-to-peak) of octapole 1
XRS	X-ray spectroscopy

List of Appendices

Chapter 1

Introduction and Overview

1.1 General introduction

Thiosalts are sulfur oxyanion species that are produced in the natural sulfur-rich aqueous environments, such as in volcanic eruptions and hotsprings. These species are also produced during the crushing, milling and flotation of sulfidic ores as a result of oxidative processes. In addition, other important sources of thiosalts include produced water, photographic development wastes and waste water. [1-3] Some of the important species produced are thiosulfate, trithionate, tetrathionate, pentathionate and hexathionate. While thermodynamic considerations suggest that oxidation of sulfide minerals should lead to the production of sulfate, kinetic limitations largely lead to the formation of these intermediate species which can pass through conventional mine effluents treatment facilities (lime treatment) unaffected. These species are then discharged into surface aqueous environments where they oxidize slowly culminating in the generation of an acidic aqueous environment. The structures of the most common thiosalt species are shown in Figure 1.1.[1]

Approaches to understanding and mitigating the generation of thiosalts are areas showing intense interest from industry and have stimulated research by a number of groups[1-3]; this is primarily because of the complex chemistry of these intermediate sulfur species. Most of the thiosalt species are formed during the processing of sulfidic ores, particularly those containing pyrite (FeS_2) and pyrrhotite ($Fe_{(1-x)}S$, x = 0 to 0.2). The pathway leading to full oxidation of these mineral ores includes several oxidative processes leading to sulfate production from the intermediate sulfur species.[4-9]

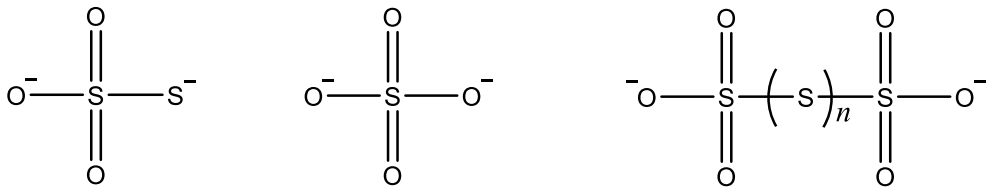

thiosulfate sulfate n=1: trithionate

n=2: tetrathionate

n=3: pentathionate

Figure 1.1. Some of the prevalent thiosalt species

Accompanying the oxidative processes of these thiosalt species is the production of hydrogen ions (H^+) which is responsible for the acidification of the freshwater that received the waste. Although thiosalts in themselves have been shown to be relatively non-toxic, acidification can cause stress to freshwater flora and fauna, which in some instances can be severe enough to lead to death of vulnerable organisms. Acidification can also result in enhanced metal migration, which can lead to toxic metal concentrations in biota.[1-3,10]

Despite extensive research on thiosalts since the 1980s, there are still many unknowns, particularly questions related to reaction kinetics and thermodynamics. The study of the reactions of thiosalts is required to better understand how to effectively treat them.

However, studies of the kinetics, which can be fast and complex, are complicated by the limitations of the quantitative analytical methods. Many current methods such as ion chromatography are time-consuming; and particularly for the partially oxidized reactive sulfur species such as thiosalts, improved methods of analysis are required. [1-4]

The aim of this research is to understand the chemistry of thiosalts, investigate capillary zone electrophoresis (CZE) with indirect detection and electrospray mass spectrometry (ESI-MS) techniques for thiosalt species analysis, particularly sulfate, thiosulfate and the higher-order polythionates. These techniques will also be optimized to achieve fast analysis with high separation efficiency in CZE and high sensitivity (low limit of detection (LOD)) in ESI-MS, and applied to real world samples such as effluents from the mineral milling process and treated tailings ponds. All species in equations presented in the chapter are in the aqueous state unless otherwise indicated.

1.2 The generation and chemistry of thiosalts from sulfidic minerals

Many of the redox reactions occurring during the oxidation of sulfide-rich minerals leading to the generation of acidic effluents are still not well understood or characterized. Pyrite and pyrrhotite are the two most commonly occurring sulfide minerals; pyrite differs stoichiometrically from pyrrhotite in the crystal structure and oxidation states of the Fe (Fe^{2+}/Fe^{3+}) which has an effect on their reactivity during oxidation in the aqueous environment. Pyrite has a simple cubic NaCl-like structure with unit cells composed of face-centered Fe atoms at the corners and face center points of the cube and the disulfide

S_2^{2-} subunits at the midpoints of the corners and in the center of the cubic structure.[11] Thus, the unit structure consists of Fe-S as well as S-S bonds or Fe^{2+} and S_2^{2-} ions. Pyrrhotite ($Fe_{(1-x)}S$) consists of Fe^{2+} and S^{2-} however the amount of Fe^{2+} present is deficient allowing for this deficiency to be compensated by the presence of Fe^{3+}. It has been shown that when the value of x approaches 0 such as in troilite (FeS), the amount of H^+ ions produced during oxidation is greatly minimized and essentially only Fe^{2+} and SO_4^{2-} are produced; however when x = 0.125 such as in the monoclinic pyrrhotite Fe_7S_8, the amount of H^+ ions reaches its maximum with each mole of Fe_7S_8 producing 0.25 mole of H^+ in addition to SO_4^{2-}.[12] Thus the reactivity of pyrrhotite is expected to be higher than pyrite due to the presence of the oxidant Fe^{3+} in its structure. Several studies have also confirmed this.[13-15]

The overall reaction leading to the production of ferric hydroxide and sulfuric acid is shown below:[16,17]

$$2FeS_2 + \frac{15}{2} O_2 + 7H_2O \longrightarrow 2Fe(OH)_3 + 4H_2SO_4 \qquad (1.1)$$

However it is now understood that during this oxidation process S_2^{2-} and SO_3^{2-} ions are formed during the milling and flotation process. These ions react with elemental sulfur to yield polysulfides that are further oxidized to thiosulfate ($S_2O_3^{2-}$), trithionate ($S_3O_6^{2-}$), tetrathionate ($S_4O_6^{2-}$) and other higher polythionates of the formula $S_xO_6^{2-}$ where $3 \leq x \leq 10$. The partially oxidized intermediate sulfur species formed during this process possess

varying kinetic properties under different conditions in aqueous systems with the oxidation state of sulfur ranging from -2 in the sulfide ion (S^{2-}) to +6 in the fully oxidized form sulfate ion (SO_4^{2-}).[1,8,9,10,18,19]

The chemistry and reaction kinetics of sulfur compounds and especially thiosalts are complex and several studies [1-4, 10, 20-23] have shown that reactivity strongly depends on temperature, pH, and presence of oxygen as well as other thiosalt species, metals and microorganisms[24] in the environment. According to thermodynamic and equilibrium calculations, complete oxidation of these sulfur oxyanions lead to the formation of sulfate. However, as mentioned in Section 1.1, these partially oxidized species remain in the mining effluent due to limits imposed by mass transfer and kinetics.[1, 20-25]

1.2.1 Chemical oxidation of sulfidic ores

The oxidation of FeS_2 and $Fe_{1-x}S$ to SO_4^{2-} and ferrous iron Fe^{2+} in natural aqueous systems involves many complex redox and biochemical reactions leading to the transfer of electrons from the sulfur atoms of the sulfidic ore to the oxidizing agent present in the environment. Some of the earliest investigations on the oxidation of sulfidic ores were reported by Garrels *et al.*[26] in 1960 and Singer *et al.*[27] in 1970. In these studies, the investigators identified the main oxidants as Fe^{3+} and dissolved O_2 in their papers on aqueous oxidation of pyrite and acidic mine drainage, respectively.

Recent research has also confirmed the results of this work and has shown that these oxidants (Fe^{3+} and dissolved O_2) accept electrons from the pyritic sulfur and are reduced in the system. Other pathways of aqueous oxidation of pyrite and pyrrhotite have been reported in literature.[28-30] The reactions below show that the pyritic-S is oxidized to SO_4^{2-} while the pyritic-Fe remains unaffected (Fe^{2+}) by the oxidation process with the oxidant (Fe^{3+} being reduced to Fe^{2+}) as shown in equations 1.2 and 1.3.[31]

$$FeS_2 + 14\ Fe^{3+} + 8\ H_2O \rightarrow 15\ Fe^{2+} + 16\ H^+ + 2\ SO_4^{2-} \qquad (1.2)$$

$$FeS_2 + \frac{7}{2}\ O_2 + H_2O \rightarrow Fe^{2+} + 2\ H^+ + 2\ SO_4^{2-} \qquad (1.3)$$

The non-stoichiometric sulfide ore pyrrhotite ($Fe_{1-x}S$) has been shown to be more reactive than pyrite due to presence of Fe^{3+} in its lattice structure to compensate for the deficiency of Fe^{2+} as mentioned in Section 1.2. The higher the amount of Fe^{3+} the more reactive the ore is. Nordstom *et al.*[32] showed that pyrrhotite in aqueous systems with pH > 4 is mainly oxidized by both dissolved oxygen and Fe^{3+} ions. Benner *et al.*[33] also showed that the presence of dissolved O_2 is essential in the oxidation of pyrrhotite in mine wastes. Thus in the oxidation of pyrrhotite in natural aqueous systems both O_2 as well as Fe^{3+} ions have been shown to be responsible for the oxidation to SO_4^{2-} and protons (H^+) as shown by equations reaction 1.4 and 1.5.[34]

$$Fe_{1-x}S + (2-\frac{x}{2})\ O_2 + xH_2O \rightarrow (1-x)\ Fe^{2+} + SO_4^{2-} + 2xH^+ \qquad (1.4)$$

$$Fe_{1-x}S + (8-2x)\ Fe^{3+} + 4H_2O \rightarrow (9-3x)\ Fe^{2+} + SO_4^{2-} + 8H^+ \qquad (1.5)$$

1.2.2 Enzymatic oxidation of sulfidic ores in aqueous systems

In addition to chemical oxidation described above aqueous oxidation also involves bacteria-catalyzed reaction pathways. Several *Thiobacillus* species have been shown to produce S-oxidizing enzymes that can oxidize S-species such as $S_2O_3^{2-}$ and some polythionates to sulfate.[35] Kelly and Wood[36] showed that thiosalt species serve as electron-donating substrates for *Thiobacilli* metabolism. However as with many other enzymatic reactions, pH and concentration of dissolved oxygen play an important role in the mechanism and efficiency of these conversions in aqueous systems. The most important *Thiobacillus* species characterized in thiosalt oxidation include *T. acidophilus*, *T. ferroxidans* and *T. thiooxidans*.

T. acidophilus produces the trithionate hydrolase enzyme that catalyzes the conversion of the $S_4O_6^{2-}$ and $S_3O_6^{2-}$ ions to $S_2O_3^{2-}$ according to the following reaction scheme:

$$S_3O_6^{2-} + H_2O \rightarrow S_2O_3^{2-} + SO_4^{2-} + 2H^+ \quad (1.6)$$

$$S_4O_6^{2-} + H_2O \rightarrow S_2O_3^{2-} + S^0 + SO_4^{2-} + 2H^+ \quad (1.7)$$

T. ferroxidans produces tetrathionate hydrolase that catalyzes the oxidation of $S_4O_6^{2-}$ to SO_4^{2-} in several steps. The overall reaction scheme is shown below:

$$S_4O_6^{2-} + \frac{7}{2}O_2 + 3H_2O \rightarrow 4SO_4^{2-} + 6H^+ \quad (1.8)$$

The tetrathionate hydrolase from *T. thiooxidans* produces $S_2O_3^{2-}$ from $S_4O_6^{2-}$ by a mechanism which has been shown to be catalyzed by Cu^{2+} ions. The net reaction is shown below: [36]

$$4S_4O_6^{2-} + 5H_2O \longrightarrow 7S_2O_3^{2-} + SO_4^{2-} + 10H^+ \quad (1.9)$$

1.3 Thermodynamic and kinetic properties of thiosalts in aqueous systems

The chemistry and kinetics of sulfur compounds and particularly thiosalts are very complex and extensive work continues to be done to understand reactivity of these compounds especially in terms of the influence of pH and temperature on the reaction kinetics of these species. Thiosalts are known to behave differently in different conditions of pH, temperature, presence of catalyst and even the type of thiosalt since each species has varying chemical and physical properties.[20-25]

1.3.1 Reactions involving the thiosulfate ion

Through a reaction of elemental sulfur S^0 formed in the processing of sulfidic ores with SO_3^{2-} ions, thiosulfate ions are produced by the reaction below:

$$S_8 + 8SO_3^{2-} \longrightarrow 8S_2O_3^{2-} \quad (1.10)$$

Thiosulfate has been shown to be stable in neutral and alkaline aqueous systems at temperatures below 70 °C but oxidizes at temperatures above 70 °C, where it decomposes to SO_4^{2-}. However in acidic media it is oxidized to $S_4O_6^{2-}$ in the net reaction in the presence of oxidizing agents such as O_2.[37,38]

In the presence of other thiosalt species and mild acidic conditions, $S_2O_3^{2-}$ ions react to yield polythionates and other S-compounds. Thus $S_2O_3^{2-}$ acts as a catalyst for the production of polythionates in the aqueous system.[39]

$$2S_2O_3^{2-} + 2S_xO_6^{2-} \rightarrow 2S_{x+1}O_6^{2-} + SO_3^{2-} + S^{2-} \quad (1.11)$$

Complete oxidation of thiosulfate under basic conditions results in the formation of SO_4^{2-} ions.

$$S_2O_3^{2-} + 2O_2 + 2OH^- \rightarrow 2SO_4^{2-} + H_2O \quad (1.12)$$

Extensive work on thiosalts in aqueous systems has been performed in the Bottaro Lab to monitor the oxidation and degradation pathways of various thiosalt species. Vongporm[40] reported on thiosalt behavior in aqueous systems. It was shown that the thiosulfate ion $S_2O_3^{2-}$ is stable at pH between 4 and 9 and at temperatures up to 30°C. It decomposes to $S_3O_6^{2-}$ and SO_4^{2-} under acidic conditions with pH $\leq$ 2. In addition there is also precipitation of elemental sulfur as can be shown by the equation below:

$$4S_2O_3^{2-} + 4H^+ \rightarrow S_3O_6^{2-} + SO_4^{2-} + 4S^0 + 2H_2O \quad (1.13)$$

However under strong basic conditions (pH > 10) $S_2O_3^{2-}$ decomposes to $S_3O_6^{2-}$ and $S_4O_6^{2-}$:

$$5S_2O_3^{2-} + 6OH^- \rightarrow 2S_3O_6^{2-} + S_4O_6^{2-} + 3H_2O \quad (1.14)$$

Treatment options for thiosulfate in treated mine tailings include oxidation with hydrogen peroxide (H_2O_2), with ferric sulfate ($Fe_2(SO_4)_3$) and some copper complexes as catalysts. The oxidative process involving $S_2O_3^{2-}$ in a H_2O_2 - $S_2O_3^{2-}$ system was shown to be dependent on the pH and the concentration of oxidant.[41] Kinetic studies (Figure 1.2) also

showed that the reaction is first order with respect to each of the reactants. Complete oxidation of $S_2O_3^{2-}$ led to the production of SO_4^{2-}.

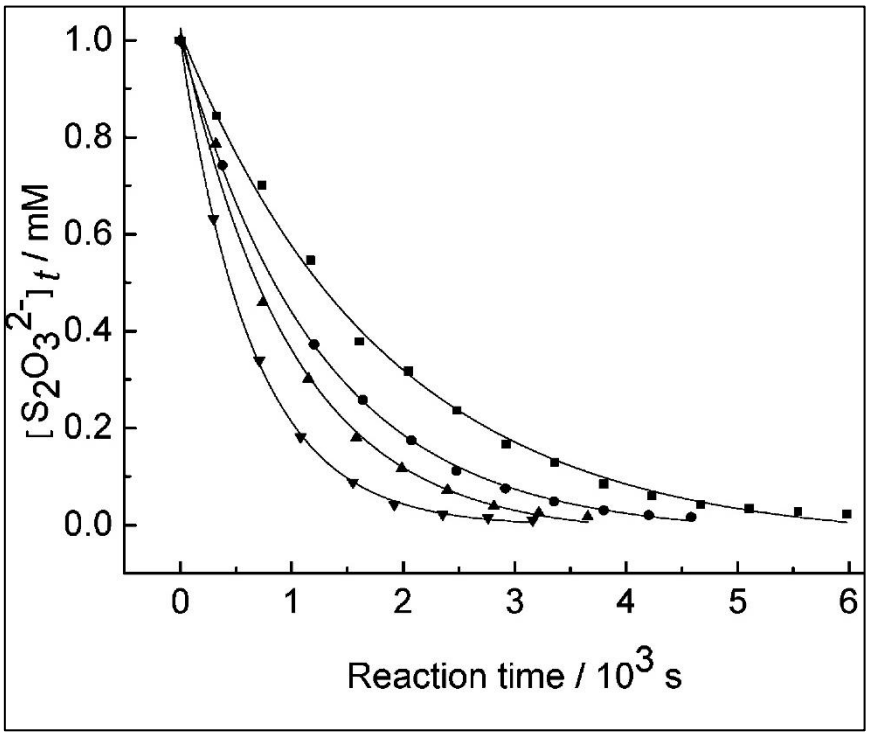

Figure 1.2. Kinetic analysis showing changes in concentration of thiosulfate in a hydrogen peroxide-thiosulfate reaction mixture with different initial concentration ratios. $[S_2O_3^{2-}]_0$ = 0.001 M; $[H_2O_2]_0$ = 0.010 M (■), 0.015 M(●), 0.020 M (▲) and 0.025 M (▼); pH 5.0; 25 °C. (Reprinted with permission from Ref 41, Copyright 2012 American Chemical Society)

1.3.2 Reactions involving the trithionate ion

Trithionate is essentially stable below 4 ^oC for pH between 2 and 9, with increase in temperatures from 15 ^oC to 30 ^oC leading to the formation of trace quantities of SO_4^{2-},

$S_2O_3^{2-}$ and $S_4O_6^{2}$. Meyer *et al.*[42] showed that trithionate breaks down to SO_4^{2-}, S^0 and SO_4^{2-} at pH between 3.5 and 4 and temperatures above 20 °C. The upper limit of the experiment was 70 °C and the reaction rate depended on the temperature at least over the range studied.

The reactions are shown below:

$$3S_3O_6^{2-} \rightarrow S_4O_6^{2-} + \frac{1}{8}S_8 + 2SO_4^{2-} + 2SO_2 \quad (1.15)$$

$$S_3O_6^{2-} \rightarrow \frac{1}{8}S_8 + SO_4^{2-} + SO_2 \quad (1.16)$$

Zhang and Jeffrey[43] showed that at pH 7, $S_3O_6^{2-}$ is hydrolyzed to $S_2O_3^{2-}$ and SO_4^{2-}. They found that the reaction has a pseudo first-order rate constant of $6.2 \pm 0.2 \times 10^{-7}\ M^{-1}\ s^{-1}$ for the pH range of 5.5-10.5.

$$S_3O_6^{2-} + H_2O \rightarrow S_2O_3^{2-} + SO_4^{2-} + 2H^+ \quad (1.17)$$

However in strongly basic media (pH > 11) $S_3O_6^{2-}$ decomposes to SO_3^{2-} and $S_2O_3^{2-}$:

$$2S_3O_6^{2-} + 6OH^- \rightarrow S_2O_3^{2-} + 4SO_3^{2-} + 3H_2O \quad (1.18)$$

Oxidation reactions involving the trithionate ion in a chlorine dioxide – trithionate system, buffered by acetic acid-acetate solution between 4.35 and 5.70, has been shown to produce mainly SO_4^{2-} as shown in Equation 1.19 or SO_4^{2-} and ClO_3^- in the presence of excess chlorine dioxide (Equation 1.20).[44]

$$5S_3O_6^{2-} + 8ClO_2 + 14H_2O \rightarrow 15SO_4^{2-} + 8Cl^- + 28H^+ \quad (1.19)$$

$$S_3O_6^{2-} + 4ClO_2 + 4H_2O \rightarrow 3SO_4^{2-} + 2Cl^- + 2ClO_3^- + 8H^+ \qquad (1.20)$$

The reaction has been shown to be first order with respect to the concentration of $S_3O_6^{2-}$. In the presence of excess chlorine dioxide, ClO_3^- is also generated in high concentrations as shown in Figure 1.3.

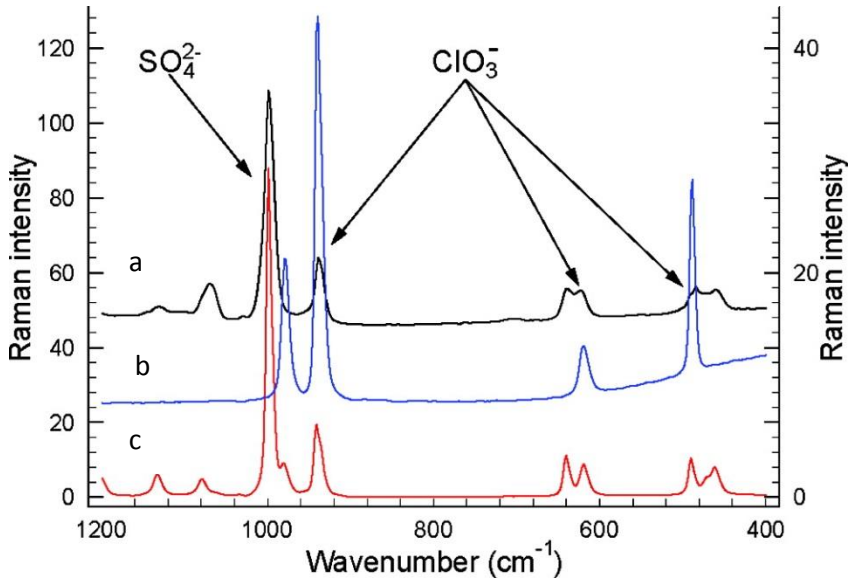

Figure 1.3. (a) Raman spectrum of the vacuum-evaporated reacting solution at $[S_3O_6^{2-}]_0$ = 1.75 mM and $[ClO_2]_0$ = 17.5 mM in unbuffered medium. (b) Raman spectrum of solid potassium chlorate shifted by +25 Raman intensity units along the left *Y*-axis; (c) Raman spectrum of the evaporated solution containing potassium chlorate, sodium sulfate and sodium chloride in alkaline pH (Reprinted with permission from Ref 44. Copyright 2012 American Chemical Society)

1.3.3 Reactions involving the tetrathionate ion

Work done in the Bottaro lab also showed that tetrathionate is relatively stable between pH 2 and pH 9 for temperatures up to 30 ^{o}C; it only starts to break down when the pH is elevated above 9. Thus in varying the pH and temperature conditions, thiosalts in mixtures exhibit a complex relationship as the concentration of one form decreases and the concentrations of the other species increase. In addition to the above pentathionate $S_5O_6^{2-}$ ions are generated.

These are consistent with work done by Zhang *et al.*[45] where they showed that in the pH range of 6 and 8 degradation of $S_4O_6^{2-}$ is catalyzed by $S_2O_3^{2-}$ through a rearrangement mechanism to form $S_3O_6^{2-}$ and $S_5O_6^{2-}$. Subsequently, $S_3O_6^{2-}$ further hydrolyzes to $S_2O_3^{2-}$ and $S_5O_6^{2-}$ undergoes a further rearrangement reaction.

The reactions involving the transformation of $S_4O_3^{2-}$ are shown below:

$$S_4O_6^{2-} + S_2O_3^{2-} \rightarrow S_5O_6^{2-} + SO_3^{2-} \quad (1.21)$$

$$S_4O_6^{2-} + SO_3^{2-} \rightarrow S_2O_3^{2-} + S_3O_6^{2-} \quad (1.22)$$

At pH > 11 the predominant decomposition pathway of $S_4O_6^{2-}$ is the formation of $S_2O_3^{2-}$ and $S_3O_6^{2-}$:

$$4S_4O_6^{2-} + 6OH^- \rightarrow 5S_2O_3^{2-} + 2S_3O_6^{2-} + 3H_2O \quad (1.23)$$

Tetrathionate oxidation to sulfate ions by hydroxyl radicals provides a much better alternative to treating the polythionates in acid mine drainage (AMD) environments than the addition of lime or carbonate neutralization. Work done by Druschel *et al.*[21] showed that enhanced oxidation of $S_4O_6^{2-}$ to SO_4^{2-} is achieved by using OH radicals generated by Fenton's reagent. The kinetics suggested a rate constant greater than 10^8 M^{-1} s^{-1}.

Thiosalts have limited reactivity in the presence of hydrogen peroxide but this is improved in the presence of Fenton's reagent. To generate the hydroxyl radicals, H_2O_2 is treated with Fe^{2+} in an acidified solution according to the equation below.

$$H_2O_2 + H^+ + Fe^{2+} \longrightarrow OH^{\cdot} + H_2O + Fe^{3+} \qquad (1.24)$$

1.3.4 Reactions involving the pentathionate and hexathionate ions

Higher order polythionates are formed at low concentrations during the redox and microbial oxidation of sulfidic ores particularly pyrites and pyrrhotites. Lu *et al.*[47,48] have shown that during the oxidation of thiosulfate with hydrogen peroxide (H_2O_2) and chlorite (ClO_2^-) higher polythionates including $S_4O_6^{2-}$, $S_5O_6^{2-}$, $S_6O_6^{2-}$ and $S_7O_6^{2-}$ are formed. These higher order species consequently hydrolyse or oxidize to form other S-species such as SO_4^{2-}, $S_2O_3^{2-}$ and $S_3O_6^{2-}$.

Some of the intermediate reactions leading to the formation of some of $S_4O_6^{2-}$ and $S_5O_6^{2-}$ are shown below:

$$S_2O_3^{2-} + H_2O_2 \longrightarrow HS_2O_4^{2-} + OH^- \qquad (1.25)$$

$$S_2O_3^{2-} + HS_2O_4^{2-} + H^+ \rightarrow S_4O_6^{2-} + H_2O \quad (1.26)$$

$$S_4O_6^{2-} + S_2O_3^{2-} \rightarrow S_5O_6^{2-} + SO_3^{2-} \quad (1.27)$$

$S_5O_6^{2-}$ degradation has been shown to be dependent on the concentration of OH^- ions and initial $S_5O_6^{2-}$ concentration; higher concentrations of OH^- (high pH) lead to higher degradation rates.[49] The net reaction for the degradation of $S_5O_6^{2-}$ is shown in equation 1.28 below:

$$2S_5O_6^{2-} + 6OH^- \rightarrow 5S_2O_3^{2-} + 3H_2O \quad (1.28)$$

However the formation of elemental sulfur S^0 suggests that $S_5O_6^{2-}$ decomposes via a $S_4O_6^{2-}$ pathway:

$$S_5O_6^{2-} \rightarrow S_4O_6^{2-} + S^0 \quad (1.29)$$

$$S^0 + SO_3^{2-} \rightarrow S_2O_3^{2-} \quad (1.30)$$

Figure 1.4 shows the HPLC chromatograms of the oxidation pathways of $S_5O_6^{2-}$ to the major products $S_2O_3^{2-}$ and $S_4O_6^{2-}$ in an alkaline medium. Other thiosalt species such as $S_6O_6^{2-}$ and SO_3^{2-} were also detected in the reaction mixture indicating that side reactions may also be occurring.

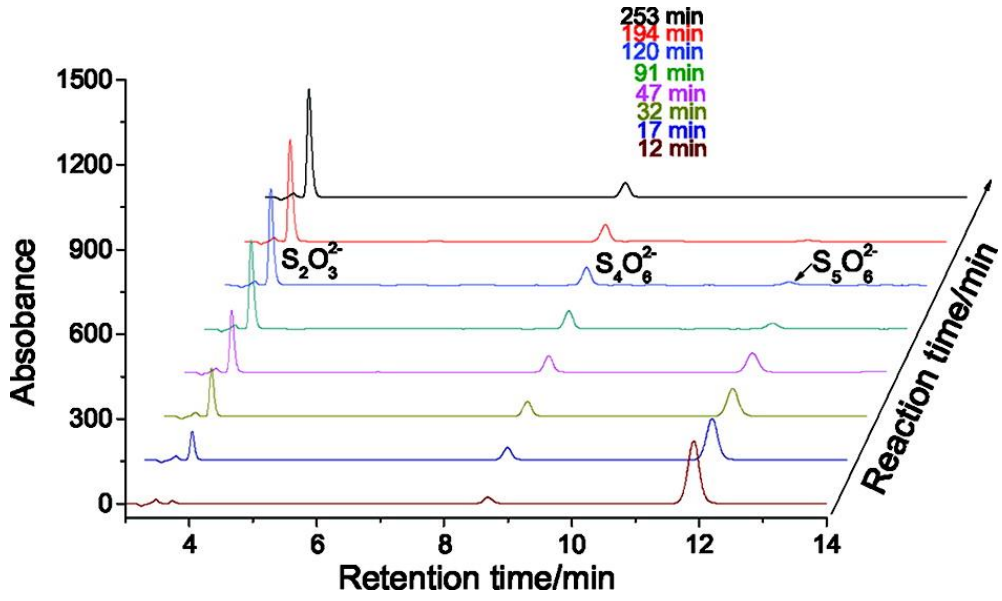

Figure 1.4. Chromatogram showing the oxidation of $S_5O_6^{2-}$ monitored by HPLC (Reprinted with permission from Ref. 49 Copyright 2011 American Chemical Society)

Pan *et al.*[49] showed that $S_2O_3^{2-}$ has no effect on the kinetics of the conversion of $S_5O_6^{2-}$ to $S_6O_6^{2-}$ and $S_4O_6^{2-}$ therefore the most probable mechanism will be:

$$S_5O_6^{2-} + S_3O_3OH^- \rightarrow S_6O_6^{2-} + S_2O_3OH^- \quad (1.31)$$

$$S_5O_6^{2-} + SO_3^{2-} \rightarrow S_4O_6^{2-} + S_2O_3^{2-} \quad (1.32)$$

Experiments studying alkaline decomposition of hexathionate have been shown to mainly yield $S_2O_3^{2-}$ and $S_5O_6^{2-}$. In addition to these, elemental sulfur S^0, $S_4O_6^{2-}$ and $S_7O_6^{2-}$ have also been observed in small but detectable concentrations. Since higher polythionates are

not stable in strongly alkaline conditions over a longer period of time, it is proposed that $S_6O_6^{2-}$ decomposition will favour the formation of the more stable species $S_2O_3^{2-}$ and elemental sulfur S^0:

$$2S_6O_6^{2-} + 6OH^- \longrightarrow 5S_2O_3^{2-} + 2S^0 + 3H_2O \quad (1.33)$$

Pan *et al.*[50] also proposed a kinetic model that shows the formation of the major species shown above as well as the intermediate species such as $S_4O_6^{2-}$, $S_5O_6^{2-}$ and SO_4^{2-}. Some of the potential reactions are shown below:

$$S_6O_6^{2-} + OH^- \longrightarrow S_2O_3^{2-} + S_4O_3OH^- \quad (1.34)$$

$$2S_6O_6^{2-} \longrightarrow S_5O_6^{2-} + S_7O_6^{2-} \quad (1.35)$$

$$S_4O_6^{2-} + S_2O_3^{2-} \longrightarrow S_5O_6^{2-} + SO_3^{2-} \quad (1.36)$$

$$S_5O_6^{2-} + S_2O_3^{2-} \longrightarrow S_6O_6^{2-} + SO_3^{2-} \quad (1.37)$$

$$S_5O_6^{2-} + OH^- \longrightarrow S_2O_3^{2-} + S_3O_4H^- \quad (1.38)$$

The decomposition pathway of $S_5O_6^{2-}$ follows a similar trend to that of $S_5O_6^{2-}$ with the generation of higher polythionates such as $S_7O_6^{2-}$ in the reaction mixture as shown in Figure 1.5.

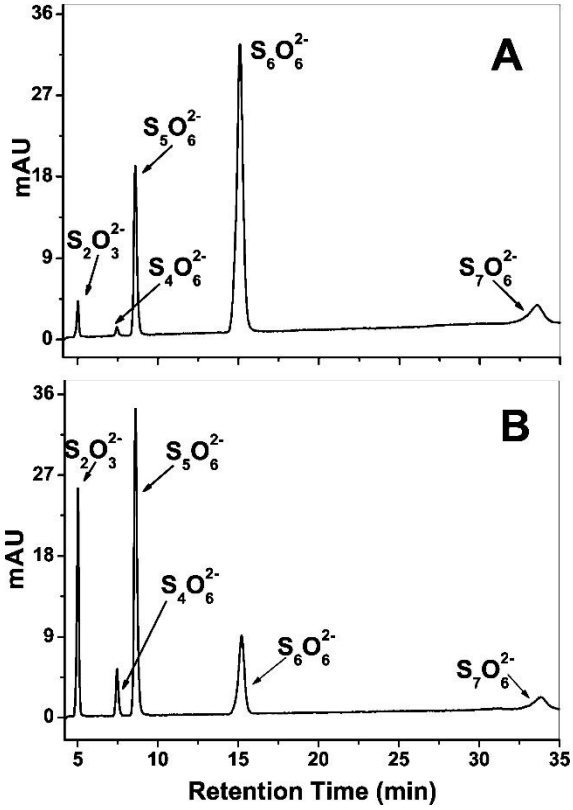

Figure 1.5. HPLC chromatograms of the alkaline decomposition of hexathionate (Reprinted with permission from Ref. 50 Copyright 2013 American Chemical Society)

1.4 An overview of analytical techniques for detecting and quantifying thiosalts

1.4.1 Chromatographic techniques

Extensive analytical work has been done in the area of separation and quantitation of sulfur species in the natural environment including water, air, and soil.[51-64] Because these species are essentially inorganic anions, ion exchange chromatography (IC) coupled with different detection systems has been most commonly used for their determination and quantitation. IC is a well-established and robust technique with broad application in the determination of inorganic anions with good reliability.[51] The technique makes use of columns packed with either anion or cation exchange resins with suitable detectors such as spectrophotometric, conductivity and electrochemical. Several variations of the technique also exist. Until recently the most analyzed species of sulfur was sulfate but awareness of the environmental impact of the intermediate sulfur species particularly the thiosalts have led to the development of IC techniques for their analysis.[51-54]

In 1993, Friedhelm *et al.*[52] developed an IC technique for the determination of thiosulfate and tetrathionate ions present in natural water samples and in some microbial cultures containing sulfur-metabolizing bacteria. They were able to achieve complete separation (Figure 1.6) by eluting the samples with acetonitrile/methanol mixture on a Sykam LCA A08 polymer-coated, silica-based anion exchange column coupled to UV detector at 216 nm. Up to lower μM range of concentrations could be detected for the analytes.

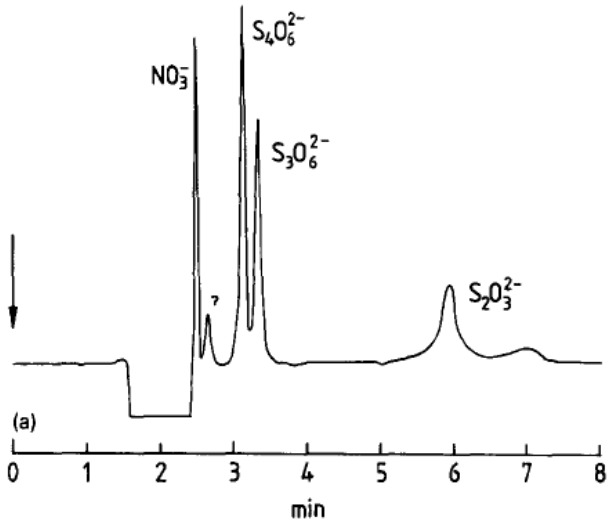

Figure 1.6. Ion chromatogram of some sulfur oxyanions. Eluent consisted of 70% ACN, 10% MeOH and 200 mM NaCl. Concentration of sulfur anions were 10 μM $S_4O_6^{2-}$, 50 μM $S_3O_6^{2-}$ and 25 μM $S_2O_3^{2-}$ (Reprinted with permission from Ref. 52 Copyright 2006 John Wiley and Sons)

Miura *et al.*[53] demonstrated the separation and detection of thiosalt species by postcolumn iodine-azide reaction. In this work five S-species ($S_2O_3^{2-}$, $S_3O_6^{2-}$, $S_4O_6^{2-}$, $S_5O_6^{2-}$ and $S_6O_6^{2-}$) were separated on an octadecylsilica (ODS) column and eluted with acetonitrile-water mobile phase using tetrapropylammonium salt as an ion-pair agent in the separation. Iodine was detected as triiodide spectrophotometrically at 350 nm catalyzed by each thiosalt species after separation in the column. The method was

successfully applied to determining thiosulfate and polythionates in diluted hotspring samples. Figure 1.7 below shows the separation of the sulfur species on an ODS column.

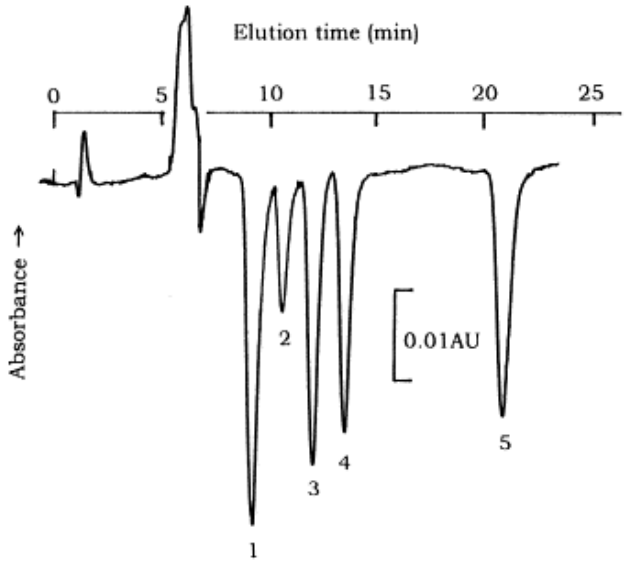

Figure 1.7. Chromatograms of five sulfur oxyanions in a mixture. Peak identification: 1. $S_2O_3^{2-}$ (50 n*M*), 2. $S_3O_6^{2-}$ (70 μ*M*), 3. $S_4O_6^{2-}$ (3.5 μ*M*), 4. $S_5O_6^{2-}$ (0.10 μ*M*), 5. $S_6O_6^{2-}$ (0.15 μ*M*). (Reprinted with permission from Ref. 54 Copyright 2001 Elsevier)

In another study Chen *et al.*[54] analyzed five sulfur species used as food additives using IC with post-column derivatization with iodine and UV detection at 288 nm. A Dionex Ionpac AS22A (250 mm x 4mm ID) column was used for the separation with an eluent mixture of 4.5 mM sodium carbonate and 0.8 mM sodium bicarbonate. The time for the

last eluting peak was 35 min. The chromatogram below (Figure 1.8) shows the separation of the sulfur species.

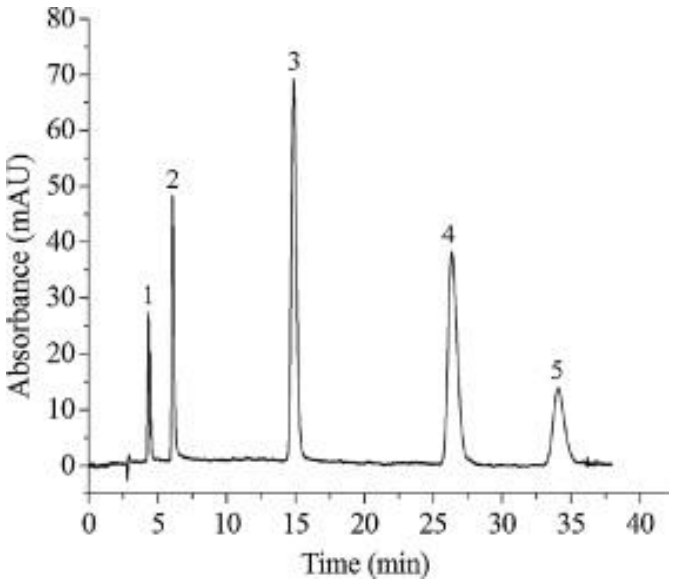

Figure 1.8. Chromatogram of a mixture of five sulfur anions. Peaks: 1. formaldehyde sulfoxylate (1.0 mg/L); 2. sulfide (10 mg/L); 3. sulfite (10 mg/L); 4. thiocyanate (10 mg/L); 5. thiosulfate (7.0 mg/L). (0.15 μ*M*). (Reprinted with permission from Ref. 54)

Despite the good results obtained using IC, there is a high cost of consumables, only moderate separation efficiency and speed, as well as lack of tolerance to some sample matrices, such as those with high ionic strength. Therefore high speed and cost effective as well as robust methods such as those using CE are attractive complements to IC.[55-66]

1.4.2 Capillary electrophoresis

Since Michaelis[67] coined the word 'electrophoresis' in 1909 after studying the migration of colloids in an electric field, and Tiselius[68] in 1937 applied the technique to performing 'moving boundary electrophoresis' to characterize the mobility of ionic protein analytes, the development of capillary electrophoresis (CE) has seen a significant growth from the early 1980s until now. CE is a powerful analytical separation technique for speciation analysis of environmental and biological molecules, inorganic ions and a variety of other compounds. Separation performance in terms of analysis time and throughput in CE is superior to most analytical techniques, such as HPLC and IC.[51] In addition, CE also required small amounts of consumables such as solvents and small sample volumes (nL range) leading to low waste generation (green). As mentioned previously, CE detection in nearly all cases requires a shorter analysis time compared to other analytical separations and this leads to reduced costs and improvement in quality control procedures. Despite the obvious advantages CE offers over more common analytical methods, adoption by industry for routine analysis has been slow, primarily hindered by a lack of robust methods and limited knowledge held by traditional analytical chemists of the technique's operational parameters.

CE is well suited for the analysis of thiosalts particularly with regard to industrial application of the technique, as these species are unstable and CE provides the high throughput analysis needed for better correlation between the analytical results and characteristics of the source. In addition, proper process and environmental controls

require detailed and reliable knowledge of speciation, which can be best obtained using CE. Therefore, CE can be used for analysis of thiosalts in studying their kinetic and thermodynamic properties required for optimization of the hydrometallurgical processing as well as waste-stream treatment. Furthermore CE can be coupled to MS to provide identification of the species on the basis of their mass-to-charge ratios. Studies involving analysis of some thiosalt species using CE have been a great success showing superior speed, sensitivity and reliability.[1,4,7,52,53] Consequently, CE has been applied for the separation of various inorganic sulfur oxyanions as well as other sulfur-containing species based on direct and indirect modes of CE detection.[4,5,7,56,71] Indirect methods are more commonly used for sulfur oxyanion species due to the fact that some of the important species such as SO_4^{2-} and SO_3^{2-} exhibit very weak or no UV absorbance in the direct CE mode. Hence CE with indirect UV detection helps to compensate for this challenge.

Fundamentally, separation of analytes in CE is generally due to differences in mobilities of analyte ions in an electrolyte solution under an applied electric field and this is a function of the hydrodynamic radius and charge of the analytes. Movement of the analytes are due to combined action of their electrophoretic mobility, which is an inherent property of the ion, as well as the electroosmotic flow (EOF) both of which are a result of the applied electric field across the capillary. Several variations (modes) of CE separation techniques are in use in CE including capillary zone electrophoresis (CZE), capillary isoelectric focusing (CIEF), capillary gel electrophoresis (CGE), capillary

isotachophoresis (CITP), micellar electrokinetic chromatography (MEKC) and capillary electro-chromatography (CEC).[69]

The migration velocity, v, of an analyte under the influence of an electric field is given by:[70]

$$v = \mu_{ep} E = \mu_{ep} \frac{V}{L} \tag{1.39}$$

where v is the migration velocity (cm s^{-1}), μ_{ep} is the electrophoretic mobility (cm^{-2} $V^{-1}s^{-1}$), V is the applied voltage (V) and L is the length of the capillary (cm). The μ_{ep} is an inherent property of the charged analyte and is given by:

$$\mu_{ep} = \frac{q}{6\pi\eta r} \tag{1.40}$$

where q is net charge on the ion, η is the viscosity of the buffer system, and r is the Stokes' ionic radius of the analyte.

Above pH 3, the silanol (Si-OH) groups inside a fused-silica capillary are deprotonated leaving negatively charged groups ($Si\text{-}O^-$) at the surface.[71] An electric double layer consisting of the immobile negatively charged silanol groups on the wall of the capillary and excess cations tightly adsorbed onto the surface of the capillary to compensate for the negatively charged wall is formed (Figure 1.9). The formation of this electric double layer results in a potential - zeta potential - that decays exponentially from the wall of the capillary towards the bulk solution. For a 1 mM electrolyte solution made of monovalent

ions, the thickness of the electric double layer will be 10 nm and at a concentration of 0.1 M, the thickness will be 1 nm.[72] When an electric field (E) is applied to the capillary, the excess cations in the diffuse part of the electric double layer cause a uniform bulk plug-like flow (as opposed to the parabolic flow of hydrodynamic profile of pressure-driven systems such as in HPLC) of the buffer solution within the capillary towards the cathode (Figure 1.10). This bulk flow phenomenon is called *electroosmotic flow* (EOF).

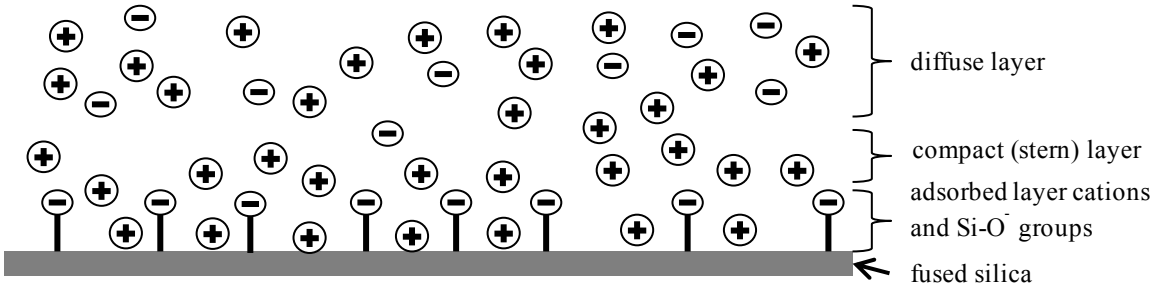

Figure 1.9. Charged fused-silica capillary surface showing the charged silica wall ($Si\text{-}O^-$ groups) and the electric double layer (compact and diffuse layers of excess cations)

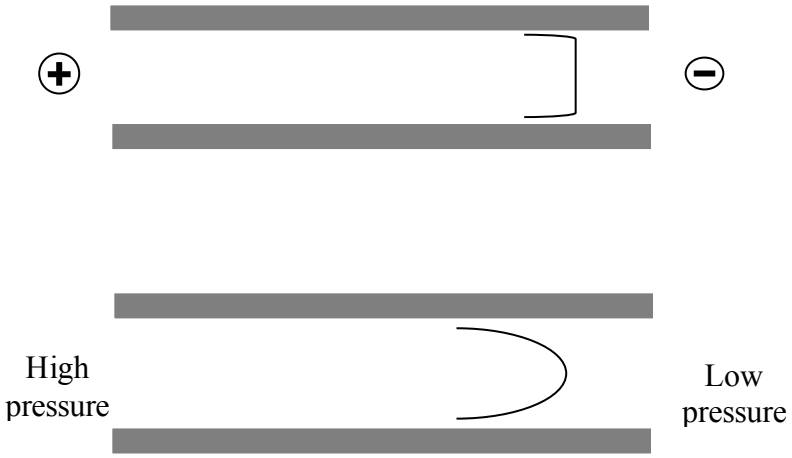

Figure 1.10. Comparison of flow profiles of electroosmotic flow (such as in CE) and hydrodynamic flow (such as in HPLC)

Under cathodic EOF conditions, cations are attracted towards the cathode and the anions towards the anode. When the EOF exceeds that of the electrophoretic mobilities of the anionic constituents, detection of all constituents (cation, anions, neutrals) can occur. The EOF depends on factors such as the buffer pH and concentration, applied voltage (V) and the addition of organic modifiers. The EOF (ν_{eo}) is defined by the Helmholtz-Smoluchowski equation[73]:

$$\nu_{eo} = \frac{\varepsilon\zeta}{\eta} \tag{1.41}$$

where ε is the dielectric constant, ζ is the zeta potential close to the wall, and η is the viscosity of the buffer system.

The zeta potential increases as a reciprocal square-root of the ionic strength I of the background electrolyte system (Equation 1.42).

$$\zeta \sim \frac{1}{\sqrt{I}} \tag{1.42}$$

During electrophoretic separation, with the detector placed at the cathode, the observed or apparent mobility, μ_{app}, of an ion is given by the sum of the electroosmotic mobility, μ_{eo}, of the solution and the electrophoretic mobility μ_{ep} of the ion (Equation 1.43).

$$\mu_{app} = \mu_{eo} + \mu_{ep} \tag{1.43}$$

Under cathodic conditions (positive polarity), a cation has μ_{ep} with the same sign as the μ_{eo} and therefore the $\mu_{app} > \mu_{ep}$. For anions, the two terms μ_{eo} and μ_{ep} have different signs. Under these conditions, high mobility anions may never reach the detector and therefore reversal of polarity is necessary to detect such anions.

1.4.2.1 CE Separation techniques for inorganic ions

Capillary zone electrophoresis (CZE) is the most common CE mode for the separation of inorganic anions. There are important parameters that need to be considered when applying CZE for separations. These include the background electrolyte (BGE), pH, organic modifiers (additives), applied voltage and polarity, capillary dimensions and capillary temperatures, among others. For the detection of inorganic anions such as sulfur oxyanions, an additional requirement will be to also select the most appropriate EOF

modifier to allow for the detection of the anions in the shortest possible time. EOF modifiers, such as cationic surfactants, are added to the BGE to form a dynamic coating on the surface of the capillary and impart a positive charge to the surface of the capillary. A reversed polarity electric field can then be applied for the separation. As the EOF and the anions are moving in opposite directions, modification of the EOF to either slow it down substantially or to reverse it is necessary to achieve fast analysis times.[74] Some of the selected BGE systems for inorganic sulfur anions reported are presented in Table 1.1.

In micellar electrokinetic chromatography (MEKC), one of the most important modes of electrokinetic chromatography (EKC), a pseudo-stationary phase in the form of an anionic or cationic surfactant is added to the BGE at a concentration above its critical micelle concentration (CMC) in order to form micelles. The analytes are separated based on their differential affinity for the micelles and as a result of their partitioning behaviour between the micellar phase and the aqueous phase.[79] The most common surfactants used for anionic separation in MEKC are sodium dodecyl sulfate (SDS) and cetyltrimethyl-ammonium bromide or chloride (CTAB or CTAC), tetradecyltrimethylammonium bromide (TTAB), sodium cholate and sodium deoxycholate.[80-81]

Table 1.1. Selected CZE applications for the analysis inorganic sulfur anions

BGE system	Buffer additives	Sulfur species analyzed	Reference
5 mM Na_2CrO_4, pH = 9.4, λ = 374 nm	4 mM TTAOH, 10 mM CHES (anti-coagulant)	SO_4^{2-}, SO_3^{2-}, $S_2O_3^{2-}$, $S_2O_4^{2-}$	[5]
1.5 mM PMA + 10 mM Tris; pH = 8.0, λ = 214 nm	0.5 mM CTAB	$S_2O_3^{2-}$, $S_2O_3^{2-}$, SCN^-	[57]
2.25 mM PMA + 6.5 mM NaOH + 1.6 mM TEA; pH = 10, λ = 254 nm	0.75 mM HMOH	S^{2-}, SO_4^{2-}, SO_3^{2-}, SCN^-, $S_2O_3^{2-}$, $S_2O_6^{2-}$, $S_2O_8^{2-}$	[76]
10 mM Na_2CrO_4, pH = 11, λ = 275 nm	2 mM TTAOH	S^{2-}, SO_4^{2-}, SO_3^{2-}, $S_2O_3^{2-}$	[77]
1.5 mM PMA + 10 mM Tris; pH = 7.0, λ = 214 nm	0.5 mM DETA, 0.1% formaldehyde (stabilizer)	S^{2-}, SO_4^{2-}, SO_3^{2-}, $S_2O_3^{2-}$, $S_2O_4^{2-}$	[78]

TTAOH – tetradecyltrimethylammonium hydroxide

CHES – 2-(cyclohexylamino) ethanesulfonic acid

HMOH – hexamethonium hydroxide

DETA – diethylenetriamine (dien)

Although not many MEKC methods have been published on inorganic anions, there have been numerous applications of the method to important environmental analytes such as polyaromatic hydrocarbons (PAHs),[82] pesticide samples[83] and phenolic compounds[84,85] One interesting application of MEKC with ESI-MS was the use of ammonium perfluorooctanoate (PFOA) as a volatile surfactant for the analysis of *N*-methylcarbamate pesticides by MEKC-ESI-MS in the Bottaro lab.[86] Table 1.2 summarizes the application of MEKC for other environmental samples and sulfur anions of interest.

Table 1.2. Some MEKC application for environmental analysis

BGE system	Surfactant used	Analyte	Reference
Phosphate-borate, pH = 8.0	SDS	*N*-methylcarbamates and metabolites in water	[87]
Ammonium chloride-ammonia, pH = 8.5	SDS	Imidachloprid and metabolites in tomato	[88]
Borate, pH = 9.0	SDS/β-cyclodextrin (CD)	2,4-dinitrophenyl-hydrazine (DNPH)-aldehyde derivatives in emissions from vehicles	[89]
20 mM 2-(N-morpholino) ethanesulfonic acid (MES), 20 mM Histidine (His), pH = 6.2	0.2 mM CTAB	SO_4^{2-}, NO_3^-, Cl^-	[90]
5 mM chromate, pH = 8.0	0.25 mM CTAC, MeOH (30%)	SO_4^{2-}, NO_3^-, Cl^-, F^-, ClO_4^-	[91]

Several inorganic ions have also been analyzed by microchip electrophoresis (MCE).[92-98] Table 1.3 shows some of the important inorganic ions analyzed by MCE.

Table 1.3. Selected MCE analysis of inorganic anions in the environment

MCE system and mode	Detection system	Analytes	LOD	Reference
PMMA, CZE	CD	Cl^-, SO_4^{2-}, NO_3^-	0.4 – 1.2 μM	[95]
PMMA, isotachophoresis (ITP) - CZE	CD	F^-, PO_4^{2-}, NO_2^-	0.5-0.7 μM	[96]
PDMS, CZE	CD	SO_4^{2-}, NO_3^-	1 μM	[97]
Borofloat glass, CZE	CD	SO_4^{2-}, HCO_3^-, Cl^-	10 μM	[98]

1.4.2.2 Detection of inorganic ions in CE

UV-vis detectors have been used most frequently for detection in CE. This is achieved as the analytes are separated into zones during electrophoresis and the absorbance of the analytes zone correlated to the concentration of the analyte. In addition to UV-vis detection for CE, other detectors have been employed based on techniques such as laser-induced fluorescence, conductivity, and mass spectrometry. Compared to HPLC the LOD obtained in CE is generally higher. This is partly due to typically nL sample volume injection in CE compared to μL in HPLC. In addition on-column detection in small capillary diameters (short pathlengths) in the 25 – 100 μm range account for the higher detection limits. However advances in on-column detection techniques such as the use of extended light pathlengths, Z-shaped capillary design at the detection and the use of liquid-core waveguides have led to higher sensitivities (~ 3 – 10 fold in LOD improvements).[99] In addition more sensitive detection techniques such as conductivity and mass spectrometry have led to lower LODs in CE. A summary of typical LODs for the different detection modes for CE are presented in Table 1.4.

Table 1.4. Detection techniques in CE and detection limits [adapted from Ref. 100]

Detection Mode	Typical LOD range (M)
Direct UV absorption	$10^{-5} – 10^{-7}$ (standard pathlength) 10^{-8} (extended pathlength)
Indirect UV absorption	$10^{-5} – 10^{-7}$
Direct laser-induced fluorescence LIF (on-column)	$10^{-10} – 10^{-11}$
Indirect LIF	$10^{-5} – 10^{-7}$
Post-column LIF	10^{-16} (single molecule)
Refractive index	$10^{-5} – 10^{-6}$ (capillary) 10^{-5} (microchip)
Conductivity	$10^{-7} – 10^{-8}$
Amperometry	$10^{-7} – 10^{-8}$
Potentiometry	$10^{-7} – 10^{-8}$
Raman	$10^{-3} – 10^{-6}$ (pre-concentration required)
MS	$10^{-8} – 10^{-9}$

1.4.2.2.1 CE with direct UV-vis detection

In direct UV-vis detection, an electrolyte with very low or no absorption at the desired wavelength is used and the positive absorbance peaks are monitored for each analyte zone. The obvious advantages of using direct UV-vis detection are the ease of monitoring UV absorbing analytes and the possible use of high concentration of the carrier electrolytes. LODs are generally in the range of $10^{-5} – 10^{-6}$ M for both direct UV-vis detection with standard capillary window pathlengths. Extended pathlengths can give LOD values well below 10^{-6} M.[100]

1.4.2.2.2 CE with indirect UV-vis detection

Whereas in CE with direct UV detection, a buffer system with low or no UV absorbance is used to detect UV absorbing analytes, CE with indirect UV detection makes use of a strongly absorbing probe added to the buffer system to give a consistently high absorption during the electrophoretic run. Thus, both UV-absorbing and non UV-absorbing analytes can be detected. Some additional considerations, however, must be taken into account with indirect UV-vis detection. The chromophoric probes selected for the analysis must meet certain conditions such as high molar extinction coefficient at the chosen detection wavelength, reasonable mobility match to the anions for improved sensitivity (symmetrical peak shape) and be unreactive toward the analytes.[5-7,53]

During electrophoretic separation, the analyte ions form zones (termed eigenzones) as a function of their electrophoretic mobilities. In the 'eigenzone' the composition of the BGE may be slightly different from the surrounding buffer environment. [101-103] Here, competitive processes, such as charge repulsion, allow analytes having the same charge as the probes to displace chromophoric probes and reduce their concentration in the eigenzone, which leads to a reduction in the background absorption resulting in 'negative' peaks. The area of the peak is then correlated to the concentration of the analytes in the eigenzone. Structures of some of the chromophoric probes are shown in Figures 1.11. [54, 101-103]

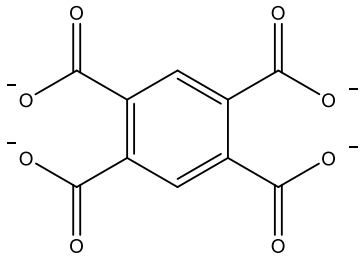

pyromellitate (PMA)

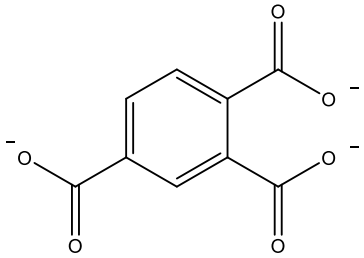

trimellitate (TMA)

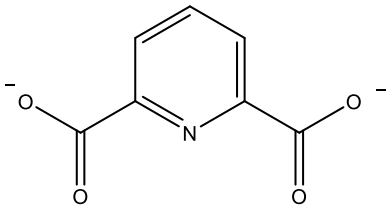

2,6-pyridine dicarboxylate (PDC)

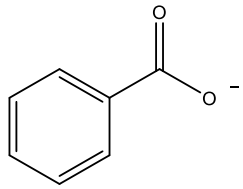

benzoate

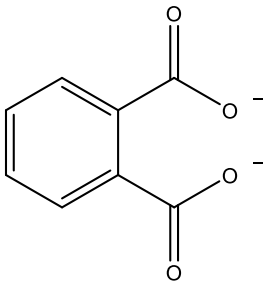

phthalate

Figure 1.11. Some chromophoric probes (fully charged) used in CE indirect UV-vis detection.

1.4.2.2.3 Selected applications of CE with direct UV-vis detection

O'Reilly *et al.*[8] developed a fast direct CE technique for separation of 4 sulfur anion species within 3 min in gold thiosulfate effluents. The BGE consisted of 25 mM bis(2-hydroxyethyl)amino-tris(hydroxymethyl)methane (BIS-TRIS) adjusted to pH 6.0 with H_2SO_4 and the sulfur species were detected at 195 nm (Figure 1.12). LOD values of 1 μM ($S_3O_6^{2-}$ and $S_4O_6^{2-}$) were achieved, as well as a large linear range of 10-8000 μM for the sulfur species. This method was not applied to detecting other sulfur species such as SO_4^{2-}, SO_3^{2-} and $S_6O_6^{2-}$.

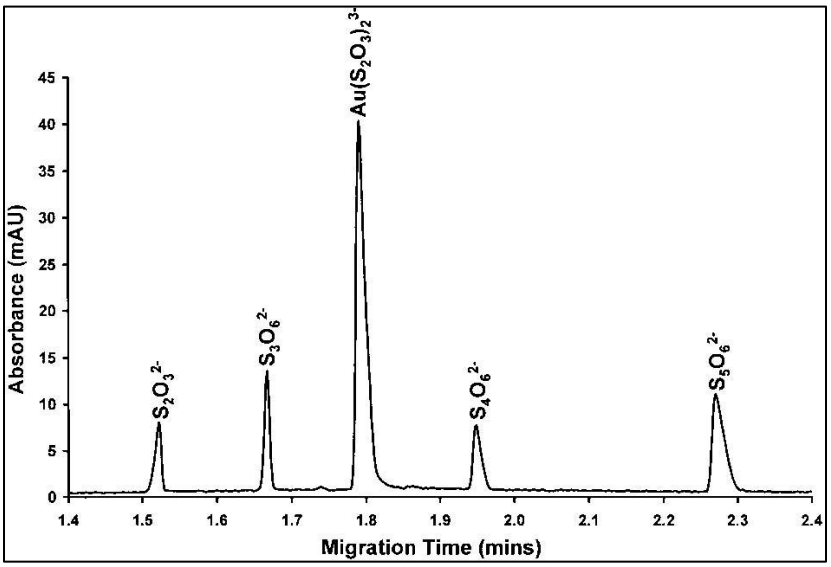

Figure 1.12: : Electropherogram showing the separation of 0.1 mM thiosulfate and 0.08 mM each of $S_2O_3^{2-}$, $S_3O_6^{2-}$, $S_5O_6^{2-}$ and the gold(I) thiosulfate complex. The BGE composed of 25 mM Bis-Tris adjusted to pH 6.0 with H_2SO_4, and a detection wavelength of 195 nm. (Reprinted with permission from Ref. 8 Copyright 2000 Wiley and Sons).

Jankovskiene *et al.*[104] developed an in-capillary derivatization method (Figure 1.12) for the analysis of some sulfur-oxyanion species using CE with direct UV-Vis detection. In this experiment sulfite was reacted with iodine and the resulting iodide ion was detected and correlated with the concentration of the sulfite ion. The principle of the in-column technique is shown in Figure 1.13. The method was applied for the analysis of a standard solution containing Br^-, I^-, $S_2O_3^{2-}$, SO_3^{2-} and NO_3^- anions. Very good correlation was obtained for all the anions analyzed. The electropherogram of the analysis is shown in Figure 1.14. For sulfite a linear calibration range between 1×10^{-5} and 8×10^{-4} M of sulfite was obtained with the LOD value determined to be 2×10^{-6} M.

:

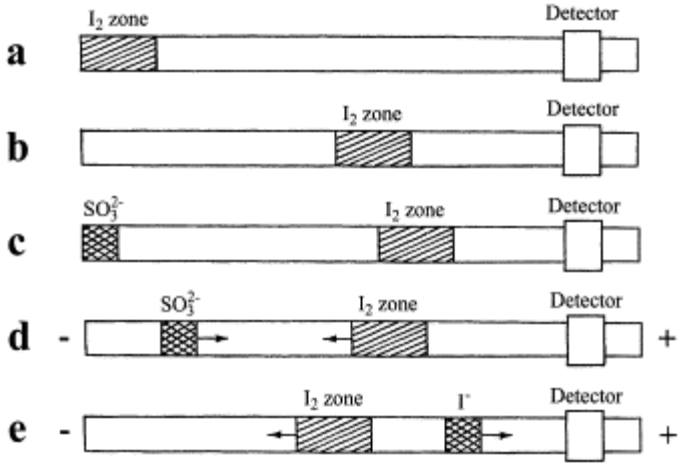

Figure 1.13. 5-step in-column derivatization of sulfite with iodine and U-detection of iodide (Reprinted with permission from Ref. 104 Copyright 2001 Elsevier)

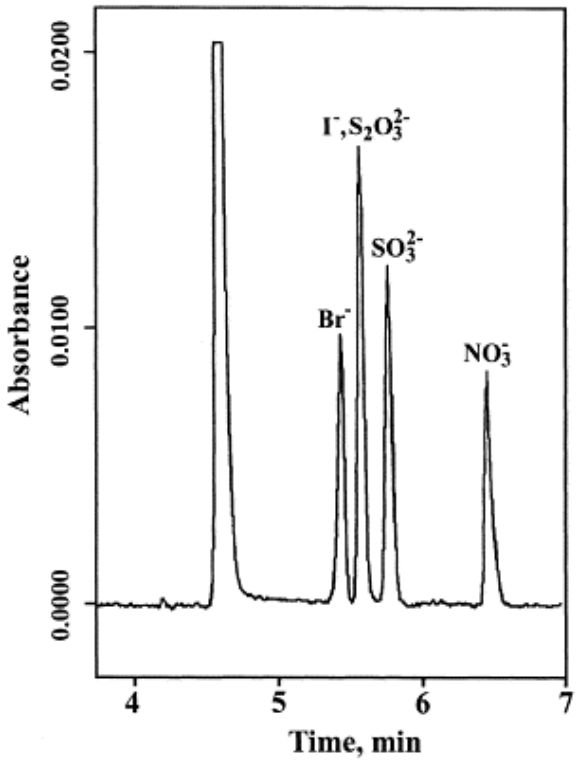

Figure 1.14. Electropherogram of a standard solution of Br^-, I^-, $S_2O_3^{2-}$, SO_3^{2-} and NO_3^- anions. Electrolyte composed of 20 mM Tris-HCl, 2 mM CH_3COONa. The electrolyte pH was 5 and the applied voltage was −20 kV. Direct UV detection was at 214 nm. (Reprinted with permission from Ref. 104 Copyright 2001 Elsevier)

In another study, Daunoravicius and Padarauskas developed a CE with direct UV detection method based on the similar iodine derivatization technique to successfully detect and quantify three sulfur anions: sulfite, sulfide and thiosulfate species in spent fixing solutions (waste from photographic developing).[105] In this study the iodine was injected from the anodic end of the capillary and a high reversed potential applied (Figure

1.15). The separated species react with iodine with the resultant iodide ion being detected and correlated to the concentration of the sulfur species. The electropherogram obtained from the analysis is shown in Figure 1.16. The LOD obtained for this technique for the three species ranged from 0.5 µM for $S_2O_3^{2-}$ to 2×10^{-6} µM SO_3^{2-}.

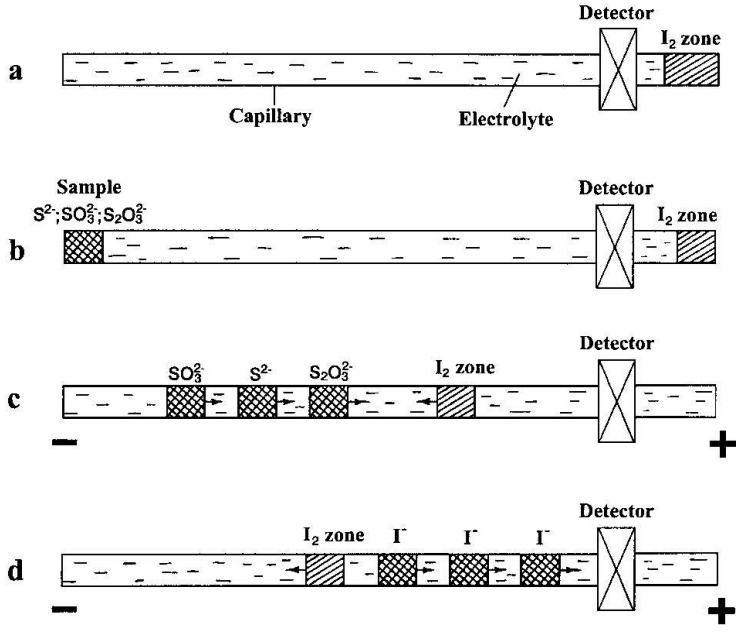

Figure 1.15. In-column derivatization and direct CE-UV detection of some sulfur anions with iodine. (Reprinted with permission from Ref. 105 Copyright 2001 Elsevier)

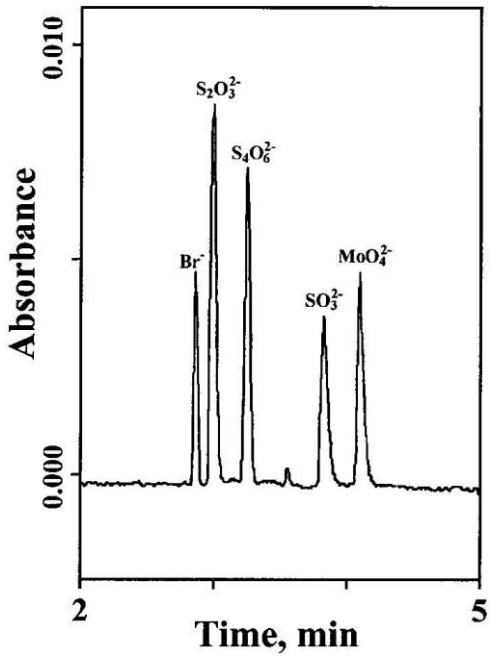

Figure 1.16. Electropherogram of 1:500 diluted spent fixing solution sample showing the presence of some sulfur anions. The electrolyte consisted of 20 mM Tris-Cl, pH 8.5. Applied voltage was -30 kV and direct UV detection made at 214 nm. (Reprinted with permission from Ref. 105 Copyright 2001 Elsevier)

1.4.2.2.4 Selected applications of CE with both direct and indirect UV-vis detection

A study by Chen *et al.*[58] utilizing both direct and indirect UV detection for CE was applied to the analysis of some sulfur species. For the indirect CE analysis 2,6-pyridinedicarboxylic (PDCA), benzoate, phthalate and trimellitate were used separately as the BGE absorbing probes with tetradecyltrimethylammonium bromide (TTAB) as the EOF modifier. The sulfur species investigated included $S_2O_3^{2-}$, SO_4^{2-}, SO_3^{2-} and S^{2-}.

Detection limit ranges achieved for the direct and indirect CE analysis were 3 – 7 μM and 2 – 6 μM respectively.

Padarauskas *et al.* developed a rapid determination of $S_2O_3^{2-}$ and some polythionate anions and applied the technique to the analysis of sulfur species in photographic spent fixing solutions (photographic developing waste).66 Both direct and indirect CE detection modes were examined. For the indirect analysis the BGE composed of 5 mM H_2CrO_4, 1 mM HMOH and the pH adjusted to 8.0 with triethanolamine. The peaks were detected at 254 nm. The sulfur species detected with the indirect CE technique included $S_2O_3^{2-}$, SO_4^{2-}, SO_3^{2-} and $S_4O_6^{2-}$ (Figure 1.17).

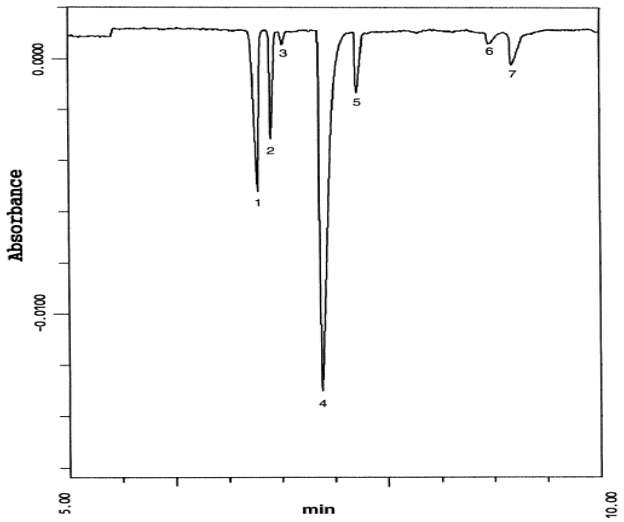

Figure 1.17: Electropherogram of 1:200 diluted spent fixing solution sample at 10 h into an anodic oxidation process. Electrolyte, 5 mM H_2CrO_4, 1 mM HMOH, pH adjusted to 8.0 with triethanolamine. Peaks: 1. $S_2O_3^{2-}$; 2. Br^-; 3. Cl^-; 4. SO_4^{2-}; 5. NO_3^-; 6. SO_3^{2-}; 7. $S_4O_6^{2-}$. (Reprinted with permission from Ref. 5 Copyright 2000 Elsevier)

1.4.2.2.5 Selected applications of CE with indirect UV-vis detection

Liang utilized an indirect CE method for the detection and quantitation of sulfur anions including SO_4^{2-}, SO_3^{2-}, $S_2O_3^{2-}$ and HS^- generated during the corrosion process of alloy production.[5] The BGE consisted of 5 mM Na_2CrO_4 as the absorbing probe, 4 mM tetradecyltrimethyl-ammonium hydroxide (TTAOH) as the EOF modifier, 10 mM 2-(cyclohexylamino) ethanesulfonic acid (CHES) as anti-coagulant (to prevent precipitation of chromate-TTAOH complex) and 0.1 mM calcium gluconate. The BGE pH was 9.4 and the detection wavelength was 374 nm. The method was however not able to resolve SO_3^{2-} and $S_2O_4^{2-}$ under any of the experimental conditions. Detection limits of 0.5 µg/mL were achieved for the sulfur anions with good repeatabilities of 0.1% and 0.5% for $S_2O_3^{2-}$ and SO_4^{2-}, respectively.

Another indirect CE method for sulfur species was developed by Motellier *et al.* for the detection of the sulfitolysis (disulfide cleavage) products of $S_4O_6^{2-}$.[55] The BGE consisted of 2 mM 5-sulfosalicylic acid (SULSAL), 0.5 mM TTAOH (EOF modifier), with pH adjusted to 7.00 with Bis-Tris. $S_4O_6^{2-}$ was determined indirectly as $S_3O_6^{2-}$ as a result of a rearrangement reaction of $S_4O_6^{2-}$. No higher order polythionates were determined with this method. A LOD value of 5 µM was achieved for $S_2O_3^{2-}$ and $S_4O_6^{2-}$, 2.5 µM for SO_4^{2-} and 6 µM for $S_3O_6^{2-}$.

1.4.2.2.6 CE with Electrochemical detection

The two most common electrochemical detection techniques in CE are conductivity and amperometric detection. LOD values in the range 0.001 µM to 0.1 µM can easily be achieved using this detection technique with CE.[106]

For environmental analysis, CE with conductivity detection has been the preferred electrochemical detection mode as it is more applicable to ions than amperometric detection (AD).[106] In this technique, two electrodes are put in contact with the electrolyte solution in a cell and a high frequency alternating current (AC) is applied across the electrodes. Analyte ions introduced in the electrolyte system cause an increase in the conductivity between the electrodes by decreasing the electrical resistance of the electrolyte as they pass through the electrode gap. The change in electrical conductivity is then correlated to the concentration of the analyte ions. CD detection is considered universal and generally has lower background noise compared to UV-vis detectors. The sensitivity of CD can be further enhanced by using suppression conductivity.[107]

Hissner *et al.*[57] utilized conductivity detection for CE (Figure 1.18) and achieved LOD values in the 8 – 50 ng/mL range. The technique worked better than CE with indirect detection as all the anions gave sufficient conductivity. The BGE was composed of 50 mM CHES, 35 mM LiOH, 0.03% Triton X-100.

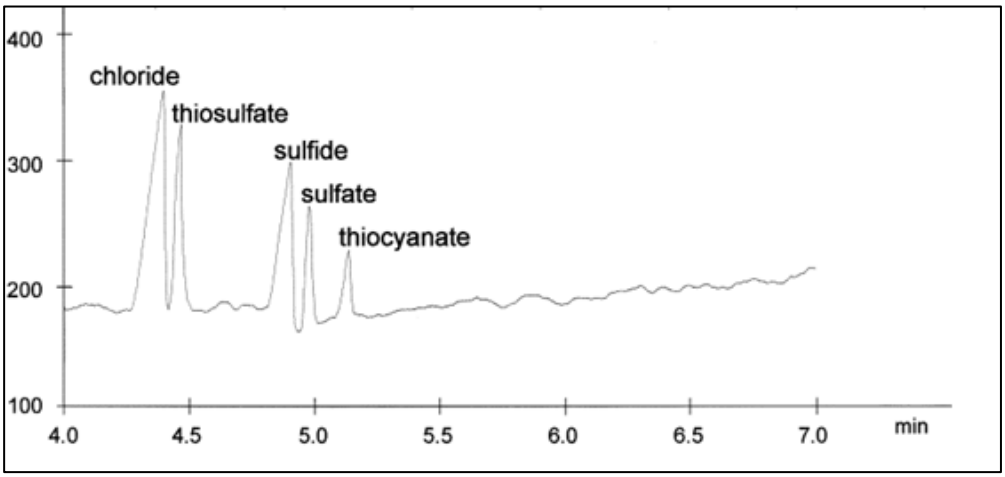

Figure 1.18. Electropherogram of some sulfur anions and chloride. BGE: 35 mM LiOH, Capillary: 72 cm × 50 μm, voltage: −25 kV, detection: conductivity 1 μS/cm, injection: 25 mbar for 12s 10 μg/mL anion standard mixture (Adapted and reprinted with permission from Ref. 57 Copyright 1999 Elsevier)

Currently capacitively coupled contactless conductivity detection (C^4D) is seeing more applications for CE and MCE systems especially for environmental inorganic ions as the design and operational performances are enhanced.[108] Table 1.5 summarizes some of the recent developments in the use of C^4D for CE and MCE. Although to our knowledge, no application has been made with CE-C^4D for the detection of sulfur anions, this will be an area where application could be seen in the near future.

Table 1.5. Some applications of CE-C^4D for environmental samples

Analytes	BGE composition	CE mode	Limit of detection	Reference
Glyphosate and its metabolites	12.0 mM His + 8.0 mM MES + 75 μM CTAB + 3% methanol, pH 6.3	CZE	0.005 μg/L 0.06 μg/L	[109]
Trace heavy metals	30 mM MES + 30 mM His	EPC-CE	0.95 – 6.8 μg/L	[110]
Chemical warfare agents	7.5 mM MES/His, pH 6	portable CE	4.1 – 5.0 μM	[111]
Nerve agents	7.5. mM MES/His, pH 6	CE portable	15.2 –26.1 μ M	[112]
Toxic metals (Cr^{3+}, Pb^{2+}, Hg^{2+}, Ni^{2+})	10 mM His + 4 mM Tart, pH 5.5, 2 mM 18-crown-6	CZE	0.005 – 2.32 μg/L	[113]

His – histidine
MES – 2-(N-morpholino)ethanesulfonic acid
EPC – electrochemical preconcentration

1.4.3 Use of ion-pairing reagents for CE-MS analysis

Mass spectrometric detection of environmental anions is not the norm as more established techniques such as IC and CE with UV-vis detection have been the routine approach to detecting these anion species. However, one of the major limitations of the current analytical methods that rely on UV-vis for quantitation is that identification is made on the basis of retention or migration time. When samples are more complex or when matrix effects interfere with expected migration behavior, confirmation of peak identity may be difficult or impossible. The main problem with direct analysis of the

anions by MS is that they must be detected in negative ESI mode, which is typically less sensitive, and their $\frac{m}{z}$ values tend to be relatively low, leaving them to be detected in the low mass region of the mass spectrum that typically suffers from poor signal-to-noise ratio, that is, there is a great deal of noise and so detection limits are high (poor).

To surmount these issues, to achieve unequivocal anion identification and push detection limits down to ultra-trace levels for thiosalt species, a novel approach for detection has been recently been reported in literature.[114-118] This technique makes use of ion-pairing reagents (IPR^{m+}) to aid detection of these anions (A^{n-}) by MS. The objective is to use these reagents to form a ion-pairs with the anions so that the ion-pair carries a positive charge which can then be detected using the more sensitive positive mode of ESI-MS. Flow injection analysis (FIA) and CE with ESI-MS have been used to detect the formation of stable gas phase adducts of the form $[IPR^{m+}+A^{n-}]^{(m-n)+}$, making these approaches suitable for analysis of a range of anions. Some of the tricationic ion-pairing reagents reported in literature are shown on the next page in Figure 1.19.[117,118]

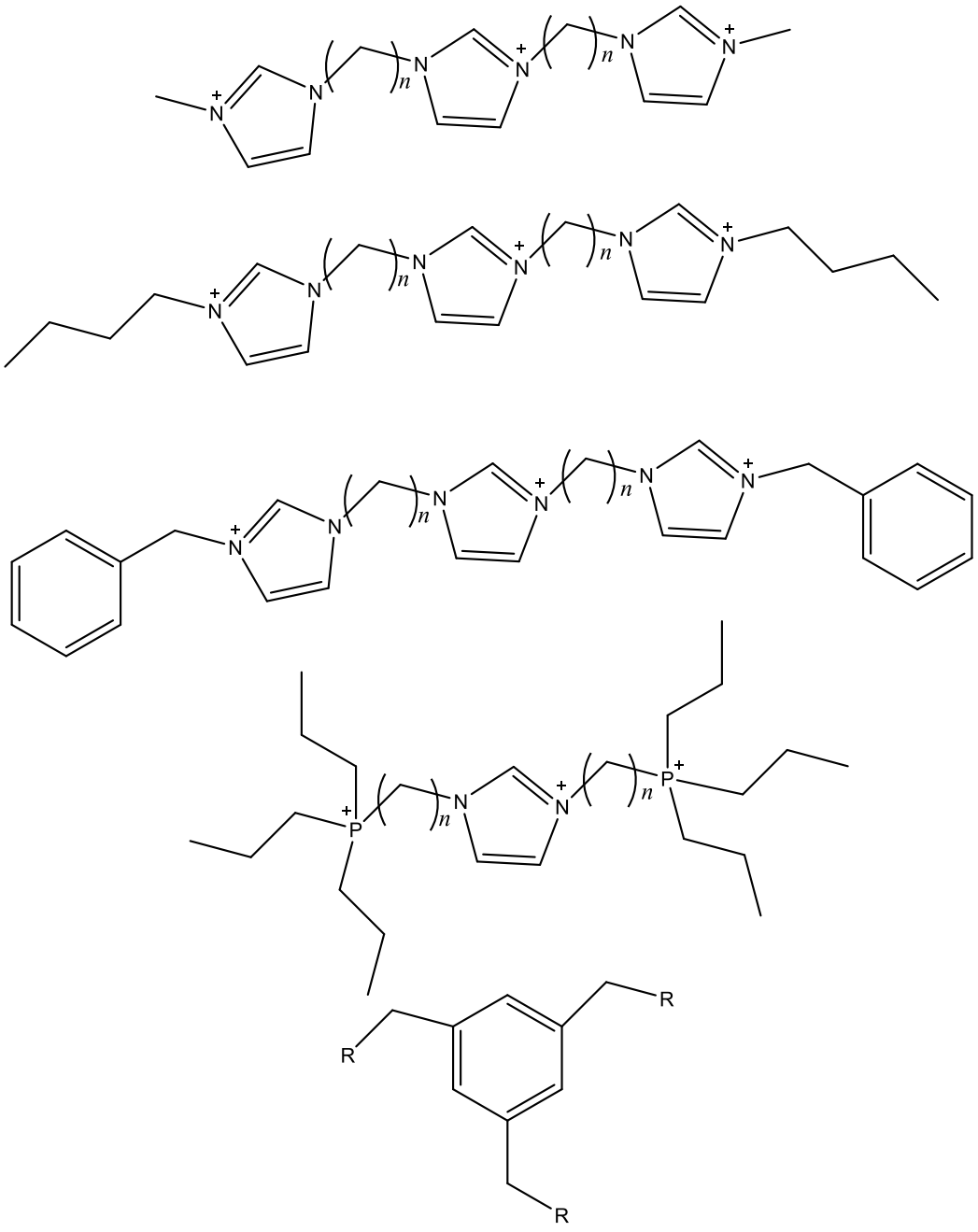

Figure 1.19. Structures of some tricationic ion-pairing reagents. (3 < n < 12; R = methylimidazolium or tripropylphosphonium)

Several applications of the use of ion-pairing reagents for environmental analysis have been published. In one study by Magnuson *et al.*, detection of trace concentration of perchlorate ions in drinking water was achieved using an ion-pairing reagent.[115] A perchlorate-decyltrimethylammonium complex was extracted with dichloromethane and detected as $\frac{m}{z}$ 380 using FIA-ESI-MS. LOD value of 100 ng/L was achieved using this technique. Though few papers have been published using this technique to detect and quantify sulfur oxyanion species, there was one of particular interest by Breitbach *et al.*[116] They evaluated 16 different tricationic ion-pairing reagents to detect divalent anions in the positive mode ESI-MS. The trication pairing reagents were made up of mostly imidazolium, phosphonium or pyrrolidinium charged groups, alkyl linkages and benzene groups. The ion-pairing reagents were added 'post-column' and mixed with the anions in a Y-type tee after the anions were injected via a 6-port injection valve. LODs achieved for the sulfur anions using this technique were remarkably lower than those seen when using CE or IC with UV-vis detection. The LOD for SO_4^{2-} ranged from 0.1 ng to 2.75 ng and $S_2O_3^{2-}$ from 0.1 ng to 5.2 ng for the 16 tricationic pairing reagents. They found out that for these analytes, the linear tricationic reagents, the alkyl linkages between the charged moieties should be between 6 and 10 carbons in length to give the optimum pairing response. In addition, the triisopropylphosphonium and benzylimidazolium charged groups gave the best pairing response with the anions analyzed. Warnke *et al.* also evaluated two linear flexible and two trigonal tricationic ion pairing reagents with imidazolium and phosphonium charged groups for several divalent anions and detected them in the positive mode ESI-MS.[117] Disulfonates, dicarboxylates and other inorganic

anions including tetrathionate were studied. Tetrathionate ion gave LOD values of 5.0×10^{-4} ng/mL and 2.2×10^{-2} ng/mL with the linear phosphonium-based and imidazolium-based trication pairing reagents, respectively, and 2.5×10^{-2} ng/mL and 5.0×10^{-2} ng/mL for the trigonal phosphonium-based and imidazolium-based trication pairing reagents respectively. Finally, in a recent work by Gerardi *et al.*[118] CE-ESI-MS was applied in separating three divalent anions and detecting the tricationic-anion ion-pair by positive mode ESI-MS. The trigonal trication was composed of a benzene core and three imidazolium charged groups. The challenge with CE-ESI-MS is the need to optimize the CE separation parameters, maintaining electric contact between the CE and ESI source as well as optimize the ESI-MS parameters. The trication pairing reagent can be added to the sample, BGE or the sheath liquid for the analysis so that must also be considered. In this work, the best and fastest separation and sensitivity were achieved when the pairing reagent was added to the BGE (Figure 1.20). LODs for SO_4^{2-} and $S_2O_3^{2-}$ were 52.3 ng/mL and 68.4 ng/mL, respectively.

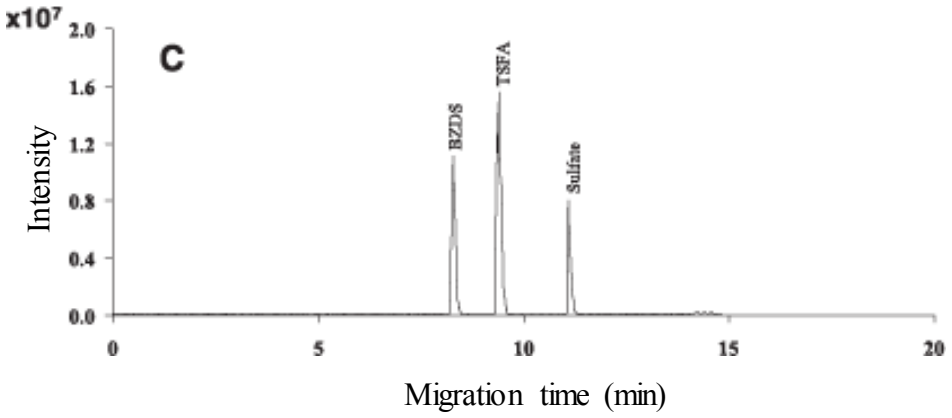

Figure 1.20. Chromatogram showing the separation of three anions (10 µg/mL benzenedisulfonate (BZDS), 100 µg/mL thiosulfate (TSFA), and 50 µg/mL of sulfate) by CE-ESI-MS in positive-ion mode with on-column ion-pairing with 20 µM 1,3,5-1-butyl-3-methyl-1*H*imidazol-3-ium-2,4,6-trimethylbenzene in the separation buffer.

In all the analytical techniques discussed, and to our knowledge, not one has been applied for the analysis of all the important thiosalt species relevant to our work although they could be optimized to analyze these species of interest.

1.5 Research objectives and organization of thesis

The primary objective of this research is to develop fast and sensitive CE method with indirect detection and ESI-MS detection for the analysis of sulfur oxyanions, particularly thiosulfate and the polythionates. Detecting and quantifying these species in the milling process and the tailings ponds will provide information that will lead to a better

understanding of thiosalts generation which is needed to develop the best treatment protocols

In the development of these methods, techniques that have been applied for thiosalt species and published will be investigated to determine the important parameters to optimize in the development of the new CE with indirect UV methods. As optimization of the several parameters of CE with UV (such as concentration of background electrolyte, concentration of chromophoric probes, pH, cassette temperature, and applied electric field) can be time consuming, an experimental design approach was utilized for screening critical factors and optimizing these factors for CE-UV-vis analysis and to study interactions between these factors for the optimum resolution of analyte peaks required for the analysis. This work incorporated several approaches including experimental designs such as fractional factorial (fFD), response surface (central composite (CCD) or Box-Behnken (BBD) designs for the selection of optimum levels of selected factors and optimization of responses.

The introduction to thiosalt chemistry and analytical approaches for their analysis are already covered in this chapter. Chapters 2, 3 and 4 are dedicated to the development of indirect CE methods for the rapid analysis of thiosalts in tailings pond samples. Chapter 2 examines the influence of factors such as the concentrations of BGE chromophoric probe and EOF modifiers, separation voltage and organic modifiers on the separation of the thiosalt species and application to real samples using a univariate approach. Chapters 3

and 4 focus on use of experimental design approach to the development of robust CE with indirect UV detection methods using two chromophoric probes and 3 EOF modifiers for thiosalts analysis. The use of CCD, fFD and BBD designs for the background electrolyte composition and instrument parameter optimization, and application for the separation of thiosalts will be described. The results of an ESI-MS study of gas phase ion-pairs formed by tricationic ion-pairing reagents and thiosalts are given in Chapter 5 which highlights the strength of association and binding energies of these ions in the gas phase via static titration. Chapter 6 describes the single crystal characterization of tri-, tetra- and pentathionates synthesized for this work. Finally in Chapter 7, future work and preliminary results of using CE-ESI-MS to detect the ion-pairs formed between the thiosalt species and the tricationic ion-pairing reagents are presented.

1.6 Co-authorship Statement

A modified version of Chapter 1 has been published as a critical review article in a peer-reviewed journal with Jorge C. Miranda-Trevino and Drs. Kelly Hawboldt and Christina S. Bottaro. Pappoe is the 2nd author and independently prepared portions of manuscripts with Miranda-Trevino. Advice and editing was given by Drs. Christina S. Bottaro and Kelly Hawboldt. For clarity, Pappoe prepared all material for the 'Analytical methods for detection and quantification of thiosalts' section of the paper and these sections have been included in Chapter 1 with modifications and updating.

Chapter 2, 'Systematic optimization of a pyromellitic acid background electrolyte for capillary zone electrophoresis with Indirect UV-Vis detection and online pre-

concentration analysis of thiosalt anions in the treated mine tailings', has been published in the RSC Journal of Analytical Methods. Manuscripts for Chapters 3, 4 and 5 have been prepared for publication. Editing and advice are given by Dr. Christina S. Bottaro. For Chapter 5, the first author proposed the evaluation of the strength of association of tricationic ion-pairing for the analysis of the thiosalt species of interest and followed through with experimental work with advice from Dr. Bottaro.

The unavailability of some thiosalt compounds warranted that synthesis and purification be performed to be able to use them as standards. The compounds included trithionate, tetrathionate, pentathionate and hexathionate salts. Pappoe performed all the synthesis with assistance from Heather Lucas in part of the project. A peer-reviewed paper on the X-ray structural characterization of some of these crystals has been published in the Journal of Chemical Crystallography with Michael Pappoe being the first author, Heather Lucas, the second, Dr. Christina S. Bottaro, the third and Dr. Louise Dawe as the fourth and corresponding author. All crystallographic analysis was done by Dr. Louise Dawe with the first author preparing part of the introduction, synthesis and acknowledgements sections. This paper is included in thesis as Chapter 6 without modification.

1.7 References

[1] Wasserlauf, M.; Dutrizac, J.E. The chemistry, generation and treatment of thiosalts in milling effluents – A non-critical summary of CANMET investigations 1976-1982, CANMET Report 82-4E, 1982.

[2] Dinardo, O.; Sally, J. In *Treatment of thiosalts in milling effluent: A review of treatment process*. Mining and Mineral Sciences Laboratories Report. Thiosalts Consortium-Phase II. CANMET-MMSL, 1998.

[3] Druschel, G. K.; Schoonen, M. A. A.; Nordstrom, D. K.; Ball, J. W.; Xu, Y.; Cohn, C.A. Sulfur geochemistry of hydrothermal waters in Yellowstone National Park, Wyoming, USA. III. An anion-exchange resin technique for sampling and preservation of sulfoxyanions in natural waters. *Geochem. Trans.* **2003**, *4*,12-19.

[4] Fahd, F.; Khan, F.; Hawboldt, K.; Abbassi, R. Developing a Novel Methodology for the Ecological Risk Assessment of Thiosalts. *Stoch. Environ. Res. Risk Assess.* **2014,** *28*, 383-391.

[5] Liang, H., Method development and validation for the determination of various sulfur-containing anions and other anions in the corrosion process by capillary ion electrophoresis with indirect detection. *J. Chromatogr. Sci.* **2001**, *39*, 12-20.

[6] Motellier, S.; Gurdale, K.; Pitsch, H., Sulfur speciation by capillary electrophoresis with indirect spectrophotometric detection: In search of a

suitable carrier electrolyte to maximize sensitivity. *J. Chromatogr. A*, **1997**, *770*, 311-319.

[7] Hissner, F.; Mattusch, J.; Heinig, K. Determination of sulfur-containing inorganic anions by dual ion chromatography and capillary electrophoresis – application to the characterization of bacteria sulfur degradation. *Fresenius' J. Anal. Chem*. **1999**, *365*, 647 – 653.

[8] O'Reilly, J.W.; Dicinoski, G.W.; Miura Y.; Haddad P.R.; Separation of thiosulfate and the polythionates in gold thiosulfate leach solutions by CE. *Electrophoresis*, **2003**, *24*, 2228-2234.

[9] Druschel, G. K.; Schoonen, M. A. A.; Nordstrom, D. K.; Ball, J. W.; Xu, Y.; Cohn, C.A. Sulfur geochemistry of hydrothermal waters in Yellowstone National Park, Wyoming, USA. III. An anion-exchange resin technique for sampling and preservation of sulfoxyanions in natural waters. *Geochem. Trans.* **2003**, *4*, 12-19.

[10] Mizoguchi, T.; Takei, Y.; Okabe T. The chemical behavior of low valence sulfur compounds. X. Disproportionation of thiosulfate, trithionate, tetrathionate and sulfite under acidic conditions. *Bull. Chem. Soc. Jpn.* **1976**, *49*, 70-75.

[11] Wu, R.; Zheng, Y.F.; Zhang, X.G.; Sun, Y.F.; Xu, J.B.; Jian, J.K.; Hydrothermal synthesis and crystal structure of pyrite. *J. Cryst. Growth*. **2004**, *266*, 523–527.

[12] Fox, D.; Robinson, C.; Zentilli, M.; Pyrrhotite and associated sulphides and their relationship to acid rock drainage in the Halifax Formation, Meguma Group, Nova Scotia. *Atl. Geol.* 1997, *33*, 87-103.

[13] Chinchón-Payá, S.; Aguado, A.; Chinchón, S. A comparative investigation of the degradation of pyrite and pyrrhotite under simulated laboratory conditions. *Eng. Geol.* **2012**, *127*, 75-80.

[14] Klein, B.; Higgs, T.W.; Poling, G.W.; In: *A New Test Procedure to Characterize the Reactivity of Mining Waste*. The Technical and Research Committee on Reclamation Proceedings of the 18th Annual British Columbia Mine Reclamation Symposium in Vernon, BC, 1994.

[15] Wu, R.; Zheng, Y.F.; Zhang, X.G.; Sun, Y.F.; Xu, J.B.; Jian, J.K.; Hydrothermal synthesis and crystal structure of pyrite. *J. Cryst. Growth*. **2004**, *266*, 523–527.

[16] H.W. Nesbitt, H.W.; Bancroft, G.M.; Pratt, A.R.; Scaini, M.J. Sulfur and iron surface states on fractured pyrite surfaces, *Am. Mineral.* **1998**, *83*, 1067–1076.

[17] Ferguson, K.D.; Erickson, P.M. In: *Will It Generate AMD? An Overview of Methods to Predict Acid Mine Drainage*. The Technical and Research Committee on Reclamation Proceedings of the 11th Annual British Columbia Mine Reclamation Symposium in Campbell River, BC, 1987.

[18] R.A. Knapp., In: *The Biogeochemistry of Acid Generation in Sulfide Tailings and Waste Rock*. Proceedings of Acid Mine Drainage Seminar in Halifax, NS, 1987.

[19] Williamson, M.A.; Rimstidt, J.D. Correlation between structure and thermodynamic properties of aqueous sulfur species. *Geochim. Cosmochim. Acta*. **1992**, *56*, 3867-3880.

[20] Druschel, G.K.; Hamers, R.J.; Banfield, J.F. Kinetics and mechanism of polythionate oxidation to sulfate at low pH by O_2 and Fe^{3+}. *Geochim. Cosmochim. Acta*, **2003**, *67*, 4457-4469.

[21] Druschel, G.K.; Hamers, R.J.; Luther, G.W.; Banfield, J.F. Kinetics and mechanism of trithionate and tetrathionate oxidation at low pH by hydroxyl radicals. *Aquat. Geochem*. **2003**, *9*, 145-164.

[22] Garcia, C.; Ballester, A.; Gonzalez, F.; Blazquez, M.L. Pyrite behavior in a tailings pond. *Hydrometallurgy*, **2005**, *76*, 25-36.

[23] Goldhaber, M. Experimental study of metastable sulfur oxyanion formation during pyrite oxidation at pH 6-9 and 30 C. *Am. J. Sci.* **1983**, *283*, 193-217.

[24] Masau, R.; Oh, J.; Suzuki, I. Mechanism of oxidation of inorganic sulfur compounds by thiosulfate-grown *Thiobacillus thioxidans*. *Can. J. Microbiol.* **2001**, *47*, 348-358.

[25] Holmes, P.R.; Crundwell, F.K. The kinetics of the oxidation of pyrite by ferric ions and dissolved oxygen: An electrochemical study. *Geochim. Cosmochim. Acta*. **2000**, *64*, 263-274.

[26] Garrels, R.M., Thompson, M.E. Oxidation of pyrites by iron sulfate solutions. *Am. J. Sci.* **1960,** *258-A*, 57–67.

[27] Singer, P.C., Stumm, W. Acidic Mine Drainage: The Rate-Determining Step. *Science*, **1970,** *167,* 1121–1123.

[28] Hu, G; Dam-Johansen K.; Wedel, S.; Hansen, J.P. Decomposition and oxidation of pyrite. *Prog. Energy Combust. Sci.* **2006**, *32*, 295-314.

[29] Bain, G.W. Pyrite oxidation. *Econ. Geol. Bull. Soc. Econ. Geol.* **1935**, *30*, 166-169.

[30] Belzile, N.; Chen, Y.; Cai, M.; Li, Y. A review on pyrrhotite oxidation. *J Geochem. Explor.* **2004**, *84*, 65-76.

[31] Rimstidt, J.D.; Vaughan, D.J. Pyrite oxidation: A state-of-the-art assessment of the reaction mechanism. *Geochim. Cosmochim. Acta*. **2003**, *67*, 873-880.

[32] Nordstrom, D.K.; Alpers C.N. Geochemistry of acid mine waters. *Rev. Econ. Geol.* **1999**, *6A*, 133-160.

[33] Benner, S.G.; Gould, W.D.; Blowes, D.W., Microbial populations associated with the generation and treatment of acid mine drainage. *Chem. Geol.* **2000**, *169*, 435 – 448.

[34] Fox, D.; Robinson, C.; Zentilli, M. Pyrrhotite and associated sulfides and their relationship to acid rock drainage in the Halifax Formation, Meguma Group, Nova Scotia. *Atl. Geol.* **1997**, *33*, 87-103.

[35] Suzuki, I. Oxidation of Inorganic Sulfur Compounds: Chemical and Enzymatic Reactions. *Can. J. Microbiol.* **1999**, *45*, 97-105.

[36] Kelly, D.P.; Wood, A.P. Enzymes Involved in Microbial Oxidation of Thiosulfate and Polythionates. *Methods Enzymol.* **1994**, *243*, 501-510.

[37] Xu, Y.; Schoonen, M.A.A. The stability of thiosulfate in the presence of pyrite in low-temperature aqueous solutions. *Geochimica. Cosmochimica. Acta*, **1995**, *59*, 4605-4622.

[38] Rabin, S.B. The redox kinetics and reaction mechanisms of some sulfur oxyanions. Ph.D Thesis, Rice University, 1998.

[39] J. Zopfi, T.G; Ferdelman, H. Distribution and fate of sulfur intermediates—sulfite, tetrathionate, thiosulfate, and elemental sulfur—in marine sediments. *Geol. Soc. Am. Spec. Pap.* **2004**, *379*, 97-116.

[40] Vongporm, Y. Thiosalt behavior in aqueous media. Master in Engineering Thesis. Memorial University of Newfoundland, 2008.

[41] Lu, Y. C.; Gao, Q. Y.; Xu, L.; Zhao, Y. M.; Epstein, I. R. Oxygen-Sulfur Species Distribution and Kinetic Analysis in the Hydrogen Peroxide-Thiosulfate System. *Inorg. Chem.* **2010**, *49*, 6026–6034.

[42] Meyer, B.; Ospina, M. Raman spectrometric study of the thermal decomposition of aqueous tri- and tetrathionate. *Phosphorus, Sulfur, Silicon Relat. Elem.* **1982**, *14*, 23-36.

[43] Zhang H.; Jeffrey M.I. A Kinetic Study of Rearrangement and Degradation Reactions of Tetrathionate and Trithionate in Near-Neutral Solutions. *Inorg. Chem.* **2010**, *49*, 10273–10282.

[44] Csekő G.; Horváth A.K., Kinetics and Mechanism of the Chlorine Dioxide−Trithionate. *J. Phys. Chem. A*, **2012**, *116*, 2911−2919.

[45] Zhang H.; Jeffrey M. I. A Kinetic Study of Rearrangement and Degradation Reactions of Tetrathionate and Trithionate in Near-Neutral Solutions. *Inorg. Chem*. **2010**, *49*, 10273–10282.

[46] Lu, Y. C.; Gao, Q. Y.; Xu, L.; Zhao, Y. M.; Epstein, I. R. Oxygen-Sulfur Species Distribution and Kinetic Analysis in the Hydrogen Peroxide-Thiosulfate System. *Inorg. Chem*. **2010**, *49*, 6026–6034.

[47] Lu, Y. C.; Gao, Q. Y.; Xu, L.; Zhao, Y. M.; Epstein, I. R. Oxygen-Sulfur Species Distribution and Kinetic Analysis in the Hydrogen Peroxide-Thiosulfate System. *Inorg. Chem*. **2010**, *49*, 6026–6034.

[48] Xu, L.; Horváth, A. K.; Hu, Y.; Ji, C.; Zhao, Y. M.; Gao, Q. Y. High Performance Liquid Chromatography Study on the Kinetics and Mechanism of Chlorite-Thiosulfate Reaction in Slightly Alkaline Medium. *J. Phys. Chem. A*, **2011**, *115*, 1853–1860.

[49] Pan, C.; Wang, W.; Horváth, A. K.; Xie, J.; Lu, Y.; Wang, Z.; Hu, Y.; Ji, C., Zhao, Y.; Gao, Q., Kinetics and Mechanism of Alkaline Decomposition of the Pentathionate Ion by the Simultaneous Tracking of Different Sulfur Species by High-Performance Liquid Chromatography. *Inorg. Chem*. **2011**, *50*, 9670-9677.

[50] Pan, C.; Liu Y.; Horváth, A. K.; Wang, Z.; Hu, Y.; Ji, C.; Zhao, Y.; Gao, Q.; Kinetics and Mechanism of the Alkaline Decomposition of Hexathionate Ion. *J. Phys. Chem. A*. **2013,** *117*, 2924−2931.

[51] Haddad, P.R., Comparison of ion chromatography and capillary electrophoresis for the determination of inorganic ions. *J. Chromatogr. A.* **1997**, *770*, 281-290.

[52] Friedhelm, B.; Schuhmann, A.; Jansen, K. Determination of tetrathionate and thiosulfate in natural samples and microbial cultures by a new, fast and sensitive ion chromatographic technique. *FEMS Microbiol. Ecol.* **1993**, *12*, 257-264.

[53] Miura, Y.; Watanabe, M. Ion-pair chromatography of polythionates and thiosulfate with detection based on their catalytic effects on the postcolumn azide-iodine reaction. *J. Chromatogr A*. **2001,** *920*, 163-171.

[54] Chen, M. L.; Ye, M. L.; Zeng, X. L.; Fan, Y. C.; Yan, Z. Determination of sulfur anions by ion chromatography–postcolumn derivation and UV detection. *Chin. Chem. Lett*. **2009**, *20*, 1241–1244.

[55] Motellier, S., Sulfur speciation and tetrathionate sulfitolysis monitoring by capillary electrophoresis. *J. Chromatogr. A*, **2001**, *907*, 329-335.

[56] Jeffrey, M. I.; Brunt, S. D., The quantification of thiosulfate and polythionates in gold leach solutions. *Hydrometallurgy*. **2007**, *89*, 52-60.

[57] Hissner, F.; Mattusch, J.; Heinig, K. Quantitative determination of sulfur-containing anions in complex matrices with capillary electrophoresis and conductivity detection. *J. Chromatogr. A*. **1999**, *848*, 503-513.

[58] Chen, Z.; Naidu, R., Separation of sulfur species in water by co-electroosmotic capillary electrophoresis with direct and indirect UV detection. *Int. J. Environ. Anal. Chem*. **2003**, *83*, 749-759.

[59] Timberbaev, A. R., Analysis of inorganic pollutants by capillary electrophoresis. *Electrophoresis.* **1997**, *18*, 185-195.

[60] Kaniansky, D.; Masár, M.; Marák, J.; Bodor., Capillary electrophoresis of inorganic anions. *J. Chromatogr. A.* **1999**, *834*, 133-178.

[61] Mazzeo, J. R.; Mazzeo, J.R. Capillary electrophoresis of inorganic anions. In *High Performance Capillary Electrophoresis, Theory, Techniques and Applications.* Khaledi, M.G., Ed.; Wiley: New York, 1998; p 825-852.

[62] Jones, W. R.; Jandik, P., Controlled changes of selectivity in the separation of ions by capillary electrophoresis. *J. Chromatogr.* **1991**, *546*, 445-458.

[63] Camilleri, P., Determination of inorganic anions and metal cations. In *Capillary electrophoresis, Theory and Practice.* Camilleri P., Ed.; CRC Press, 1998; p 246-272.

[64] Kelly, D. P.; Wood, A. P., Synthesis and determination of thiosulfate and polythionates. *Methods Enzymol.* **1994**, *243*, 475-500.

[65] Paull, B.; King, M., Quantitative capillary zone electrophoresis of inorganic anions. *Electrophoresis*. **2003**, *24*, 1892-1934.

[66] Padarauskas, A.; Paliulionyte, V.; Ragauskas, R.; Dikcius, A. Capillary electrophoretic determination of thiosulfate and its oxidation products. *J. Chromatogr. A.* **2000**, *879*, 235-243.

[67] Michaelis, L.; Electric transport of enzymes, malt distaste and pepsin. *Biochemische Zeitschrift*. **1909**, *17*, 231-234.

[68] Tiselius, A. A new apparatus for electrophoretic analysis of colloidal mixtures. *Trans. Faraday Soc.* **1932**, *33*, 524-531.

[69] Frost, N. W.; Jing, M.; Bowser, M. T. Capillary Electrophoresis. *Anal. Chem.* **2010**, *82*, 4682–4698.

[70] Jorgenson, J. W.; Lukacs, K. D. Zone electrophoresis in open-tubular glass capillaries. *Anal. Chem.* **1981**, *53*, 1298 – 1302.

[71] Huanga, X.; Wangb, Q.; Huangb, B. Preparation and evaluation of stable coating for capillary electrophoresis using coupled chitosan as coated modifier. *Talanta*, **2006**, *69*, 463–468.

[72] Koesdjojo, M. T.; Gonzalez, C. F.; Remcho, V.T. Principles and Practice of Capillary Electrochromatography. In *Handbook of Capillary and Microchip Electrophoresis and Associated Microtechniques* (3rd Edn.); Landers, J.P., Ed.; CRC Press, Taylor & Fracis Group, New York, 2008; 184-186.

[73] Wei Wang, Fang Zhou, Liang Zhao, Jian-Rong Zhang, Jun-Jie Zhu, Measurement of electroosmotic flow in capillary and microchip electrophoresis, *J. Chromatogr. A*, **1170**, 1-8.

[74] Melanson, J. E.; Baryla, N.E.; Lucy, C.A. Dynamic capillary coatings for electroosmotic flow control in capillary electrophoresis. *Trends Anal. Chem.* **2001,** *20*, 365-374.

[75] Pobozy, E.; Jarczynska, M.; Trojanowicz, M. Speciation of sulfur-containing anions by use of capillary electrophoresis. *Chromatographia.* **2002**, *56*, 723-728.

[76] Sullivan, J.; Douek, M. Analysis of hydroxide, inorganic sulphur species and organic anions in kraft pulping liquors by capillary electrophoresis. *J. Chromatogr. A*. **2004**, *1039*, 215–225.

[77] de Carvalho, L.M.; Schwedt, G. Sulfur speciation by capillary zone electrophoresis: Determination of dithionite and its decomposition products sulfite, sulfate and thiosulfate in commercial bleaching agents. *J. Chromatogr. A*. **2005**, *1099*, 185-190.

[78] Koji, O.; Shigeru, T. Micellar electrokinetic chromatography. *Mol. Biotechnol.* **1998**, *9*, 253-271.

[79] Benrraou, M.; Bales, B. L.; Zana, R. Effect of the nature of the counterion on the properties of anionic surfactants. 1. CMC, ionization degree at the CMC and aggregation number of micelles of sodium, cesium, tetramethylammonium, tetraethylammonium, tetrapropylammonium, and tetrabutylammonium dodecyl sulfates. *J. Phys. Chem. B.* **2003**, *107*, 13432-13440.

[80] Tedeschi, A. M.; Franco, L.; Ruzzi, M.; Paduano, L.; Corvaja, C.; D'Errico, G. Micellar aggregation of alkyltrimethylammonium bromide surfactants studied by electron paramagnetic resonance of an anionic nitroxide, *Phys. Chem. Chem. Phys*. **2003**, 5, 4204-4209.

[81] Aguiar, J.; Carpena, P.; Molina-Bolívar, J.A.; Ruiz, C.C. On the determination of the critical micelle concentration by the pyrene 1:3 ratio method. *J. Colloid Interface Sci.* **2003**, *258*, 116–122.

[82] Eduardo, D. P; Bernabé, L. R.; Iván, P.; Paola, G.; Valeska, F. Poly(sodium-10-undecylenate) as pseudo-stationary phase in the separation and quantification of polyaromatic hydrocarbons by micellar electrokinetic chromatography. *J. Chilean Chem. Soc*. **2010**, *55*, 31-34.

[83] Ravelo-Pérez, L. M.; Hernández-Borges, J.; Borges-Miquel, T. M.; Rodríguez-Delgado, M.A. *Electrophoresis*. **2007**. *28*, 4072 – 4081.

[84] Niu, J.; Qiu, H.; Li, J.; Liu, X.; Jiang, S. 1-Hexadecyl-3-methylimidazolium Ionic Liquid as a New Cationic Surfactant for Separation of Phenolic Compounds by MEKC. *Chromatographia*. **2009**, *69*, 1093 – 1096.

[85] Zhang, Yaohai and Jiao, Bining. Dispersive liquid-liquid microextraction combined with online preconcentration MEKC for the determination of some phenoxyacetic acids in drinking water. *J. Sep. Sci*. **2013**, *36*, 3067 – 3074.

[86] Van Biesen, G.; Bottaro, C. S. Ammonium perfluorooctanoate as a volatile surfactant for the analysis of N-methylcarbamates by MEKC-ESI-MS. *Electrophoresis*. **2006**, *27*, 4456-4468.

[87] Molina, M. Multi-residue analysis of N-methylcarbamate pesticides and their hydrolytic metabolites in environmental waters by use of solid-phase extraction and micellar electrokinetic chromatography. *Electrophoresis*. **1999**, *20*, 3439 – 3449.

[88] Carretero, A. S.; Cruces-Blanco, C.; Durán, S. P.; Gutiérrez, A. F. Determination of imidacloprid and its metabolite 6-chloronicotinic acid in greenhouse air by application of micellar electrokinetic capillary

chromatography with solid-phase extraction. *J. Chromatogr. A*. **2003,** *1003*, 189–195.

[89] Pereira, E. A.; Tavares, M. F. M; Cardoso. A. A. Alternative methodologies for the determination of aldehydes by capillary electrophoresis: environmental analysis using capillary electrophoresis and related techniques, including capillary electrochromatography. *J. AOAC Int*. **1999**, *82*, 1562-1570.

[90] Fornaro, A.; Gutz, I. G. R. Wet deposition and related atmospheric chemistry in the São Paulo metropolis, Brazil: Part 2—contribution of formic and acetic acids. *Atmos. Environ*. **2003**, *37*, 117-128.

[91] Diress, A. G.; Lucy, C. A. Study of the selectivity of inorganic anions in hydro-organic solvents using indirect capillary electrophoresis, *J. Chromatogr. A*. **2005**, *1085*, 155-163.

[92] Manz, A.; Graber, N.; Widmer, H. M. Miniaturized total chemical analysis systems: A novel concept for chemical sensing. *Sens. Actuators, B*: *Chemical*, **1990**, *1*, 244-248.

[93] Legendre, L. A.; Ferrance, J. P.; Landers, P. J. Microfluidic devices for electrophoretic separations: fabrication and use. In *Handbook of Capillary and Microchip Electrophoresis and Associated Microtechniques* (3rd Edn.); Landers, J. P., Ed.; CRC Press, Taylor & Francis Group, New York, 2008; 335-347.

[94] Kitagawa, F.; Otsuka, K. Recent progress in microchip electrophoresis–mass spectrometry. *J. Pharm. Biochem. Anal*. **2011**, *55*, 668–678.

[95] Masár, M.; Bomastyk, B.; Bodor, R.; Horčičiak, M.; Danč, L.; Troška, P.; Kuss, H. Determination of chloride, sulfate and nitrate in drinking water by microchip electrophoresis. *Microchim. Acta*. **2012**. *177*, 309–316.

[96] Bodor, R.; Madajová, V.; Kaniansky, D.; Masár, M.; Jöhnck, M.; Stanislawski, B. Isotachophoresis and isotachophoresis — zone electrophoresis separations of inorganic anions present in water samples on a planar chip with column-coupling separation channels and conductivity detection, *J. Chrom. A*. **2001**, *916*, 155-165.

[97] Liu, Y.; MacDonald, D. A.; Yu, X.; Hering, S. V.; Collett Jr. J. L.; Henry, C. S. Analysis of anions in ambient aerosols by microchip capillary electrophoresis. *Analyst*. **2006**, *131*, 1226–1231.

[98] Vrouwe, E. X.; Luttge, R.; Olthuis, W.; van den Berg, A. Rapid inorganic ion analysis using quantitative microchip capillary electrophoresis. *J. Chromatogr. A*. **2006**, *1102*, 287-293.

[99] Okada, T. Liquid-core waveguide in CE. *Electrophoresis*, **2007**, *28*, 3414–3419.

[100] Scalan, C.; Lapainis, T.; Sweedler, J.V. Light-based detection methods in capillary electrophoresis. In *Handbook of Capillary and Microchip Electrophoresis and Associated Microtechniques* (3rd Edn.); Landers, J.P., Ed.; CRC Press, Taylor & Francis Group, New York, 2008; 305 – 312.

[101] Heiger, D.; Weinberger, R.; Agilent application note [Online]. https://www.chem.agilent.com/Library/applications/59631138.pdf (accessed December 2, 2013).

[102] Gaš, B.; Kenndler, E. System zones in capillary zone electrophoresis. *Electrophoresis.* **2004**, *25*, 3901–3912.

[103] Erny, G. L.; Esteves, V. I. Robustness of the co-ion transfer ratio in capillary electrophoresis. *J. Sep. Sci.* **2009**, *32*, 3007 – 3012.

[104] Jankovskiene, G.; Daunoravicius, Z.; Padarauskas, A. Capillary electrophoretic determination of sulfite using the zone-passing technique of in-capillary derivatization. *J. Chromatogr. A.* **2001**, *934*, 67-73.

[105] Daunoravicius, Z.; Padarauskas, A. Capillary electrophoretic determination of thiosulfate, sulfide and sulfite using in-capillary derivatization with iodine. *Electrophoresis.* **2002**, *23*, 2439–2444.

[106] Yu, H.; Xu, X.; Sun, J.; You, T.; Recent progress for capillary electrophoresis with electrochemical detection. *Cent. Eur. J. Chem*. **2012**, *10*, 639-651.

[107] Tonin, F. G.; Tavares, M. F. M. Separation strategies for environmental analysis. In *Handbook of Capillary and Microchip Electrophoresis and Associated Microtechniques* (3rd Edn.); Landers, J.P., Ed.; CRC Press, Taylor & Francis Group, New York, 2008; 913 – 962.

[108] Elbashira, A. A.; Aboul-Eneinb, H. Y. Recent advances in applications of capillary electrophoresis with capacitively coupled contactless conductivity detection (CE-C4D): an update. *Biomed. Chromatogr*. **2012,** *26*, 990–1000.

[109] See, H. H.; Hauser, P. C.; Sanagi, M. M.; Ibrahim, W. A. W. Dynamic supported liquid membrane tip extraction of glyphosate and aminomethylphosphonic acid followed by capillary electrophoresis with contactless conductivity detection. *J. Chromatogr. A* **2010**, *1217*, 5832–5838.

[110] Lopes, F. S.; Junior, O. A.; Gutz, I. G. R. Fully electrochemical hyphenated flow system for preconcentration, cleanup, stripping, capillary electrophoresis with stacking and contactless conductivity detection of trace heavy metals. *Electrochem. Commun.* **2010**, *12*, 1387–1390.

[111] Kubáň, P.; Seiman, A.; Kaljurand, M. Improving precision of manual hydrodynamic injection in capillary electrophoresis with contactless conductivity detection. *J. Chromatogr.* A. **2011,** *1218*, 1273–1280.

[112] Kubáň, P.; Seiman, A. Makarõtševa, N.; Vaher, M.; Kaljurand, M. In situ determination of nerve agents in various matrices by portable capillary electropherograph with contactless conductivity detection. *J. Chromatogr. A.* **2011,** *1218*, 2618–2625.

[113] Lau, H. F.; Quek, N. M.; Law, W. S.; Zhao, J. H.; Hauser, P. C.; Li, S. F. Optimization of separation of heavy metals by capillary electrophoresis with contactless conductivity detection. *Electrophoresis*, **2011**, *32*, 1190–1194.

[114] Warnke, M. M.; Breitbach, Z. S.; Dodbiba, E.; Crank, J. A.; Payagala, T.; Sharma, P.; Wanigasekara, E.; Zhang, X.; Armstrong, D.W. Positive mode electrospray ionization mass spectrometry of bisphosphonates using dicationic and tricationic ion-pairing agents. *Anal. Chimica. Acta*. **2009**, *633*, 232–237.

[115] Magnuson, M. M.; Urbansky, E. T.; Kelty, C. A. Determination of Perchlorate at Trace Levels in Drinking Water by Ion-Pair Extraction with Electrospray Ionization Mass Spectrometry. *Anal. Chem*. **2000**, *72*, 25-29.

[116] Breitbach, Z. S.; Warnke, M. M.; Wanigasekara, E.; Zhang, X.; Armstrong, D. W. Evaluation of Flexible Linear Tricationic Salts as Gas-Phase Ion-Pairing Reagents for the Detection of Divalent Anions in Positive Mode ESI-MS. *Anal. Chem*. **2008**, *80*, 8828–8834.

[117] Warnke, M. M.; Breitbach, Z. S.; Dodbiba, E.; Wanigasekara, E.; Zhang, X.; Sharma, P.; Armstrong, D. W. The Evaluation and Comparison of Trigonal and Linear Tricationic Ion-Pairing Reagents for the Detection of Anions in Positive Mode ESI-MS. *J. Am. Soc. Mass. Spectrom*. **2009**, *20*, 529 –538.

[118] Gerardi, A. R.; Lin, X., Breitbach, Z. S.; Armstrong, D. W.; Colyer, C.L. CE-ESI-MS separation of divalent organic and inorganic anions using a tricationic complexing reagent. *Electrophoresis*, **2012**, *33*, 734–740.

Chapter 2

Systematic Optimization of a Pyromellitic Acid Background Electrolyte for Capillary Zone Electrophoresis with Indirect UV-Vis Detection and Online Pre-concentration Analysis of Thiosalt Anions in the Treated Mine Tailings

2.1 Introduction

Thiosalts are sulfur oxyanions formed during the incomplete oxidation of sulfur-rich minerals. Most thiosalt species are produced during the milling and flotation of these sulfidic ores, particularly those containing pyrite (FeS_2) and pyrrhotite ($Fe_{(1-x)}S$, x = 0 to 0.2).[1] The major thiosalt species are sulfate (SO_4^{2-}), thiosulfate ($S_2O_3^{2-}$), trithionate ($S_3O_6^{2-}$), tetrathionate ($S_4O_6^{2-}$) and higher polythionates such as pentathionate ($S_5O_6^{2-}$). Thiosalts can be oxidized to sulfate, along with concomitant production of acid, which can lead to acidification of receiving waters.[2] Although thiosalts have been shown to be relatively non-toxic, acidification can cause stress to freshwater flora and fauna, which in some instances can be severe enough to lead to death of vulnerable organisms. Acidification can also result in enhanced metal migration and toxic metal concentrations.[1,2]

Although not currently regulated, thiosalts represent a significant challenge to both the mining and metals processing industries, particularly with respect to effective mitigation and treatment.[3] Analysis of thiosalts in milling process waters and tailings ponds is necessary for effective treatment and the data are also needed to develop a better understanding of how thiosalts are generated, which in turn influences the treatment protocols. Despite extensive research in the area since the 1980s, there are still many unknowns, specifically questions related to reaction kinetics and thermodynamics of thiosalt transformations, which are complex and interrelated.[4] To study thiosalt reaction kinetics, which can show significant changes on a time-scale of minutes, improved

methods of analysis are required.[3,4] Ion chromatography (IC) coupled with various detection techniques has been used generally for their determination and quantitation.[5] IC is a well-established technique with numerous well-developed methods for the determination of inorganic anions with good measures of reliability and sensitivity.[5-10] However, consumables can be costly, separations have only moderate resolution and analyses tend to be time consuming. IC can also be intolerant of some sample matrices, such as those with high ionic strength. Capillary zone electrophoresis (CZE) has inherent advantages such as fast analysis, tolerance for a range of sample matrices, potential for high-throughput analysis, low consumption of reagents and simple instrumentation making it an attractive complement to IC. [6-11]

A substantial amount of analytical work[5, 13-18] has been done in the area of quantitation of sulfur anions in water, air and soil samples. Table 2.1 summarizes some of the methods published for sulfur anions by CZE with indirect UV-vis detection. As exemplified in the table, the most common chromophoric probes for the analysis of sulfur oxyanion species in CZE include pyromellitic acid (PMA) and sodium chromate (Na_2CrO_4); EOF modifiers include hexadecyltrimethylammonium bromide (CTAB), tetradecyltrimethyl-ammonium hydroxide (TTAOH) and diethylenetriamine (DETA). From these applications, it can be concluded that the most important factors influencing separation efficiency of CZE with indirect detection are concentrations of chromophoric probe and electroosmotic flow (EOF) modifier, use of organic modifiers, pH, capillary temperature, and applied electric field.

Table 2.1. Selected indirect CZE applications for the analysis of inorganic sulfur anions

BGE system	BGE additives	Sulfur species analysed	LOD range (μg/mL)	Reference
1.5 mM PMA + 10 mM Tris; pH = 8.0, λ = 214 nm	0.5 mM CTAB	$S_2O_3^{2-}$, $S_2O_3^{2-}$, SCN^-, SO_3^{2-}	0.17 - 0.50	[7]
5 mM Na_2CrO_4, pH = 9.4, λ = 374 nm	4 mM TTAOH, 10 mM 2-cyclo-hexylamino-ethanesulfonic acid (CHES) (anti-coagulant)	SO_4^{2-}, SO_3^{2-}, $S_2O_3^{2-}$, $S_2O_4^{2-}$	0.45 - 0.48	[14]
2.25 mM PMA + 6.5 mM NaOH + 1.6 mM TEA; pH = 10, λ = 254 nm	0.75 mM HMOH	S^{2-}, SO_4^{2-}, SO_3^{2-}, SCN^-, $S_2O_3^{2-}$, $S_2O_6^{2-}$, $S_2O_8^{2-}$	0.35 - 0.35,	[18]
10 mM Na_2CrO_4, pH = 11, λ = 275 nm	2 mM TTAOH	S^{2-}, SO_4^{2-}, SO_3^{2-}, $S_2O_3^{2-}$	N/R	[19]
1.5 mM PMA + 10 mM Tris; pH = 7.0, λ = 214 nm	0.5 mM DETA, 0.1% formaldehyde (stabilizer)	SO_4^{2-}, SO_3^{2-}, $S_2O_3^{2-}$, $S_2O_4^{2-}$	0.45 - 1.0	[20]

N/R – not reported

In addition to optimizing instrument and BGE parameters, there have been several reports on improving the detection sensitivity of CZE using on-line pre-concentration sample stacking techniques such as field-amplified sample stacking,[19,20] large volume sample stacking[21,22] and pH-mediated sample stacking.[23,24] These techniques work on the principle of introducing a plug of the sample at low ionic strength relative to the BGE into a BGE-filled capillary and applying a high potential. The high electric field

experienced by the analytes in the sample plug causes them to move rapidly until they reach the BGE interface at which point the analytes slow down and 'stack' leading to a concentrated zone of analytes and increased sensitivity.

In this work, we report the systematic development of a CZE with indirect UV-vis method with PMA as the chromophoric probe and three EOF modifiers: tetramethylammonium hydroxide (TMAOH), CTAB and hexamethonium hydroxide (HMOH). The BGE was further optimized by varying the most important factors (concentration of chromophoric probe and EOF modifier, pH and applied field voltage) for the fast separation (under 3 min) of five key thiosalt species (sulfate (SO_4^{2-}), thiosulfate ($S_2O_3^{2-}$), trithionate ($S_3O_6^{2-}$), tetrathionate ($S_4O_6^{2-}$) and pentathionate ($S_5O_6^{2-}$)), which have not been analysed together by CZE previously. The optimized BGE was compared with a costly commercially available PMA BGE solution and it was found to provide much better sensitivity and complete separation of the five species, which could not be resolved using the commercial PMA BGE solution. Finally, the field amplified sample stacking (FASS) technique for online sample pre-concentration was used, resulting in an improvement in the sensitivity and detection limits (S/N = 3) by at least 3-fold. The optimized method was applied for the analysis of treated tailings pond samples.

2.2. Experimental

2.2.1 Chemicals

All chemicals used for this work were of analytical grade unless otherwise noted. PMA, HMOH (0.1 M), TMAOH (25% v/v in H_2O, trace select), CTAB (> 99%) and buffer solution HPCE pH 7.7 (commercial PMA BGE) were all purchased from Sigma (Sigma-Aldrich, MO, USA). The pH of the BGE was adjusted to 7.0, 8.0.and 9.0 with triethanolamine (TEA; Sigma, MO, USA). CE grade sodium hydroxide solution (1 M) was purchased from Agilent (Agilent Technologies Canada Inc., Mississauga, Ontario). Stock solutions of sulfur oxyanions were prepared daily from sodium thiosulfate ($Na_2S_2O_3$, > 99.9% purity, Sigma), sodium tetrathionate ($Na_2S_4O_6$, > 99.9% purity, Sigma), sodium trithionate ($Na_2S_3O_6$), and potassium pentathionate ($K_2S_5O_6$). Sodium trithionate ($Na_2S_3O_6$), and potassium pentathionate ($K_2S_5O_6$) were synthesized and purified using modified known methods.[25] The description of the synthesis and characterization of the single crystals used in this work have been published elsewhere.[26] Nanopure water from Barnstead Nanopure II (Barnstead Nanopure, CA, USA) with ionic purity of 18.2 MΩ·cm was used for this work. All solutions were degassed and filtered with a 0.22 µm nylon syringe filter (Canadian Life Science, ON).

2.2.2 Instrumentation

All CE analyses were performed on an Agilent 7100 ^{3D}CE System (Agilent Technologies Canada Inc., Mississauga, ON) equipped with a diode array UV-vis detector. Data were acquired at 350.10 nm with references at 191 nm, 200 nm, 214 nm and 254 nm (to invert

the negative peaks) and processed using Agilent OpenLAB Chromatography Data System (CDS) ChemStation Edition for corrected peak areas, peak widths and heights, and migration times. Bare fused-silica capillaries (internal diameter, 50 μm id) were obtained from MicroSolv Technology Corporation (NJ, USA) and were accurately cut to the desired length (48.5 cm). A 'window' was made 8.5 cm from detector by removal of the polyimide coating using the MicroSolv Window Maker™; approximately 2 mm of polyimide at the beginning and at the end of the capillaries was similarly removed. Initial conditioning was as follows: flushing at ~ 940 mbar with 1.0 M NaOH for 1 hr, water for 1 hr and BGE for another 1 hr. The capillary was conditioned daily with 0.1 M NaOH for 10 min, water for 10 min and BGE for another 10 min. Between injections, the capillary was flushed with 0.1 M NaOH for 1 min, water for 1 min and BGE for 3 min. Except stated otherwise, samples were injected hydrodynamically at 50 mbar for 10 s, and negative potential of between -20 kV and -30 kV was applied for the separation with indirect detection at the wavelengths specified above. The temperature of the capillary was maintained at 25 $^{\circ}$C for the separation. UV-vis analyses of the thiosalt species to determine their maximum absorption wavelengths (λ_{max}) and molar extinction coefficients were performed on a Varian Cary 6000i UV-Vis-NIR spectrophotometer (Varian Inc., Palo Alto) with 1 cm quartz cuvettes (International Crystal Laboratories, NJ, USA).

2.2.3 Overview of factors studied

Table 2.2 shows the factors and the levels at which they were studied. Each factor was optimized in a univariate approach (one factor at a time). The rationale for choosing the selected ranges is based on previous experiments on thiosalt standards and analysis reported in literature. Values at lower and higher levels than reported are included to ensure that the optimum levels could be determined from this experiment without unnecessary constraints.

Table 2.2. Factors influencing separation and levels studied

Factor	Levels
[PMA] (mM)	1.00 – 1.50 – 2.00 – 2.50 – 3.00 (5 levels)
[TMAOH] (mM)	0.20 – 0.40 – 0.60 – 0.80 – 1.00 (5 levels)
[CTAB] (mM)	0.20 – 0.40 – 0.60 – 0.80 – 1.00 (5 levels)
[HM^{2+}] (mM)	0.20 – 0.40 – 0.60 – 0.80 – 1.00 (5 levels)
pH	7 – 8 – 9 (3 levels)
Applied potential (kV)	20 – 25 – 30 (3 levels)

2.3. Results and discussions

2.3.1 UV-vis analysis of thiosalts

UV-vis spectra were acquired for all the thiosalt species and BGE chromophoric probes to determine their molar absorptivities at the wavelengths of maximum absorbance (λ_{max})

to guide the choice of chromophoric probes for use for the experimental design. For the most sensitive results, analytes should not absorb at the λ_{max} of the probe. Figure 2.1 shows the UV absorption spectra of the thiosalt species.

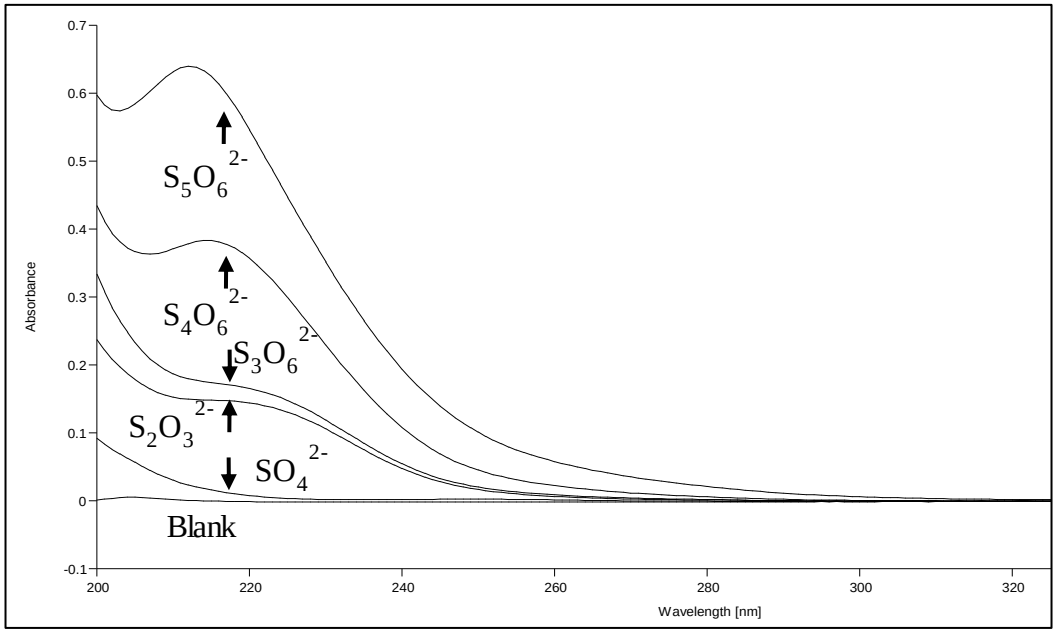

Figure 2.1: UV-vis absorption spectra of five thiosalt species (concentration of 200 µg/mL each in water).

2.3.2 Influence of EOF modifier concentration

EOF modifiers are usually cationic surfactants that adsorb onto the surface of bare-fused silica due to strong electrostatic attraction between the negatively charged wall ($Si\text{-}O^-$)

and the positively charged group of the modifier. This imparts a positive charge to the surface of the wall and greatly suppresses or reverses the EOF. In this work three EOF modifiers (Figure 2.2) were used: TMAOH, CTAB and HMOH. With a constant concentration of the PMA probe of 3.00 mM, [TMAOH], [CTAB] and [HMOH] were varied from 0.2 mM to 1.0 mM to test the ability to enhance the separation speed of the analysis. Since the electrophoretic mobilities of the sulfur anions are counter-EOF, suppressing or reversing the EOF will lead to rapid separation or resolution of the analytes.

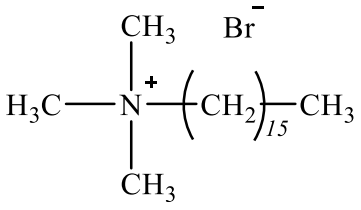

Hexadecyltrimethylammonium bromide (CTAB)

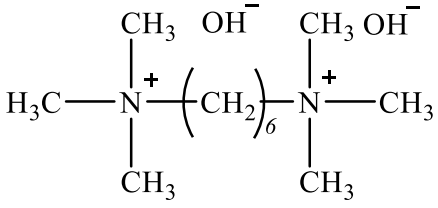

Hexamethonium hydroxide (HMOH)

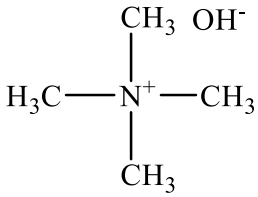

Tetramethylammonium hydroxide (TMAOH)

Figure 2.2. EOF modifiers used in this work

As expected, the addition of all the EOF modifiers reduced the EOF, which led to higher effective electrophoretic mobilities of all the thiosalt species and faster migration towards the detector. Figure 2.3 shows the effective mobilities of the thiosalt species with respect to the concentration of the EOF modifiers. However, increases in [TMAOH] and [CTAB] even at low concentrations led to other undesirable separation issues. As [TMAOH] was increased from 0.20 mM to 1.00 mM, total analysis time decreased from 10.7 min to 4.2 min, however under these conditions SO_4^{2-} and $S_3O_6^{2-}$ were not resolvable. It was found that it was not possible to find a combination of conditions that would give short analysis time and satisfactory resolution using TMAOH, thus it was not used further. CTAB was also evaluated for its effectiveness and influence on the EOF modifier in many studies. For instance, Chen *et al.*[7] used CTAB with PMA in a TRIS buffer to separate $S_2O_3^{2-}$, $S_2O_3^{2-}$, SCN^- and SO_3^{2-} leading to reduced analysis time. For this work, increasing the concentration of CTAB led to a reduction of analysis time. However there was co-migration of SO_4^{2-} and $S_3O_3^{2-}$ as well as broadening of the tetrathionate peak even at low concentrations (0.20 mM). Increasing the concentration further led to co-elution of the SO_4^{2-} and $S_3O_6^{2-}$ peaks. HMOH was much more effective for regulating the EOF in the analysis of the thiosalt species than the other EOF modifiers, leading to good peak resolution, shorter analysis as well as much better peak symmetry for all the thiosalt species analyzed. Thus HMOH was used for further optimization of the BGE for the analysis. The optimum concentration of HMOH was found to be 0.80 mM giving complete separation in 4.4 min; above this concentration $S_2O_3^{2-}$ and $S_5O_6^{2-}$ start to co-

migrate and the $S_4O_6^{2-}$ peak begins to broaden. Thus [HMOH] = 0.80 mM was used for further optimization.

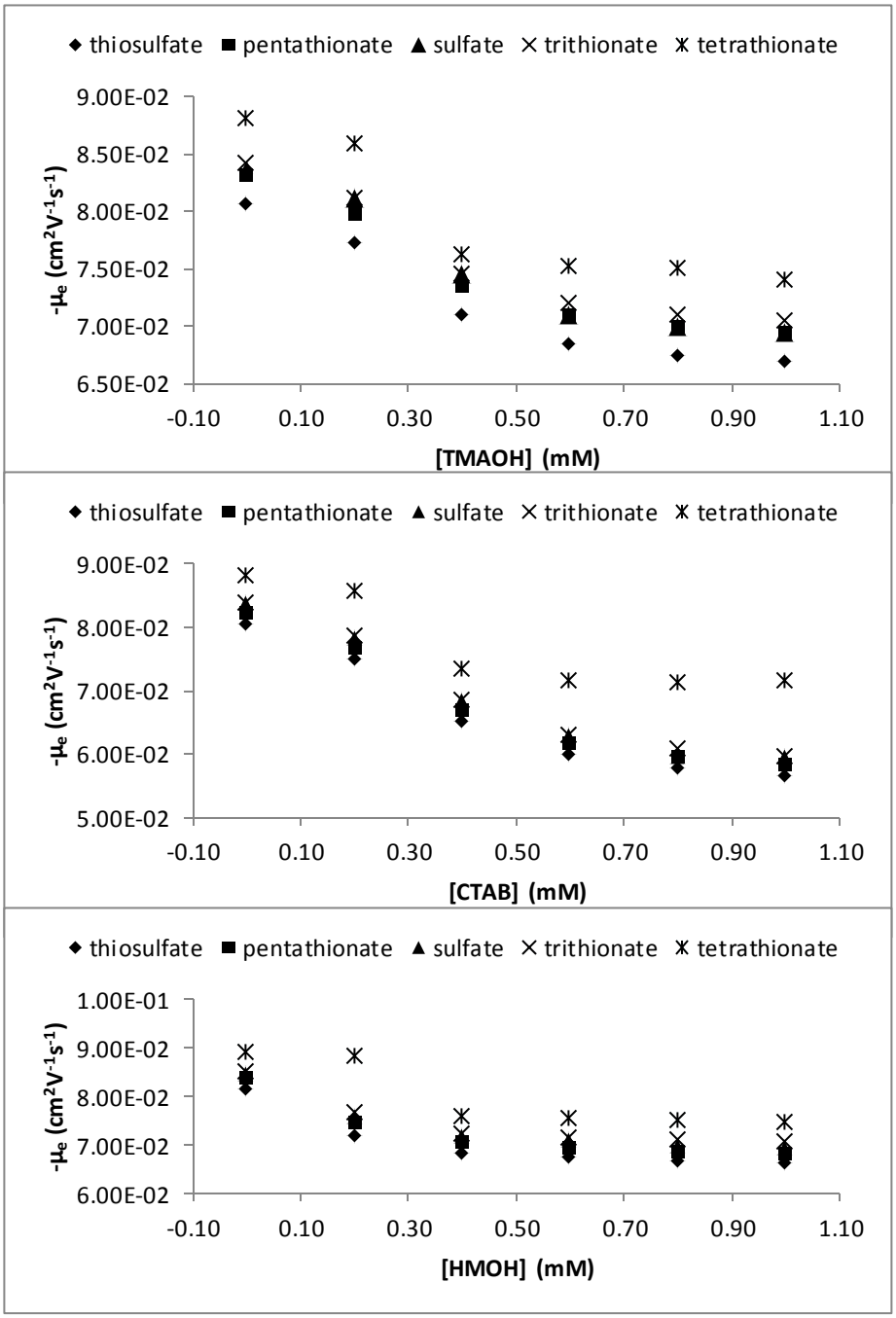

Figure 2.3. Effect of increasing [TMAOH], [CTAB] and [HMOH] on the effective electrophoretic mobilities of thiosalt species

2.3.3 Influence of PMA chromophoric probe concentration

PMA was chosen for this work because of its high molar absorptivity and close mobility match with those of the sulfur oxy-anions leading to improved sensitivity and reduced electromigration dispersion. It has no oxidizing properties or reactivity with thiosalt anions and has a high molar extinction coefficient at the chosen wavelength for this work.[7,18,19]

With the optimal concentration of HMOH at 0.80 mM, the concentration of the PMA was varied from 1.00 mM to 3.00 mM with 5 concentrations in total. With PMA at 1.00 mM, the peak symmetry and sensitivity (with respect to peak height, width and area) were very poor for all the thiosalt species; at 2.00 mM PMA gave higher sensitivity and good peak symmetry with faster migration (last peak at 4.3 min) than at all the other concentrations. Further increase in the concentration of PMA beyond 3.00 mM led to a slight increase in signal sensitivity, but poor peak symmetry (tailing and fronting), indicating that there may be some interaction of the BGE probe with the anions.

2.3.4 Influence of pH and applied field on the electrophoretic mobilities of thiosalts

The use of the EOF modifier should in principle either slow down or reverse the EOF and therefore lead to higher migration of the thiosalt anions towards the detector. An increase in pH will lead to an increase in the ionization of the silanol group on the surface of the capillary. The increase in positive charge on the surface of the capillary by the addition of cationic EOF modifiers such as HMOH will therefore increase with increasing pH until all the available silanol groups are ionized. With the BGE at pH 7, [PMA] = 2.00 mM and [HMOH] = 0.80 mM, the migration times of the thiosalt species ranged from 3.8 min to 5.7 min. At pH 8 migration times decreased to between 3.1 and 4.3 min, and at pH 9 between 3.4 and 4.9 min. At pH 9, migration times were slightly longer than at pH 8, and $S_2O_3^{2-}$ and $S_5O_6^{2-}$ co-migrated. With the optimum BGE composition of [PMA] = 2.00 mM, [HMOH] = 0.80 mM and BGE pH of 8, the applied separation field was varied from -20 kV to -30 kV. As expected, with increased potential the time for separation was reduced from 4.2 min (-20 kV) to 2.8 min (-30 kV).

2.3.5 Optimization of sensitivity

Detection wavelengths for most capillary electrophoretic analysis with indirect detection of sulfur anions have been performed at $\lambda = 254$ nm. The UV-vis diode array detector (DAD) allows for monitoring at different wavelengths, which allows for selection of wavelengths that give the most sensitivity. Wavelengths selected were 191 nm, 214 nm, 200 nm and 254 nm. Although most of these are not at the λ_{max} for the PMA chromophoric probe (214 nm), the absorbance of the UV-active thiosalts influence the

sensitivity (usually decreasing sensitivity for indirect mode). The most sensitive results for sulfate, which has low absorptivity (Figure 2.1), should be seen at 214 nm. However, for the more UV-active species, 200 nm on average gave the best sensitivity and was therefore used for further analysis. To invert the negative peaks, measurements were taken at 350 nm and 200 nm was used as the reference wavelength; since the decrease in absorbance at 200 nm will be greater than that at 350 nm, this will register as a positive peak. The optimized buffer system was determined to be 2.00 mM PMA, 0.80 mM HM^{2+}, with pH adjusted to 8.0 with triethanolamine. All five sulfur oxyanion species under investigation were successfully separated (Figure 4) under these conditions in less than 3 min. To the best of our knowledge, this is the fastest CZE method with indirect UV-vis analysis reported to date for all these species.

2.3.6 Linearity of method, sensitivity and LOD determination

Calibration curves were constructed for all thiosalt species at six concentrations (including a blank). Each standard sample was injected in triplicate and the standard deviation of the peak areas and migration times determined. Very good linearity with R^2 > 0.99 was obtained from the calibration curves for all the thiosalt species (Figure 2.4). LOD values were obtained at S/N ratios of 3 by sequential dilution of thiosalt mixtures until S/N value of the peak of interest reach 3. Table 2.3 shows the relative standard deviations (RSD) of the migration times and peak areas, linearity of standard calibration curves and LOD values for each of the thiosalt anions.

Field-amplified sample stacking (FASS) was applied to increase the sensitivity of the method and to achieve low LOD values. In this work, FASS was applied by injecting a small plug of water (1 – 5 s at 30 mbar) into a BGE-filled capillary, injecting the sample plug (5 s at 50 mbar) and applying high negative potential. LOD values for stacking and normal CZE are shown in Table 2.3 leading to a nearly 4-fold increase over normal hydrodynamic injection for some of the thiosalts (see Figure A9 in Appendix A). No further increase in sensitivity was observed after 3 s injection time of water plug before the sample. Larger volumes of water (more than 5 s at 30 mbar) led to decrease in sensitivity probably due to sample dilution.

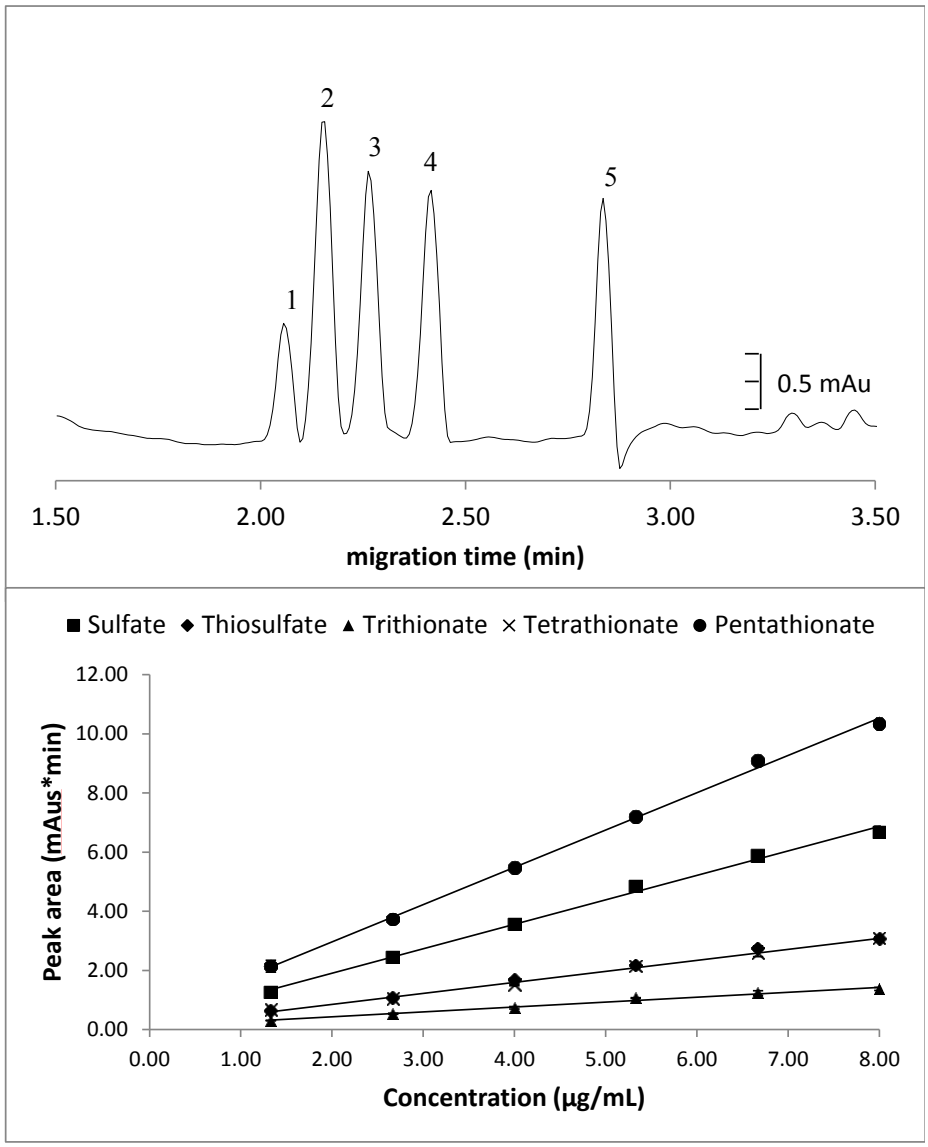

Figure 2.4: Electropherogram and standard calibration lines (error bars are standard deviation) obtained from thiosalt standards. 1. $S_2O_3^{2-}$ (40 µg/mL), 2. $S_5O_6^{2-}$ (40 µg/mL), 3. SO_4^{2-} (20 µg/mL), 4. $S_3O_6^{2-}$ (50 µg/mL), $S_4O_6^{2-}$ (50 µg/mL). CZE conditions: injection: 250 mbar·s, applied field: -30 kV, temperature: 25 °C, indirect UV detection at λ = 350 nm, Ref 200 nm. BGE 2.00 mM PMA, 0.80 mM HM^{2+}, pH adjusted to 8 with TEA

Table 2.3. Peak area and migration time repeatability, linearity of standard calibration and LOD values of thiosalt anion analysis

Thiosalt anion	Conc. (μg/mL)	RSD peak area (%) (n = 3)	RSD migration time (%) (n = 3)	coefficient of regression (R^2)	LOD without stacking (n = 3) (μg/mL)	LOD with stacking (n = 3) (μg/mL)	LOQ (μg/mL)
SO_4^{2-}	1	0.50	0.06	0.9953	0.09	0.02	0.07
	5	0.51	0.14				
	10	0.58	0.06				
	15	0.87	0.04				
	20	0.53	0.14				
$S_2O_3^{2-}$	1	2.95	0.08	0.9998	0.16	0.12	0.40
	5	2.70	0.10				
	10	1.55	0.06				
	15	0.53	0.02				
	20	1.28	0.17				
$S_3O_6^{2-}$	1	0.85	0.09	0.9454	0.34	0.11	0.37
	5	1.46	0.14				
	10	3.93	0.12				
	15	2.42	0.12				
	20	3.31	0.05				
$S_4O_6^{2-}$	1	1.40	0.02	0.9940	0.32	0.14	0.47
	5	3.77	0.14				
	10	2.85	0.06				
	15	1.74	1.68				
	20	0.39	0.03				
$S_5O_6^{2-}$	1	0.47	0.70	0.9952	0.10	0.04	0.13
	5	0.54	0.10				
	10	0.54	0.06				
	15	0.92	0.04				
	20	0.53	0.13				

2.3.7 Comparison to commercially available PMA BGE for inorganic anions

PMA BGE is commercially available for the analysis of inorganic anions. The developed PMA BGE for this application was compared to the commercial electrolyte and found to be more sensitive (greater peak areas in optimized PMA BGE) with better separation efficiency (Figure 2.5) under all injection and applied field conditions.

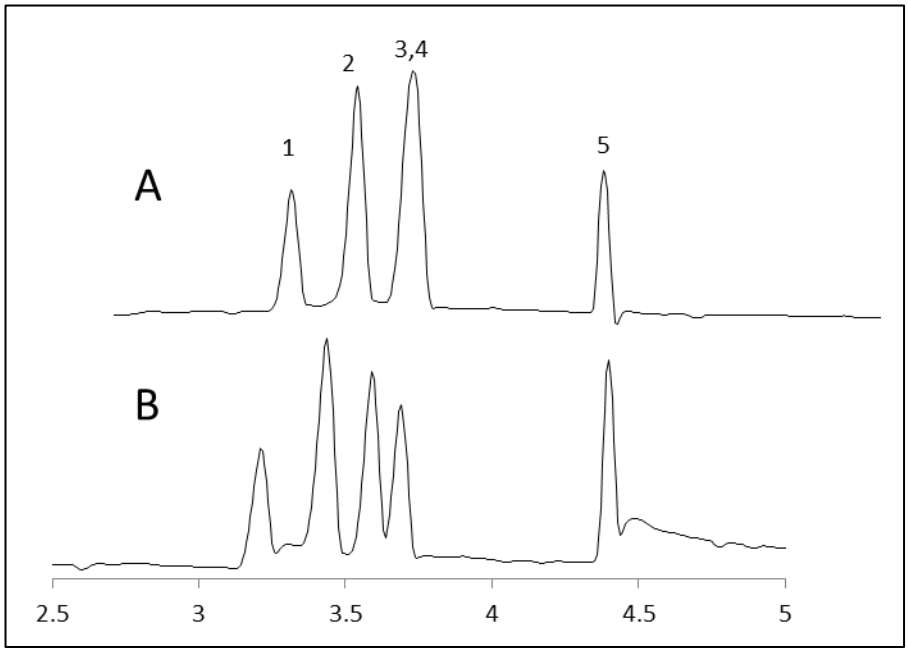

Figure 2.5. Electropherogram showing separation efficiency of five thiosalt species using commercially available PMA BGE (A) with the optimized PMA BGE (B). 1. $S_2O_3^{2-}$ (40 µg/mL), 2. $S_5O_6^{2-}$ (27 µg/mL), 3. SO_4^{2-} (20 µg/mL), 4. $S_3O_6^{2-}$ (50 µg/mL), 5. $S_4O_6^{2-}$ (50 µg/mL). Separation conditions: hydrodynamic injection, 300 mbar·s; applied field: -20 kV

2.3.8 Application of method to thiosalt standard mixture and tailings pond samples

The final BGE composition and instrument parameters were applied to the analysis of thiosalt standards and samples taken from a thiosalt tailings pond. The method was rapid

with analysis time of less than 3 min, sensitive, gave good resolution of all peaks and proved reliable for the thiosalt species analyzed. Optimal detection was achieved at 350 nm with reference wavelength at 200 nm, with good peak intensity, reproducibility and linearity for all the anions under consideration over the concentration range of 1 µg/mL to 20 µg/mL. Electropherograms of diluted spiked tailings pond water (1:100 with nano-pure water) and diluted spiked tailings pond water along with the standard addition plots of the five thiosalts are presented in Figure 2.6. Based on this dilution, the total method detection limits would be 10 and 30 µg/mL for the highly complex tailings waters. It should be noted that typical thiosalt concentrations are well above 50 µg/mL, and at this concentration are considered of low toxicity to fish so these detection limits are adequate.[2,4] By sacrificing short analysis times sought for this work, it is possible to analyze pond samples with little or no dilution and still accommodate the relatively high concentrations of sulfate and thiosulfate. For less complex samples, as measured in kinetic and thermodynamic studies, dilution is not necessary and the high method sensitivity is maintained. To prepare the samples for standard addition, 100 µL of the 1:100 diluted sample was spiked with 0, 100, 200, 300, 400 and 500 µL of the thiosalt standard mix (0.33 µg/mL sulfate, 0.45 µg/mL thiosulfate and 0.88 µg/mL each trithionate, tetrathionate and pentathionate), made up to 600 µL, mixed with a vortex and analyzed. Three samples were prepared for each standard addition point to determine the standard deviations associated with each measurement. Table 2.4 shows the results of the standard addition analysis. The main thiosalts present detected in the sample taken from

the tailings pond were sulfate (SO_4^{2-}) and thiosulfate ($S_2O_3^{2-}$) with concentrations about 300 µg/mL for SO_4^{2-} and 700 µg/mL for $S_2O_3^{2-}$.

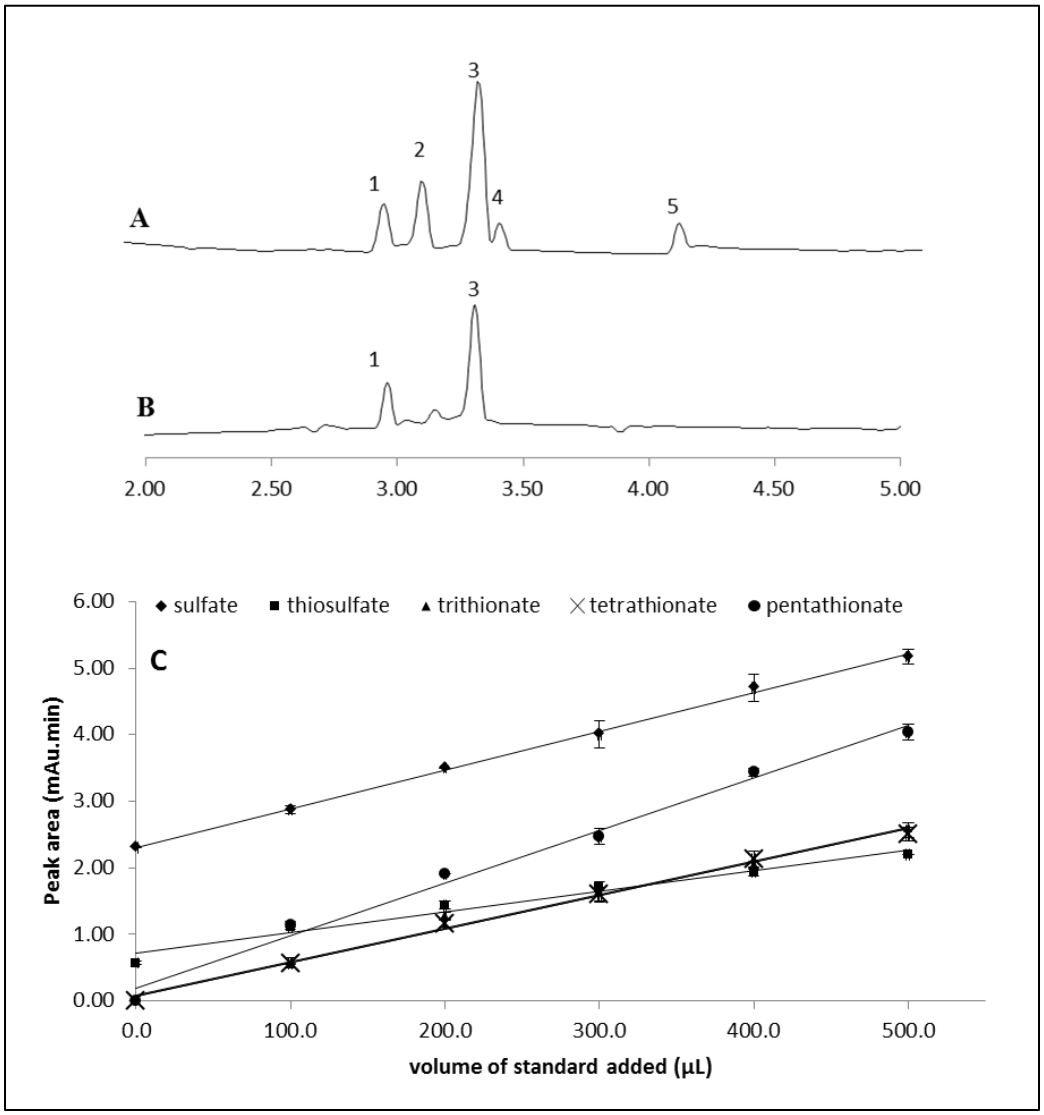

Figure 2.6: Electropherograms of A. Real sample spiked with 6 µg/mL each of the 5 thiosalt species (1. $S_2O_3^{2-}$, 2. $S_5O_6^{2-}$, 3. SO_4^{2-}, 4. $S_3O_6^{2-}$, 5. $S_4O_6^{2-}$); B. Real thiosalt tailings sample diluted 1:100. C. Standard addition calibration curves of thiosalts (Error bars are standard deviation). CE conditions: injection: 250 mbar.s, applied field: -20 kV, temperature 25 °C, BGE: 2.00 mM PMA, 0.80 mM HM^{2+}, pH adjusted to 8.0 with TEA and indirect UV detection at λ = 350 nm, Ref. 200 nm

Table 2.4. Standard addition result of thiosalt sample spiked with 0.05, 0.10 and 0.15 mL of 100 μg/mL standards (n=3)

Thiosalt anion	Average migration time (min)	Concentration found (μg/mL±SD)
SO_4^{2-}	2.39	324.3 ± 31.1
$S_2O_3^{2-}$	2.14	709.0 ± 74.1
$S_3O_6^{2-}$	2.47	43.5 ± 19.6
$S_4O_6^{2-}$	2.92	9.4 ± 7.8
$S_5O_6^{2-}$	2.30	6.1 ± 5.5

The high standard deviation values for the higher order polythionates was probably due to their very low concentrations or absence from the tailings sample.

2.4. Conclusions and future work

A fast CE method with indirect UV-vis detection was developed for the separation of five important thiosalt anions: sulfate (SO_4^{2-}), thiosulfate ($S_2O_3^{2-}$), trithionate ($S_3O_6^{2-}$), tetrathionate ($S_4O_6^{2-}$) and pentathionate ($S_5O_6^{2-}$). The optimized BGE consisted of 2.00 mM PMA, 0.80 mM HM^{2+}, pH adjusted to 8.0 with triethanolamine and indirect UV detection at λ = 200 nm. The method was rapid, sensitive, selective and reliable with complete separation of the thiosalt species under 3 min. LOD values (from 0.1 μg/mL to 0.34 μg/mL) were improved by about 4 fold (to 0.02 to 0.12 μg/mL) with the use of field-amplified sample stacking (FASS), first injection of a plug of water for 3 s at 30 mbar followed by sample injection for 5 s at 50 mbar. Results from the experiments showed

that HM as EOF modifier was superior to CTAB and TMAOH for thiosalt analysis. The optimized method was successfully applied to the quantitative analysis of thiosalt species in tailings pond samples with challenges posed by the complexity of the tailings matrix accommodated.

.

2.5. References

[1] Hißner F., Mattusch J., Heinig K., Determination of sulfur-containing inorganic anions by dual ion chromatography and capillary electrophoresis – application to the characterization of bacteria sulfur degradation. *Fresenius J. Anal. Chem*. **1999**, *365*, 647-653.

[2] Kuyucak N., Yaschyshyn D., Managing Thiosalts In Mill Effluents, "Studies Conducted at the Kidd Metallurgical"; Paper Presented at the Mining and the Environment IV Conference, Sudbury, Ontario, Canada, October 19-27, 2007.

[3] Silver M., Dinardo O., Factors Affecting Oxidation of Thiosalts by *Thiobacilli*, *Appl. Environ. Microbiol.* **1981**, *41*, 1301-1309.

[4] Wasserlauf M., Dutrizac J. E., The chemistry, generation and treatment of thiosalts in milling effluents – A non-critical summary of CANMET investigations 1976-1982, CANMET Report 82-4E, 1982.

[5] Haddad, P. R., Comparison of ion chromatography and capillary electrophoresis for the determination of inorganic ions. *J. Chromatogr. A*. **1997**, *770*, 281-290.

[6] Hissner, F.; Mattusch, J.; Heinig, K., Quantitative determination of sulfur-containing anions in complex matrices with capillary electrophoresis and conductivity detection. *J. Chromatogr. A*. **1999**, *848*, 503-513.

[7] Chen, Z.; Naidu, R., Separation of sulfur species in water by co-electroosmotic capillary electrophoresis with direct and indirect UV detection. *Int. J. Environ. Anal. Chem*. **2003**, *83*, 749-759.

[8] Timberbaev, A. R., Analysis of inorganic pollutants by capillary electrophoresis. *Electrophoresis.* **1997**, *18*, 185-195.

[9] Kaniansky, D.; Masár, M.; Marák, J.; Bodor., Capillary electrophoresis of inorganic anions. *J. Chromatogr. A.* **1999**, *834*, 133-178.

[10] Mazzeo, J. R. Capillary electrophoresis of inorganic anions. In *High Performance Capillary Electrophoresis, Theory, Techniques and Applications.* Khaledi, M.G., Ed.; Wiley: New York, 1998; p 825-852.

[11] Jones, W. R.; Jandik, P., Controlled changes of selectivity in the separation of ions by capillary electrophoresis. *J. Chromatogr.* **1991**, *546*, 445-458.

[12] Liang, H., Method development and validation for the determination of various sulfur-containing anions and other anions in the corrosion process by capillary ion electrophoresis with indirect detection. *J. Chromatogr. Sci.* **2001**, *39*, 12-20.

[13] O'Reilly, J. W.; Dicinoski, G. W.; Miura, Y.; Haddad P. R.; Separation of thiosulfate and the polythionates in gold thiosulfate leach solutions by CE. *Electrophoresis*. **2003**, *24*, 2228-2234.

[14] Jeffrey, M. I.; Brunt, S.D., The quantification of thiosulfate and polythionates in gold leach solutions. *Hydrometallurgy*. **2007**, *89*, 52-60.

[15] Motellier, S., Sulfur speciation and tetrathionate sulfitolysis monitoring by capillary electrophoresis. *J. Chromatogr. A*, **2001**, *907*, 329-335.

[16] Pobozy, E.; Jarczynska, M.; Trojanowicz, M. Speciation of sulfur-containing anions by use of capillary electrophoresis. *Chromatographia*. **2002**, *56*, 723-728.

[17] Sullivan, J.; Douek, M. Analysis of hydroxide, inorganic sulphur species and organic anions in kraft pulping liquors by capillary electrophoresis. *J. Chromatogr. A*. **2004**, *1039*, 215–225.

[18] de Carvalho, L. M.; Schwedt, G. Sulfur speciation by capillary zone electrophoresis: Determination of dithionite and its decomposition products sulfite, sulfate and thiosulfate in commercial bleaching agents. *J. Chromatogr. A*. **2005**, *1099*, 185-190.

[19] Lin, Y. T., Liu, Y. W., Cheng, Y. J., Huang, H. Y., Analyses of sulfonamide antibiotics by a successive anion- and cation-selective injection coupled to microemulsion electrokinetic chromatography. *Electrophoresis* **2010**, *31*, 2260–2266.

[20] Jiang, T. F.; Lu, Z. H.; Wang, Y. H.; Yue, M. E. On-line concentration by field-enhanced sample injection with reverse migrating micelles in micellar electrokinetic capillary chromatography for the analysis of coumarins from traditional Chinese medicine and human serum. *Biomed Chromatogr*. **2010**, *24*, 581-587.

[21] Urban, P. L.; García-Ruiz, C.; García, M. A.; Marina, M.L. Separation and online preconcentration by multistep stacking with large-volume injection of anabolic steroids by capillary electrokinetic chromatography using charged cyclodextrins and UV-absorption detection. *J. Sep. Sci*. **2005**, *28*, 2200-2209.

[22] Kawai, T.; Koino, H.; Sueyoshi, K.; Kitagawa, F.; Otsuka, K. Highly sensitive chiral analysis in capillary electrophoresis with large-volume sample stacking with an electroosmotic flow pump**.** *J. Chromatogr. A.* **2012**, *1246*, 28–34.

[23] Su, A. K.; Chang, Y. S.; Lin, C. H.; Analysis of riboflavin in beer by capillary electrophoresis/blue light emitting diode (LED)-induced fluorescence detection combined with a dynamic pH junction technique. *Talanta* **2004**, *64*, 970–974.

[24] Kim, J. B.; Okamoto, Y.; Terabe, S. On-line sample preconcentration of cationic analytes by dynamic pH junction in capillary electrophoresis. *J. Chromatogr. A* **2003**, *1018*, 251–256.

[25] Kelly, D. P.; Wood, A. P., Synthesis and determination of thiosulfate and polythionates. *Methods Enzymol.* **1994**, *243*, 475-500.

[26] Pappoe, M.; Lucas, H.; Bottaro, C.; Dawe, L. N. Single Crystal Structural Characterization of Tri-, Tetra and Pentathionates. *J. Chem. Crystallogr.* **2013**, *43*, 596–604.

Chapter 3

Central Composite Response Surface Design for the Optimization of Capillary Zone Electrophoresis with Indirect Detection Using a Triethanolamine-Buffered Pyromellitic Acid Probe for the Analysis of Thiosalts in Mine Tailings

3.1 Introduction

Thiosalt species, also known as sulfur oxyanions are naturally formed from the partial oxidation of sulfur compounds in sulfur-rich environments but are also generated during the flotation and milling of sulfidic minerals especially those containing pyrite (FeS_2) and pyrrhotite ($Fe_{(1-x)}S$, x = 0 to 0.2). These species have varying reactivities and thermodynamic properties. The full oxidation process leads to the production of sulfuric acid (H_2SO_4) and subsequently acidification of the receiving aqueous environment, which has a negative effect on plant and animal life. Acidification can also lead to toxic metal solubilization and transport.[1-6]

The properties of thiosalts and mitigating their production are areas showing intense interest from industry and has necessitated research by a number of groups.[7-9] This interest is driven by the need for treatment of thiosalts in an efficient and effective manner. Neutralization is not very effective, and ideal treatment should lead to the complete oxidation of all sulfur species to sulfate. In addition, the success of these treatment approaches is dependent on thiosalt speciation and the treatment protocol adopted. As these species have complex chemistry and are reactive, analytical techniques that can provide relatively fast analysis are desired; CZE with indirect UV-vis detection for inorganic anions is well suited for this. Indirect CZE is becoming an established technique in environmental contaminant analysis, pharmaceutical screening and analytical chemistry. In addition to providing fast separations, CZE requires only a small

amount of sample for analysis, has good reproducibility and method development is relatively easy.[10-14]

Indirect CZE, and CZE in general, can be influenced by many factors including buffers and chromophoric probe concentrations, pH; applied voltage; capillary temperature; injection volume; an experimental design can give better optimized conditions and more robust methods.[15] This is especially important in regulatory or forensic environments, where methods require not only fast analysis (short analysis time) but also reliable analytical results.[16-18] Experimental design approaches allow for simultaneous investigation of the most important factors, as well as the interactions between the factors, making them elegant in terms of efficiency of time and resources. They can also provide information about the chemistry of the system. There are several methods of experimental designs used in analytical work, most common are general full factorial (GFF), 2-level factorial, response surface designs such as central composite design (CCD) and Box-Behnken design (BBD), or a mixture design such as the simplex lattice design (SLD) and simplex centroid design (SCD). Designs such as a 2-level GFF (2^k) can easily be used to determine the most important factors (screening). Optimization of the chosen factors at appropriate levels is then performed using techniques such as CCD and BBD. One advantage in using response surface designs is that they have an embedded factorial design and the experimental domain is expected to contain the optimum values of the multivariate factors assessed in the preliminary method development. [19-23]

Experimental designs applied for screening of factors in CZE use two-level screening designs such as fractional factorial (fFD) or Plackett-Burman (PBD) designs, when screening of many factors is necessary. For the optimization stage of method development, use of GFF and response surface designs such as CCD and BBD are typical.[21-23] Not all CZE methods employ experimental design approaches, however, the number of publications on chemometric-assisted CZE and other CE modes have been on the increase especially in pharmaceutical, neutraceutical, and biochemical analyses. One application of experimental design was reported by van Biesen *et al.* in which MEKC-ESI-MS was applied for the analysis of *N*-methylcarbamate pesticides.[24] In this work, which was performed in our laboratory, the authors applied a face centered CCD design to 4 factors studied at 3 levels with factor settings capped at minima and maxima. The optimum experimental conditions gave complete resolution of 10 *N*-methylcarbamates in a mixture. Liu *et al.* optimized a non-aqueous CZE method based on orthogonal experimental design with six factors at three levels for the analysis of pesticide residues in tobacco.[25] The main factors studied were the BGE concentration, percent of ACN in BGE, applied voltage and BGE pH with the separation resolution factor and migration time optimized. Jurado-Gonzalez *et al.* used a 2^6 factorial screening design for a CE-UV method to study the influence of six factors: concentration of UV absorption probe, sample introduction time (length of sample injection), applied voltage, concentration of complexing reagent, pH and the length of the capillary, on the separation efficiency of 4 cations in water samples.[26] Responses monitored included the sensitivity, peak area and height, and migration time. Other applications of chemometrics for CZE include the use

of CCD and fFD for the analysis of caffeine in coffee,[27] BBD for polycyclic musks in perfumes,[28] fFD and CCD for cosmetic preservatives,[29] and 2-factor CCD RS with the use of a desirability function for the analysis of biogenic amines in food materials.[30] However, no papers using a multivariate experimental design have been published to optimize electrophoretic responses for environmentally important inorganic anions.[31] A recent review of multivariate experimental design approaches by Orlandini *et al.*[23] showed that the majority of applications are in the pharmaceutical, food and agricultural industries with a single environmental application in drinking water cited in which a cyclodextrin (CD)-modified MEKC method was applied for the determination of pharmaceuticals in drinking water using face centered composite design methodology for multivariate optimization of 3 factors at 3 levels.[17] Interestingly, this work was performed in the Botarro lab.

We present a multivariate experimental design approach using response surface CCD design to establish the optimal compositions of the background electrolyte and the separation voltage. As pH is critical for the stability of the thiosalt species analyzed all experiments were carried out at pH 8.0, and we determined that the concentrations of chromophoric probe used for indirect analysis and EOF modifier were the most important components for the BGE. Levels were defined based on previous experimental work using pyromellitic acid (PMA) as a BGE probe. However additional lower and higher levels were added to enable more thorough assessment of the optimum domain for these factors. The approach for the BGE design for this work was to use amine base to buffer

the chromophoric probes; these bases such as trithanolamine and tris(hydroxymethyl)-aminomethane) have been used by others for indirect capillary electrophoresis experiments.[32-34] In this work triethanolamine (TEA) was chosen as the background electrolyte buffer. With a pKa value of 7.8, the buffer capacity is expected to be very good for the chosen pH of 8.0. The optimal BGE composition yielding the highest desirability factors, after applying experimental design, were then applied for the analysis of five thiosalts standards and effluent samples from a treated mine tailings pond. The chromophoric probe used for this work, PMA, together with the pKa values, is shown in Figure 3.1.

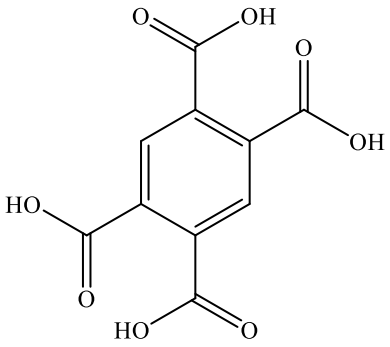

Figure 3.1. Pyromelltic acid (PMA). pKa_1 1.92, pKa_2 2.87, pKa_3 4.49, pKa_4 5.63[35-37]

3.2 Materials and Method

3.2.1 Chemicals

Sulfur oxyanion species used in this study include (1) sodium sulfate, (2) sodium thiosulfate, (3) sodium trithionate, (4) potassium tetrathionate and (5) potassium

pentathionate. Three (3) and five (5) were synthesized from a modified synthetic method described by Kelly *et al.*[38] Details of the synthesis and single crystal analysis are published elsewhere.[39] Hexamethonium hydroxide (HMOH) solution (0.1 M), benzene-1,2,4,5-tetracarboxylic (pyromellitic) acid (PMA), and triethanolamine solution (>99.0%) were all obtained from Sigma-Aldrich, MO, USA. CE-grade sodium hydroxide was purchased from Agilent Technologies, Waldbronn, Germany, and 0.22 µm nylon filters were purchased from Canadian LifeScience, ON, Canada. Nanopure water from Barnstead Nanopure II (Barnstead Nanopure, CA, USA) with ionic purity of 18.2 MΩ·cm was used for this work. For the BGE, the probe was titrated with triethanolamine to pH 8.0 to form the triethanolamine-buffered background electrolyte solutions at different concentrations of the probes. Thiosalts standards, samples and background electrolyte solution were all prepared with nanopure water, degassed and filtered through a 0.22 µm nylon filter before analysis.

3.2.2 Instrumentation

All CE analyses were performed on an Agilent 7100 ^{3D}CE System (Agilent Technologies Canada Inc., Mississauga, Ontario) equipped with a diode array UV-vis detector. To invert the negative peaks for the thiosalt species, measurements were acquired at 350 nm relative to 200 nm, since the decrease in absorbance at 200 nm will be greater than that at 350 nm. An Agilent OpenLAB Chromatography Data System (CDS) ChemStation Edition was used to process the acquired data: corrected peak areas, peak widths and heights, and migration times. Bare fused-silica capillaries (id 50 µm) were obtained from

MicroSolv Technology Corporation (NJ, USA) and were accurately cut to the desired length (48.5 cm). Polyimide coating was removed from the capillaries at 8.5 cm to create a window and at the last 2 mm of the ends of the capillaries using MicroSolv Window Maker™ (N.J. USA). Initial conditioning was as follows: flushing at ~ 940 mbar with 1.0 N NaOH for 1 hr, water for 1 hr and BGE for another 1 hr. The capillary was conditioned daily with 0.1 N NaOH for 10 min, water for 10 min and BGE for another 10 min. Between injections, the capillary was flushed with 0.1 N NaOH for 1 min, water for 1 min and BGE for 3 min. Except stated otherwise, samples were injected hydrodynamically at 50 mbar for 10 s, and negative potentials of between -18 and -30 kV (as in the experimental design) were applied for the separation with indirect detection at the wavelengths above.

3.3 Results and Discussion

3.3.1 Experimental design and optimization of separation

PMA was chosen for the analysis of thiosalts because of its high molar extinction coefficient, close mobility match with the thiosalt anions and no known oxidizing effect on these species. Previous experiments with PMA as chromophoric probe and three EOF modifiers showed that hexamethonium dication (HM^{2+}) was more effective as an EOF modifier for such species. In our previous work, a univariate approach was utilized by varying each factor to see its effect on the separation efficiency of the thiosalt species and analysis time. In this work a more robust experimental design approach was pursued. The factors that were selected for the optimization phase of the experimental method

development and the levels at which each factor were studied are shown in Table 3.1. The factor levels were set based on previous experimental work using pyromellitic acid (PMA) as a BGE probe, however additional lower and higher levels were added to ensure the domain included a truly optimal set of conditions. PMA as the chromophoric probe and HM^{2+} were examined using a CCD design for optimizing CZE conditions and BGE composition.

Table 3.1. Factors selected for the experimental design and their levels

Factor	**Levels**
[PMA]	1.00 – 3.00 – 5.00 (mM)
$[HM^{2+}]$	0.20 – 0.60 – 1.00 (mM)
Potential (-kV)	18 – 24 – 30

3.3.2 Assessment of analytical performance of PMA BGE system

Experimental designs were devised and analyzed using Minitab® design of experiment (DOE) mode. The response surface design using CCD required data for 20 points (runs) for various combinations of factors and levels. The desirability function in Minitab® enabled the optimization to be based on the desired resolution of key thiosalt peak pairs, that is, closely migrating pairs. Five representative electropherograms, with the degree of

separation of the thiosalts peaks, under different combinations of the BGE components and instrument parameters are shown in Figure 3.2.

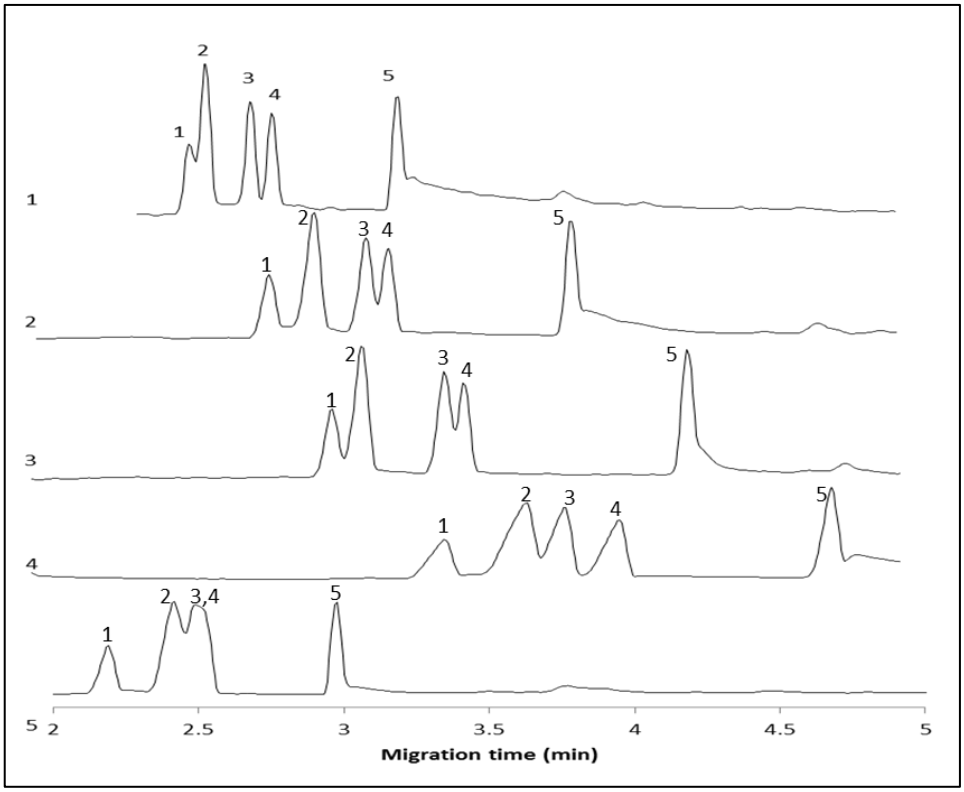

Figure 3.2. Five representative electropherograms from the 20-experiment CCD experimental design for PMA BGE system. 1. [PMA] = 5.00 mM, [HM^{2+}] = 1.00 mM, V = -30 kV; 2. [PMA] = 3.00 mM, [HM^{2+}] = 0.60 mM, V = -24 kV; 3. [PMA] = 5.00 mM, [HM^{2+}] = 0.20 mM, V = -18 kV; 4. [PMA] = 1.00 mM, [HM^{2+}] = 1.00 mM, V = -18 kV; 5. [PMA] = 1.00 mM, [HM^{2+}] = 0.20 mM, V = -30 kV; Detection λ = 350, Ref = 200 nm. Thiosalt species: 1. $S_2O_3^{2-}$ 2. $S_5O_6^{2-}$ 3. SO_4^{2-} 4. $S_3O_6^{2-}$ 5. $S_4O_6^{2-}$

The adjacent peak resolution factor (R_s) was calculated using the equation below:

$$R_{1,2} = \frac{2\,(t_2 - t_1)}{w_1 + w_2} \qquad (3.1)$$

where t_2 and t_1 are the migration times of two adjacent peaks and w_1 and w_2 are the baseline peak width (in time) .The targets for R_s and analysis time (t) are shown below in Table 3.2.

Table 3.2. Response targets for adjacent peak resolution (R_S) and analysis time (t)

Resolution response factor	Description	Goal	Target	Lower limit
$R_{1,2}$ (peak 1 and 2)	$S_2O_3^{2-}$ - $S_5O_6^{2-}$	Target	3.0	2.0
$R_{2,3}$ (peak 2 and 3)	$S_5O_6^{2-}$ - SO_4^{2-}	Target	3.0	2.0
$R_{3,4}$ (peak 3 and 4)	SO_4^{2-} - $S_3O_6^{2-}$	Target	2.5	2.0
$R_{4,5}$ (peak 4 and 5)	$S_3O_6^{2-}$ - $S_4O_6^{2-}$	Target	10	5.0
t (min)	analysis time	minimize	3.0	4.0

The separation dashboards (Minitab® feature) for the optimized conditions for R_s and t responses for the five thiosalt species analyzed are shown in Figure 3.3. The values in red show optimized conditions for best composite desirability for a minimum $R_s = 2.0$ and analysis time of at least 4 min. The dashboard above shows a high composite desirability factor of 0.74 (maximum is 1) for the optimal predicted factor settings to achieve the targeted responses in Table 3.2. The predicted settings were tested experimentally to see if the results of the model will be close to the experimental values. Triplicate experiments were performed using the optimal factor settings

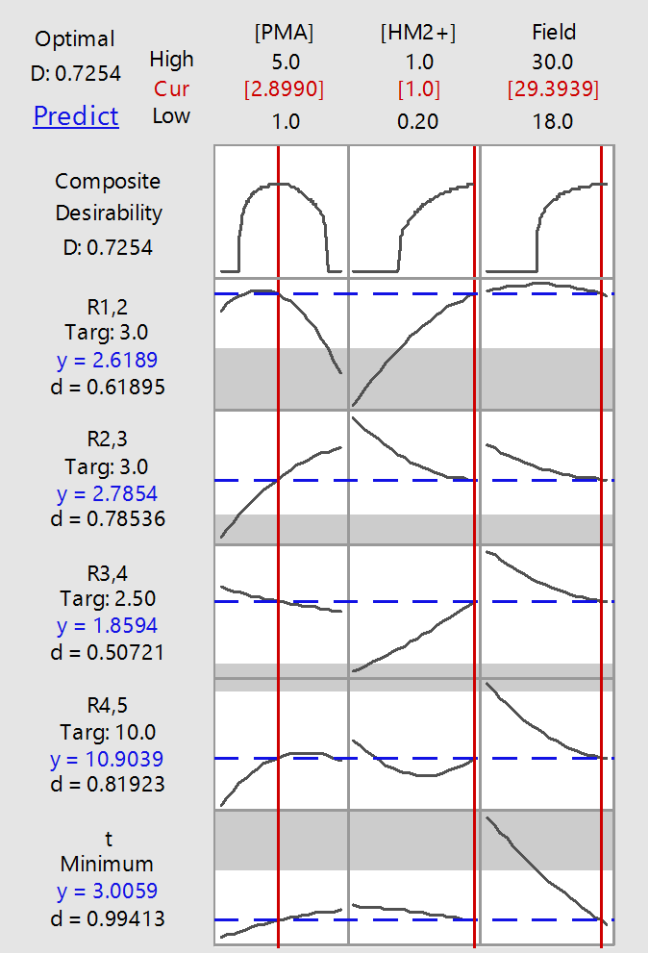

Figure 3.3. Response optimizer dashboard (Minitab®) for PMA BGE systems showing predictions for optimal factor levels and desirability of responses

The electropherogram obtained from the optimal conditions shown in the separation dashboard is shown in Figure 3.4. The results of the analysis are summarized in Table 3.3. It can be seen that there is good agreement between the predicted and the experimental values with percentage differences ranging from 1.39 % to 7.95 %.

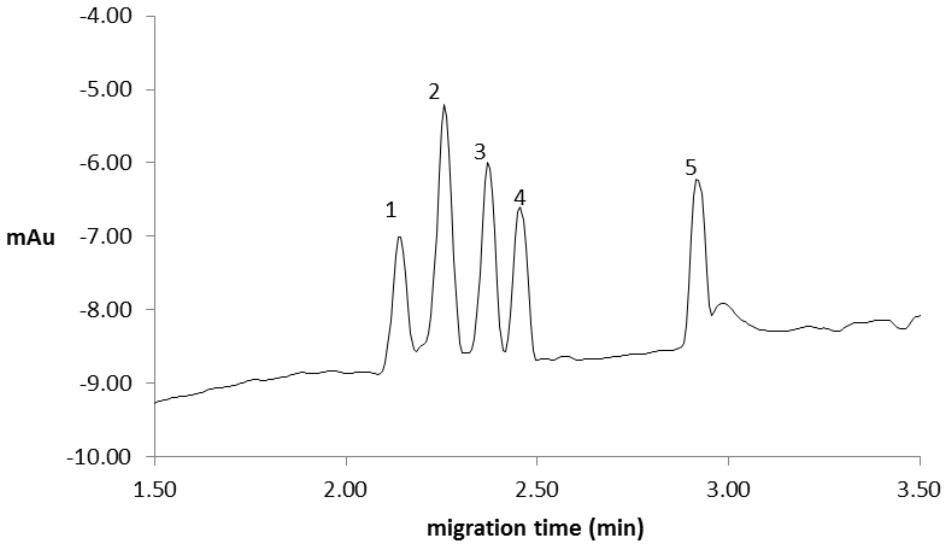

Figure 3.4. Electropherogram showing the complete separation of five thiosalt species using the optimal conditions. [PMA] = 2.90 mM, [HM^{2+}] = 1.00 mM, Applied Field = -29.4 kV. Thiosalt species: 1. $S_2O_3^{2-}$ 2. $S_5O_6^{2-}$ 3. SO_4^{2-} 4. $S_3O_6^{2-}$ 5. $S_4O_6^{2-}$. Detection wavelength: λ = 350 nm, with reference λ = 200 nm. Capillary: total length (L) = 48.5 cm, length to detector (l) = 40 cm.

Table 3.3. Predicted versus experimental values of peak resolution for PMA BGE system

Response	Predicted	Experimental (n=3)	% Difference
$R_{1,2}$	2.62	2.66	1.39
$R_{2,3}$	2.79	2.58	7.95
$R_{3,4}$	1.86	1.97	5.57
$R_{4,5}$	10.9	11.2	2.39
t (min)	3.00	2.92	2.59

3.3.3 Response Surface Plots of $R_{1,2}$, $R_{2,3}$ and $R_{3,4}$ for the PMA BGE system

The response surface plots can be used to assess the effect of interacting factors on resolution on resolution between adjacent peaks. The surface plots for $R_{1,2}$ (A), $R_{2,3}$ (B) and $R_{3,4}$ (C) as a function of [HM^{2+}] are shown in Figure 3.5. The critical peak pairs (from Figure 3.3) are $R_{1,2}$, $R_{2,3}$ and $R_{3,4}$; peaks 4 and 5 are a non-critical pair and the surface plot for this is therefore not discussed. The surface plots for (Figure 3.5A, B and C), show an increase in adjacent peak resolution $R_{1,2}$, and $R_{3,4}$ as [HM^{2+}] is increased, however a negative effect is seen in $R_{2,3}$ with this effect attenuated at high [PMA].

From the optimization experiments, the most critical peak pair was 3 and 4. The surface plot for this pair is shown in Figure 5C. A low resolution factor target of 2.5 (compared to 3.0 for the other peak pairs) was set for this peak pair to reduce the constraint on the other peak pairs and to avoid co-migration of the peaks; and to ensure complete resolution. An increase in [PMA] from 1.00 mM to 5.00 mM led to a very small increase in $R_{3,4}$. However, increasing [HM^{2+}] led to a much higher increase in the value of $R_{3,4}$ close to the target value of 2.5. Combining [PMA] and [HM^{2+}], a higher resolution factor is realized much higher than each of the factors. At [PMA] = 2.90 mM and [HM^{2+}] at 1.00 mM, the resolution factor reached 1.9. Although this is lower than the target, a baseline resolution was realized for this peak-pair.

As [PMA] was increased from 1.0 mM to 5.0 mM, $R_{1,2}$ increased to a maximum value at ~ 2.5 mM and then decreased to a minimum value. As the chromophoric probe PMA is necessary for the analyte signals and hence better signal-to-noise ratioof the peaks in the indirect CZE mode at higher concentrations, it may be necessary to trade off resolution for sensitivity. The EOF modifier HM^{2+} was added to reduce or reverse the EOF and allow for a fast separation in the negative mode; therefore $[HM^{2+}]$ is another important factor. Increasing $[HM^{2+}]$ from 0.2 mM to 1.0 mM led to an increase in the value of $R_{1,2}$ towards the targeted value but less than the target of 3.0. The response surface plot (Figure 5A) shows that $[HM^{2+}]$ works synergistically with [PMA] with the optimum $R_{1,2}$ obtained at the maximum $[HM^{2+}]$ of 1.00 mM used and ~ 3.00 mM.

The response surface plot for $R_{2,3}$ (Figure 3.5B) with respect to [PMA] and $[HM^{2+}]$ showed a very different interaction between the two factors compared to $R_{1,2}$ and $R_{3,4}$. Increasing [PMA] led to an increase in $R_{2,3}$ to maximum value above the target value of 3.0 and then a slight decrease. Increasing $[HM^{2+}]$ however led to a slight decrease in $R_{2,3}$ to a minimum value then a slight increase. Two optima are shown at high [PMA] value of 5.00 mM; with one at $[HM^{2+}]$ of 0.00 mM (no EOF modifier) and the other at high $[HM^{2+}]$ of 1.00 mM. As $[HM^{2+}]$ is required for complete resolution of the other peak pairs $R_{1,2}$ and $R_{3,4}$, a compromise is needed. Thus for $R_{2,3}$, the second maximum is more important. At the optimal condition with [PMA] = 2.90 mM and $[HM^{2+}]$ = 1.00 mM a value much closer to the predicted value is realized which is lower (but closer to the target) than that obtained at the same concentrations for only PMA or HM^{2+}.

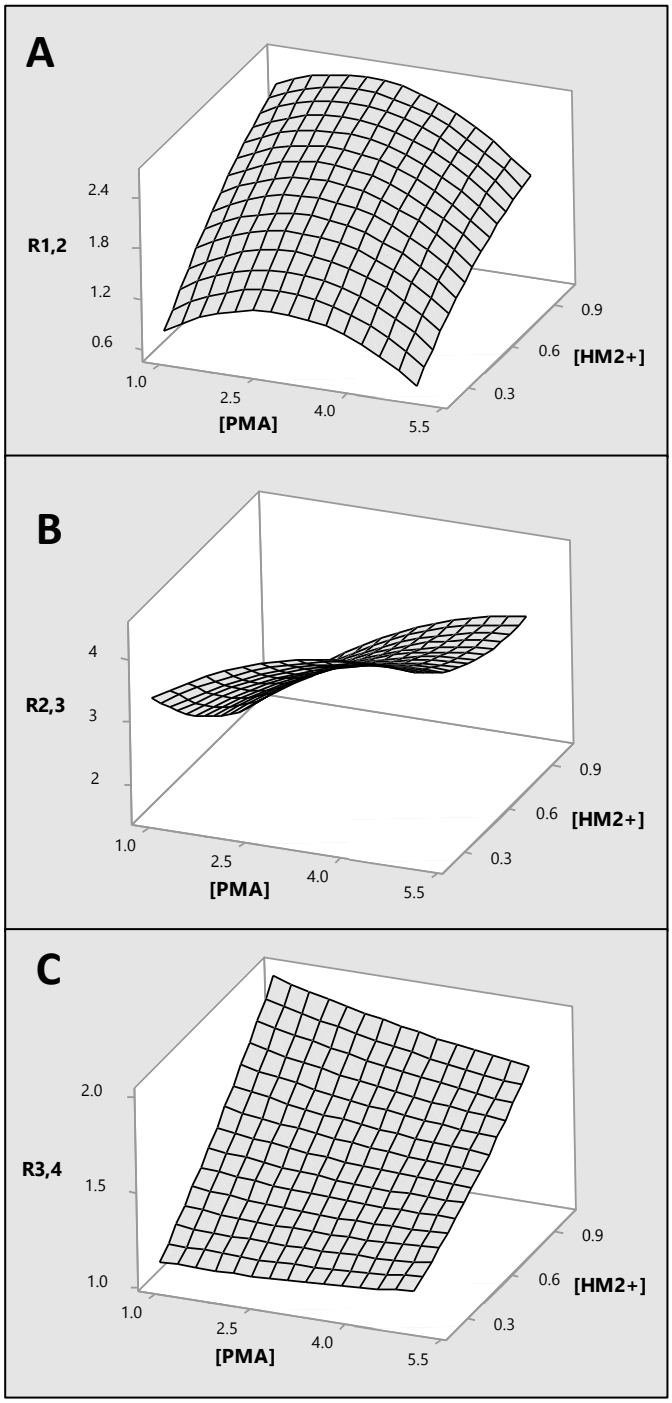

Figure 3.5. Response surface plot of Resolutions $R_{1,2}$, $R_{2,3}$ and $R_{3,4}$ vs [PMA] and [HM^{2+}]

3.3.4 Figures of merit for the optimized PMA BGE system

Limit of detection (S/N =3) values were established by sequential dilution and analysis of each of the thiosalt standards until the S/N of the analyte peak is ~ 3. Table 3.4 is a collation of the method LOD values and relative standard deviations (RSDs) of the migration times and peak areas of the analytes with triplicate analysis done.

Table 3.4. LOD values (µg/mL) and RSD values for migration time and peak areas for 5 thiosalt species (40 µg/mL each) analyzed using the optimum BGE conditions. Detection wavelength was at λ = 350, Ref = 200 nm

Analyte	Method LOD (µg/mL)	RSD migration time (%) (n = 3)	RSD peak area (%) (n = 3)
SO_4^{2-}	0.1	0.1	2.1
$S_2O_3^{2-}$	0.2	0.1	2.4
$S_3O_6^{2-}$	0.2	0.08	1.9
$S_4O_6^{2-}$	0.2	0.1	1.9
$S_5O_6^{2-}$	0.1	0.09	2.2

3.3.5 Application of three BGE systems to thiosalts samples analysis

Samples taken from a mine tailings pond were analysed for the presence of thiosalts using a standard addition method. Samples were diluted 1:100 before analysis. To prepare the calibration samples for standard addition, 500 µL of the 1:100 diluted sample was spiked with 0, 20, 40, 60, 80 and 100 µL of the thiosalt standard mix (40 µg/mL each), made up to 600 µL, mixed using a vortex and analyzed. This dilution was performed due to the relatively high concentrations of sulfate and thiosulfate in the sample. Based on this dilution, the total method detection limits would be 10 and 30 µg/mL for the highly complex tailings waters. Since the concentrations of thiosalts of concern (due to their toxicity to some fish species) in the tailings are from 50 µg/mL up, and with the low LOD values achieved for this method, the dilution of the sample at 1:100 is not expected to negatively impact the quantitation of these species. However, by sacrificing short analysis times sought for this work, it is possible to analyze pond samples with little or no dilution and still accommodate the relatively high concentrations of sulfate and thiosulfate. For less complex samples, as measured in kinetic and thermodynamic studies, dilution is not necessary and the high method sensitivity can be maintained. Three samples were prepared for each standard addition point to determine the standard deviations associated with each measurement. The results of the standard addition analysis are shown in Table 3.5. The main thiosalts detected in the sample taken from the tailings pond were sulfate (SO_4^{2-}) and thiosulfate ($S_2O_3^{2-}$) with concentrations over 450 µg/mL for SO_4^{2-} and 800 µg/mL for $S_2O_3^{2-}$.

Table 3.5. Results from the analysis of a tailings pond sample using standard addition calibration. The migration times (t_M) were measured for the 100 µL standard addition samples (last set of the six samples).

Thiosalt species (Real sample)	Average migration time (t_M)	Amount found (µg/mL±SD)
SO_4^{2-}	3.30	484.9 ± 5.2
$S_2O_3^{2-}$	2.96	823.4 ± 39.1
$S_3O_6^{2-}$	3.39	51.2 ± 5.0
$S_4O_6^{2-}$	4.06	33.5 ± 15.7
$S_5O_6^{2-}$	3.09	10.7 ± 6.4

3.4 Concluding remarks

The quest for reliable and high quality data from environmental, pharmaceutical and forensic samples has called for the need to develop robust and reliable analytical methods for their analysis. In this work, a chemometric approach using central composite response surface (CCD) design was used to establish the optimal concentrations of the background buffer probes, surfactant and the separation voltage and to develop an understanding of the interplay of these factors in achieving a complete resolution of the analyte peaks. The optimized PMA BGE composition of [PMA] = 2.90 mM, [HM^{2+}] = 1.00 mM and separation applied field -29.4 kV resulted in a fast separation of five sulfur oxyanion species with the last peak migrating at just under 3 min. The optimum values predicted were in good agreement with experimental values. In addition, LOD values of between

0.1 (SO_4^{2-} and $S_2O_3^{2-}$) and 0.2 µg/mL ($S_2O_3^{2-}$, $S_3O_6^{2-}$ and $S_4O_6^{2-}$) were achieved for the thiosalt species. The optimized method successfully applied to the analysis of thiosalt mine tailings sample for which the predominant species were sulfate (SO_4^{2-}) and thiosulfate ($S_2O_3^{2-}$).

3.5 References

[1] Vongporm, Y. Thiosalt behavior in aqueous media. Master of Engineering Thesis. Memorial University of Newfoundland, 2008.

[2] Druschel, G.K.; Hamers, R.J.; Luther, G.W.; Banfield, J.F. Kinetics and mechanism of trithionate and tetrathionate oxidation at low pH by hydroxyl radicals. *Aquat. Geochem.* **2003**, *9*, 145-164.

[3] Garcia, C.; Ballester, A.; Gonzalez, F.; Blazquez, M.L. Pyrite behavior in a tailings pond. *Hydrometallurgy.* **2005**, *76*, 25-36.

[4] Goldhaber, M. Experimental study of metastable sulfur oxyanion formation during pyrite oxidation at pH 6-9 and 30 C. *Am. J. Sci.* **1983**, *283*, 193-217.

[5] Masau, R.; Oh, J.; Suzuki, I. Mechanism of oxidation of inorganic sulfur compounds by thiosulfate-grown *Thiobacillus thioxidans*. *Can. J. Microbiol.* **2001**, *47*, 348-358.

[6] Garcia, C.; Ballester, A.; Gonzalez, F.; Blazquez, M.L. Pyrite behavior in a tailings pond. *Hydrometallurgy.* **2005**, *76*, 25-36.

[7] Wasserlauf, M.; Dutrizac, J.E. In The chemistry, generation and treatment of thiosalts in milling effluents – A non-critical summary of CANMET investigations 1976-1982, CANMET Report 82-4E, 1982.

[8] Dinardo, O.; Sally, J. In *Treatment of thiosalts in milling effluent: A review of treatment process*. Mining and Mineral Sciences Laboratories Report. Thiosalts Consortium-Phase II. CANMET-MMSL, 1998.

[9] Fahd, F.; Khan, F.; Hawboldt, K.; Abbassi, R. Developing a Novel Methodology for the Ecological Risk Assessment of Thiosalts. *Stoch. Environ. Res. Risk Assess.* **2014,** *28*, 383-391.

[10] Timberbaev, A. R., Analysis of inorganic pollutants by capillary electrophoresis. *Electrophoresis.* **1997**, *18*, 185-195.

[11] Kaniansky, D.; Masár, M.; Marák, J.; Bodor., Capillary electrophoresis of inorganic anions. *J. Chromatogr. A.* **1999**, *834*, 133-178.

[12] Timberbaev, A.R.; Dabek-Zlotorzynska, E.; van den Hoop, M. A. G. T. Inorganic Environmental Analysis by Capillary Electrophoresis. *Analyst*. **1999**, *124*, 811-826.

[13] Zhao S, Zhang R, Wang H, Tang L, Pan Y. Capillary electrophoresis enantioselective separation of vigabatrin enantiomers by precolumn derivatization with dehydroabietylisothiocyante and UV-vis detection. *J. Chromatogr. B. Analyt. Technol. Biomed. Life Sci.* **2006**, 833, 186-190.

[14] Hiissa T, Sirén H, Kotiaho T, Snellman M, Hautojärvi A. Quantification of anions and cations in environmental water samples. Measurements with capillary electrophoresis and indirect-UV detection. *J. Chromatogr. A.* **1999**, 853, 403-411.

[15] Hanrahan, G.; Lu, K. Application of factorial and response surface methodology in modern experimental design and optimization. *Crit. Rev. Anal. Chem.* **2006**, *36*, 141–151.

[16] I.M. Palabiyik, M. G. Caglayan, F. Onur, Multivariate optimization and validation of a CE method for simultaneous analysis of dorzolamide hydrochloride and timolol maleate in ophthalmic solution. *Chromatographia*. **2011**, *73*, 541–548.

[17] Drover, V. J.; Bottaro, C. S. Determination of pharmaceuticals in drinking water by CD-modified MEKC: separation optimization using experimental design, *J. Sep. Sci.* **2008**, *31*, 3740–3748.

[18] Chiang, J. F.; Hsiao, Y. T.; Ko, W. K.; Wu, S. M. Analysis of multiple abused drugs and hypnotics in urine by sweeping CE, *Electrophoresis*, **2009**, *30*, 2583–2589.

[19] McCourt, J.; Stroka, J.; Anklam, E. Experimental design-based development and single laboratory validation of a capillary zone electrophoresis method for the determination of the artificial sweetener sucralose in food matrices. *Anal. Bioanal. Chem*. **2005,** *382*, 1269-1278.

[20] Altekar, M.; Homon, C.A.; Kashem, M.A.; Mason, S.W.; Nelson, R.M.; Patnaude, L.A.; Yingling, J.; Taylor, P.B. Assay Optimization: A Statistical Design of Experiments Approach. *Clin. Lab. Med.* **2007**, 27, 139–154.

[21] Montes, R.; Dahdouh, F.; Riveros, T.A.; Hanrahant G.; Gomez, F. A. Chemometrical Experimental Design-Based Optimization Studies in Capillary Electrophoresis Applications. *LC GC North America*, **2008**, 82-88.

[22] Hanrahant G.; Montes, R.; Gomez, F. A Chemometric experimental design based optimization techniques in capillary electrophoresis: a critical review of modern applications. *Anal. Bioanal. Chem*. **2008**, *390*, 169–179.

[23] Orlandini, S.; Gotti, R.; Furlanetto, S. Multivariate optimization of capillary electrophoresis methods: A critical review. *J. Pharm. Biomed. Anal.* **2014**, *87*, 290– 307.

[24] Van Biesen, G.; Bottaro, C. S. Ammonium perfluorooctanoate as a volatile surfactant for the analysis of N-methylcarbamates by MEKC-ESI-MS. *Electrophoresis*. **2006**, *27*, 4456-4468.

[25] Liu, H.; Song, J.; Han, P.; Li, Y.; Zhang, S.; Liu, H.; Wu, Y. Separation and determination of 2,4-D, dicamba and 2,4,5-T in tobacco by nonaqueous capillary electrophoresis. *J. Sep. Sci.* **2006**, *29*, 1038-44.

[26] Jurado-González, J. A.; Galindo-Riaño, M.D.; García-Vargas, M. Factorial designs applied to the development of a capillary electrophoresis method for the analysis of zinc, sodium, calcium and magnesium in water samples. *Talanta*, **2003**, *59*, 775-783.

[27] Meinhart, A. D.; Bizzotto, C. S.; Ballus, C. A.; Prado, M. A.; Bruns, R. E.; Filho, J.T.; Godoy, H.T. Optimisation of a CE method for caffeine analysis in decaffeinated coffee. *Food Chem*. **2010**, *120*, 1155–1161.

[28] Lopez-Gazpio, J.; Garcia-Arrona, R.; Ostra, M.; Millan, E. Optimization and validation of a nonaqueous micellar electrokinetic chromatography method for determination of polycyclic musks in perfumes. *J. Sep. Sci.* **2012**, *35*, 1344–1350.

[29] Cheng, Y. C.; Wang, C. C; Chen, Y.L.; Wu, S.M. Large volume sample stacking with EOF and sweeping in CE for determination of common preservatives in

cosmetic products by chemometric experimental design. *Electrophoresis*. **2012**, *33*, 1443–1448.

[30] L. M. Swann, S. L. Forbes, S. W. Lewis, A capillary electrophoresis method for the determination of selected biogenic amines and amino acids in mammalian decomposition fluid. *Talanta*, **2010**, *81*, 1697–1702.

[31] Muzikář, M.; Havel, Miroslav, J.; Macka, M. Capillary electrophoresis determinations of trace concentrations of inorganic ions in large excess of chloride: Soft modelling using artificial neural networks for optimisation of electrolyte composition. *Electrophoresis*. **2003**, *24*, 2252–2258.

[32] Xiong, X.; Li, S. F. Y.; Selection and optimization of background electrolytes for simultaneous detection of small cations and organic acids by capillary electrophoresis with indirect photometry. *J. Chromatogr. A*. **1998**, *822*, 125-136.

[33] Doble, P.; Per Andersson, P. Buffered Chromate Electrolytes for Separation and Indirect Absorbance Detection of Inorganic Anions in Capillary Electrophoresis. *Anal. Commun*. **1997**, *34*, 351-353.

[34] Shafaati, A.; Lucy, C. Application of capillary zone electrophoresis with indirect UV detection to the determination of a model drug, vigabatrin, in dosage forms. *J. Pharm. Pharm Sci.* **2005**, 8, 190-198.

[35] Motellier, S.; Gurdale, K.; Pitsch, H., Sulfur speciation by capillary electrophoresis with indirect spectrophotometric detection: In search of a suitable carrier electrolyte to maximize sensitivity. *J. Chromatogr. A*, **1997**, *770*, 311-319.

[36] Hißner, F.; Mattusch, J.; Heinig, K. Determination of sulfur-containing inorganic anions by dual ion chromatography and capillary electrophoresis – application to the characterization of bacteria sulfur degradation. *Fresenius J. Anal. Chem*. **1999**, *365*, 647 – 653.

[37] O'Reilly, J. W.; Dicinoski, G. W.; Miura Y.; Haddad P. R.; Separation of thiosulfate and the polythionates in gold thiosulfate leach solutions by CE. *Electrophoresis*, **2003**, *24*, 2228-2234.

[38] Kelly, D. P.; Wood, A. P., Synthesis and determination of thiosulfate and polythionates. *Methods Enzymol.***1994**, *243*, 475-500.

[39] Pappoe, M.; Lucas, H.; Bottaro, C.; Dawe, L. N. Single Crystal Structural Characterization of Tri-, Tetra and Pentathionates. *J. Chem. Crystallogr.* **2013**, *43*, 596–604.

[40] Bartels, K. UV spectral characteristics of selected thiosalts. Canada Centre for Mineral and Energy Technology (CANMET), CANMET Report, Toronto, 1981

[41] Padarauskas, A.; Paliulionyte, V.; Ragauskas, R.; Dikcius, A. Capillary electrophoretic determination of thiosulfate and its oxidation products. *J. Chromatogr. A.* **2000**, *879*, 235-243.

Chapter 4

Use of fractional factorial and Box-Behnken response surface designs for the screening and optimization of factors for capillary zone electrophoresis separation and indirect UV-vis detection of thiosalts

4.1 Introduction

Although research in thiosalts has been ongoing since the 1980s, their reactivity and thermodynamic properties are still not completely understood due to their complex chemistry and reaction pathways under certain conditions such as temperature, pH and oxygen concentration.[1-9] As these intermediate sulfur species are only metastable, a fast, reliable and robust analytical technique is needed to quantify all the important thiosalt species at the various stages in sulfide mineral processing, to provide the relevant information of their generation and to aid in their treatment upstream of the tailings pond as well as to implement the appropriate risk assessment model for these species.[7]

Capillary zone electrophoresis (CZE) and CE in general, is a powerful separation technique due to its high speed, high separation efficiency, and good tolerance to sample matrices, such as high pH. Combined with low consumption and cost of consumables, such as solvents, and low waste generation, CZE can be considered a green analytical technique.[8-10] CZE has been applied to speciation analysis of environmental and biological samples, as well as other systems. Separation performance in CE is superior to most analytical techniques, such as ion chromatography.[11-12] CE detection in nearly all cases requires a shorter analysis time compared to these separation techniques leading to reduced costs and improvement in quality control procedures. CE can therefore be used as a complementary technique to IC or other well-established separation techniques for process monitoring in industry.

The use of multivariate experimental design approaches in developing robust analytical techniques particularly for CZE methods is increasing in pharmaceutical, forensic and environment sectors due to stringent regulatory enforcement and the benefit for faster and more thorough optimization. However, CZE separation are often considered complex because of the number of factors that can be modified to influence the separation.[13]

After the goals and objectives of the experiment are determined, the process of applying multivariate experimental design is straight-forward. First, screening designs (for 6 – 15 factors) are used to identify the critical factors that have the greatest effect on the interested responses such as peak resolution and analysis time. Typically, a 2-level GFF (2^k) or fractional factorial design (2^{k-p}) are used for screening, where k is the number of factors and p a chosen number (k > p) that gives the degree of fractionality of the fractional factorial design. The critical factors (2 – 5) from the screening stage can be used in the optimization stage using models such as factorial design (2-level, Plackett-Burman or GFF), response surface design (central composite (CCD) or Box-Behnken (BBD)), mixture design (simplex centroid, simplex lattice or extreme vertices) or Taguchi design (2-5 level or mixed levels).[14-20]

A large number of applications of multivariate approaches to the optimization of CZE methods have been reported.[21-26] In a study by Zhu *et al.*, a CCD was used to optimize a CE separation with electrochemiluminescence detection of six antihistamine drugs.[21] The factors studied were buffer concentration, buffer pH and voltage. The responses

optimized were the peak resolution factor (R_s) and analysis time. Meinhart *et al.* optimized an MEKC method for caffeine analysis in decaffeinated coffee using CCD for screening and FFD for optimizing five critical factors: sodium carbonate concentration, SDS concentration, voltage, injection time and injection pressure for seven responses: peak separation, peak area, background noise intensity, baseline variation, analysis time, system current and peak area.[22] Other applications include the use of BBD for CZE separation of polycyclic musks in perfumes,[23] fFD and CCD for screening and optimization of CZE separation of cosmetic preservatives,[24] and fFD for the optimization of CZE method for quinine, propranolol and atropine.[25] There are few reports on the application of multivariate experimental design in CZE for environmentally important anions and none for thiosalt species.[26]

In this work, a multivariate approach was used to screen and optimize critical factors for CZE with indirect UV-vis detection of five important thiosalt species: sulfate (SO_4^{2-}), thiosulfate ($S_2O_3^{2-}$), trithionate ($S_3O_6^{2-}$), tetrathionate ($S_4O_6^{2-}$) and pentathionate ($S_5O_6^{2-}$). A fractional factorial design (fFD) was used to screen 6 factors: concentration of trimellitic acid ([TMA]), concentration of the electroosmotic flow modifier hexamethonium hydroxide ([HMOH]), injection time (s), cassette temperature (ºC), applied field (kV) and detection wavelength. At the optimization stage, the four critical factors: [TMA], [HMOH], injection time (s) and applied field (kV) were optimized using a Box-Behnken response surface design (BBD). The optimized BGE composition and separation conditions in the model were tested experimentally and were found to be in

good agreement. The method was applied for the analysis of thiosalts in mine treated tailings pond samples.

4.2 Materials and Method

4.2.1 Chemicals

Sulfur oxyanion species used in this study include sodium sulfate (1), sodium thiosulfate (2), potassium tetrathionate (3), sodium trithionate (4), potassium pentathionate (5), and potassium hexathionate (6). The latter three (4-6) were synthesized from a modified synthetic method described by Kelly *et al.*[27] Details of the synthesis and crystal analysis is published elsewhere.[28] Benzene-1,2,4-tricarboxylic (trimellitic) acid (> 99%), and hexamethonium hydroxide (HMOH) solution (0.1 M) were all purchased from Sigma-Aldrich, MO, USA. CE-grade sodium hydroxide (1.0 N) was purchased from Agilent Technologies, Waldbronn, Germany, 0.22 μm nylon filters were purchased from Canadian LifeScience, ON, Canada and hydrochloric acid (HCl) was purchased from Fisher Scientific, Canada. Nanopure water (18.2 MΩ·cm) from Barnstead Nanopure II was used for this work. Most of the thiosalt species are reactive below pH o4 and close to or above pH 9. TMA was titrated with triethanolamine to a pH 8.0 to form the triethanolamine-buffered TMA BGE solution. At this pH TMA is in the fully ionized form and thiosalts are relatively stable. The thiosalts standards, samples and background electrolyte solution were all prepared with nanopure water, degassed and filtered through a 0.22 μm nylon filter before analysis.

4.2.2 Instrumentation

All CE analyses were performed on an Agilent 7100 ^{3D}CE System (Agilent Technologies Canada Inc., Mississauga, Ontario) equipped with a diode array UV-vis detector. Data were acquired at 350.10 nm with references at 200.10 and 254.10 nm (to invert the negative peaks) and processed using an Agilent OpenLAB Chromatography Data System (CDS) ChemStation Edition for corrected peak areas, peak widths and heights, and migration times. Bare fused-silica capillaries (id 50 µm) were obtained from MicroSolv (MicroSolv Technology Corporation, NJ, USA) and were accurately cut to the desired length (48.5 cm) with a 'window' made at 8.5 cm from the detector by burning, using the MicroSolv Window Maker™ (N.J. USA), to remove the polyimide coating. Also, 2 mm of polyimide at the beginning and at the end of the capillaries was removed. Initial conditioning was as follows: flushing at ~ 940 mbar with 1.0 N NaOH for 1 hr, water for 1 hr and BGE for another hr. Daily, the capillary was conditioned with 0.1 N NaOH for 10 min, water for 10 min and BGE for another 10 min. Between injections, the capillary was flushed with 0.1 N NaOH for 1 min, water for 1 min and BGE for 3 min.

4.3. Results and Discussion

4.3.1 Screening design using fractional factorial Design (fFD)

The criteria for choosing the factors and levels for this work were based on previous work done with a pyromellitic (similar in structure to TMA, Figure 4.1) acid BGE system using both univariate and multivariate approaches as well as literature reports.

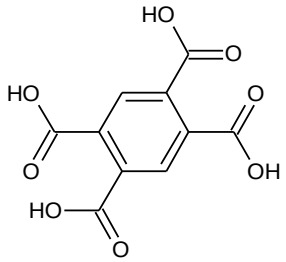

Pyromellitic acid (PMA)

pK_as: 1.91, 2.27, 4,49, 5,63

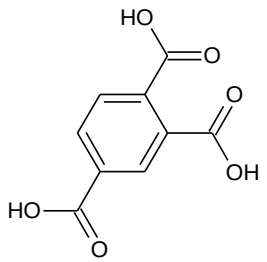

Trimellitic acid (TMA) used in this work

pk_as: 2.52, 3.84, 5.20

Figure 4.1.Structures of BGE chromophoric probes PMA and TMA

In this experimental design setup, six factors ([TMA], [HMOH], injection time (s), cassette temperature (ºC), applied field (kV) and detection wavelength) were selected for the fFD screening experiments to identify the most critical factors for optimization. A resolution of IV was chosen where main effects of the selected factors are confounded by 3-way interactions. This allows for better estimation of the effects of the factors on the desired responses in order to select the critical factors for optimization. A 2-level ¼ fFD with low (-1) and high (+1) settings was chosen yielding 16 experiments plus 1 center point, giving a total of 17 points for the factor screening (Table 4.1).

Table 4.1. Factors and levels for fFD (2^{6-2}) screening experiments

Factor	-1	0	+1
[TMA] (mM)	2.00	3.50	5.00
[HMOH] (mM)	0.50	1.00	1.50
Injection time (s)	2	6	10
Cassette temperature (ºC)	20.0	22.5	25.0
Applied field (kV)	20.0	25.0	30.0
Detection wavelength	200	227	254

The responses studied for this analysis were peak resolution factor (R_s) of adjacent peaks, symmetry (Sym) of the peaks and the analysis time (t). R_s was calculated using the following equation:

$$R_{1,2} = \frac{2\,(t_2 - t_1)}{w_1 + w_2} \qquad 44$$

where t_2 and t_1 are the migration times of two adjacent peaks and w_1 and w_2 are the baseline peak width. See Table 4.2 for further explanation.

Table 4.2. Responses selected for the screening analysis

Response factor	Description
$R_{1,2}$	Adjacent peaks 1 and 2 ($S_2O_3^{2-}$ - $S_5O_6^{2-}$)
$R_{2,3}$	Adjacent peaks 2 and 3 ($S_5O_6^{2-}$ - SO_4^{2-})
$R_{3,4}$	Adjacent peaks 3 and 4 (SO_4^{2-} - $S_3O_6^{2-}$)
$R_{4,5}$	Adjacent peaks 4 and 5 ($S_3O_6^{2-}$ - $S_4O_6^{2-}$)
Sym1	Peak 1 symmetry
Sym2	Peak 2 symmetry
Sym3	Peak 3 symmetry
Sym4	Peak 4 symmetry
Sym4	Peak 5 symmetry
t	Analysis time (min)

Pareto charts of the effects of the factors on the responses were constructed to determine the magnitude and statistical importance of the factors effects at 95% confidence level for all factor level intervals. From the analysis the critical responses identified were $R_{1,2}$, $R_{3,4}$ and t. The Pareto charts (Figure 4.2 A, B and C) show that for $R_{1,2}$, $R_{3,4}$ although none of the factors were statistically critical (beyond the red line) the one most significant factor combination is that for [TMA] and [HMOH]. The other most important factor having effect on the responses was the injection time. For the analysis time (t) (Figure 4.2 C), it was found that several factors and factor combinations were statistically critical for achieving a short migration time (and analysis time). Thus, the factors that have the most influence on the critical responses $R_{1,2}$, $R_{3,4}$ and analysis time (t), selected from the screening experiments for optimization were [TMA], [HMOH], injection time and

applied potential, with the cassette temperature and analysis wavelength set at 25 ºC and 200 nm, respectively.

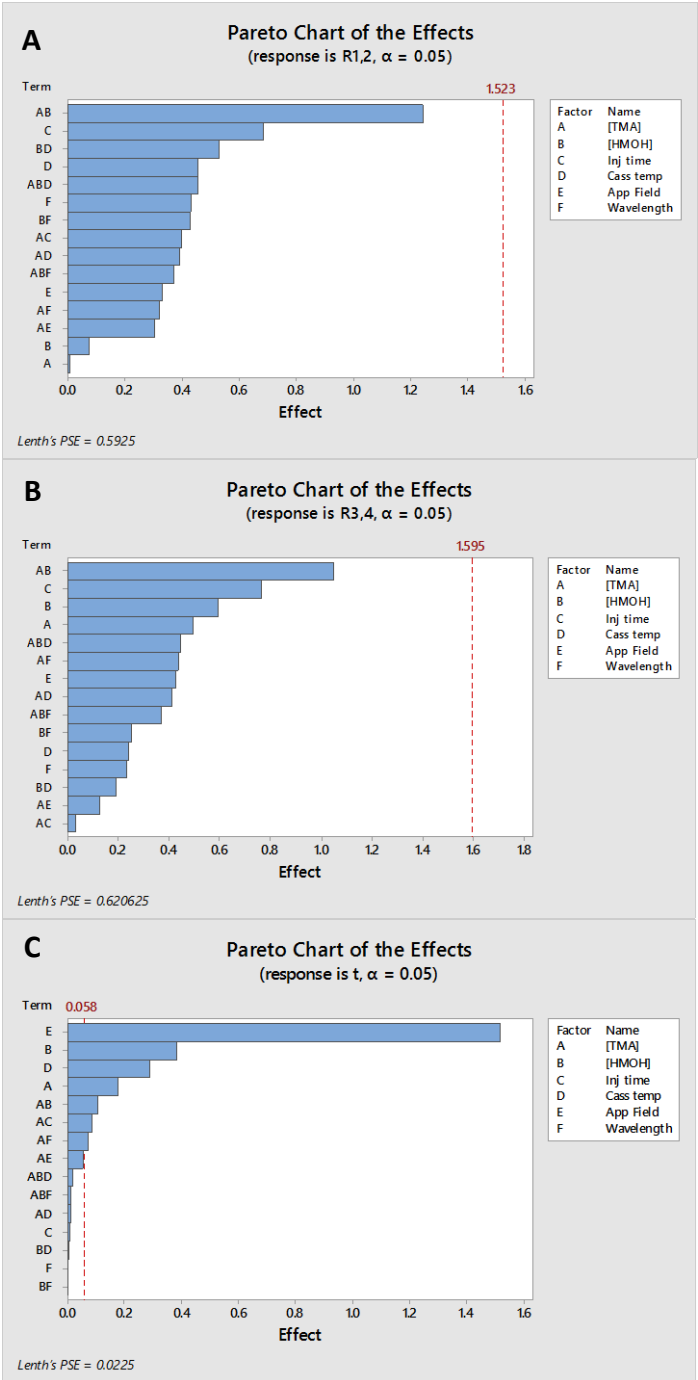

Figure 4.2. Pareto Charts showing the effects of the 6 factors on A. $R_{1,2}$ B. $R_{3,4}$ and C. Analysis time (t)

4.3.2 Optimization design using Box-Behnken response surface design (BBD)

A BBD allows for efficient estimation of the first- and second-order coefficients of the design model using the factor levels selected. The optimal factor levels for the desired responses are expected to be in the experimental domain. The four critical factors selected from the screening experiments that have statistically significant effect on the responses chosen for this work and their levels are shown in Table 4.3. These factors were optimized using a BBD surface response methodology. The BBD required 27 experiments. The results of the optimization analysis are shown in Table 4.4. Figure 4.3 shows five representative electropherograms for the factors at different levels; and the degree of separation of the five thiosalt species.

Table 4.3. Factors and their levels selected for the BBD optimization experiments

Factor	Levels
[TMA]	2.00 – 3.50 – 5.00 (mM)
[HMOH]	0.50 – 1.00 – 1.50 (mM)
Injection time (s)	2 – 6 – 10
Potential (-kV)	20 – 25 – 30

Table 4.4. Results of BBD optimizing experiments

RunOrder	[TMA]	[HMOH]	Inj time	App Field	$R_{1,2}$	$R_{2,3}$	$R_{3,4}$	$R_{4,5}$	t
1	2.00	1.00	6	30	1.39	1.52	1.49	4.85	2.69
2	2.00	1.00	2	25	2.21	2.16	2.05	9.22	3.24
3	3.50	1.50	10	25	0.78	1.32	0.00	4.48	3.21
4	5.00	1.00	6	30	2.41	1.04	0.00	3.79	2.82
5	3.50	1.00	6	25	1.48	2.49	1.30	5.16	3.33
6	5.00	0.50	6	25	1.42	3.68	1.01	10.26	3.74
7	3.50	1.00	6	25	1.55	2.56	1.28	4.96	3.35
8	3.50	1.50	6	20	1.09	2.87	2.15	7.31	4.05
9	2.00	1.50	6	25	1.23	1.76	1.97	5.96	3.22
10	2.00	1.00	10	25	1.21	1.35	1.41	5.79	3.28
11	3.50	0.50	6	20	1.77	2.91	1.04	9.25	4.48
12	2.00	0.50	6	25	2.19	1.65	0.93	9.41	3.47
13	3.50	0.50	10	25	1.45	2.68	0.98	8.64	3.57
14	5.00	1.00	6	20	1.00	3.39	1.02	3.51	3.43
15	3.50	0.50	2	25	2.17	3.91	1.37	10.83	3.58
16	5.00	1.00	2	25	1.34	4.13	0.93	2.93	3.44
17	3.50	1.00	6	25	1.48	2.42	1.18	4.52	3.34
18	3.50	1.00	2	20	1.99	3.53	1.28	6.47	4.10
19	2.00	1.00	6	20	1.72	1.65	1.38	5.45	4.09
20	3.50	1.50	6	30	1.11	2.38	1.94	6.09	2.69
21	3.50	1.00	2	30	1.68	2.77	1.80	8.82	2.79
22	3.50	1.00	10	20	1.29	2.23	1.06	4.47	4.18
23	5.00	1.50	6	25	2.13	1.47	0.00	4.63	3.29
24	5.00	1.00	10	25	2.38	0.93	0.00	3.27	3.42
25	3.50	0.50	6	30	1.75	2.81	1.08	8.75	2.96
26	3.50	1.50	2	25	1.57	3.35	2.41	7.04	3.26
27	3.50	1.00	10	30	1.24	2.09	1.34	4.72	2.78

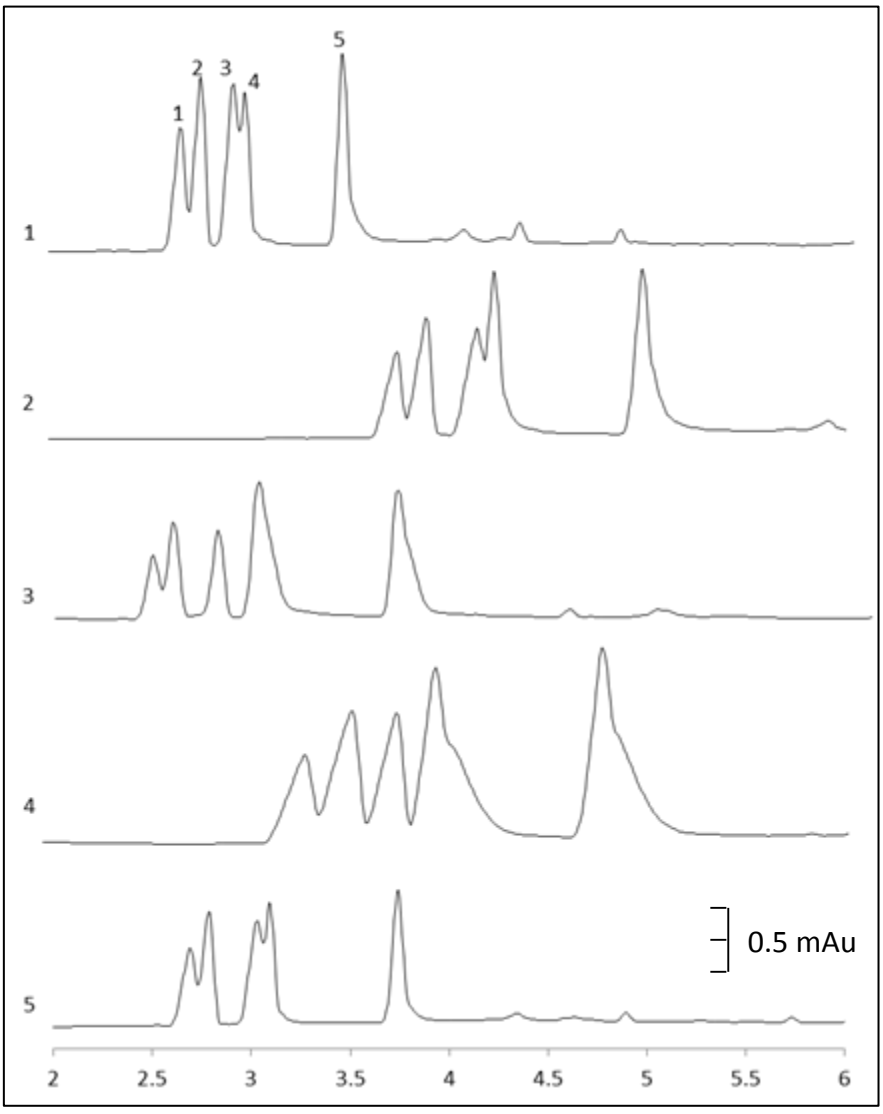

Figure 4.3. Five representative electropherograms from the optimization experiments using BBD experimental design (see Table 4). 1. RunOrder 6; 2. RunOrder 11; 3. RunOrder 19; 4. RunOrder 25; 5. RunOrder 26. Detection $\lambda = 350$, Ref = 200 nm. Thiosalt species: 1. $S_2O_3^{2-}$ (50 µg/mL); 2. $S_5O_6^{2-}$ (25 µg/mL); 3. SO_4^{2-} (20 µg/mL); 4. $S_3O_6^{2-}$ (50 µg/mL); and 5. $S_4O_6^{2-}$ (50 µg/mL)

Table 4.5 shows the targets set for the resolution response factors $R_{1,2}$, $R_{2,3}$, $R_{3,4}$ and $R_{4,5}$; the symmetry factors (Sym) and analysis time (t).

Table 4.5. Response targets for adjacent peak resolution (R_S) and analysis time (t) for the optimizing experiments using BBD

Resolution response	Goal	Target	Minimum	Maximum
$R_{1,2}$ (peak 1 and 2)	Target	2.5	2.0	3.0
$R_{2,3}$ (peak 2 and 3)	Target	2.5	2.0	3.0
$R_{3,4}$ (peak 3 and 4)	Target	2.5	2.0	3.0
$R_{4,5}$ (peak 4 and 5)	Target	5.0	4.0	8.0
Sym1	Target	1.00	0.60	1.60
Sym2	Target	1.00	0.60	1.60
Sym3	Target	1.00	0.60	1.60
Sym4	Target	1.00	0.60	1.60
Sym5	Target	1.00	0.60	1.60
t (min)	minimize	3.0	3.0	3.5

Figure 4.4 below shows the optimization response dashboard of the influence of the separation factors on the targeted responses. The values in red show optimized levels of the factors and instrumental conditions for best desirability for the responses. The individual desirabilities (d) of each response show how the factor levels optimize that response; and the composite desirability (D) shows the overall influence of the factors at different levels, on all the responses. The maximum value for d or D is 1. Each factor can influence one or more of the responses.

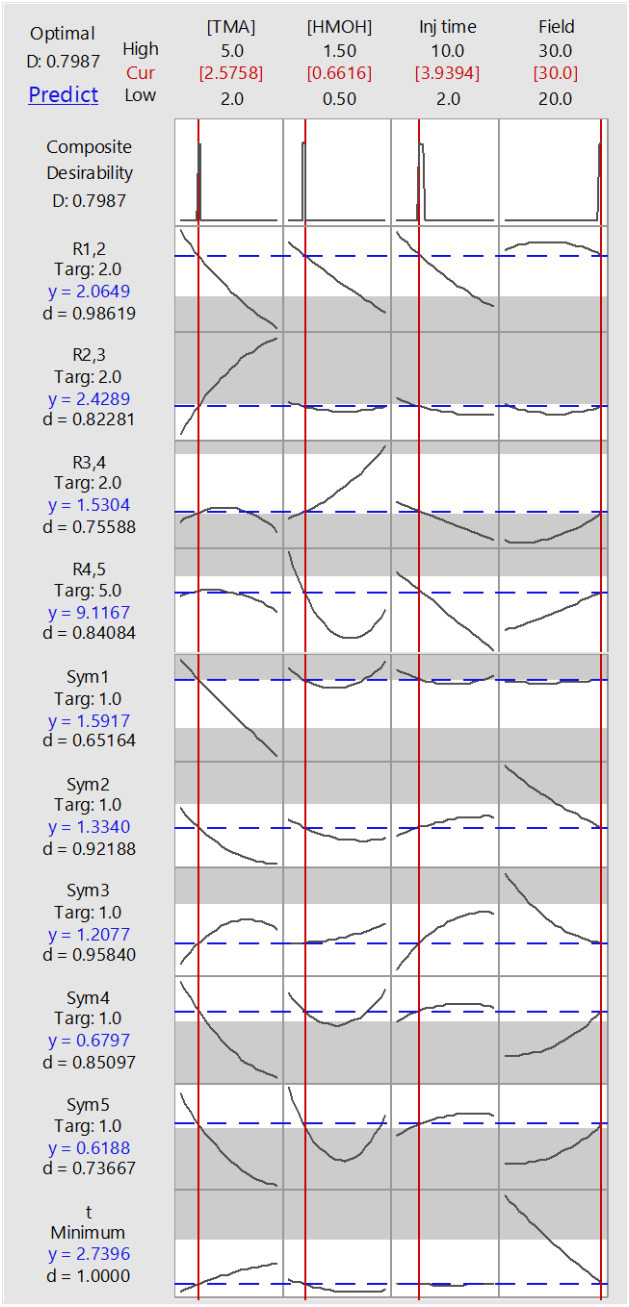

Figure 4.4. Response dashboard showing the optimized factors and levels and their effect on the selected responses

The optimization windows of the factors are very narrow, indicating that a small change in the factor setting can significantly impact the responses. For instance, increasing [TMA] above ~2.70 mM will negatively compromise $R_{1,2}$, Sym1, 2, 4 and 5. In addition, it will be impossible to simultaneously improve $R_{1,2}$ and $R_{2,3}$ with [TMA] as an increase in concentration will lead to a decrease in $R_{1,2}$ and an increase in $R_{2,3}$, although the desirabilities for these responses, at the optimized factor levels are close to the target values with good desirabilities (d = 0.98 and 0.82 respectively). With the exception of Sym3, the peak symmetries Sym1, 2, 4 and 5 are negatively impacted with an increase in [TMA]. For [HMOH], the optimum factor setting was 0.66 mM. Above this concentration, the responses that will be negatively impacted include $R_{1,2}$, $R_{4,5}$ and Sym5. As well, the injection time of between 2 and 10 s (as a function of a constant pressure of 50 mbar), is shown to impact the responses. Different injection times (at constant pressure), will translate to different injection volumes and hence loading. Increasing the loading will lead to increased peak widths and therefore reduction in peak resolution R_s. To ensure that peaks are completely resolved, it may be necessary to sacrifice a little sensitivity for resolution. Injection times were varied from 2 s to 10 s to assess their impact on the responses. An injection time of ~ 4 s, together with the optimum settings of the other factors, led to a high overall desirability factor of 0.8. Finally, as expected, the applied field at the optimum setting of -30 kV was shown to greatly improve the analysis time. Thus, the optimized factor level settings of [TMA] of 2.58 mM, [HMOH] of 0.66 mM, injection time of 4 s and applied field of -30 kV were necessary to attain good desirabilities for all the targeted responses.

4.3.3 Validation and analysis of optimized conditions for TMA BGE system

The optimized values were tested experimentally and the results were compared with the mathematically predicted values for the peak resolution factors (R_s), peak symmetry (Sym) and analysis time (t) of the five thiosalt species. The results of the analysis are summarized in Table 4.6. It can be shown that there was generally good agreement between the predicted and the experimental values with percentage differences ranging from 3.4% to 42.4%. Interestingly, the values yielding the high percentage differences (> 10%) gave experimental results closer (more favourable) to the targeted values than predicted.

Table 4.6. Predicted versus experimental values of peak resolution for PMA BGE system

Response	Predicted	Experimental (n = 3)	% Difference
$R_{1,2}$	2.06	2.32	11.7
$R_{2,3}$	2.43	2.24	8.1
$R_{3,4}$	1.53	1.40	8.9
$R_{4,5}$	9.12	8.76	4.0
Sym1	1.59	1.03	42.4
Sym2	1.33	1.29	3.4
Sym3	1.21	1.06	12.8
Sym4	0.68	0.88	26.1
Sym5	0.62	0.86	32.2
t (min)	2.74	2.89	9.7

In the following section (Section 3.3.4), the response surface plots for optimization analysis of the TMA BGE system are analyzed. The electropherogram obtained from the the optimization experiments showed that the most critical response factors were $R_{1,2}$, $R_{3,4}$, Sym4 and Sym5. Thus only the surface plots for these responses are discussed.

4.3.4 Surface Plot analysis of $R_{1,2}$ and $R_{3,4}$ vs [TMA[and [HMOH]

Using the optimized settings of injection time set of 4 s (at 50 mbar) and applied field at -30 kV (optimum conditions), the influence of the change in [TMA] and [HMOH] on $R_{1,2}$ can be seen in Figure 4.5A. An increase in [TMA] from 2.00 mM to 5.00 mM led to a reduction of $R_{1,2}$ to a minimum value lower than the target value of 2.0. This may be attributed to interaction between the probe ions and the analyte ions at higher probe concentration. Since sensitivity is related to molar displacement ratio of probe ions by the analyte ions, the molar concentration of analyte is important; typically, a low sample concentration relative to that of the probe is expected to reduce peak distortions (broadening, fronting and tailing). Although, the surface plot maxima correspond to low [TMA] of 2.00 mM and low [HMOH] of 0.50 mM, the adjacent peak resolution $R_{1,2}$ at this maximum is higher than the target of 2.0, therefore an increase in [TMA] and [HMOH] is needed to reach the required target setting.

In the surface plot of the effect of interaction between [TMA] and [HMOH] on peak resolution factor $R_{3,4}$ (Figure 4.5B), a different trend to that of $R_{1,2}$, is seen. The

maximum point (corresponding to $R_{3,4}$ of ~ 2.5) corresponds to low [TMA] at 2.00 mM and high [HMOH] at 1.50 mM. To reach the target of 2.0, a mid-point may be favorable. The final optimum conditions of [TMA] = 2.58 mM, [HMOH] = 0.66 mM shows that a compromise is needed between [TMA] and [HMOH] to achieve the target and not compromise the other response targets.

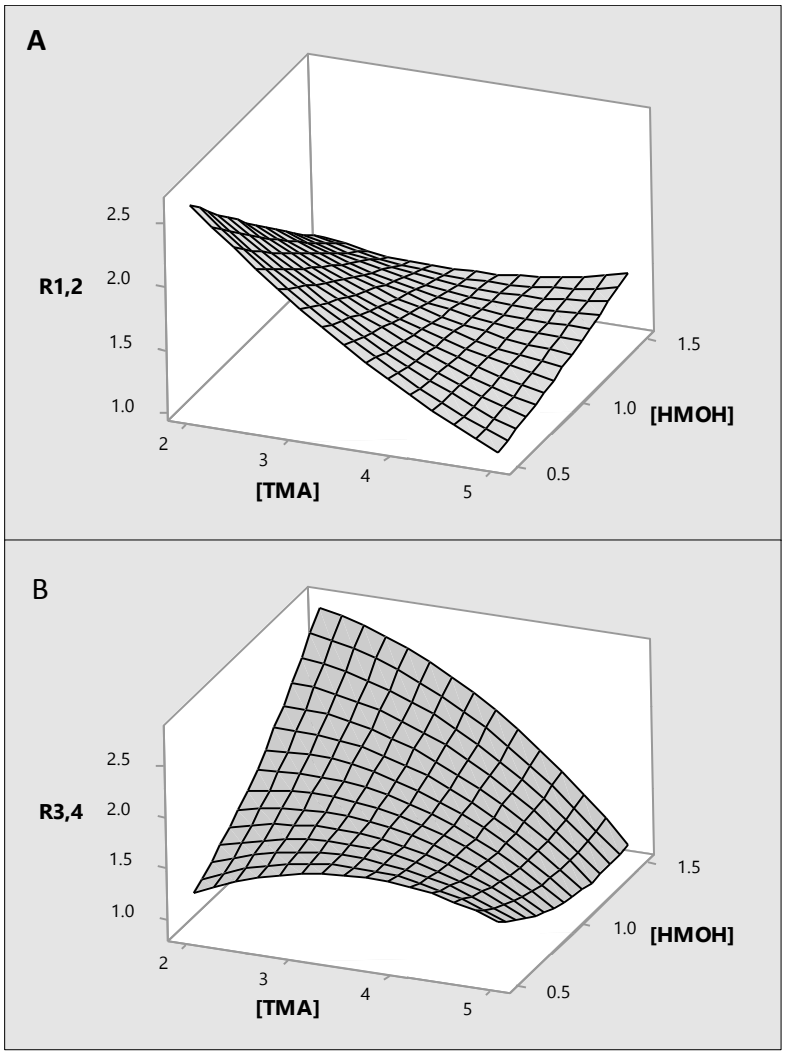

Figure 4.5. 3-D response surface plots of the effect of interaction between [TMA] and [HMOH] on peak resolution factors (A) $R_{1,2}$ and (B) $R_{3,4}$.

4.3.5 Surface Plot analysis of Sym4 and Sym5 vs [TMA[and [HMOH]

The 3-D surface plots of the effect of [TMA] and [HMOH] on peak symmetry are shown in Figure 4.6 A and B. Interestingly, these two plots look similar with slighted folded 'slide' shapes. Thus the maxima occurred at low [TMA] and either low or high [HMOH]. An increase in [TMA] led to a significant reduction in the peak symmetries of $S_3O_6^{2-}$ and $S_4O_6^{2-}$ however at every [TMA] (from 2.00 mM to 5.00 mM), a high or a low value (0.50 mM or 1.50 mM) of [HMOH] was needed to improve the symmetries. For better peak symmetries (close to 1.0), it is preferable to have low [TMA] and avoiding the mid-point value of 1.00 mM for [HMOH]. A compromise was reached for Sym4 and Sym5 at the optimum concentrations of TMA and HMOH set with the model ([TMA] = 2.58 mM, [HMOH] = 0.66 mM) with values (0.68 and 0.88 respectively) that were closer to the target value of 1.00. Interestingly, however the experimental values (0.88 and 0.86) were much better (closer to 1.00).

4.3.6 Peak splitting in TMA BGE

Peak splitting was observed for some of the analyte peaks as shoulder peaks on the tail side of the main analyte peak (Figure 4.7). Peak splittings have been seen by other researchers and are thought to be caused by a number of factors such as high analyte concentration, particularly thiosulfate;[29] presence of ionizable groups in the analyte molecule that can form complexes with the buffer constituents,[30] and excessive dispersion and separation of neutral and charged species of the same analyte.[31] In this work, peak splitting occurred for trithionate and tetrathionate peaks at low ($\leq$ 0.5 mM)

and high concentrations (≥ 1.5 mM) of [HMOH]. This may be attributed to interactions with the analytes, possibly incomplete formation of ion-pair complexes at low concentrations and interactions with HM^{2+} adsorbed to the capillary surface. Further research is required to fully understand more clearly this phenomenon.

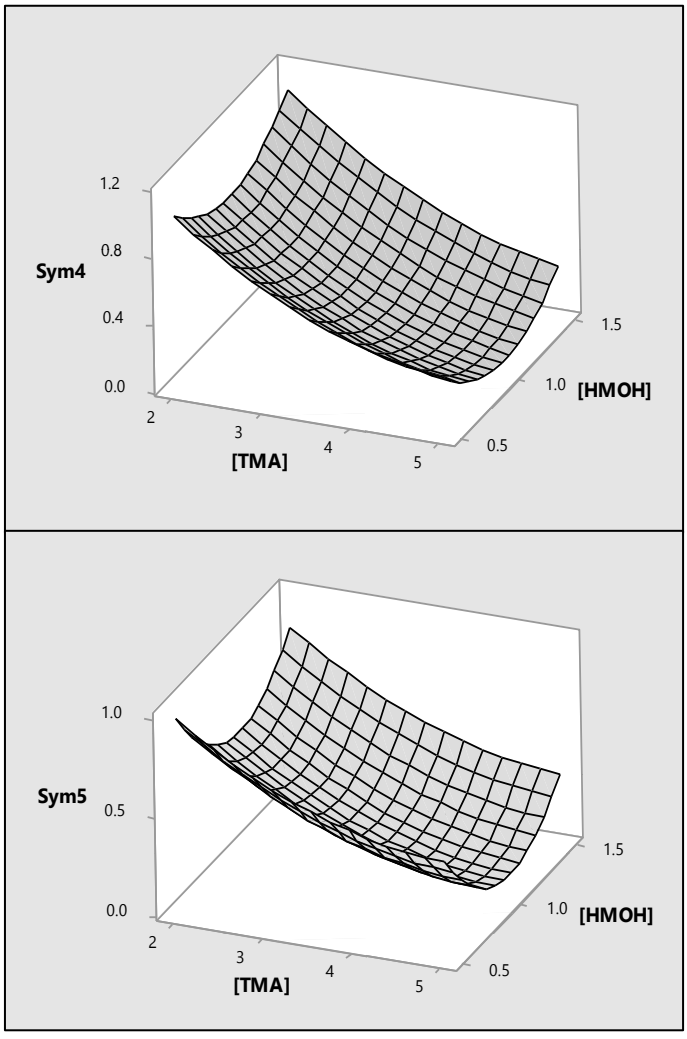

Figure 4.6. 3-D response surface plots of the effect of interaction between [TMA] and [HMOH] on peak symmetry factor Sym4.

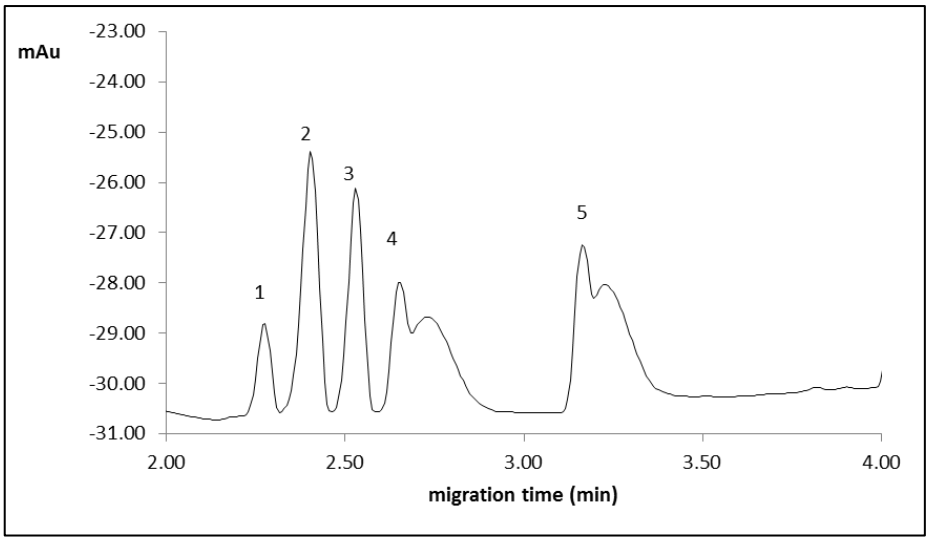

Figure 4.7. Electropherogram showing peak splitting of trithionate and tetrathionate peaks. 1. $S_2O_3^{2-}$ (50 µg/mL); 2. $S_5O_6^{2-}$ (25 µg/mL); 3. SO_4^{2-} (20 µg/mL); 4. $S_3O_6^{2-}$ (50 µg/mL); and 5. $S_4O_6^{2-}$ (50 µg/mL)

4.3.7 Figures of merit and application of optimized method for real world samples

The optimal conditions were applied to the analysis of five thiosalt anion mixtures. Good separation of all analyte peaks (Figures 4.8A) was achieved in less than 3 min. However, as can be seen $R_{3,4}$ was not completely baseline as predicted by the model ($R_{3,4}$ = 1.5 predicted and experimental $R_{3,4}$ = 1.5). Thus, the separation was further optimized by reducing the applied field to -25 kV (Figure 4.8B). The final optimized conditions gave good reproducibility for migration times and peak areas for all the thiosalt species. The concentrations of the standards used were as follows: 1. $S_2O_3^{2-}$ (50 µg/mL); 2. $S_5O_6^{2-}$ (25 µg/mL); 3. SO_4^{2-} (20 µg/mL); 4. $S_3O_6^{2-}$ (50 µg/mL); and 5. $S_4O_6^{2-}$ (50 µg/mL);

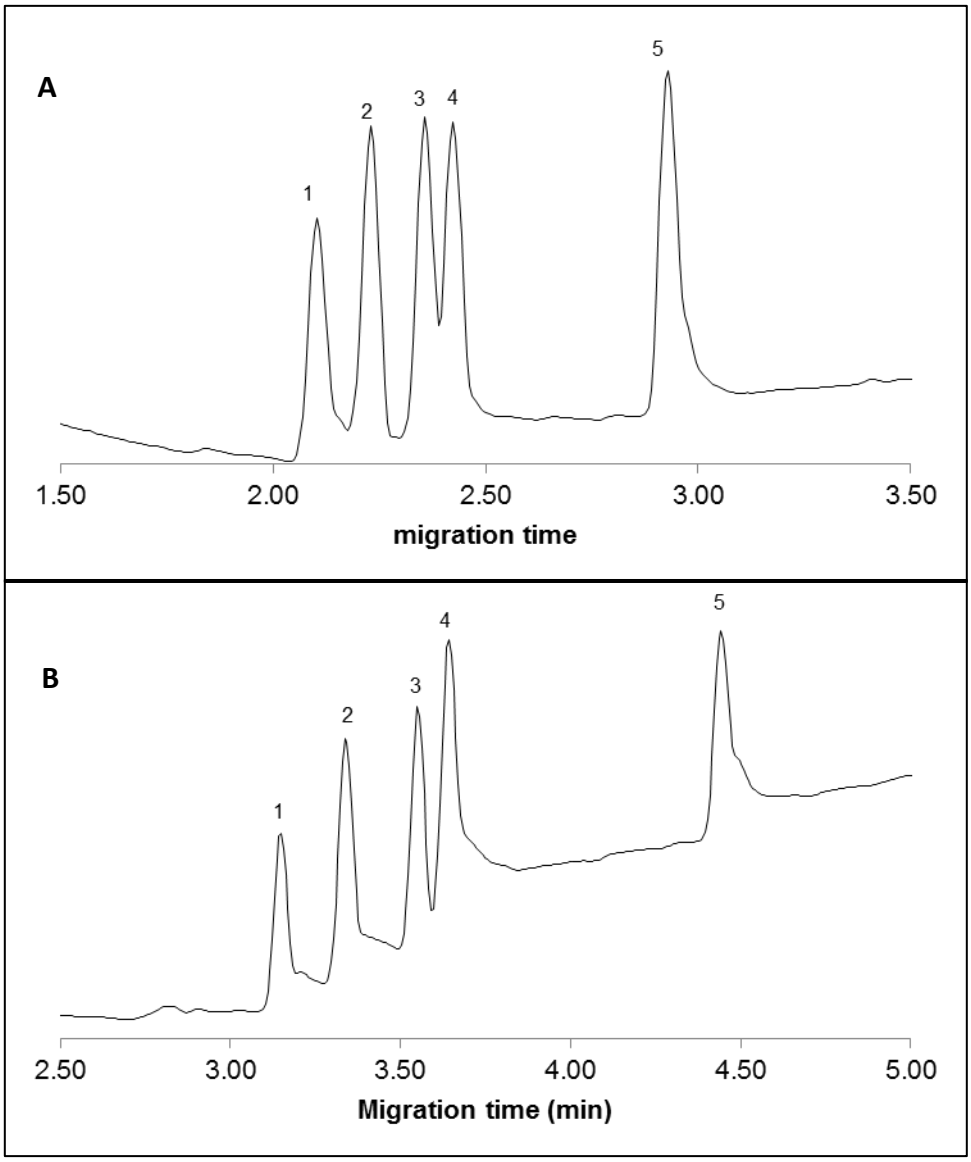

Figure 4.8. Electropherogram showing (A) the separation of five thiosalt species using optimized separation conditions: [TMA]: 2.58 mM, [HMOH]: 0.66 mM, applied field: -30 kV. (B) Same conditions as (A) but applied field: -25 kV Thiosalt species: 1. $S_2O_3^{2-}$ 2. $S_6O_6^{2-}$ 3. SO_4^{2-} 4. $S_3O_6^{2-}$ 5. $S_4O_6^{2-}$ 6. $S_5O_6^{2-}$

Figures of merit are presented in Table 4.7 including migration times, LODs, relative standard deviations (RSD) of migration times and peak areas. The LOD values determined for the thiosalt species were much better than reported values in the literature for these species. The RSD values were calculated for a mixture of the five species at 40 µg/mL each.

Table 4.7. Limit of LOD values (µg/mL) and RSD values for migration time and peak areas for five thiosalt species analyzed at the optimum BGE conditions. Number of analysis (n) = 3 and detection λ = 350 nm, Ref λ = 200 nm.

Analyte	Average migration time (min)	LOD (µg/mL)	RSD migration time (%) (n = 3)	RSD peak area (%) (n = 3)
SO_4^{2-}	2.1	0.2	0.1	1.7
$S_2O_3^{2-}$	2.2	0.3	0.2	3.9
$S_3O_6^{2-}$	2.3	0.4	0.2	6.4
$S_4O_6^{2-}$	2.4	0.3	0.2	9.7
$S_5O_6^{2-}$	2.9	0.2	0.3	4.5

For the real world analysis, samples were taken from a mine tailings pond and analyzed for the presence of thiosalts using a standard addition method. Samples were diluted 1:50, spiked with different concentration of thiosalt standards and analyzed. Figure 4.9 shows the electropherogram of 1:50 real sample and a spiked sample with 40 µL of thiosalt standard mixture containing 6 µg/mL of each of the five species. Table 4.8 shows the

results from the analysis. All the five thiosalt species were detected in the tailings sample, with the concentration of thiosulfate (SO_4^{2-}) > 500 µg/mL, that of sulfate (SO_4^{2-}) close to 400 µg/mL, and [$S_3O_6^{2-}$] and [$S_5O_6^{2-}$] > 50 µg/mL. The concentration of $S_4O_6^{2-}$ was found to be < 50 µg/mL.

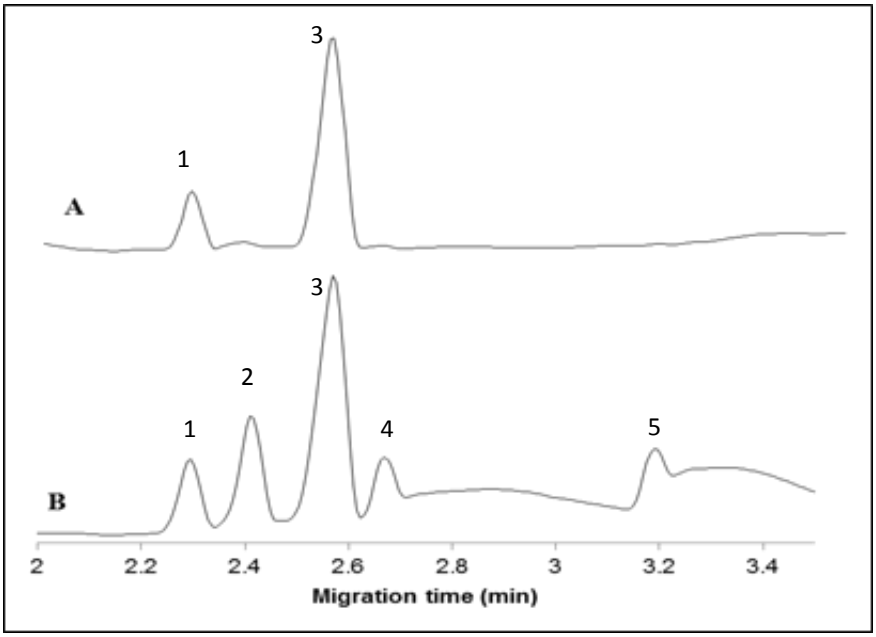

Figure 4.9. Electropherograms of 1:50 diluted real sample (A) and real sample spiked with 40 µL of 6 µg/mL thiosalt mixture standard solution. 1. $S_2O_3^{2-}$ 2. $S_5O_6^{2-}$ 3. SO_4^{2-} 4. $S_3O_6^{2-}$ 5. $S_4O_6^{2-}$

Table 4.8. Results from the analysis of a tailings pond sample using standard addition calibration

Thiosalt species	Amount in tailings pond sample (μg/mL±SD)
SO_4^{2-}	521.4 ± 52.1
$S_2O_3^{2-}$	379.5 ± 25.5
$S_3O_6^{2-}$	54.3 ± 6.6
$S_4O_6^{2-}$	39.5 ± 7.4
$S_5O_6^{2-}$	59.2 ± 2.7

4.4 Concluding remarks

The quest for reliable and high quality data from environmental, pharmaceutical and forensic samples has called for the need to develop robust and reliable analytical methods for their analysis. The complexity of such samples requires techniques that can resolve all the components and quantify them accurately. Furthermore, the instability of thiosalts requires high throughput. In this work, a CZE with indirect detection was developed using fFD for screening six factors from which four factors were chosen ([TMA], [HMOH], injection time and applied field) as critical to optimization. The important responses assessed in method optimization using BBD, were peak resolution $R_{1,2}$ and $R_{3,4}$; and peak symmetry (Sym4 and Sym5). The final optimized conditions gave good separation of all five analyte peaks in 3 min with highly reproducible migration times (RSD < 0.3 %) and peak areas (RSD < 10 %). The method gave LOD values of < 0.5 μg/mL. Finally the optimized method was applied successfully to the analysis of real thiosalt tailings pond sample.

4.5 References

[1] Wasserlauf, M.; Dutrizac, J.E. In The chemistry, generation and treatment of thiosalts in milling effluents – A non-critical summary of CANMET investigations 1976-1982, CANMET Report 82-4E, 1982.

[2] Garcia, C.; Ballester, A.; Gonzalez, F.; Blazquez, M.L. Pyrite behavior in a tailings pond. *Hydrometallurgy*. **2005**, *76*, 25-36.

[3] Vongporm, Y. Thiosalt behavior in aqueous media. Master of Engineering Thesis. Memorial University of Newfoundland, 2008.

[4] Goldhaber, M. Experimental study of metastable sulfur oxyanion formation during pyrite oxidation at pH 6-9 and 30 C. *Am. J. Sci.* **1983**, *283*, 193-217.

[5] Masau, R.; Oh, J.; Suzuki, I. Mechanism of oxidation of inorganic sulfur compounds by thiosulfate-grown *Thiobacillus thioxidans*. *Can. J. Microbiol.* **2001**, *47*, 348-358.

[6] Dinardo, O.; Sally, J. In *Treatment of thiosalts in milling effluent: A review of treatment process*. Mining and Mineral Sciences Laboratories Report. Thiosalts Consortium-Phase II. CANMET-MMSL, 1998.

[7] Fahd, F.; Khan, F.; Hawboldt, K.; Abbassi, R. Developing a Novel Methodology for the Ecological Risk Assessment of Thiosalts. *Stoch. Environ. Res. Risk Assess.* **2014,** *28*, 383-391.

[8] Timberbaev, A. R., Analysis of inorganic pollutants by capillary electrophoresis. *Electrophoresis.* **1997**, *18*, 185-195.

[9] Kaniansky, D.; Masár, M.; Marák, J.; Bodor. Capillary electrophoresis of inorganic anions. *J. Chromatogr. A*. **1999**, *834*, 133-178.

[10] Timberbaev, A.R.; Dabek-Zlotorzynska, E.; van den Hoop, M.AG.T. Inorganic Environmental Analysis by Capillary Electrophoresis. *Analyst*. **1999**, *124*, 811-826.

[11] Zhao, S., Zhang, R., Wang, H., Tang, L., Pan, Y. Capillary electrophoresis enantioselective separation of vigabatrin enantiomers by precolumn derivatization with dehydroabietylisothiocyante and UV-vis detection. *J.Chromatogr. B. Anal. Technol. Biomed. Life Sci*. **2006**, 833, 186-190.

[12] Hiissa, T., Sirén, H., Kotiaho, T., Snellman, M., Hautojärvi, A. Quantification of anions and cations in environmental water samples. Measurements with capillary electrophoresis and indirect-UV detection. *J. Chromatogr. A*. **1999**, 853, 403-411.

[13] Orlandini, S.; Gotti, R.; Furlanetto, S. Multivariate optimization of capillary electrophoresis methods: A critical review. *J. Pharm. Biomed. Anal.* **2014**, *87*, 290– 307.

[14] Hanrahan, G.; Lu, K. Application of factorial and response surface methodology in modern experimental design and optimization. *Crit. Rev. Anal. Chem*. **2006**, *36*, 141–151.

[15] McCourt, J.; Stroka, J.; Anklam, E. Experimental design-based development and single laboratory validation of a capillary zone electrophoresis method for the determination of the artificial sweetener sucralose in food matrices. *Anal. Bioanal. Chem*. **2005,** *382*, 1269-1278.

[16] Altekar, M.; Homon, C.A.; Kashem, M.A.; Mason, S.W.; Nelson, R.M.; Patnaude, L.A.; Yingling, J.; Taylor, P.B. Assay Optimization: A Statistical Design of Experiments Approach. *Clin. Lab. Med.* **2007**, 27, 139–154.

[17] Montes, R.; Dahdouh, F.; Riveros, T.A.; Hanrahant G.; Gomez, F.A. Chemometrical Experimental Design-Based Optimization Studies in Capillary Electrophoresis Applications. *LC GC North America*. **2008**, 82-88.

[18] Hanrahant G.; Montes, R.; Gomez, F. A Chemometric experimental design based optimization techniques in capillary electrophoresis: a critical review of modern applications. *Anal. Bioanal. Chem*. **2008**, *390*, 169–179.

[19] Liu, H.; Song, J.; Han, P.; Li, Y.; Zhang, S.; Liu, H.; Wu, Y. Separation and determination of 2,4-D, dicamba and 2,4,5-T in tobacco by nonaqueous capillary electrophoresis. *J. Sep. Sci.* **2006**, *29*, 1038-44.

[20] José Antonio Jurado-González, J.A.; Galindo-Riaño, M.D.; García-Vargas, M. Factorial designs applied to the development of a capillary electrophoresis method for the analysis of zinc, sodium,calcium and magnesium in water samples. *Talanta*. **2003**, *59*, 775-783.

[21] Zhu, D.; X. Li, X.; Sun, J.; You, T. Chemometrics optimization of six antihistamines separations by capillary electrophoresis with electrochemiluminescence detection. *Talanta*. **2012**, *88*, 265–271.

[22] Meinhart, A.D.; Bizzotto, C.S.; Ballus, C.A.; Prado, M.A.; Bruns, R.E.; Filho, J.T.; Godoy, H.T. Optimisation of a CE method for caffeine analysis in decaffeinated coffee. *Food Chem*. **2010**, *120*, 1155–1161.

[23] Lopez-Gazpio, J.; Garcia-Arrona, R.; Ostra, M.; Millan, E. Optimization and validation of a nonaqueous micellar electrokinetic chromatography method for determination of polycyclic musks in perfumes. *J. Sep. Sci.* **2012**, *35*, 1344–1350.

[24] Y.-C. Cheng, Y.-C.; Wang, C.-C.; Chen, Y.-L.; Wu, S.-M. Large volume sample stacking with EOF and sweeping in CE for determination of common preservatives in cosmetic products by chemometric experimental design. *Electrophoresis.* **2012**, *33*, 1443–1448.

[25] Anres, P.; Delaunay, N.; Vial, J.; Gareil, P. A chemometric approach for the elucidation of the parameter impact in the hyphenation of field-enhanced sample injection and sweeping in capillary electrophoresis. *Electrophoresis*. **2012**, *33*, 1169–1181.

[26] Muzikář, M.; Havel, Miroslav, J.; Macka, M. Capillary electrophoresis determinations of trace concentrations of inorganic ions in large excess of chloride: Soft modelling using artificial neural networks for optimization of electrolyte composition. *Electrophoresis*. **2003**, *24*, 2252–2258.

[27] Kelly, D. P.; Wood, A. P. Synthesis and determination of thiosulfate and polythionates. *Methods Enzymol.* **1994**, *243*, 475-500.

[28] Pappoe, M.; Lucas, H.; Bottaro, C.; Dawe, L.N. Single Crystal Structural Characterization of Tri-, Tetra and Pentathionates. *J. Chem. Crystallogr.* **2013**, *43*, 596–604.

[29] O'Reilly, J.W.; Dicinoski, G.W.; Miura Y.; Haddad P.R. Separation of thiosulfate and the polythionates in gold thiosulfate leach solutions by CE. *Electrophoresis*. **2003**, *24*, 2228-2234.

[30] Chen, X., Xie, J.; Li, C.; Hu, Z.; Chen, X. Investigation of the factors that induce analyte peak splitting in capillary electrophoresis. *J. Sep. Sci.* **2004**, *27*, 1005-1010.

[31] Ermakov, S. V.; Zhukov, M. Yu; Capelli, L.; Righetti, P. Experimental and Theoretical Study of Artifactual Peak Splitting in Capillary Electrophoresis. *Anal. Chem*. **1994**, *66*, 4034 – 4042.

Chapter 5

Determination of Association Constants of Trication-Thiosalt Ion pairs using positive mode electrospray ionization time-of-flight mass spectrometry

5.1 Introduction

Thiosalts are sulfur oxyanions associated with mining and milling of sulfidic minerals; their key impact is acidification of receiving environments.[1,2] These anions are usually analyzed by ion exchange chromatography (IEC),[3,4] or more recently capillary zone electrophoresis (CZE) with UV-vis detection.[5-8] When samples are complex or when matrix effects interfere with expected migration behaviour, the use of retention or migration time for anion identification maybe impossible and UV-vis lacks necessary specificity. New approaches for thiosalt analysis, particularly mass spectrometric (MS) techniques for detection, can yield improved detection limits and unequivocal anion identification. In recent years, tricationic alkyl-linked imidazolium and phosphonium salts have been shown to be good ion-pairing reagents for singly and doubly charged anions, forming stable gas-phase adducts with these anions. Divalent ions studied with these ion-pairing reagents included thiosalt species such as sulfate (SO_4^{2-}), thiosulfate ($S_2O_3^{2-}$) and tetrathionate ($S_4O_6^{2-}$).[9-13] Ion-pairs with these bulky ion-pairing reagents are formed in a 1:1 ratio with net charge of +1 making thiosalt analysis more sensitive by increasing the m/z at which the analyte species are measured, and facilitating use of the more sensitive positive-mode ESI-MS.

Conceptually, ion-pair formation in solution is a multistep process involving the successive exclusion of solvent molecules in the solvation sphere of the ions and formation of a compact ion pair. Thus, there is a transition from solvent-separated ion-

pair (SSIP), through a solvent-shared ion-pair (SIP) to the final compact ion-pair (CIP) system. When the ion-pairs are successfully transferred to the gas-phase by ESI, desolvation strengthens non-covalent interactions (such as electrostatic, π-π and hydrogen bonding) between these ion pairs.[14] A summary of the steps involved in ion-pairing between a thiosalt (TS) ion and an ion-pairing (IP) reagent in solution and the transition through the desolvation stages are shown in Figure 5.1.

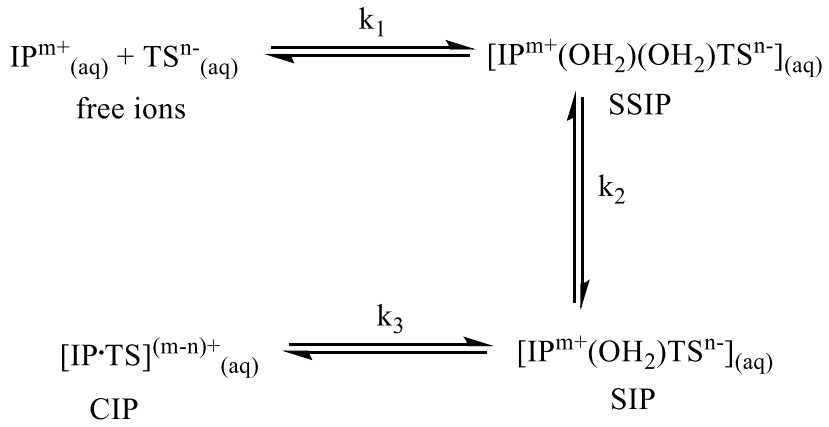

Figure 5.1. A multistep equilibrium for ion-pair formation between a thiosalt (TS) and an ion-pairing reagent (IP). k_1, k_2 and k_3 are step-wise equilibrium constants. (Adapted from Ref. 14)

Ion-pairing reagents have been evaluated in a number of analytical systems in terms of their efficiencies in analytical separations, spectroscopic behaviour, binding affinities for non-covalent ion-pairs, etc.[15-18] Research has focused on understanding the mechanisms involved in the formation of these ion-pairs, such as thermodynamic properties, influence

of the solvation environment, and kinetics.[19-24] Particularly important is the study of the association (stability) constants of these ion-pairs in solution and the gas phase. Nuclear magnetic resonance (NMR), mass spectrometry (MS), UV-vis and Raman spectroscopy have all been used in these studies. Studies involving MS are of special interest since formation of an ion-pair that remains stable in the ionization process and in gas phase is required for detection.[25] The transfer of such non-covalent ion-pairs into the gas phase by ESI has been well documented.[26-27]

Some environmentally-important studies of ionic analytes using ion-pairing reagents with ESI-MS have been reported.[10,12,28,29] For example, this technique was applied by Magnuson *et al.*[28] for the analysis of perchlorate in drinking water with detection limits of 100 ng/L This approach was extended to some sulfur oxyanions species by Warnke *et al.*,[2] Breitbach *et al.*,[4] and Gerardi *et al.*[29] Breitbach *et al.* evaluated 16 different tricationic ion-pairing reagents of various types with ESI-MS to detect divalent anions including SO_4^{2-} and $S_2O_3^{2-}$. LODs achieved for the sulfur oxyanions with these imidazolium, phosphonium or pyrrolidinium containing ion-pair reagents were much lower than using CE or IC with UV-Vis: 0.1 ng to 2.75 ng for SO_4^{2-} and 0.1 ng to 5.2 ng for $S_2O_3^{2-}$. They found that for the linear tricationic reagents, alkyl linkages between charged moieties of six to ten carbons gave optimal pairing response. Warnke *et al.*[2] also evaluated two trigonal and two linear tricationic pairing reagents for several divalent anions including tetrathionate ($S_4O_6^{2-}$) and detected them in the positive mode ESI-MS. For tetrathionate LOD values of 5.0×10^{-4} ng/mL and 2.2×10^{-2} ng/mL were measured

for the linear phosphonium-based and imidazolium-based trication pairing reagents respectively, and 2.5 x 10^{-2} ng/mL and 5.0 x 10^{-2} ng/mL for the trigonal phosphonium-based and imidazolium-based trication pairing reagents respectively. In 2012, Gerardi *et al.*[29] used CE-ESI-MS with 1,3,5-tris [(tripropylphosphonium) methyl]benzene (IP-T-Imid) to analyze sulfate, thiosulfate and benzenedisulfonate with good separation and LODs in tens of ng/mL.

The primary objective of the work presented here is to evaluate the strength of the interactions (binding energies) between three tricationic ion-pairing reagents (Figure 5.2) and a suite of four key environmentally-occurring thiosalt anions (Figure 5.3) using flow injection analysis (FIA) technique for the anions and post-column addition (via a mixing tee) of tricationic ion-pair reagents, followed by ESI-MS analysis. This type of study, especially the strength of ion-pairing interactions between tricationic ligands and thiosalts, has not been undertaken or published. In addition to elucidating the strength of association, the data obtained from this study will enable selectivity tuning as well as sensitivity determination for the thiosalt species in complex environmental media.

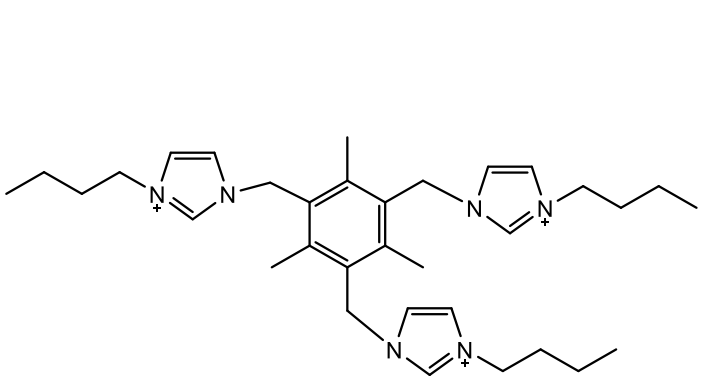

IP-T-Imid

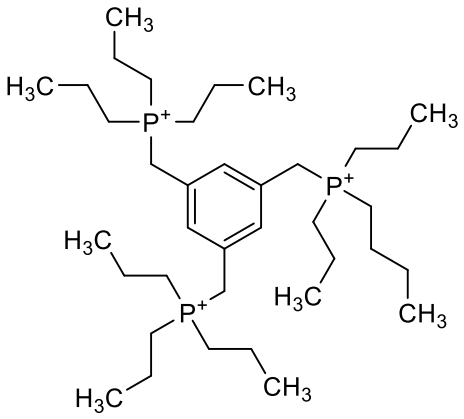

IP-T-Phos

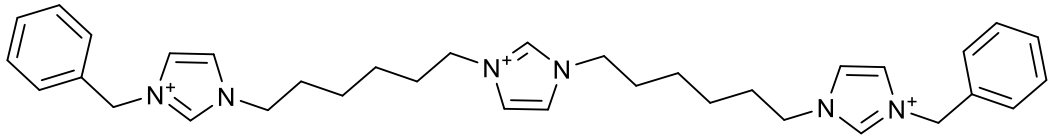

IP-L-Imid

Figure 5.2. Structures of trigonal and linear tricationic ion-pairing reagents: 1,3,5-tris[(3-butyl-imidazolium)methyl]-2,4,6-trimethylbenzene (IP-T-Imid); 1,3,5-tris[(tripropylphosphonium) methyl]benzene (IP-T-Phos); and 1,3-bis[6-(3-benzyl-1-imidazolio)-hexyl]imidazolium (IP-L-Imid)

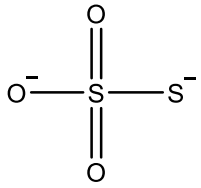

thiosulfate

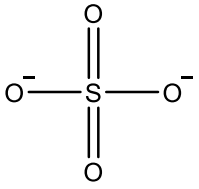

sulfate

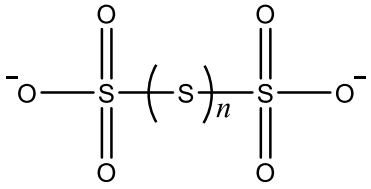

n=1: trithionate

n=2: tetrathionate

Figure 5.3. Structures and names of thiosalt species used in this study

5.2 Materials and methods

5.2.1 Chemical reagents, solutions and sample preparation

All reagents and solvents used for this study were of analytical grade unless otherwise noted. Thiosalt (sulfur oxyanion) species (Figure 5.3) were purchased from Sigma-Aldrich (MO, USA) except sodium trithionate, which was synthesized using a modified method after Kelly *et al.*[30] Details of the synthesis and characterization of the single crystals of sodium trithionate have been published elsewhere.[31] Tricationic ion-pairing reagents 1,3,5-tris[(3-butyl-imidazolium)methyl]-2,4,6-trimethylbenzene (IP-T-Imid); 1,3,5-tris [(tripropylphosphonium)methyl]benzene (IP-T-Phos); 1,3-bis[6-(3-benzyl-1-imidazolio)-hexyl]imidazolium (IP-L-Imid) in the fluoride form (in 50/50 v/v methanol/water) were all obtained from Sigma-Aldrich, MO, USA. These were diluted as needed with 50/50 v/v nanopure water/HPLC grade methanol (Sigma-Aldrich, MO, USA). Nanopure water (18.2 MΩ·cm) used for this work was from a Barnstead Nanopure II (CA, USA) water purification system. HPLC grade sodium hydroxide was purchased from Agilent Technologies (Waldbronn, Germany), 0.22 µm nylon filters were obtained from Canadian Life Sciences (ON, Canada) and hydrochloric acid (trace metal grade) was from Fisher Scientific, Canada.

5.2.2 Instrumentation and experimental setup

Analyses were performed with an Agilent 1260 Infinity LC System coupled to an Agilent 6230 time-of-flight (TOF) LC/MS System (Agilent Technologies, Mississauga, ON).

Methanol/water (50/50 v/v) system was used as eluting solvent. The ionization source was a dual electrospray ionization (ESI) source operated in the positive mode. In the ionization chamber, the nebulizer pressure was set at 10 psi; the drying gas flow rate and temperature were set at 13.0 L/min and 300 °C, respectively. With the ESI parameters held constant and capillary voltage at 4 kV, the TOF parameters were optimized using a surface response experimental design approach to achieve the highest signal count for the ion-pair reagent ion ($[IP]^{3+}$) and trication-thiosalt ion-pair ($[IP{\cdot}TS]^{+}$). The final conditions were: fragmentor voltage 96 V, skimmer 20 V and Oct 1 RF V_{pp} 652 V. The scan range was set to the range 100 – 1000 m/z. Mass calibration and tuning were performed each day before experiments were performed. Data collection and analysis were performed using MassHunter workstation software (version B.05.00). The concentrations of the four thiosalt species were set at 2 μM and the ion-pair reagents were varied from 0.5 μM to 10 μM. The volume of samples injected was 5 μL except for sulfate for which 20 μL was injected. Each titration had seven levels and was performed at least two times.

5.3 Results and discussion

5.3.1 Mass spectrometric analysis

All full scan spectra obtained showed the presence of the 1:1 trication-thiosalt ion-pairs. Table 5.1 shows the ion-pairs monitored in this work. The mass spectra of an equimolar amount (10 µM) of IP-T-Imid and $S_2O_3^{2-}$ is shown in Figure 5.4.

Table 5.1. Trication-thiosalt ion- pairs $[IP{\cdot}TS]^+$ and their corresponding m/z value monitored in positive mode ESI-TOF for the 12 systems

Ion-pair system	Thiosalt ion	m/z of ion-pair
IP-T-Phos	SO_4^{2-}	693
	$S_2O_3^{2-}$	709
	$S_3O_6^{2-}$	789
	$S_4O_6^{2-}$	821
IP-T-Imid	SO_4^{2-}	627
	$S_2O_3^{2-}$	643
	$S_3O_6^{2-}$	723
	$S_4O_6^{2-}$	755
IP-L-Imid	SO_4^{2-}	647
	$S_2O_3^{2-}$	663
	$S_3O_6^{2-}$	743
	$S_4O_6^{2-}$	775

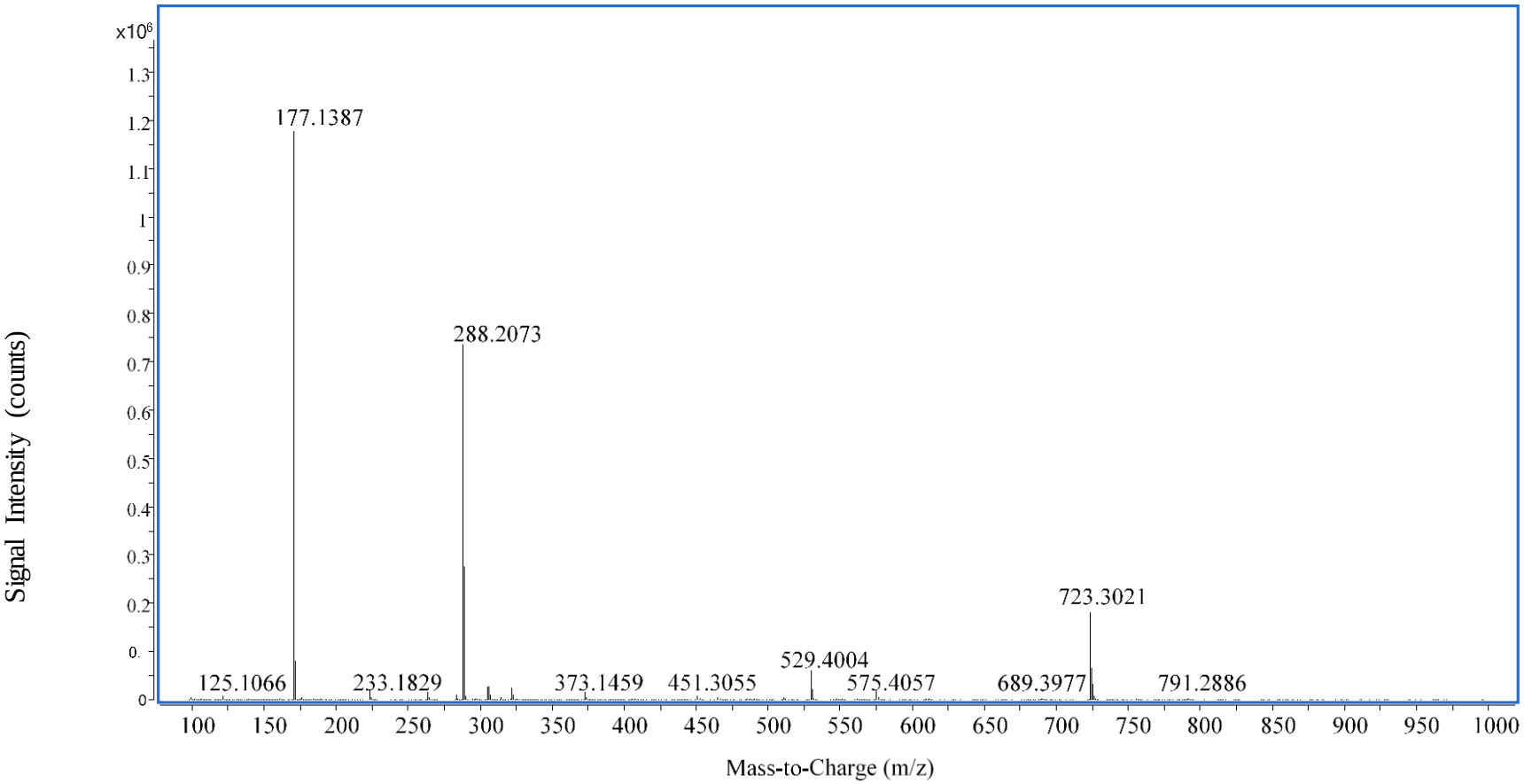

Figure 5.4. FIA-ESI-TOF mass spectrum showing ion-pair signals for equimolar (10 µM each) of IP-T-Imid and $S_3O_6^{2-}$ showing $[IP\text{-}T\text{-}Imid \cdot S_3O_6^{2-}]^+$ (m/z 723) and that of $[IP\text{-}T\text{-}Imid^{3+}]$ alone (m/z 177)

5.3.2 Gas phase evaluation of association constant K_{assoc}

The basic assumption for the evaluation of the gas phase K_{assoc} is that there is a 1:1 binding of the ion-pair reagent and the thiosalt species. The tricationic ion- pairing reagents have three permanent positive charges (IP^{3+}) and the thiosalt anions have two negative charges (TS^{2-}). The ion-pairs observed in the ESI-MS experiments (see Figure 5.5 and 5.6) all confirm the formation of $[IP{\cdot}TS]^{+}$. In a 1:2 ($IP{\cdot}2TS$) system, the resulting ion-pair will carry a -1 charge and will not be observed in the positive mode ESI. A 2:1 (2 IP·TS) ratio will result in aggregate ion-pairs with a 2+ charge state, none of which were observed for any of these systems. For the purposes of this work, we can assume the exclusive formation of the 1:1 ion-pairs. Thus a 1:1 binding model was applied for all the ion-pairs in thisstudy. Figure 5.4 shows the effect of the concentration of the ion-pair reagents on the signal intensities of the ion-pairs monitored in this study.

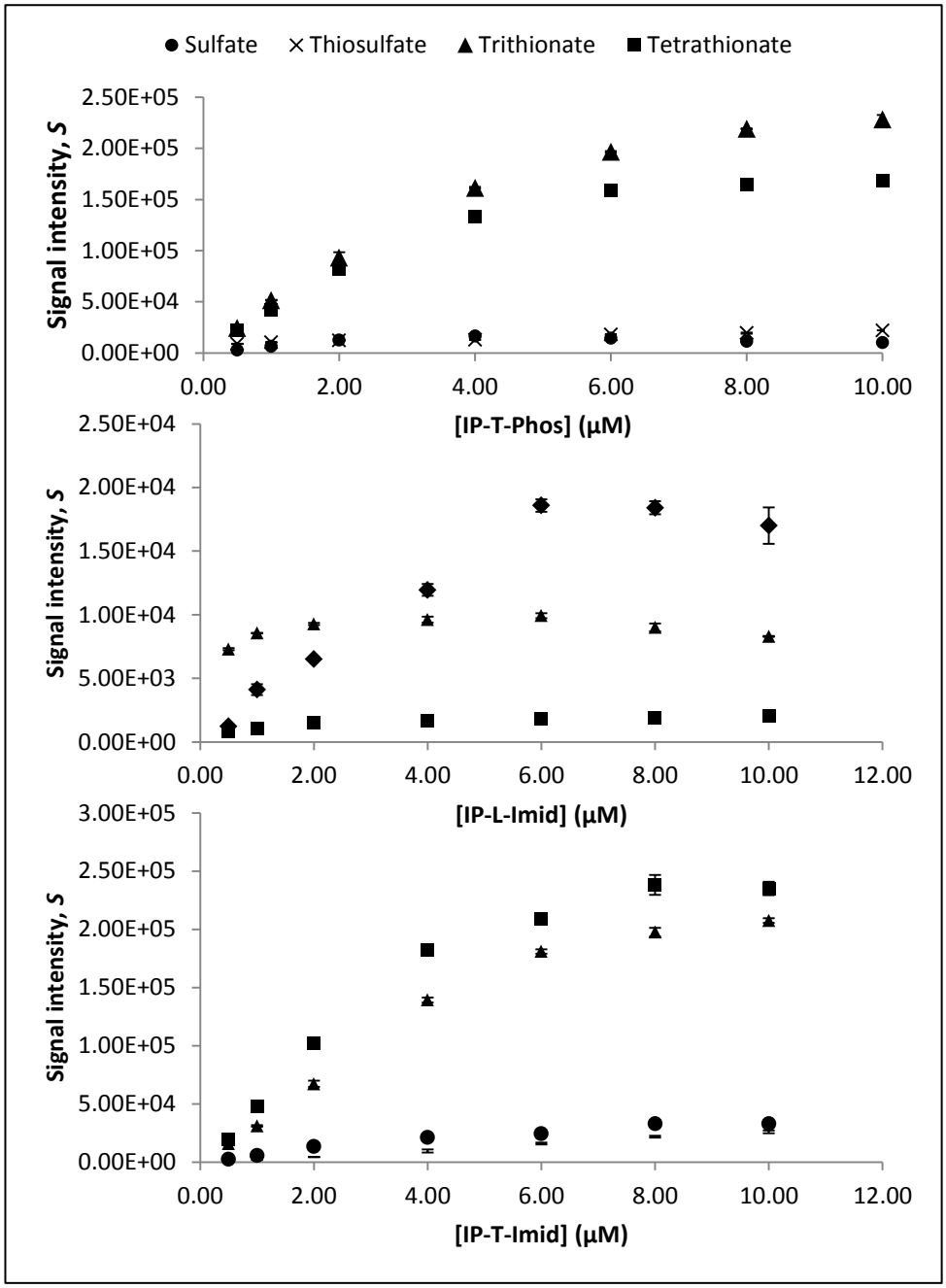

Figure 5.5. Effect of concentration of three ion-pair reagents (IP-L-Imid, IP-T-Imid and IP-T-Phos) on the signal intensities of the trication – thiosalt ion-pair. Thiosalt concentrations were 2.0 µM. Error bars represent standard deviation.

5.3.3 Data treatment of 1:1 association constant model

The equilibria for the reaction between a thiosalt ion (TS^{2-}) and tricationic ion-pairing reagent (IP^{3+}) in the aqueous phase and transfer to the gas phase (equilibrium constants not shown) can be represented as:

$$IP^{3+}{}_{(aq)} + TS^{2-}{}_{(aq)} \leftrightarrows [IP \cdot TS]^{+}{}_{(aq)} \leftrightarrows [IP \cdot TS]^{+}{}_{(g)} \quad (5\text{-}1)$$

The overall equilibrium constant is given as:

$$\beta_{assoc} = \frac{[IP_i \cdot TS_t]}{[IP]^i[TS]^t} \quad (5\text{-}2)$$

where *t*, *i* are the stoichiometric coefficients for the TS and IP, respectively in the reaction. For this work the basic assumption is that a 1:1 association occurs in the ion-pair formation, thus Equation 5-2 can therefore be written as:

$$K_{assoc} = \frac{[IP \cdot TS]}{[IP][TS]} \quad (5\text{-}3)$$

In these experiments $[IP]_0$ was fixed and $[TS]_0$ varied while monitoring the signal count, *S* of the ion-pair $[IP \cdot TS]^+$ for each titration step. Binding isotherms were the constructed for each of the twelve $[IP \cdot TS]^+$ systems. In evaluating K_{assoc}, the signal intensities of the free ion-pair reagent (S_{IP}) and the trication ($S_{IP \cdot TS}$) were monitored at each titration point. It was assumed that the response factors for the free ion-pair (f_{IP}) and the ion-pair ($f_{IP \cdot TS}$) were similar, that is, F =1.

Thus the value for S_R in Equation 5-4 was determined for each titration point:

$$\frac{[IP \cdot TS]}{[IP]} = \frac{S_{IP \cdot TS}/f_{IP \cdot TS}}{S_{IP}/f_{IP}} = \frac{S_{IP \cdot TS}}{S_{IP}} \cdot \frac{f_{IP}}{f_{IP \cdot TS}} = S_R F = S_R \qquad (5\text{-}4)$$

where S_R is the ratio of the ion intensities for the ion-pair ($S_{IP \cdot TS}$) and free trication (S_{IP}), and F is the ratio between the response factors of the free trication (f_{IP}) and the ion-pair ($f_{IP \cdot TS}$). F is assumed to be equal to 1.

Using the mass balance equations 5-5 and 5-6, together with Equations 5-3 and 5-4, we can begin to develop a relationship between S_R, K_{assoc} and the total concentrations of ion-pair reagent ($[IP]_0$) and thiosalt ($[TS]_0$).

$$[IP]_0 = [IP] + [IP \cdot TS] \qquad (5\text{-}5)$$

$$[TS]_0 = [TS] + [IP \cdot TS] \qquad (5\text{-}6)$$

Substituting Equation 5-6 into 5-3 will yield Equation 5-7.

$$K_{assoc} = \frac{[IP \cdot TS]}{[IP]([TS]_0 - [IP \cdot TS])} \qquad (5\text{-}7)$$

Given that:

$$\frac{[IP \cdot TS]}{[IP]_0} = \frac{[IP \cdot TS]}{[IP] + [IP \cdot TS]} \qquad (5\text{-}8)$$

and $$[IP \cdot TS] = [IP]_0 \cdot \frac{[IP \cdot TS]}{[IP] + [IP \cdot TS]} \qquad (5\text{-}9)$$

Equation 5-7 can be re-written as:

$$K_{assoc} = \frac{[IP \cdot TS]}{[IP]} \cdot \frac{1}{[TS]_0 - ([IP]_0 \cdot \frac{1}{\frac{[IP]}{[IP \cdot TS]} + 1})} \quad (5\text{-}10)$$

Substituting S_R from Equation 5-4 into 5-10, and given that F is unity; we can derive the following quadratic equation:

$$S_R{}^2 + S_R(1 + K_{assoc}[IP]_0 - K_{assoc}[TS]_0) - K_{assoc}[TS]_0 = 0 \quad (5\text{-}11)$$

The only real root of the quadratic equation (5-11) is given in Equation 5-12.

$$S_R = \frac{-(1+K_{assoc}[IP]_0 - K_{assoc}[TS]_0) + \sqrt{(1+K_{assoc}[IP]_0 - K_{assoc}[TS]_0)^2 + 4K_{assoc}[TS]_0}}{2} \quad (5\text{-}12)$$

Thus, we have obtained a relationship between the ratio of the signal intensities (S_R), K_{assoc} and the initial total concentrations of the ion-pair reagent $[IP]_0$ and the thiosalt species $[TS]_0$, the only unknown being K_{assoc}. A non-linear curve fitting method can then be used to obtain the value of K_{assoc}. An initial estimated value of $K_{assoc} = 1.00 \times 10^3\ M^{-1}$ based on literature was used in iterative successive approximations until reaching the lowest sum of the square of the differences (residuals) between the observed and calculated signal ratios $\Sigma(S_R - S_{calc})^2$. In this work, convergence was assumed when the percent difference of successive K_{assoc} values was < 1%,[34] with convergence tolerances of the residuals ranging from 0.00003 to 0.1 for the twelve systems.

5.3.4 Evaluation of K_{assoc} for thiosalt-tricationic ion pairs

The K_{assoc} values obtained from the titration experiment are shown in Figure 5.6. Overall the K_{assoc} determined showed that the tricationic ion pairing reagents paired well with all the thiosalt species. These K_{assoc} values (in the range of $10^3 - 10^5\ M^{-1}$) are comparable and in agreement with other solution and gas phase binding constants reported in literature for these types of ion-pairs.[35,39]

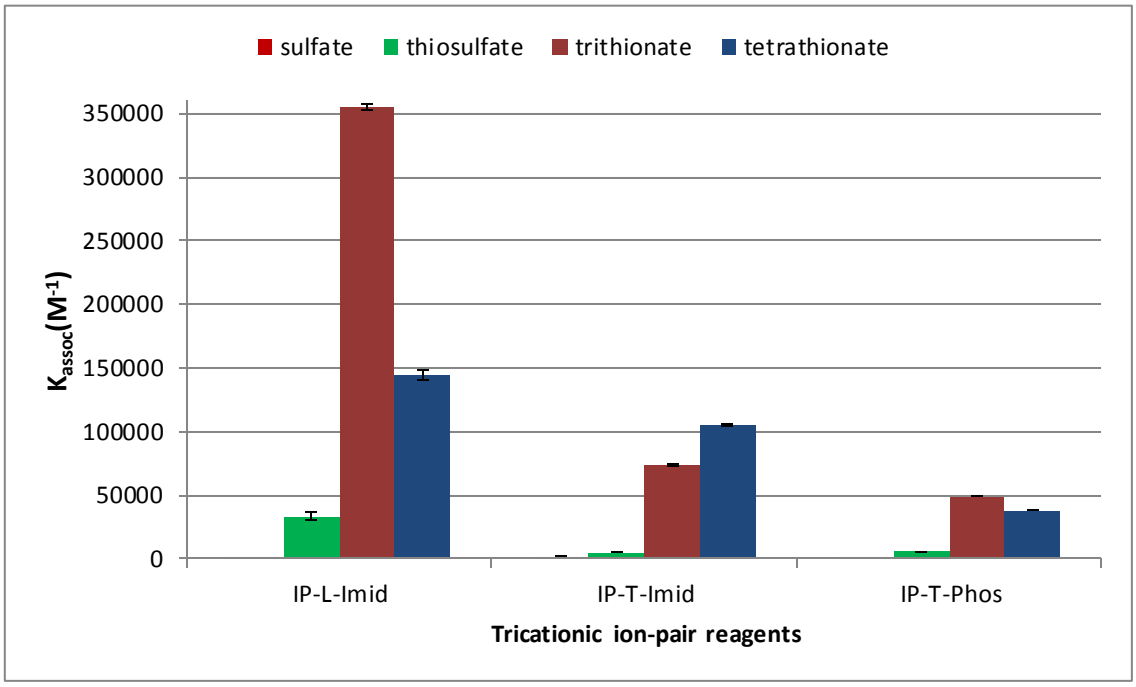

Figure 5.6. Bar graphs showing the association constants (K_{assoc}) of the trication- thiosalt ion-pair ($[IP{\cdot}TS]^+$) determined for 4 thiosalt species and 3 ion-pair reagents (12 systems) by titration and ESI-TOF MS. Error bars represent standard deviation in K_{assoc}.

It has been shown that electrostatic interactions mainly account for the strong interactions between ion-pairs in the gas-phase, such as thiosalt anion and the tricationic ion-pairing reagents.[36-37] In addition, we may expect the strength of association to be influenced by the structure of the ion-pairing reagent and the thiosalt species. IP-L-Imid is a flexible linear imidazolium ion-pairing reagent and IP-T-Imid and IP-T-Phos are trigonal shaped molecules with imidazolium and phosphonium groups attached at a central core. There were a few notable features of the K_{assoc} values determined. Perhaps most importantly is that the reproducibility of the measurements and resulting calculated K_{assoc} is quite good, with %RSD values ranging from 0.56% to 4.05%, except for 11.4% for the thiosulfate·IP-L-Imid ion-pairs. The association constants and binding strength typically increased with thiosalt sulfur content, with very small values for sulfate and highest values for trithionate and tetrathionate. This is clearly shown in the log version of the K_{assoc} plot in Figure 5.7. Though the trend held for the range of thiosalts studied with IP-T-Imid, tetrathionate gave K_{assoc} values lower than trithionate for IP-L-Imid and IP-T-Phos. The highest K_{assoc} was found for the interaction of trithionate with IP-L-Imid at $3.56 \times 10^5\ M^{-1}$, followed by the ion-pairing with tetrathionate by the same ligand at $1.45 \times 10^5\ M^{-1}$. IP-L-Imid also gave the higher K_{assoc} value for thiosulfate. Trithionate and tetrathionate were alsopaired strongly by IP-T-Imid (K_{assoc} of 7.30×10^4 and 1.05×10^5 M^{-1}, respectively). Although the linear imidazolium was generally considered the best ion-pairing agent for the thiosalts, it also gave lowest K_{assoc} in the 12 systems studied with values of $6.85 \times 10^2\ M^{-1}$ for sulfate $[IP\text{-}L\text{-}Imid{:}SO_4]^+$). The best result for sulfate was for $1.89 \times 10^3\ M^{-1}$ for IP-T-Imid·SO_4^{2-}.

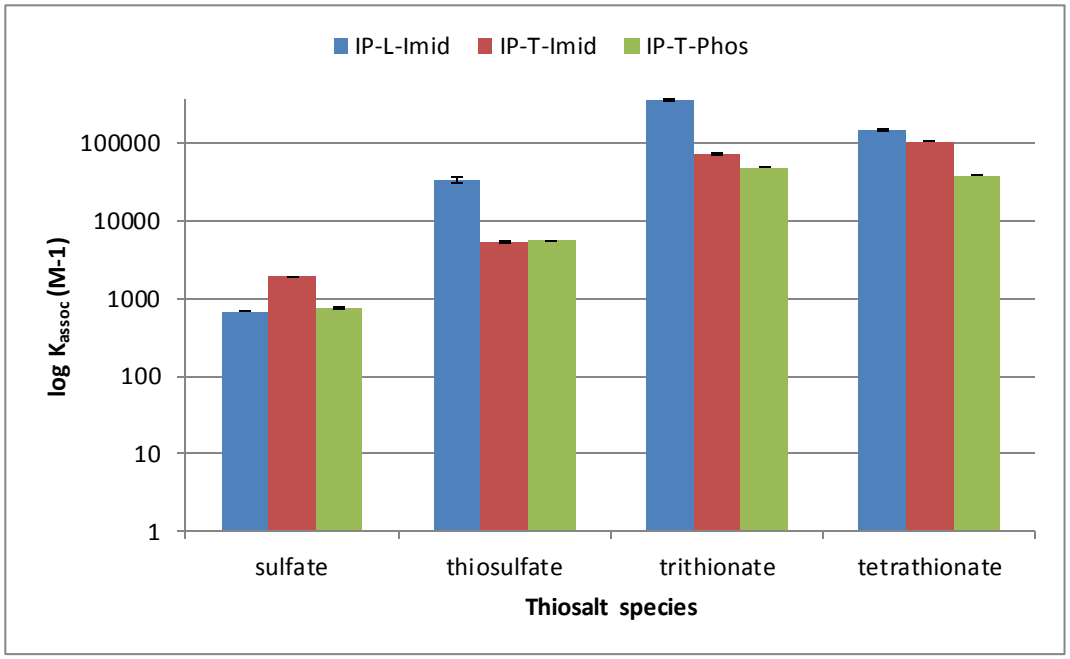

Figure 5.7. Log scale showing the trends in increasing association constants (K_{assoc}) values with increasing sulfur content in the ion-pair reagent – thiosalt ($[IP{\cdot}TS]^{+}$) ion-pairs

The formation of strong association constants between the linear imidazolium tricationic ion pairing reagent IP-L-Imid is likely due to the ability of the flexible arms with terminal imidazolium groups to wrap around the thiosalt and coordinate the thiosalt species through electrostatic interactions and hydrogen bonding between the acidic hydrogen on the imidazolium core groups and the oxygen on the thiosalt anions. The much higher K_{assoc} for trithionate and tetrathionate might be due to hydrophobic interactions between the hydrophobic sulfur linkages and hydrophobic character of the alkyl tether of the IP-L-Imid or the terminal phenyl moiety. The trigonal shaped reagents IP-T-Imid and IP-T-Phos also paired strongly with the two thionate species. The higher K_{assoc} value for IP-T-Imid can also be attributed to electrostatic and hydrophobic interactions with the thiosalt species, but since they are lower than with the linear IP reagent, steric considerations are likely implicated.

The weakness of the sulfate associations may be due to its small size and high charge density associated with sulfate suggests the possibility a strongly bound solvation sphere that would be somewhat less amenable to displacement of water and coordination to the large ion-pairing reagents, therefore weak interactions result. The IP-T-Imid give the best results of the three ion pairing reagents, suggesting that the geometry may allow the sulfate to fit well between two imidazolium groups, and that the hydrophobic terminal phenyl groups and less structured nature of the IP-L-Imid works against ion-pairing. The IP-T-Phos seems to be limited by hindered access to the charged phosphorus, which has three alkyl substituents and bound by the tether. Thiosulfate also showed lower K_{assoc}

values, but though only slightly larger than sulfate (one sulfur replaces one oxygen) it has much higher association constants. The charged terminal sulfur seems to yield stronger electrostatic and hydrogen bonding than oxygen in the sulfate. It is notable that the two sulfur atoms in thiosulfate are in different oxidation states, ther central S being +6 and terminal S -2, thus giving thiosulfate very different chemistry than the other thiosalt species.[40]

A look at the change in standard Gibbs energy of formation ($\Delta_r G^o$) for the ion-pairs (Figure 5.8) shows the general trend of the formation of lower energy ion-pairs with increasing sulfur content of the thiosalt species. $\Delta_r G^o$ was calculated from the relationship $\Delta_r G^o = RTInK_{assoc}$, where R is the gas constant (8.31 J K^{-1} mol^{-1}) and T is the temperature in kelvin (298 K for this work). The trigonal shaped tricationic pairing reagents (IP-T-Imid and IP-T-Phos) show similar trends in the energies of the ion-pairs formed with the thiosalt anions. The linear tricationic ion-pair reagent (IP-L-Imid) also show a similar trend with the exception in the ion-pair formed with $S_3O_6^{2-}$ for which the Gibbs energy of formation was much lower than that of $S_4O_6^{2-}$. This suggests that the mechanism (due to their shape and coordination geometry) for ion-pairing may be similar for both pairing reagents. Sulfate also has the smallest change in formation energies for all the three ion-pairing reagents, ranging from a formation energy of -16 kJ mol^{-1} with both the linear flexible IP-L-Imid and trigonal IP-T-Phos, to -18 kJ mol^{-1} with trigonal IP-T-Imid. This gives credence to the suggestions that the high charge density, small ionic radius and hardness of sulfate may contribute to the weak coordination with the bulky reagents.

Trithionate and tetrathionate formed the lowest energy ion-pairs with the three ion-pairing reagents. These trends and differences in K_{assoc} and $\Delta_r G^o$ will help to select the appropriate ion-pairing reagents to tune the ion-pairing for specific thiosalt species.

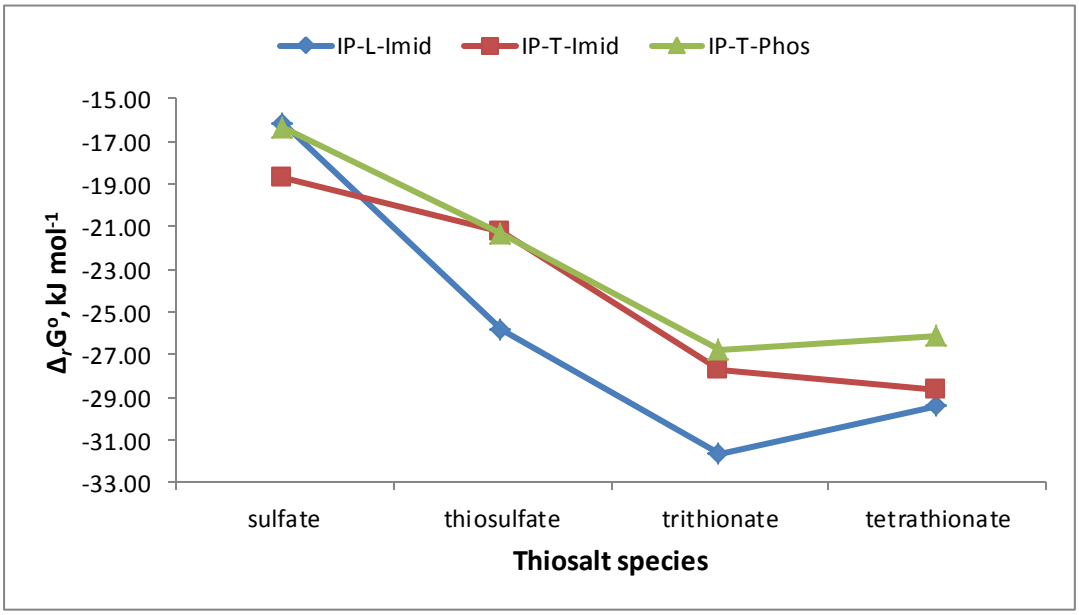

Figure 5.8. Trends in change in standard Gibbs energy of formation ($\Delta_r G^o$), kJ mol^{-1} for trication-thiosalt ion-pairs

5.4 Concluding remarks

Tricationic ion-pairing reagents provide an alternative to analyzing thiosalt ions directly with mass spectrometry. We evaluated three tricationic ion-pairing reagents for their ability to form gas-phase ion-pairs with four thiosalt species using FIA with positive mode ESI-TOF MS. The m/z (mass-to-charge) values of the free ion-pair reagent ion

$[IP^{3+}]$ and the trication–thiosalt ion-pairs $[IP{\cdot}TS]^{+}$ were monitored. All the ion-pairing reagents paired very well with the thiosalt species (except sulfate and thiosulfate) in the gas-phase and formed +1 ion-pairs, making them amenable to ESI in the positive mode and detection at relatively high m/z values that are typically free of interferences. The strength of association (K_{assoc}) for these ion-pairs were greater than those reported in the solution phase for similar system ($60 – 120\ M^{-1}$) by about two to three orders of magnitude.[39] The gas-phase association constant (K_{assoc}) values obtained for the thiosalt ion-pairs with IP-L-Imid, IP-T-Imid and IP-T-Phos were in the range of $6.85 \times 10^{2}\ M^{-1}$ to $3.56 \times 10^{5}\ M^{-1}$. Overall, except for sulfate, the K_{assoc} values obtained for these ion-pairs showed that favourable ion-pairs were formed between the tricationic ion-pairing reagents and the thiosalt species in the gas-phase. Selectivity tuning will be useful in detecting these thiosalt species with minimal interference such as in the case of the high sulfate concentration common in real samples.

5.5 Future direction

Thiosalts present in treated tailings ponds and in mill effluent present a challenge for analysis due to the complexity of the matrix, especially in natural receiving waters, in which these partially oxidized sulfur species exist. With the known sensitivity limitation of UV-vis compared with mass spectrometry, this work presents an alternative way forward for the accurate trace analysis of these thiosalt species in complex environmental samples. Once successfully coupled to an ESI-TOF-MS interface, a CZE method will

developed and utilized for the fast separation of these thiosalt species and the trication-thiosalt ion-pairs detected with ESI-TOF-MS. This future work will also employ experimental design approach to optimize the most important parameters to develop a robust and reliable method for the analysis of these anions.

5.6 References

[1] Soukup-Hein, R. J.; Remsburg, J. W.; Breitbach, Z. S.; Sharma, P. S.; Payagala, T.; Wanigasekara, E.; Huang, J.; Armstrong, D. W. Evaluating the Use of Tricationic Reagents for the Detection of Doubly Charged Anions in the Positive Mode by ESI-MS. *Anal. Chem*. **2008**, *80*, 2612-2616.

[2] Warnke, M. M.; Breitbach, Z. S.; Dodbiba, E.; Wanigasekara, E.; Zhang, X.; Sharma, P.; Armstrong, D. W. The Evaluation and Comparison of Trigonal and Linear Tricationic Ion-Pairing Reagents for the Detection of Anions in Positive Mode ESI-MS. *J. Am. Soc. Mass Spectrom*. **2009**, *20*, 529 –538.

[3] Remsburg, J. W.; Soukup-Hein, R. J.; Crank, J. A.; Breitbach, Z. S.; Payagala, T.; Armstrong, D. W. Evaluation of Dicationic Reagents for their Use in Detection of Anions Using Positive Ion Mode ESI-MS Via Gas Phase Ion Association. *J. Am. Soc. Mass Spectrom*. **2008**, *19*, 261-269.

[4] Breitbach, Z. S.; Warnke, M. W.; Wanigasekara, E.; Zhang, X.; Armstrong, D. W. Evaluation of Flexible Linear Tricationic Salts as Gas-Phase Ion-Pairing Reagents for the Detection of Divalent Anions in Positive Mode ESI-MS. *Anal. Chem*. **2008**, *80*, 8828–8834.

[5] Soukup-Hein, R. J.; Remsburg, J. W.; Dasgupta, P. K.; Armstrong, D. W. A General, Positive Ion Mode ESI-MS Approach for the Analysis of Singly Charged Inorganic and Organic Anions Using a Dicationic Reagent. *Anal. Chem*. **2007**, *79*, 7346-7352.

[6] Lin, X.; Gerardi, A. R.; Breitbach, Z. S.; Armstrong, D. W.; Colyer, C.L. CE-ESI-MS Analysis of Singly Charged Inorganic and Organic Anions Using a Dicationic Reagent as a Complexing Agent. *Electrophoresis*. **2009**, *30*, 3918-3925.

[7] Anderson, J. L.; Ding, J.; Welton, T.; Armstrong, D. W. Characterizing Ionic Liquids On the Basis of Multiple Solvation Interaction. *J. Am. Chem. Soc.*, **2002**, *124*, 14247–14254.

[8] Visser, A. E., Swatloski, R. P., Reichert, W.M., Mayton, R., Sheff, S., Wierzbicki, A., Davis, J.H. Jr, Rogers, R. D. Task-Specific Ionic Liquids Incorporating Novel Cations for the Coordination and Extraction of $Hg^{2+}$and Cd^{2+}: Synthesis, Characterization, and Extraction Studies. *Environ. Sci. Technol.* **2002**, *36*, 2523–2529.

[9] Gholap, A. R.; Venkatesan, K.; Daniel, T.; Lahoti, R.J.; Srinivasan, K.V. Ultrasound Promoted Acetylation of Alcohols in Room Temperature Ionic Liquid Under Ambient Conditions. *Green Chem*. **2003**, *5*, 693–696.

[10] Salimi, A.; Mamkhezri, H.; Mohebbi, S. Electrodless Deposition of Vanadium-Schiff Base Complex Onto Carbon Nanotubes Modified Glassy Carbon Electrode: Application to the Low Potential Detection of Iodate, Periodate, Bromate and Nitrite. *Electrochem. Comm*. **2006**, *8*, 688-696.

[11] Deck, P. A.; Marks, T. J. Cationic Metallocene Olefin Polymerization Catalysts. Thermodynamic and Kinetic Parameters for Ion Pair Formation, Dissociation, and Reorganization. *J. Am. Chem. Soc*. **1995**, *117*, 6128-6129.

[12] Álvarez , J. G.; Gomis, D. B.; Abrodo, P. A.; Llorente, D. D.; Busto, E.; Lombardía, N. R.; Fernández, V. G.; Álvarez, M. D. G. Evaluation of New Ionic Liquids as High Stability Selective Stationary Phases in Gas Chromatography. *Anal. Bioanal. Chem*. **2011**, *400*, 1209–1216.

[13] Soukup-Hein,R.J.; Warnke, M.M.; Armstrong, D.W. Ionic Liquids in Analytical Chemistry. *Annu. Rev*. *Anal. Chem*. **2009**, *2*, 145–168.

[14] Hefter, G. When spectroscopy fails: The measurement of ion pairing. *Pure Appl. Chem.*, **2006**, *78*, 1571–1586.

[15] Garcia-Araez, N.; Climent, V.; Rodriguez, P.; Feliu, J.M. Thermodynamic evidence for K^+–SO_4^{2-} ion pair formation on Pt(111). New Insight into Cation Specific Adsorption. *Phys. Chem. Chem. Phys*. **2010**, *12*, 12146-12152.

[16] Sevim, A. M.; Hojiyev, R.; Gül, A.; Çelik, M. S. An Investigation of the Kinetics and Thermodynamics of the Adsorption of a Cationic Cobalt Porphyrazine onto Sepiolite. *Dyes Pigm*. **2011**, *88*, 25-38.

[17] Fryčák, P.; Schug, K.A. Dynamic Titration: Determination of Dissociation Constants for Noncovalent Complexes in Multiplexed Format Using HPLC-ESI-MS. *Anal. Chem*. **2008**, *80*, 1385-1393.

[18] Warnke, M. M.; Breitbach, Z. S.; Dodbiba, E.; Crank, J. A.; Payagala, T.; Sharma, P.; Wanigasekara, E.; Zhang, X.; Armstrong, D.W. Positive Mode Electrospray Ionization Mass Spectrometry of Bisphosphonates Using Dicationic and Tricationic Ion-Pairing Agents. *Anal. Chim. Acta*. **2009**, *633*, 232–237.

[19] Pramanik, B. N.; Bartner, P. L.; Mirza, U. A.; Liu, Y.; Ganguly, A. K. Electrospray Ionization Mass Spectrometry for the Study of Non-covalent Complexes: An Emerging Technology. *J. Mass Spectrom*. **1998**, *33*, 911-920.

[20] Nasioudis, A.; van Velde, J. W.; Heeren, R. M. A.; van den Brink, O. F. Electrospray Ionization Mass Spectrometry of the Non-Covalent Complexes Of Ammonium Ions With High Molar Mass Polyethers. *Int. J. Mass Spectrom*. **2011**, *303*, 63-68.

[21] Daniel, J. M.; Friess, S. D.; Rajagopalan, S.; Wendt, S.; Zenobi, R. Quantitative Determination of Noncovalent Binding Interactions Using Soft Ionization Mass Spectrometry. *Int. J. Mass Spectrom*. **2002**, *216*, 1–27.

[22] Ross, A.R.S.; Ikonomou, M.G.; Orians, K.J. Characterization of Dissolved Tannins and Their Metal-Ion Complexes by Electrospray Ionization Mass Spectrometry. *Anal. Chim. Acta*. **2000**, *411*, 91-102.

[23] Coulier, L.; Bas, R.; Jespersen, S.; Verheij, E.; van der Werf, M. T. J.; Hankemeier, T. Simultaneous Quantitative Analysis of Metabolites Simultaneous Quantitative Analysis of Metabolites Using Ion-Pair Liquid Chromatography-Electrospray Ionization Mass Spectrometry. *Anal. Chem*. **2006,** *78*, 6573-6582.

[24] Dyke, J. V.; Kirk, A. B.; Martinelango, P. K.; Dasgupta, P. K. Sample Processing Method for the Determination Of Perchlorate In Milk *Anal. Chim. Acta*. **2006**, *567*, 73-78.

[25] Martinelango, P. K.; Gömös, G.; Dasgupta, P. K. Matrix Interference Free Determination of Perchlorate in Urine by Ion Association–Ion Chromatography–Mass Spectrometry. *Anal. Chim. Acta*. **2006**, *567*, 79-86.

[26] Martinelango, P. K.; Tian, K.; Dasgupta, P. K. Perchlorate in Seawater Bioconcentration of Iodide and Perchlorate by Various Seaweed Species. *Anal. Chim. Acta.* **2006**, *567*, 100-107.

[27] Huston, M. E. Chelation Enhanced Fluorescence Detection of Nonmetal Ions. *J. Am. Chem. Soc.* **1989**, *111*, 8735-8737.

[28] Magnuson, M. M.; Urbansky, E.T.; Kelty, C. A. Determination of Perchlorate at Trace Levels in Drinking Water by Ion-Pair Extraction with Electrospray Ionization Mass Spectrometry. *Anal. Chem.* **2000**, *72*, 25-29.

[29] Gerardi, A. R.; Lin, X., Breitbach, Z. S.; Armstrong, D. W.; Colyer, C. L. CE-ESI-MS Separation Of Divalent Organic and Inorganic Anions Using a Tricationic Complexing Reagent. *Electrophoresis.* **2012**, *33*, 734–740.

[30] Kelly, D. P.; Wood, A. P., Synthesis and Determination of Thiosulfate and Polythionates. *Methods Enzymol.***1994**, *243*, 475-500.

[31] Pappoe, M.; Lucas, H.; Bottaro, C.; Dawe, L. N. Single Crystal Structural Characterization of Tri-, Tetra and Pentathionates. *J. Chem. Crystallogr.* **2013**, *43*, 596–604.

[32] Tsukube, H.; Furuta, H.; Odani, A.; Takeda, Y.; Kudo,Y.; Inoue,Y.; Liu, Y.; Sakamoto, H.; Kimura, K.; *In* Comprehensive Supramolecular Chemistry, ed. Atwood, J. L.; Davies, J. E. D., MacNicol, D. D.; Vögtle, F. Pergamon, Oxford, 1996, vol. 8, ch. 10, pp. 425–482.

[33] Thordarson, P. Determining association constants from titration experiments in supramolecular chemistry. *Chem. Soc. Rev.*, **2011**, *40*, 1305–1323.

[34] Macombe, R. S. An Introduction to NMR Titration for Studying Rapid Reversible Complexation. J. *Chem*. *Edu*. **1992**, *69*, 375-378.

[35] Daniel, J. M.; Friess, S. D.; Rajagopalan, S.; Wendt, S.; Zenobi, R. Quantitative Determination of Non-Covalent Binding Interactions Using Soft Ionization Mass Spectrometry – Review. *Int*. *J. Mass Spectrom*. **2002**, *216*, 1–27.

[36] Guevremont, R.; Siu, K. W. M.; Le Blanc, J. C. Y.; Berman, S. S. Are the Electrospray Mass Spectra of Proteins Related to Their Aqueous Solution Chemistry? *J. Am*. *Soc. Mass Spectrom*. **1992**, *3*, 216-224.

[37] Visser, A. E.; Swatloski, R. P.; Reichert, W. M.; Mayton, R.; Sheff, S.; Wierzbicki, A.; Davis, J. H. Jr.; Rogers, R. D. Task-Specific Ionic Liquids Incorporating Novel Cations for the Coordination and Extraction of $Hg^{2+}$and Cd^{2+}: Synthesis, Characterization, and Extraction Studies. *Environ. Sci. Technol.* **2002**, *36*, 2523–2529.

[38] Detecting Anions in the Positive Mode Using Cationic Pairing Agents. *Anal. Chem*. **2010**, *82*, 9066–9073.

[39] Breitbach, Z. S.; Wanigasekara, E.; Dodbiba, E.; Shug, K. A.; Armstrong, D. W. Mechanisms of ESI-MS Selectivity and Sensitivity Enhancements When Detecting Anions in the Positive Mode Using Cationic Pairing Agents. *Anal. Chem*. **2010**, *82*, 9066-9073.

[40] Greenwood, N. N.; Earnshaw, A. Chemistry of the Elements 2nd ed.,1997, p 705.

Chapter 6

Single Crystal Structural Characterization of Tri–, Tetra– and Pentathionates

Michael Pappoe,[a] Heather Lucas,[a] Christina Bottaro,[a] Louise Dawe,[a,b]

a. Department of Chemistry, Memorial University of Newfoundland, St. Johns, NL, A1B 3X7, Canada

b. Centre for Chemical Analysis, Research and Training (X-ray Diffraction Lab), Memorial University of Newfoundland, St. Johns, NL, A1B 3X7, Canada

6.1 Introduction

Thiosulfate and polythionates, also known as thiosalts, are partially oxidized sulfur oxyanions formed during the milling and flotation of sulfide ores. In these processes, sulfide and sulfite react with elemental sulfur to yield linear polysulfides, which are oxidized to form thiosulfate ($S_2O_3^{2-}$), trithionate ($S_3O_6^{2-}$), tetrathionate ($S_4O_6^{2-}$) and other higher polythionates of the formula $S_xO_6^{2-}$ where $3 \leq x \leq 10$. Higher order polythionates are usually formed at very low concentrations. Thiosalts easily undergo further oxidation to sulfuric acid in natural water systems. The environmental implications lie in the formation of the acid; this leads to depression of the pH of the receiving water, which directly impacts organic organisms, and also facilitates mobilization and increased bioavailability of toxic metal species.[1-3]

Room temperature determinations of anhydrous potassium trithionate and tetrathionate have been previously reported, though the atom coordinates are not available in the Cambridge Structural Database.[4,5] Only five structurally characterized examples of the pentathionate anion have been previously reported, including the potassium pentathionate hemihydrate, which crystallized in an orthorhombic space group.[6,6d] Herein, we report the low temperature determinations of the sodium trithionate trihydrate analogue and the redetermination of potassium tetrathionate, with an emphasis on the different potassium coordination environments for the independent formula moieties contained in the asymmetric unit. Further, the new monoclinic form of potassium pentathionate is reported.

6.2 Synthesis

Syntheses of sodium trithionate trihydrate, S_3O_6•2Na•3H_2O, (**1**), Potassium tetrathionate, S_4O_6•2K (**2**) and Potassium pentathionate hydrate, S_5O_6•2K•1.5H_2O (**3**) salts were carried out using methods modified from those described by Kelly *et al.*[7] Crystal growth of the trithionate and tetrathionate salts were accomplished by adding ice–chilled 95 % ethanol to the synthesized but amorphous trithionate and tetrathionate salts and leaving for 12 hours at 4 °C. The crystallized salts were then filtered by vacuum and dried in a desiccator. Pentathionate was recrystallized by heating in 0.1 M H_2SO_4 and cooling rapidly to 0 °C. Vacuum-filtered crystals were washed with absolute ethanol and dried in a desiccator.

6.3 X–Ray Experimental

Crystals of **1** – **3** were mounted on low temperature diffraction loops and measured on a Rigaku Saturn CCD area detector with graphite monochromated Mo–Kα radiation. Structures were solved by direct methods and expanded using Fourier techniques.[8,9] Neutral atom scattering factors were taken from Cromer and Waber.[10] Anomalous dispersion effects were included in F_{calc};[11] the values for Δf' and Δf'' were those of Creagh and McAuley.[12] The values for the mass attenuation coefficients are those of Creagh and Hubbell.[13] All calculations were performed using CrystalStructure[14,15] and OLEX2[16] crystallographic software packages, except for refinement, which was performed using SHELXL–97.[9] Non–hydrogen atoms were refined anisotropically, while hydrogen atoms were introduced in difference map positions and refined positionally with *U*iso = 1.5 *U*eq

of the atom to which they were bonded. Distance and angle restraints were applied to the bonds involving hydrogen atoms. A summary of the X–ray crystallographic data can be found in Table 6.1.

6.4 Structural Descriptions

Sodium trithionate trihydrate, S_3O_6•2Na•3H_2O, (**1**): crystallized in *Pmmn* with half the chemical formula moiety contained in the asymmetric unit (Z' = 0.5; Figure 6.1). S–S and S–O bond distances are given in Table 6.2. There are oxygen contacts to the sodium atom from thiodisulfate atoms (O1, O2), from a bridging-water molecule (O3), and from the symmetry generated equivalents of these atoms, filling the sodium valence in a six-coordinate octahedral environment (Table 6.3, Figure 6.1), and leading to a three-dimensional coordination network for this structure (Figure 6.2). A single, uncoordinated, lattice solvent water molecule (O4) is present in the network for each formula unit equivalent, forming hydrogen–bonds to both the coordinated bridging water molecule (O3), and to the thiodisulfate oxygen atoms (O2; Table 6.4).

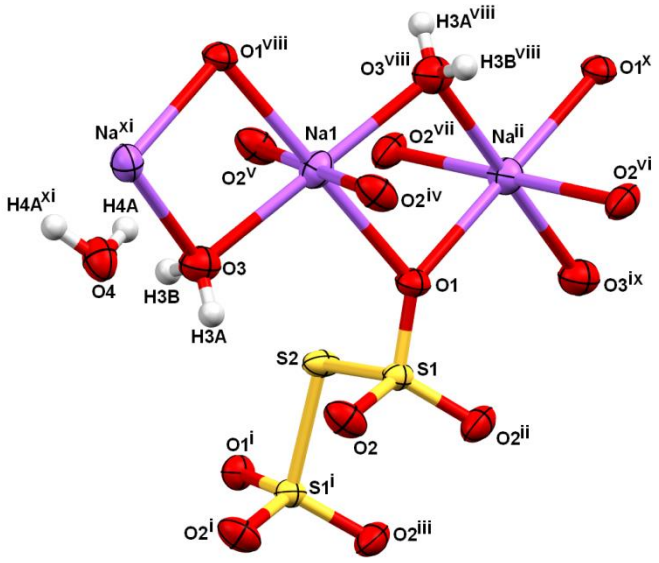

Figure 6.1. Fragment of the polymeric motif in **1**, represented with 50% probability ellipsoids; symmetry codes (i) = x, ½−y, z; (ii) = 1.5−x, y, z; (iii) = 1.5−x, ½−y, z; (iv) = 1−x, 1−y, 2−z; (v) = x, y, z−1; (vi) = ½+x, 1−y, 2−z; (vii) = ½−x, y, z−1; (viii) = 1−x, 1−y, 1−z; (ix) = 1+x, y, z; (x) = 2−x, 1−y, 1−z; (xi) = ½−x, y, z.

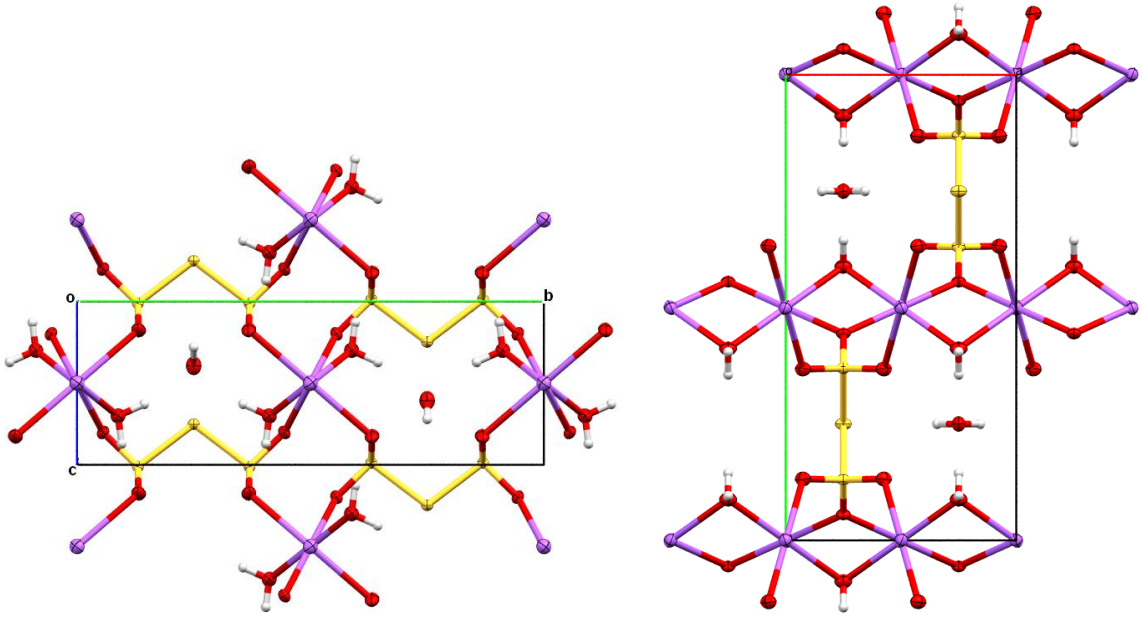

(a) (b)

Figure 6.2. Unit cell of **1**, (a) viewed down the a–axis (b) viewed down the c–axis.

Potassium tetrathionate, S_4O_6•2K (**2**): Crystallized in *Cc* with two chemical formula moieties contained in the asymmetric unit ($Z' = 2$; Figure 6.3). S–S and S–O bond distances are given in Table 6.5. Each of the unique potassium cations possesses a different coordination sphere filled by oxygen and sulfur donors from the thiodisulfate atoms: K1 – S_2O_6; K2 – S_1O_6; K3 – O_9; K4 – O_8 (see Figure 6.4 and Table 6.6). In the previous report,[5] the authors make note of the variable coordination number about potassium (*i.e.*, 6, 6, 9 and 8), however, they considered only the coordination sphere out to 3.4 Å. As reported here, the coordination spheres are less variable (with coordination numbers 7 – 9), since K1 and K2 are involved in a total of three K–S coordinative interactions (K1–S2 = 3.4572(19) Å, K1–$S3^{v}$ = 3.5484(19) Å, K2–$S2^{vii}$ = 3.6814(19) Å). In order to support these assignments, a search in the Cambridge Structure Database (*v*. 5.34)[17] was performed, revealing 144 structures with known coordinates containing a total of 367 K–S bonds, with 48 having a bond length between 3.4 and 3.7 Å (Table 6.7). Combining this information with coordination environment further revealed seven structures that posses an S_2O_6 coordination sphere,[18,19] while 14 are S_1O_6 coordinated.[19,20] However, these differ from the reported tetrathionate in that all but three[19] have all oxygen donors from 18–crown–6. Of the exceptions, one contains a combinations of methanol and calixarene–type donors,[19a] while the other two are 1,10–dithia–18–crown–6.[19b,c] This is therefore the first structurally reported example of a tetrathionate sulfur–metal interaction.

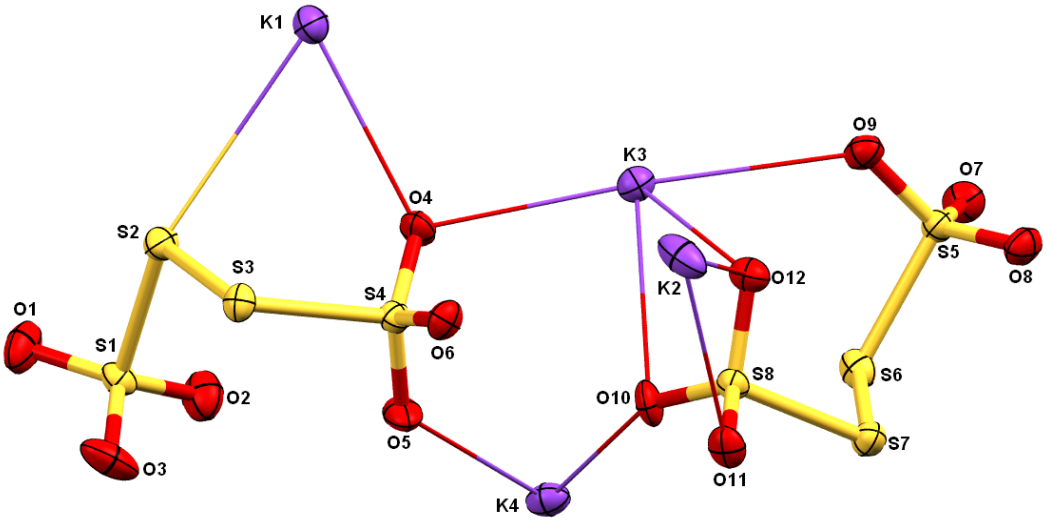

Figure 6.3. Asymmetric unit of **2**, represented with 50% probability ellipsoids.

The potassium–oxygen/sulfur bridges lead to the formation of an extended, solvent–free, three dimensional network (Figure 6.5). Intermolecular sulfur–sulfur distances that slightly exceed the van der Waals radius of the sulfur atoms are present and run parallel to the b–axis (S2−S6^{iv} = 3.663(2) Å; symmetry code: (iv) $x-1/2, y-1/2, z$). The tetrathionate ions adopt a conformation such that only one of the two crystallographically independent molecules is involved in K–S coordinative bonds. The S–S–S–S torsion angle for the tetrathionate involved in the K–S interactions is slightly acute at 87.28(9)^{o} while that of the non–interacting tetrathionate is very near to a right angle, at 90.93(8)^{o}. A search in the Cambridge Structural Database[17] shows 22 other structurally characterized models containing at least one tetrathionate anion, but none with acute angles (all fall in the range of 93.9^{o} – 127.3^{o}).[12]

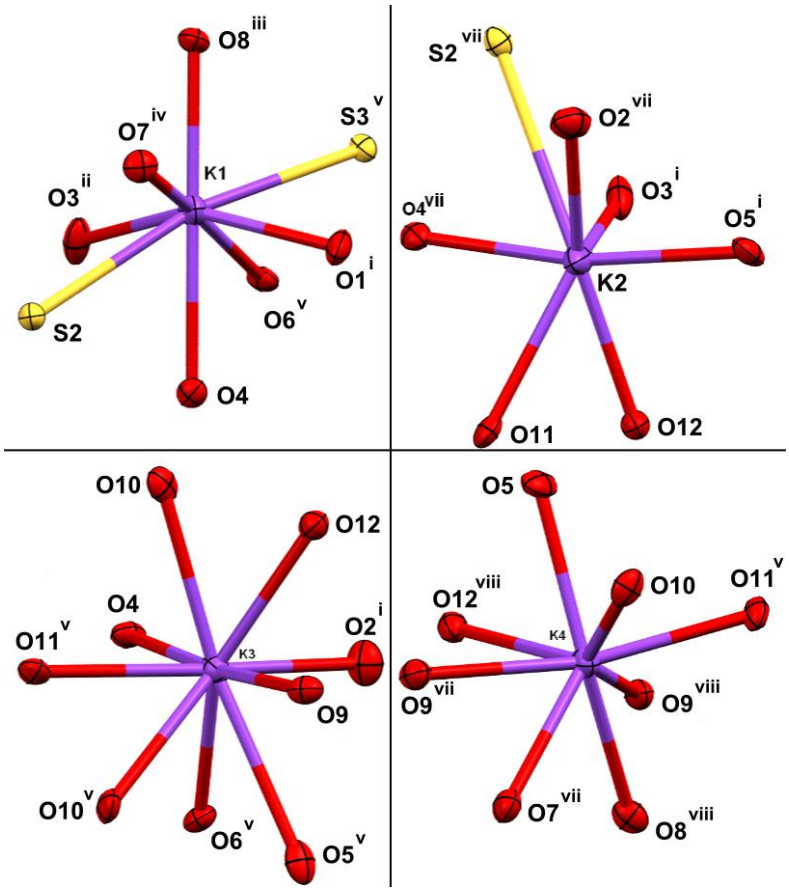

Figure 6.4. Coordination environments of each of the crystallographically unique potassium cations in **2**, represented with 50% probability ellipsoids. Symmetry codes: (i) $x, y+1, z$; (ii) $x, -y, z-1/2$; (iii) $x-1/2, -y+3/2, z-1/2$; (iv) $x-1/2, y-1/2, z$; (v) $x, -y+1, z-1/2$; (vi) $x-1/2, -y+1/2, z-1/2$; (vii) $x, -y+1, z+1/2$; (viii) $x, y-1, z$.

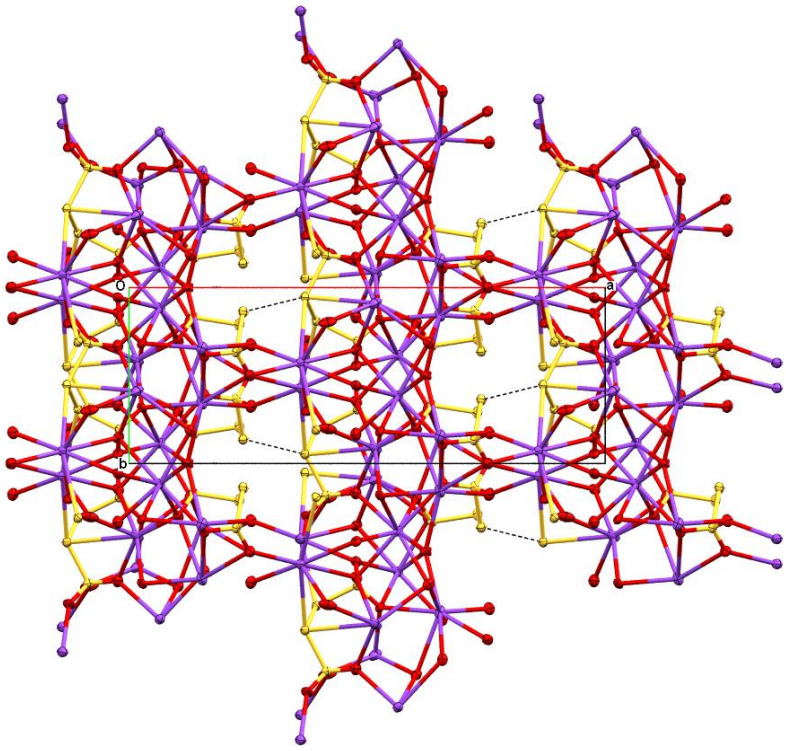

Figure 6.5. Three–dimensional coordination network of **2**, represented with 50% probability ellipsoids, view down the c–axis. Short intermolecular S–S separations indicated with dashed lines.

Potassium pentathionate hydrate, S_5O_6•2K•1.5H_2O (**3**): crystallized in $P2_1/c$ with two chemically identical formula unit moieties contained in the asymmetric unit ($Z' = 2$; Figure 6.6). S–S and S–O bond distances are given in Table 6.8. Unlike, **2**, however, 1.5 potassium–coordinated lattice solvent water molecules per formula unit are also present, and each are involved in hydrogen bonding interactions with pentathionate oxygen-acceptor atoms (Table 6.9). There are oxygen and sulfur contacts to the potassium atoms from pentathionate atoms, again, filling the coordination sphere of each of the unique

potassium cations with a different complement of donor atoms: K1 – S_2O_7; K2 – S_1O_7; K3 – S_1O_8; K4 – O_9 (see Figure 6.7 and Table 6.10). The S_2O_7 coordination sphere for potassium is previously unreported, while only 11 structures have been recorded with an S_1O_7 environment for potassium,[22] all but one where six of the oxygen donors are from 18–crown–6 derivatives (the other contains both methanol and maltose oxygen–donor atoms).[22a] In contrast to **2**, the pentathionate ions have adopted a conformation such that both of the crystallographically independent molecules are involved in K–S coordinative bonds. This structure also represents the first example of a metal–sulfur bond involving a pentathionate sulfur donor atom. In the previously reported potassium pentahydrate, each potassium ion is considered to only have a coordination sphere consisting of seven pentathionate oxygen donors.[6d]

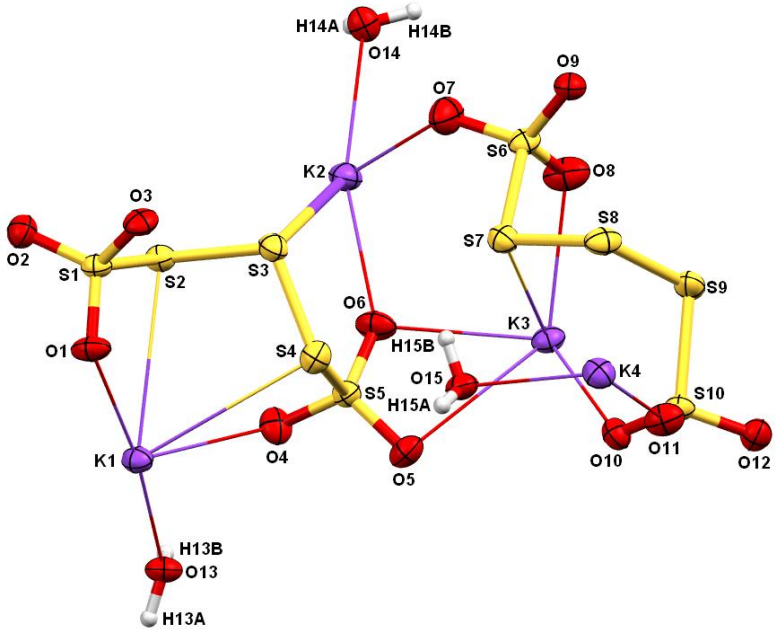

Figure 6.6. Asymmetric unit of **3**, represented with 50% probability ellipsoids.

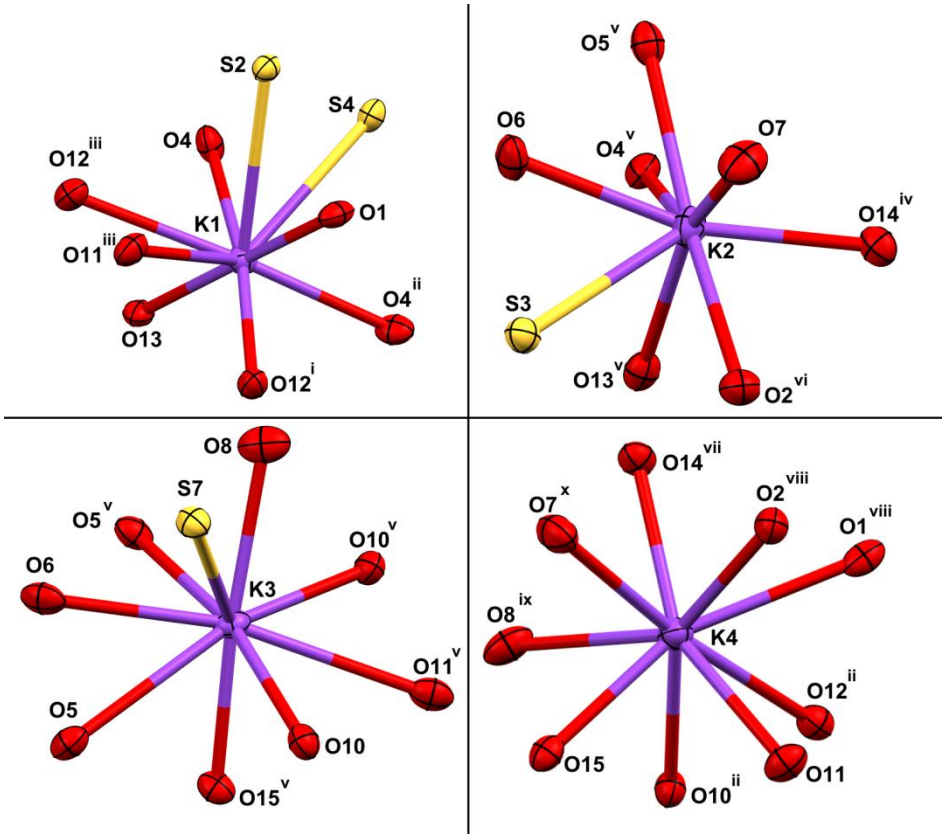

Figure 6.7. Coordination environments of each of the crystallographically unique potassium cations in **3**, represented with 50% probability ellipsoids. Symmetry codes: (i) $x-1, -y+1/2, z-1/2$; (ii) $x, -y+1/2, z-1/2$; (iii) $x-1, y, z$; (iv) $x, y, z+1$; (v) $x, -y+1/2, z+1/2$; (vi) $-x+1, -y, -z+1$; (vii) $-x+2, -y, -z$; (viii) $x+1, y, z$; (ix) $x, y, z-1$; (x) $-x+2, -y, -z+1$.

The potassium bridges lead to the formation of an extended, three dimensional network in which sulfur–rich channels are present parallel to the a–axis (Figure 6.8). The sulfur–rich channels result from the formation of intermolecular eight–membered sulfur rings, where covalently bonded S2 and S3 form contacts at the edge of their van der Waals radii to S8

and S9, on different neighboring molecules (Figure 6.9; S2−S9^{vii} 3.601(2) Å and S3−S8^{x} 3.600(3) Å). In the previously reported orthorhombic form of this structure, the closest S–S approach was notably longer at 3.697(6) Å.[6d] A Cambridge Structural Database[17] analysis revealed 85 other structures with a similar motif (S–S intermolecular contacts out to 3.8 Å were considered), many present in nominal intramolecular cyclic polysulfur structures (S_8 [23], HNS_9 [24], HNS_8 [24], HNS_7 [25]) as well as 1,7–bis(trichloromethyl)heptasulfane (Table 6.11).[26]

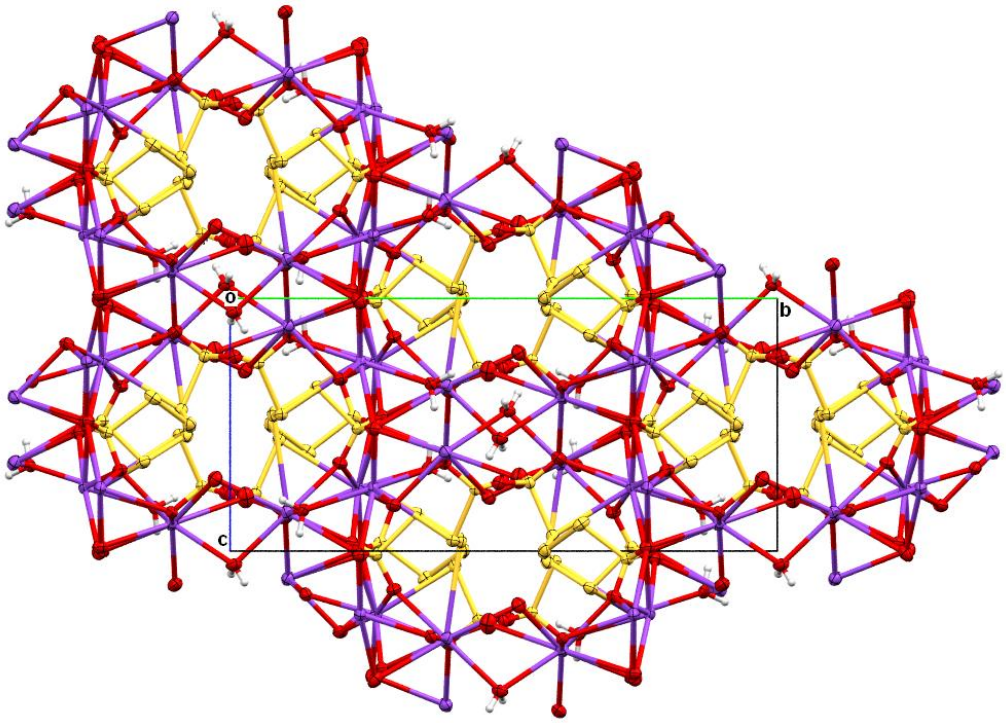

Figure 6.8. Three–dimensional coordination network of **3**, represented with 50% probability ellipsoids, view down the a–axis.

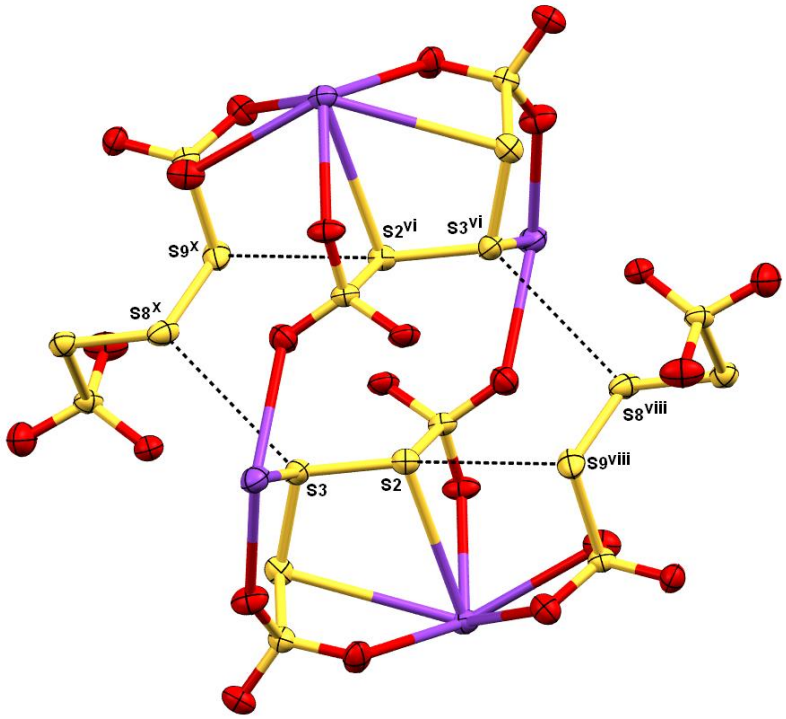

Figure 6.9. Intermolecular sulfur–sulfur contacts in **3** leading to the formation of an eight–membered ring about an inversion centre. Symmetry codes: (vi) $-x+1, -y, -z+1$; (viii) $x+1, y, z$; (x) $-x+2, -y, -z+1$.

6.5 Conclusions

The polythionate complexes of sodium (tri-) and potassium (tetra- and penta-) are reported, and the coordination sphere of the potassium ions discussed. Higher polythionates at very low concentrations are known to form during the milling and flotation of sulfide ores. Thus far, only one structure containing the hexathionate anion has been reported.[27] Future work towards the characterization of this structure is planned.

TABLES

Table 6.1. Summary of Crystallographic Data

Compound reference	1	2	3
Chemical formula	S_3O_6•2Na•3H_2O	S_4O_6•2K	S_5O_6•2K•1.5H_2O
Formula Mass	292.21	302.43	361.52
Crystal system	Orthorhombic	Monoclinic	Monoclinic
Space group	*Pmmn* (#59)	*Cc* (#9)	$P2_1/c$ (#14)
a/Å	6.8486(15)	22.081(4)	12.131(3)
b/Å	13.945(3)	7.955(2)	19.917(5)
c/Å	4.8446(10)	10.0934(15)	9.198(2)
α/°	90.00	90.00	90.00
β/°	90.00	102.573(8)	91.398(5)
γ/°	90.00	90.00	90.00
Unit cell volume/Å^3	462.69(17)	1730.4(6)	2221.8(9)
Temperature/K	153(2)	163(2)	138(2)
Z	2	8	8
Reflections (Total/Unique/$I>2\sigma I$)	4761/588/583	9400/ 3550/ 3509	12740/4559/ 3943
R_{int}	0.0247	0.0279	0.0553
R_1 ($I > 2\sigma(I)$)	0.0275	0.0412	0.0709
$wR(F^2)$ (all data)	0.0769	0.0946	0.1952
Goodness of fit on F^2	1.247	1.211	1.050
CCDC number	928014	928015	928016

Table 6.2. Selected S–S and S–O Bond Lengths (Å) and Angles (°) in **1**

S1–O1	1.4603(16)	S1–S2	2.0973(7)
S1–O2	1.4514(12)	S2–S1^{i}	2.0973(7)
S1–O2^{ii}	1.4514(12)		
S1–S2–S1^{i}	105.30(4)		

Symmetry codes: (i) = x, ½−y, z, (ii) = 1.5−x, y, z

Table 6.3. Na–O Bond Lengths (Å) and Angles (°) in **1**

Na1–O1	2.3858(11)	O1–Na1–O1^{vii}	180.0
Na1–O1^{vii}	2.3858(11)	O1–Na1–O2^{iv}	90.0
Na1–O2^{iv}	2.4687(12)	O1–Na1–O2^{v}	90.26(5)
Na1–O2^{v}	2.4687(12)	O1^{vii}–Na1–O2^{iv}	90.26(5)
Na1–O3^{vii}	2.3213(12)	O1^{vii}–Na1–O2^{v}	89.74(5)
Na1–O3	2.3213(12)	O2^{iv}–Na1–O2^{v}	180.0
O3^{vii}–Na1–O3	180.0		
O3^{vii}–Na1–O1	84.46(4)		
O3–Na1–O1	95.54(4)		
O3^{vii}–Na1–O1^{vii}	95.54(4)		
O3–Na1–O1^{vii}	84.46(4)		
O3^{vii}–Na1–O2^{iv}	91.72(5)		
O3–Na1–O2^{iv}	88.28(5)		
O3^{vii}–Na1–O2^{v}	88.28(5)		
O3–Na1–O2^{v}	90.26(5)		

Symmetry codes: (iv) = 1−*x*, 1−*y*, 2−*z*, (v) = *x*, *y*, *z*−1, (viii) = 1–*x*, 1–*y*, 1–*z*

Table 6.4. Hydrogen–bond Interactions in **1**

Donor	H	Acceptor	D···A	D–H	H···A	D–H···A
O3	H3B	O4	2.706(2)	0.843(17)	1.891(18)	162(3)
O3	H3B	O4^{xi}	2.706(2)	0.843(17)	11.891(18)	162(3)

Symmetry code: (xi) = ½−*x*, *y*, *z*

Table 6.5. Selected S–S and S–O Bond Lengths (Å) and Angles (°) in **2**

S1–O1	1.445(4)	S1–S2	2.1313(19)
S1–O3	1.447(4)	S3–S4	2.1195(17)
S1–O2	1.454(4)	S5–S6	2.138(2)
S4–O4	1.444(4)	S7–S8	2.1069(18)
S4–O6	1.449(4)		
S4–O5	1.456(4)	S3–S2–S1	102.62(8)
S5–O8	1.440(4)	S2–S3–S4	105.86(7)
S5–O7	1.452(4)	S7–S6–S5	104.31(8)
S5–O9	1.465(4)	S6–S7–S8	100.25(8)
S6–S7	2.030(2)		
S8–O10	1.453(4)		
S8–O12	1.455(4)		
S8–O11	1.462(4)		

Table 6.6. K–O and K–S Bond Lengths (Å) in **2**

K1–O1^{i}	2.612(4)	K2–O3^{i}	2.680(6)
K1–O3^{ii}	2.684(5)	K2–O2^{vii}	2.747(5)
K1–O8^{iii}	2.775(4)	K2–O5^{i}	2.770(4)
K1–O7^{iv}	2.885(4)	K2–O12	2.775(4)
K1–O6^{v}	2.973(4)	K2–O4^{vii}	2.806(4)
K1–O4	2.993(4)	K2–O11	3.042(4)
K1–S2	3.4572(19)	K2–S2^{vii}	3.6814(19)
K1–S3^{v}	3.5484(19)		
K3–O2^{i}	2.676(5)	K4–O11^{v}	2.689(4)
K3–O6^{v}	2.798(4)	K4–O5	2.783(4)
K3–O12	2.811(4)	K4–O8^{viii}	2.806(4)
K3–O11^{v}	2.837(4)	K4–O7^{vii}	2.829(4)
K3–O4	2.897(4)	K4–O9^{vii}	2.843(4)
K3–O10^{v}	2.944(4)	K4–O10	2.918(4)
K3–O10	2.974(4)	K4–O12^{vii}	3.084(4)
K3–O9	2.985(4)	K4–O9^{viii}	3.096(4)
K3–O5^{v}	3.228(5)		

Symmetry codes: (i) $x, y+1, z$; (ii) $x, -y, z-1/2$; (iii) $x-1/2, -y+3/2, z-1/2$; (iv) $x-1/2, y-1/2, z$; (v) $x, -y+1, z-1/2$; (vi) $x-1/2, -y+1/2, z-1/2$; (vii) $x, -y+1, z+1/2$; (viii) $x, y-1, z$.

Table 6.7. Histogram of K–S bond distances, generated using the Cambridge Structural Database [17] suite of programs (ConQuest and Mercury.)

Number of Observations	367
Minimum/Maximum Distance	2.832/3.86 Å
Mean Distance	3.28(14) Å
Median Distance	3.254 Å
Skewness/Kurtosis	0.856/2.091
Upper/Lower Quantiles	3.19/3.332 Å
Number of Low/High Outliers	1/6

Table 6.8 Selected S–S and S–O Bond Lengths (Å) and Angles (^{o}) in **3**

S1–O2	1.445(5)	S1–S2	2.132(2)
S1–O3	1.450(5)	S2–S3	2.040(2)
S1–O1	1.450(5)	S3–S4	2.040(3)
S5–O5	1.444(5)	S4–S5	2.127(2)
S5–O6	1.445(5)	S6–S7	2.125(2)
S5–O4	1.450(5)	S7–S8	2.036(3)
S6–O7	1.440(6)	S8–S9	2.033(3)
S6–O9	1.444(5)	S9–S10	2.118(2)
S6–O8	1.450(5)		
S10–O11	1.441(5)		
S10–O12	1.447(5)		
S10–O10	1.448(5)		
S3–S2–S1	102.74(10)		
S2–S3–S4	107.88(10)		
S3–S4–S5	101.82(10)		
S8–S7–S6	101.52(10)		
S9–S8–S7	107.81(11)		
S8–S9–S10	102.85(10)		

Table 6.9 Hydrogen–bond Interactions in **3** (Å,°)

Donor	H	Acceptor	D···A	D–H	H···A	D–H···A
O13	H13B	$O1^{v}$	2.977(7)	0.87(2)	2.11(2)	174(8)
O13	H13A	$O3^{xii}$	2.763(7)	0.87(2)	1.94(4)	159(8)
O14	H14B	$O9^{vii}$	2.788(7)	0.87(2)	1.96(4)	158(7)
O15	H15A	$O8^{x}$	2.957(7)	0.86(2)	2.18(5)	149(8)
O15	H15B	$O9^{vii}$	2.810(7)	0.86(2)	1.98(3)	161(7)

Symmetry codes: (v) $x, -y+1/2, z+1/2$; (vii) $-x+2, -y, -z+1$; (x) $x, y, z-1$; (xii) $-x+1, y+1/2, -z+1/2$.

Table 6.10. K–O and K–S Bond Lengths (Å) in **3**

K1–O13	2.689(5)	K2–O7	2.649(6)
K1–O12	2.753(5)	$K2–O14^{iv}$	2.716(5)
K1–O1	2.762(5)	K2–O6	2.742(5)
$K1–O4^{ii}$	2.927(5)	$K2–O13^{v}$	2.747(5)
K1–O4	3.042(5)	$K2–O5^{v}$	2.994(5)
$K1–O11^{iii}$	3.049(6)	$K2–O2^{vi}$	3.059(5)
$K1–O12^{iii}$	3.104(5)	$K2–O4^{v}$	3.094(6)
K1–S2	3.475(2)	K2–S3	3.639(3)
K1–S4	3.585(2)		
$K3–O15^{v}$	2.658(5)	K4–O11	2.760(5)
$K3–O10^{v}$	2.767(5)	K4–O15	2.767(5)
K3–O8	2.873(6)	$K4–O14^{vii}$	2.796(5)
$K3–O5^{v}$	2.878(5)	$K4–O2^{viii}$	2.806(5)
K3–O10	2.979(5)	$K4–O10^{ii}$	2.965(5)
K3–O6	2.981(6)	$K4–O8^{ix}$	3.036(6)
$K3–O11^{v}$	3.315(6)	$K4–O1^{viii}$	3.066(6)
K3–O5	3.365(5)	$K4–O7^{x}$	3.119(6)
K3–S7	3.372(2)	$K4–O12^{ii}$	3.214(5)

Symmetry codes: (i) $x-1, -y+1/2, z-1/2$; (ii) $x, -y+1/2, z-1/2$; (iii) $x-1, y, z$; (iv) $x, y, z+1$; (v) $x, -y+1/2, z+1/2$; (vi) $-x+1, -y, -z+1$; (vii) $-x+2, -y, -z$; (viii) $x+1, y, z$; (ix) $x, y, z-1$; (x) $-x+2, -y, -z+1$.

Table 6.11 Geometric comparison (Å,°) for some intermolecular S_8 rings

Compound	S···S	S−S···S	Reference
Potassium pentathionate hydrate	3.601(2) 3.600(3)	98.2 129.8	This work
C70 Fullerene hexakis(octathiocane) (S_8)	3.38 3.52 3.54 3.67	169.6 116.2 94.7 144.6	23
Nonasulfur imide (HNS_9)	3.41 3.58	93.0 120.0	24
Octasulfur imide (HNS_8)	3.64 3.71 3.62 3.72	93.9 96.5 114.1 165.9	24
Heptasulfur imide (HNS_7)	3.63 3.57	139.5 92.8	25
Heptasulfur imide (HNS_7)	3.72 3.60	139.9 91.8	25
1,7–bis(trichloromethyl)heptasulfane	3.44 3.67	114.6 149.7	26

Note 1: For structures where less than four distances and angles are provided, the remaining ones are symmetry equivalent to those listed.
Note 2: There are two entries for HNS_7 as there are two difference intermolecular S_8 rings present in this structure.

6.6 References

[1] Silver, M., Dinardo, O. Factors Affecting Oxidation of Thiosalts by Thiobacilli, *Appl. Environ. Microbiol.* **1981**, *41*, 1301-1309.

[2] Druschel, G.K., Hamers, R.J., Banfield, J. F. *Geochimica et Cosmochimica Act*. *2003*, **67**, 4457–4469.

[3] Pan C., Wang W., Horváth A. K., Xie J, Lu Y., Wang Z., Ji C., Gao Q., *Inorg. Chem*. 2011, **50**, *9670–9677*.

[4] Steward, J.M., Szymanski, J.T. *Acta Cryst*. **1979**, *B35*, 1967–1970.

[5] (a) Steward, J.M., Szymanski, J.T. *Acta Cryst*. 1979, **B35**, 1971–1974. (b) Hartman, P. (1994) *Zeitschrift für Kristallographie-Crystalline Materials*. 209: 1–6.

[6] (a) Harrison, B., Hathaway, B.J., Kennedy, D. *Acta Cryst*. **1979**, *B35*, 2301-2306. (b) Chun, H, Bernal, I. *Eur. J. Inorg. Chem*. **1999**, 717-722. (c) Freire, E. Baggio, S., Baggio, R. *Aust. J. Chem*., 2001, *54*, 131-134. (d) Maroy, K. *Acta Chem.Scand*. **1971**, *25*, 2580-2590.

[7] Kelly, D. P.; Wood, A. P., Synthesis and determination of thiosulfate and polythionates. Methods Enzymol. 1994, 243, 475-500

[8] Sheldrick, G.M. *Acta Cryst*. **2008**, *A64*, 112–122.

[9] DIRDIF99: Beurskens, P.T., Admiraal, G., Beurskens, G., Bosman, W.P., de Gelder, R., Israel, R., Smits, J.M.M. (1999). The DIRDIF–99 program system, Technical Report of the Crystallography Laboratory, University of Nijmegen, The Netherlands.

[10] Cromer, D.T., Waber, J.T. (1974) "International Tables for X–ray Crystallography", Vol. IV, The Kynoch Press, Birmingham, England, Table 2.2 A.

[11] Ibers, J.A., Hamilton, W.C. (1964) *Acta Cryst.*,17: 781-782.

[12] Creagh, D.C., McAuley, W.J. (1992) "International Tables for Crystallography", Vol C, (A.J.C. Wilson, ed.), Kluwer Academic Publishers, Boston, Table 4.2.6.8, pp 219–222.

[13] Creagh, D.C., Hubbell, J.H. (1992) "International Tables for Crystallography", Vol C, (A.J.C. Wilson, ed.), Kluwer Academic Publishers, Boston, Table 4.2.4.3, pp. 200–206.

[14] CrystalStructure 3.7.0: Crystal Structure Analysis Package, Rigaku and Rigaku/MSC (2000–2005). 9009 New Trails Dr. The Woodlands TX 77381 USA.

[15] CRYSTALS Issue 10: Watkin, D.J., Prout, C.K., Carruthers, J.R., Betteridge, P.W. (1996) Chemical Crystallography Laboratory, Oxford, UK.

[16] Dolomanov, O.V., Bourhis, L.J., Gildea, R. J., Howard, J.A.K., Puschmann, H., *J. Appl. Cryst.***2009**, *42*, 339–341.

[17] Cambridge Structural Database System, Version 5.34 with February 2013 Update. Allen, F. H. *Acta Cryst*., **2002**, *B58*, 380–388.

[18] (a) Chen, C.–H., Chiou, S.–J., Chen, H.–Y. (2010) *Inorg.Chem*., 49: 2023. CCDC # 830207. (b) Wang, D.–Q., Dou, J.–M., Niu, M.–J., Li, D.–C., Liu, Y., Xuebao, H. Chin. (2002) *Acta. Chim. Sinica*, 60: 2145. CCDC # 179813. (c) Wang, D.–Q., Yu, Q.–J., Dou, J.–M. (2002) *Chin. J. Chem*., 20: 191. CCDC # 179801. (d) Harrington, J.M., Jones, S.B., White, P.H., Hancock, R.D. *Inorg. Chem*., **2004**, *43*, 4456.

CCDC # 247113. (e) Gjikaj, M. Adam, A., Duewel, M., Brockner, W. (2005) *Z. Kristallogr.–New Cryst. Struct.*, 220: 67. CCDC # 272790.

[19] (a) Kondo, Y., Endo, K., Hamada, F. *Chem. Commun.* **2005**, 711. CCDC # #240391 (b) Rottgers, T., Sheldrick, W.S. (2000) *J. Solid State Chem.*, 152: 271. CCDC # 135285. (c) Rottgers, T., Sheldrick, W.S. *Z. Anorg. Allg. Chem.*, 2002, *628*, 1305. CCDC # 177281

[20] (a) Ilyukhin, A.B., Petrosyants, *S.P. Koord.Khim.(Russ.)(Coord.Chem.*), **2009**, *35*, 576. CCDC # 705833. (b) Ming, W., Peiju, Z., Jing–Zhi, Z., Zhong, C., Jin–Ming, S., Yong–Hui, Y. *Acta Cryst.*, **1987**, *C43*, 1544. IUCr A27314. (c) Suturina, E.A., Semenov, N.A., Lonchakov, A.V., Bagryanskaya, I.Y., Gatilov, Y.V., Irtegova, I.G., Vasilieva, N.V., Lork, E., Mews, R., Gritsan, N.P., Zibarev, A.V. *J. Phys. Chem. A*, **2011**, *115*, 485. CCDC # 805366. (d) Dornhaus, F., Bolte, M., Lerner, H.–W., Wagner, M. *Eur. J. Inorg. Chem.*,**2006**, 5138. CCDC # 616916 and 616921. (e) Bacher, A.–D., Muller, U., Ruhlandt–Senge, K. *Z. Naturforsch.,B: Chem.Sci.*, **1992**, *47*, 1673. CSD 56566 (FIZ Karlsruhe). (f) Chadwick, S., Englich, U., Ruhlandt–Senge, K., *Organometallics*, **1997**, *16*, 5792. CSD Ref Codes PAYSAJ, PAYSEN and PAYSOX (g) Steinborn, D., Rosenstock, T., Sieler, J. *J.Prakt.Chem.–Chem.–Zeitung*, **1996**, *338*, 264. CCDC # 106996. (h) Naganuma, K., Kawashima, T., *J. Organomet. Chem.*, **2002**, *643*, 504. CCDC # 166131. (i) Chadwick, S., Englich, U., Ruhlandt–Senge, K., Watson, C., Bruce, A.E., Bruce, M.R.M. *J. Chem. Soc., Dalton Trans.*, **2000**, 2167. CCDC # 147524. (j) Solov'yev,

V.N., Chekhlov, A.N., Zabirov, N.G., Martynov, I.V. *Dokl.Akad.Nauk SSSR(Russ.) (Proc. Nat. Acad. Sci. USSR),* **1992**, 323: 1132. CSD Ref Code WAJGET.

[21] (a) Sharma, R.P, Singh, A., Venugopalan, P., Brandao, P., Felix, V. *Polyhedron*. **2012**, *40*, 175. CCDC # 708965, 838192 and 854931. (b) Chun, H., Bill, E., Bothe, E., Weyhermuller, T., Wieghardt, K. *Inorg.Chem*., **2002**, *41*, 5091. CCDC # 242247. (c) Harrison, W.D., Hathaway, B.J. *Acta Cryst*.., **1978**, *B34*, 2843. IUCr A16395. (d) Chun, H., Bernal, I. *Eur. J. Inorg. Chem*., **1999**, 717. CCDC # 101865. (e) Bernal, I., Cetrullo, J., Jackson, W.G. *Inorg. Chem*., **1993**, *32*, 4098. (f) Freire, E., Baggio, S., Garland, M.T., Baggio, R. *Acta Cryst*., **2001**, *C57*, 1403. CCDC # 179259. (g) Freire, E., Baggio, S., Baggio, R., Garland, M.T. *Acta Cryst*., **1998**, *C54*, 464. IUCr FG1333 and FG1333. (h) Liu, Y.–F., Xia, H.–T., Chen, H.–W., Wang, D.–Q. *Acta Cryst*., 2006, *E62*, m3089. CCDC # 607472. (i) Youngme, S., Wannarit, N., Pakawatchai, C., Chaichit, N., Somsook, E., Turpeinen, U., Mutikainen, I. *Polyhedron*. **2007**, *26*, 1459. CCDC # 616539. (j) Singh, A., Sharma, R.P., Ferretti, V., Rossetti, S., Venugopalan, P. *J. Mol. Struct*., **2009**, *927*, 111. CCDC # 694961. (k) Casadesus, M., Coogan, M.P., Davies, E., Ooi, L.–L. *Inorg. Chim. Acta*, **2008**, *361*, 63. CCDC # 616723, 616724, 616726 and 616725. (l) Bernal, I., Cetrullo, J., Somoza, F. *J. Coord. Chem*., **1996**, *40*, 57. (m) Sharma, R.P., Sharma, R., Bala, R., Pretto, L, Ferretti, V. *J. Mol. Struct*., **2006**, *794*, 303. CCDC # 285722. (n) Freire, E., Baggio, S., Baggio, R., Mombru, A. *Acta Cryst*., **2001**, *C57*, 14. CCDC # 158226. (o) Youngme, S., Chaichit, N. *Polyhedron*, **2002**,

21, 247. CCDC # 168976. (p) Marsh, R.E. *Acta Cryst*. 2004, *B60*, 252. CCDC # 237407.

[22] (a) Fujimoto, T., Kato, T., Usui, Y., Kamo, O., Furihata, K., Tsubono, K., Kato, T., Machinami, T., Tashiro, M. *Carbohydr.Res.,* **2011**, *346*, 1991. CCDC # 816367. (b) .Ilyukhin, A.B., Petrosyants, S.P., *Koord.Khim.(Russ.)(Coord.Chem.),* **2010**, *36*: 563. CCDC # 751415. (c) Petrosyants, S.P., .Ilyukhin, A.B. *Koord. Khim. (Russ.) (Coord. Chem.)*, **2007**, *33*, 163. CCDC # 602813. (c) Song, X.–M., Huang, X.–Q., Dou, J.–M., Li, D.–C. *Acta Cryst*. 2008, *E64*, m489. CCDC # 252235. (d) Chekhlov, A.N. *Koord. Khim. (Russ.) (Coord.Chem.)*, **2009**, *35*, 151. CCDC # 677868. (e) Englich, U., Chadwick, S., Ruhlandt–Senge, K. *Inorg. Chem*., **1998**, *37*, 283. (f) Ilyukhin, A., Dobrokhotova, Z., Petrosyants, S., Novotortsev, V. *Polyhedron*, **2011**, *30*, 2654. CCDC # 815245 and 815244. (g) Chadwick, S., Englich, U., Ruhlandt–Senge, K. *Organometallics*, **1997**, *16*, 5792. (h) Chekhlov, A.N. *Kristallografiya (Russ.) (Crystallogr. Rep.),***1997**, *42*, 100. (i) Chekhlov, A.N. *Koord. Khim. (Russ.) (Coord.Chem.)*, **2008**, *34*, 856.

[23] Burgi, H.B., Venugopalan, P., Schwarzenbach, D., Diederich, F., Thilgen, C. *Helv.Chim.Acta*, **1993**, *76*, 2155

[24] Steudel, R., Bergemann, K., Buschmann, J., Luger, P. *Angew.Chem.,Int.Ed.*, **1996**, *35*, 2537

[25] Wang, C.C., Hong, Y.–Y., Ueng, C.–H., Wang, Y. *J.Chem.Soc.,Dalton Trans.* **1992**, 3331.

[26] Steudel, R., Pridohl, M., Buschmann, J., Luger, P. *Chem.Ber.*, **1995**, *128*, 725. CSD 401546 (FIZ Karlsruhe)

[27] (a) Maroy, K. *Acta Chem.Scand.*, **1973**, *27*, 1705. (b) Foss, O., Maroy, K. *Acta Chem.Scand.*, **1959**, *13*, 201.

Chapter 7

Conclusions and future work

7.1 General Conclusions

Currently, ion exchange chromatography (IEC) is used in industry to measure thiosulfate, trithionate and tetrathionate. However, IEC suffers from long analysis times during which thiosalt species can undergo transformations (e.g., oxidation) leading to inaccuracies in the data. As well, the inability to measure key species such as sulfate and pentathionate makes computation of sulfur balances unreliable. Thus, the development of fast, quantitative and comprehensive analytical methods for the analysis of key thiosalts is valuable for industry, government and academia. Although there are several groups involved in this endeavor, not many advances in high throughput analysis have been made recently.[1-3] In this thesis,capillary zone electrophoresis (CZE) with indirect UV-vis (Chapters 2 – 4) and CE coupled with MS are shown to be suitable for the analysis of five key thiosulfate species sulfate, thiosulfate, trithionate, tetrathionate and pentathionate. Given the range of parameters that can be varied to tailor the CE methods to be robust, high throughput and suitable for environmental samples, design of experimental principles have been demonstrated to be very effective in this work. The methods developed here show that CE is a viable an alternative to IEC. They are expected to contribute immensely to ongoing research on thiosalts, and can be used by industry to better quantify thiosalts and other sulfur compounds, which will facilitate implementation of better means to mitigating the effects of thiosalts in mineral processing and in tailings. The work on CE-ESI-MS can be extended from proof of principle to the detection of thiosalts in complex environmental media and for trace analysis of these species. The work presented in this thesis also serves as the starting point for expanding the analytical

method to include a broader suite of sulfur species such as sulfide (S^{2-}), hydrosulfide (HS^-) and sulfite (SO_3^{2-}), which will give a more detailed picture of sulfur speciation and facilitate refinement of thiosalts treatment.

In Chapter 2, a univariate approach was used to systematically develop and optimize a CZE method with hexamethonium dication (HM^{2+}) as the EOF modifier and indirect detection of the thiosalts based on pyromellitic acid (PMA) as the chromophoric probe. The final method provided fast and quantitative analysis of the five thiosalt species in under 3 min. To the best of our knowledge no CZE method has been applied for all five species. Field amplified sample stacking (FASS) was also used to lower the detection limits by about 4 folds, from 0.09 and 0.34 μg/mL to between 0.02 and 0.12 μg/mL, making the method useful in trace and sub-trace analysis of these species.

A follow-up to the work described in Chapter 2 was pursued and the result are presented in Chapter 3, in which a multivariate experimental design approach using central composite (CCD) response surface was applied to method optimization. The objective for this was to improve on the previously optimized univariate method, study the influence of the main electrophoretic factors on the separation, and optimize these factors simultaneously to achieve better sensitivity, resolution and analysis times. Although the optimized method used a different EOF modifier and different BGE component concentrations than described in Chapter 2, the analysis times in both instances were ~ 2.9 min. However, the LODs were better (except for sulfate) for the method optimized

using multivariate analysis (between 0.1 to 0.2 μg/mL) than with univariate method without sample stacking, 0.09 μg/mL compared to 0.34 μg/mL. Moreover, a better understanding of the influence of the electrophoretic factors and how best to approach optimization was gained in the course of this study. This will aid in future work exploring application of the approach to more complex systems with a greater range of sulfur anions.

In Chapter 4, a new chromophoric probe (trimellitic acid –TMA) for thiosalts was used together with hexamethonium hydroxide in the development of a new CZE method with indirect UV-vis detection for the five thiosalt anions. As this probe has not been exploited previously for these species, full use was made of a multivariate experimental design approach. Six factors were studied at the screening stage using a fractional factorial design, of these, four critical factors were selected for optimization using Box-Behnken response surface design. The responses studied included peak resolution, peak symmetry and analysis time. It was observed that some peaks, particularly those of trithionate and tetrathionate, showed splitting at certain concentration of TMA and HMOH. By optimizing the factors to desired levels, this problem was reduced and complete separation of the five species was obtained. The LOD values obtained with TMA (0.2 – 0.4 μg/mL) were higher than those obtained using PMA, which is not unexpected since TMA has a lower molar extinction coefficient than PMA.[4]

In Chapter 5, a positive mode ESI-MS method was used to study the association constants of the five thiosalt species using three tricationic ion-pairing reagents: (3,5-tris[(3-butyl-imidazolium)- methyl]-2,4,6-trimethylbenzene (IP-L-Imid), 1,3,5-tris [(tripropylphosphonium) methyl]benzene (IP-T-Imid) and 1,3-bis[6-(3-benzyl-1-imidazolio)-hexyl]imidazolium (IP-T-Phos). All ion-pairing reagents formed favourable associations with thiosalts in the gas-phase. To the best of our knowledge, only two papers have been published in which ion-pairing reagents have been applied for CE-ESI-MS experiments.[5,6] The use of tricationic ion-pairing reagents with all the thiosalts described in this chapter has not been reported elsewhere. Based on the results obtained in this Chapter 5, it is anticipated that the use of these ion-paring reagents can be extended to a full CE-ESI-MS for a comprehensive range of thiosalts for fast and sensitive analyses.

Chapter 6 a low temperature X-ray structural determinations of sodium trithionate trihydrate, anhydrous potassium tetrathionate and potassium pentathionate hydrate are reported. A statistical survey of potassium-sulfur interactions has been performed, and the K–S (tetra- and pentathionate donors) bonds highlighted. An intermolecular S8 ring motif has been found in the structure of the pentathionate.

7.2 Future research work outlook

The future of work on thiosalts based on the results obtained in this study looks bright. First, it has been established that CZE with indirect UV-vis detection is more attractive

than the currently used IC technique for analysis of thiosalts. One challenge with the CZE methods was that of real sample analysis in the presence of a large excess of sulfate. One way this was overcome was to dilute the real sample fifty (50x) and one hundred times (100x), with the assumption that environmentally relevant concentrations could still be measured reliably. However, based on the principles of standard addition, dilutions should not be more than 20% of the original sample. In the future, further methods developed for the analysis of real thiosalt samples should be optimized to accommodate large excesses of single analytes without compromising the efficiency of the separation and loss of sensitivity for trace concentrations of certain species, which may become undetectable upon dilution. A similar challenge was encountered by Muzikář *et al.* when analyzing sulfate in the presence of large excess of chloride.[7] The approach was to provide a means on accommodating this peak using experimental design. Finally, for the multivariate CZE method optimization, care should be taken in the screening and selecting of the most critical factors for optimum separation efficiency. For instance, the selection of injection time as a critical factor may not be necessary if the aim of the method was for to achieve high sensitivity. The selection of the type of experimental design should also be given due consideration. A response surface central composite design (CCD) may be better than a Box-Behnken design (BBD), especially for new factors, such as the new chromophoric probe (e.g. TMA Chapter 4). CCD has an embedded factorial design and allows for testing for higher and lower factor levels than can be accommodated by a BBD design. Since it may be possible that higher

concentrations of TMA or HMOH would be required to eliminate undesirable results, such as peak splitting, CCD design would be more efficient than BBD.

For the FIA-ESI-MS work on determination of association constants for trication-thiosalt ion-pairs (Chapter 5), some improvement may be required to fine-tune the results obtained. For example, a diffusion pump malfunction made it difficult to maintain a constant flow of the ion-pairing reagents and will need to be addressed. For example, a separate isocratic pump may be a more reliable pumping system for the post-column addition, and this affords the option of using higher flow rates to infuse the ion-pairing reagents. Secondly, MS/MS analysis of the ion-pairs can provide insight into the stability of these ion-pairs and their fragmentation pathways, enabling the ability to 'fingerprint' these ion-pairs.

The work on CE-ESI-MS for the analysis of tricationic-thiosalts ion- pairs was largely left uncompleted and will need further development. As mentioned previously, method development should include the application of a multivariate experimental design and the analysis of the ion-pairs should further exploit the selectivity of the ion-pairing reagents with the thiosalts. The association constants measured in Chapter 5 will provide a good starting point for this work.

7.3 References

[1] Wasserlauf, M.; Dutrizac, J.E. In The chemistry, Generation and Treatment of Thiosalts in Milling Effluents – A Non-critical Summary of CANMET investigations 1976-1982, CANMET Report 82-4E, 1982.

[2] Dinardo, O.; Sally, J. In *Treatment of thiosalts in milling effluent: A review of treatment process*. Mining and Mineral Sciences Laboratories Report. Thiosalts Consortium-Phase II. CANMET-MMSL, 1998.

[3] Fahd, F.; Khan, F.; Hawboldt, K.; Abbassi, R. Developing a Novel Methodology for the Ecological Risk Assessment of Thiosalts. *Stoch. Environ. Res. Risk Assess.* **2014,** *28,* 383-391.

[4] Sørensen, S.; Sørense, H.; Bjergegaard, C.; Michaelsen, S. High Performance Capillary Electrophoresis. In *Handbook of Capillary and Microchip Electrophoresis and Associated Microtecnques*; Belton, P.S. Ed.; RSC, Cambridge, UK 1999, 2008; 208-277.

[5] Lin, X.; Gerardi, A.R.; Breitbach, Z.S.; Armstrong, D.W.; Colyer, C.L. CE-ESI-MS Analysis of Singly Charged Inorganic and Organic Anions Using a Dicationic Reagent As a Complexing Agent. *Electrophoresis,*.**2009**, *30,* 3918-3925.

[6] Anthony R. Gerardi, A.R.; Lin, X., Breitbach, Z.S.; Armstrong, D.W.; Colyer, C.L. CE-ESI-MS Separation of Divalent Organic and Inorganic Anions Using a Tricationic Complexing Reagent. *Electrophoresis.* **2012**, *33,* 734–740.

[7] Muzikář, M.; Havel, J.; Macka, M. Capillary Electrophoresis Determinations of Trace Concentrations of Inorganic Ions in Large Excess of Chloride: Soft

Modelling Using Artificial Neural Networks for Optimisation of Electrolyte Composition. *Electrophoresis*. **2003**, *24*, 2252–2258

Appendices

Appendix A

Systematic optimization of a pyromellitic acid background electrolyte for capillary electrophoresis with indirect UV-Vis detection and online pre-concentration analysis of thiosalt anions in the treated mine tailings pond

In this section we present additional information on the influence of [TMAOH] on EOF and thiosalts separation efficiency (Figures A 1), of influence of [CTAB] on EOF and thiosalts separation efficiency (Figures A 2) and influence of [HMOH] on EOF and thiosalts separation efficiency (Figures A 3); influence of [PMA] on the sensitivity and separation efficiency of thiosalt species (Figure A 4), pH on the separation efficiency using the optimized PMA BGE (Figures A 5), influence of applied voltage on separation efficiency using optimized PMA BGE (Figures A 6); comparison of commercially available PMA BGE vs optimized PMA BGE under different applied voltage conditions (Figures A 7 and 8); effect of sampling stacking on sensitivity of analysis (Figure A 9); electropherogram of real thiosalt tailings pond sample and addition of thiosalts standards (Figure A 10, and standard addition calibration curves of thiosalts tailings pond sample (Figures A 11 - 15). Unless otherwise stated all migration times are in min.

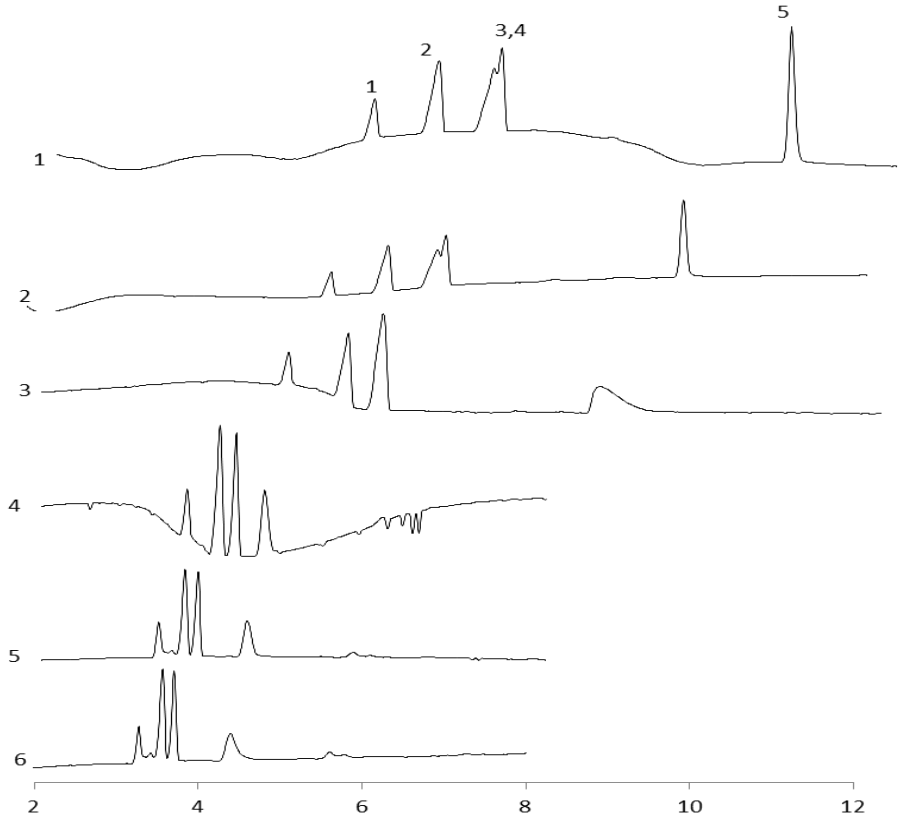

Figure A 1. Electropherograms showing the effect of increase in [TMAOH] on separation efficiency of 5 thiosalt species. 1. No TMAOH, 2. [TMAOH] = 0.20 mM, 3. [TMAOH] = 0.40, 4. [TMAOH] = 0.60 mM, 5. [TMAOH] = 0.80 mM, 6. [TMAOH] = 1.00 mM. CZE conditions: injection: 250 mbar.s, applied field: -20 kV, temperature: 25 ^{o}C, indirect UV detection at λ = 350 nm, Ref 200 nm. BGE 2.00 mM PMA pH adjusted to 8 with TEA.

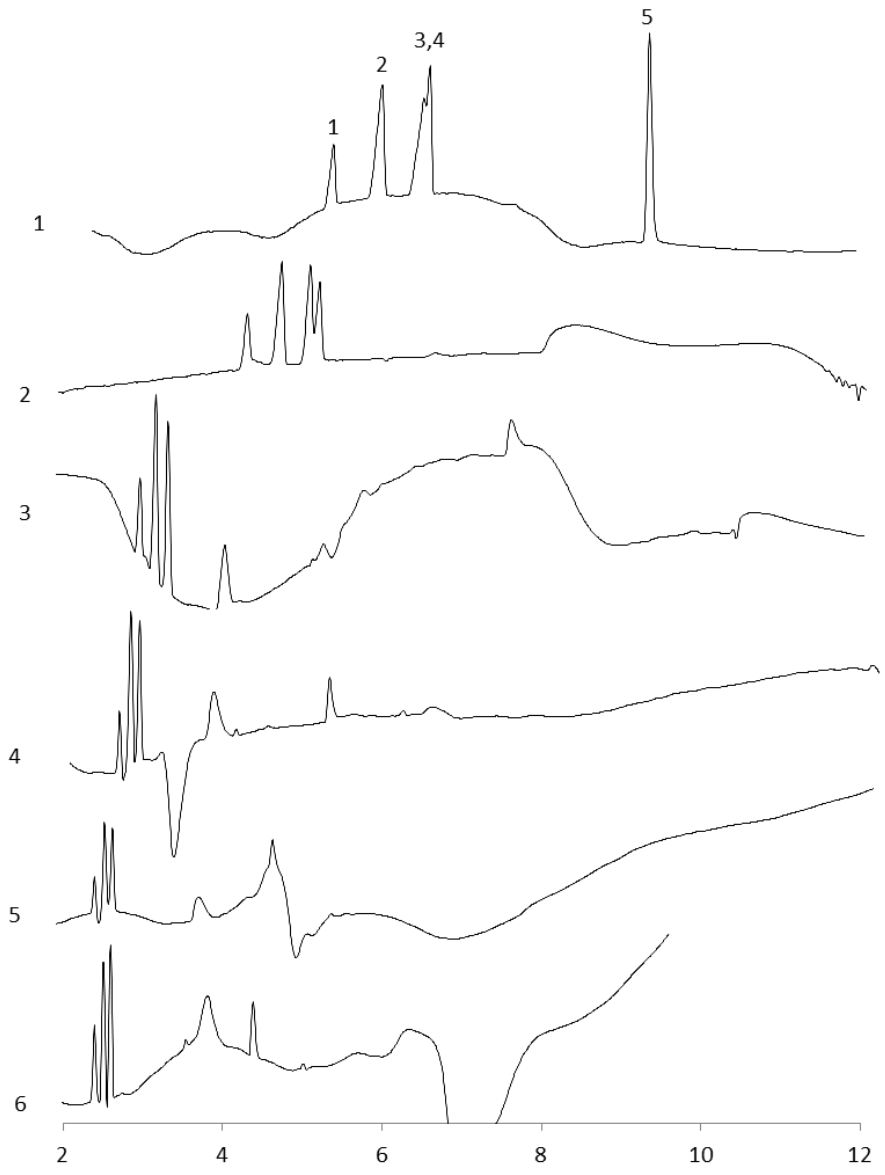

Figure A 2. Electropherograms showing the effect of increase in [CTAB] on separation efficiency of 5 thiosalt species. 1. [CTAB] = 0.00 mM, 2. [CTAB] = 0.20 mM, 3. [CTAB] = 0.40, 4. [CTAB] = 0.60 mM, 5. [CTAB] = 0.80 mM, 6. [CTAB] = 1.00 mM. CZE conditions: injection: 250 mbar.s, applied field: -20 kV, temperature: 25 ^{o}C, indirect UV detection at λ = 350 nm, Ref 200 nm. BGE 2.00 mM PMA pH adjusted to 8 with TEA.

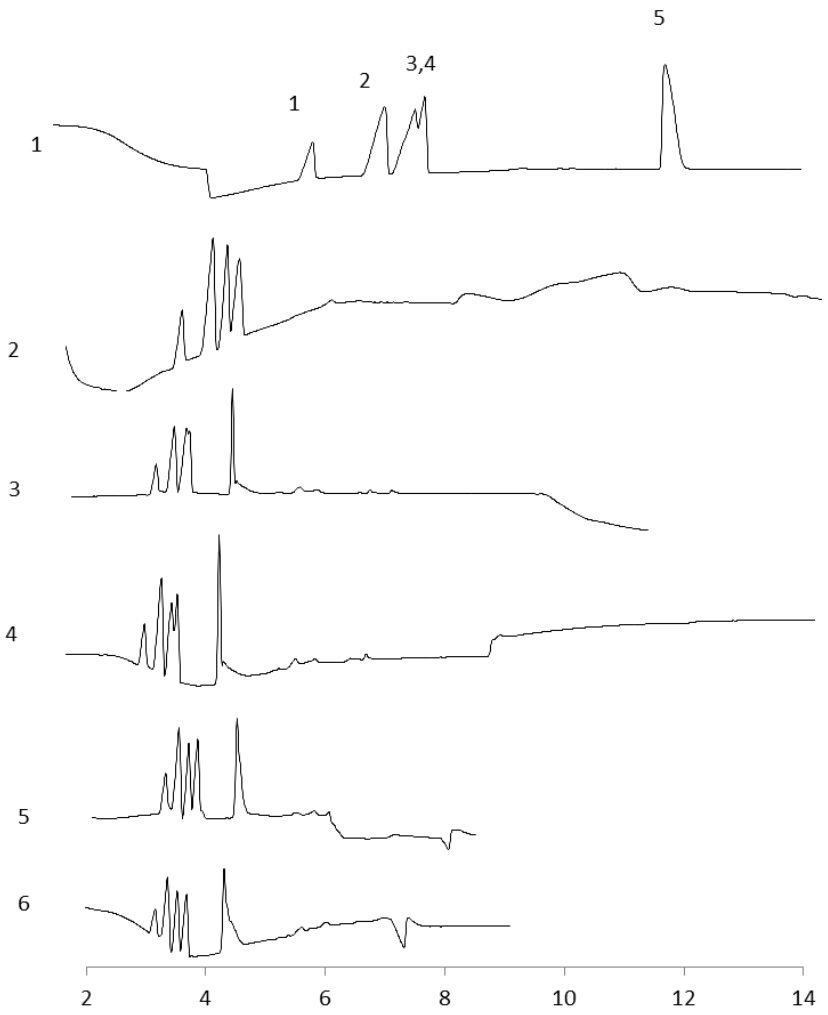

Figure A 3. Electropherograms showing the effect of increase in [HMOH] on separation efficiency of 5 thiosalt species. 1. [HMOH] = 0.00 mM, 2. [HMOH] = 0.20 mM, 3. [HMOH] = 0.40, 4. [HMOH] = 0.60 mM, 5. [HMOH] = 0.80 mM, 6. [HMOH] = 1.00 mM. CZE conditions: injection: 250 mbar.s, applied field: -20 kV, temperature: 25 ^{o}C, indirect UV detection at λ = 350 nm, Ref 200 nm. BGE 2.00 mM PMA pH adjusted to 8 with TEA.

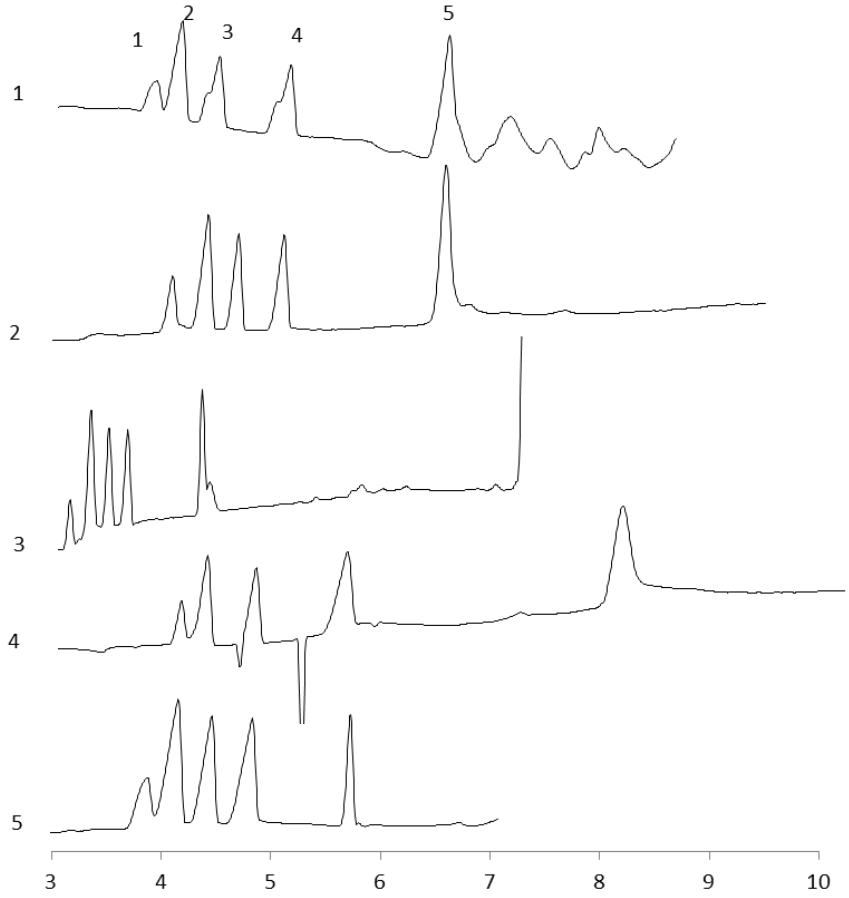

Figure A 4. Electropherograms showing the effect of increase in [PMA] on sensitivity and separation efficiency of 5 thiosalt species. 1. [PMA] = 1.00 mM, 2. [PMA] = 1.50 mM, 3. [PMA] = 2.00 mM, 4. [PMA] = 2.50 mM, 5. [PMA] = 3.00 mM. CZE conditions: injection: 250 mbar.s, applied field: -20 kV, temperature: 25 ^{o}C, indirect UV detection at λ = 350 nm, Ref 200 nm. BGE 0.80 mM HMOH with PMA pH adjusted to 8 with TEA.

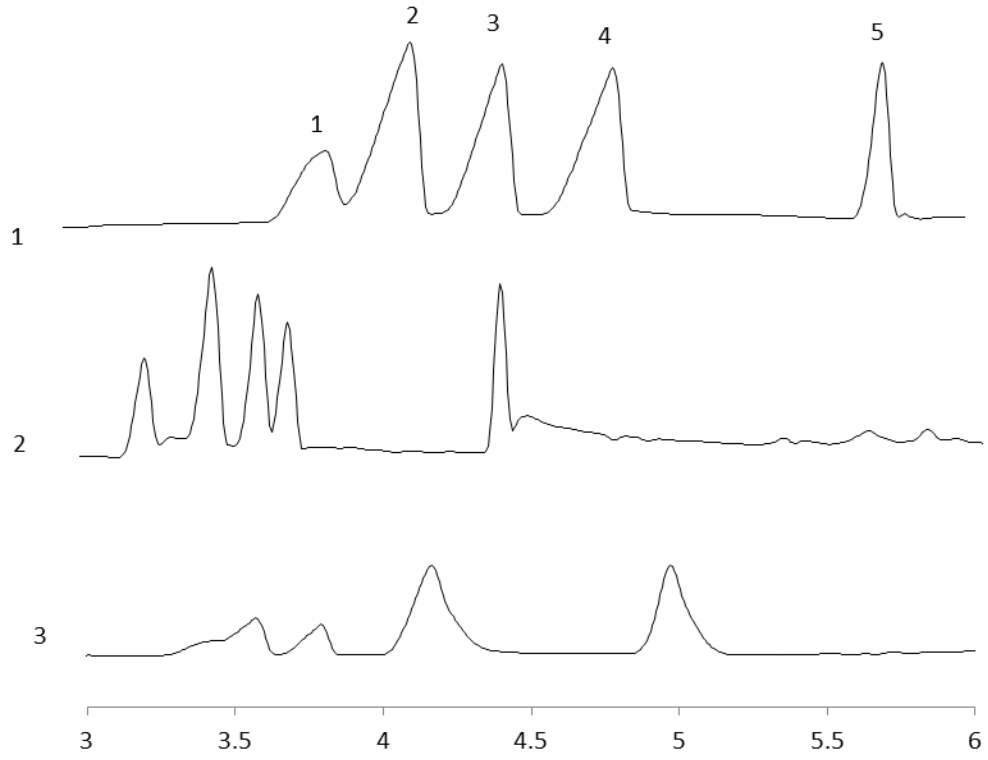

Figure A 5. Electropherograms showing the effect of increase in pH on sensitivity and separation efficiency of 5 thiosalt species. 1. pH = 7, 2. pH = 8, pH = 9 CZE conditions: injection: 250 mbar.s, applied field: -20 kV, temperature: 25 ^{o}C, indirect UV detection at λ = 350 nm, Ref 200 nm. BGE [PMA] = 2.00 mM, [HMOH] = 0.80 mM pH adjusted to 7, 8 and 9 with TEA.

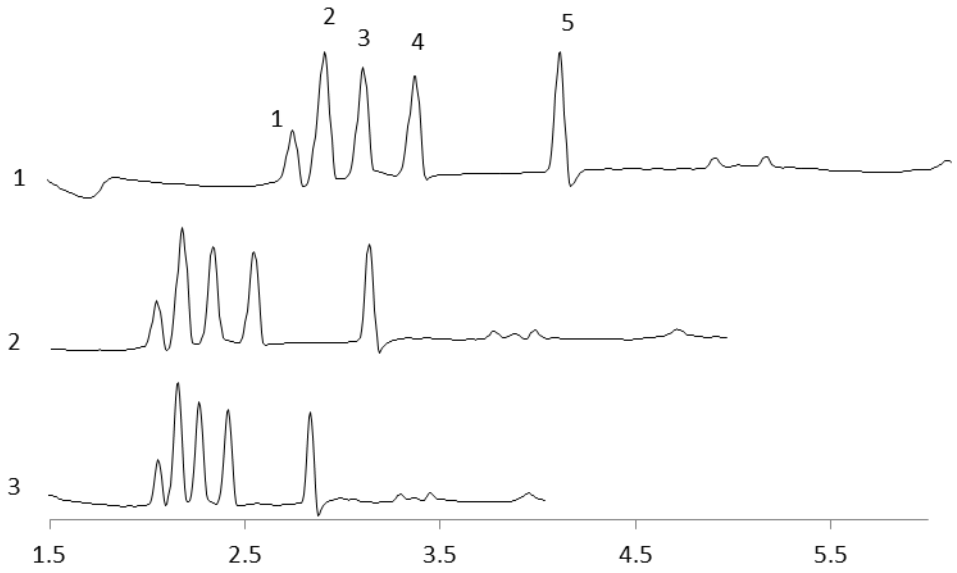

Figure A 6. Electropherograms showing the effect of increase in electric field strength on sensitivity and separation efficiency of 5 thiosalt species. 1. -20 kV, 2. -25 kV, 3. -30 kV CZE conditions: injection: 250 mbar.s, applied field: -20 kV, temperature: 25 ^{o}C, indirect UV detection at λ = 350 nm, Ref 200 nm. BGE [PMA] = 2.00 mM, [HMOH] = 0.80 mM pH adusted to with TEA.

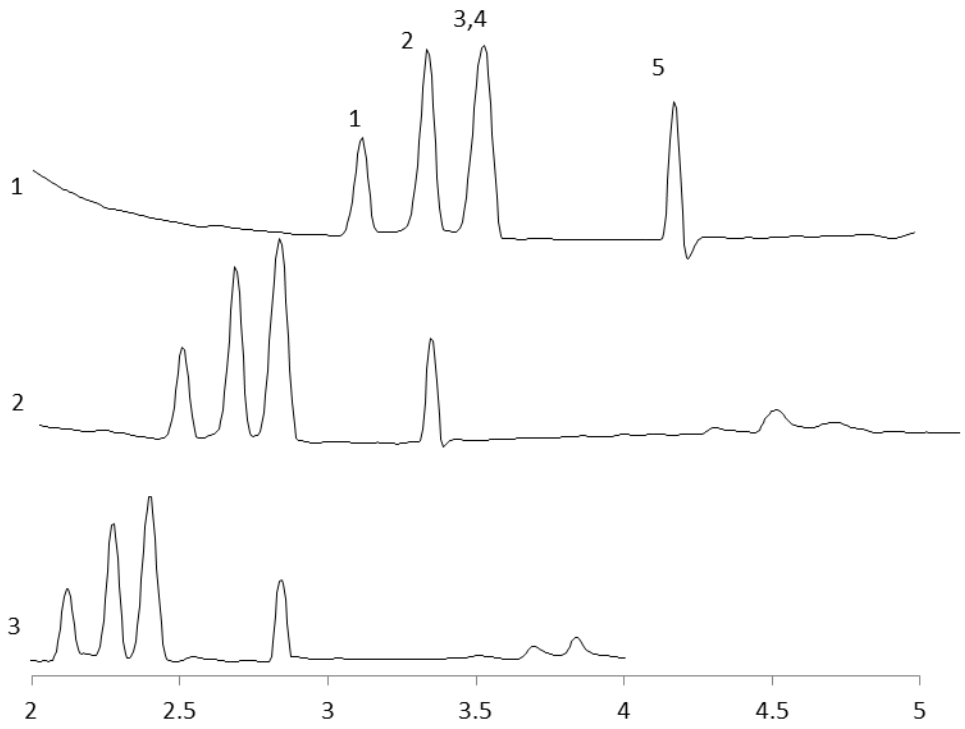

Figure A 7. Electropherograms showing the effect of increase in electric field strength on sensitivity and separation efficiency of 5 thiosalt species using commercially available PMA BGE. 1. -20 kV, 2. -25 kV, 3. -30 kV CZE conditions: injection: 250 mbar.s, applied field: -20 kV, temperature: 25 ^{o}C, indirect UV detection at λ = 350 nm, Ref 200 nm.

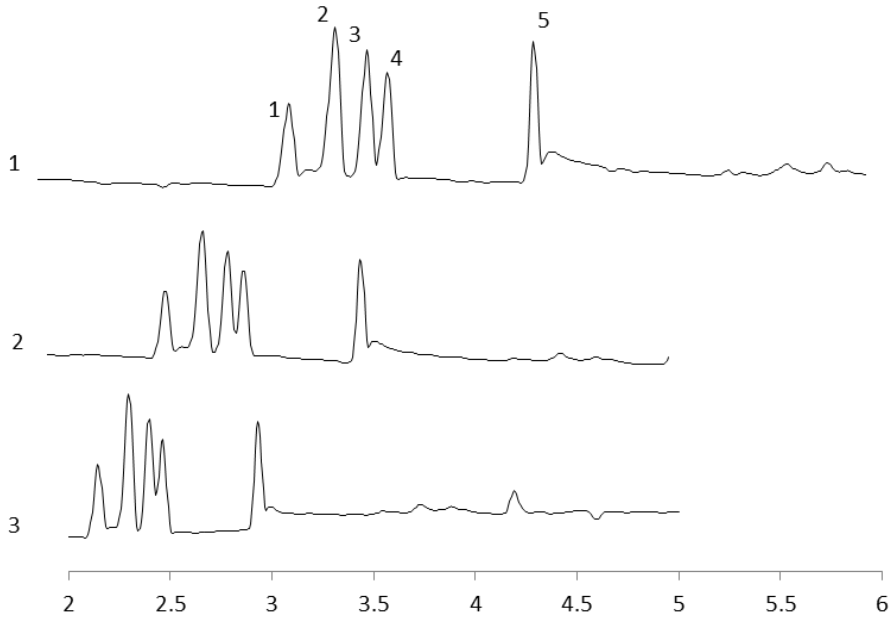

Figure A 8. Electropherograms showing the effect of increase in electric field strength on sensitivity and separation efficiency of 5 thiosalt species using the optimized PMA BGE. 1. -20 kV, 2. -25 kV, 3. -30 kV CZE conditions: injection: 250 mbar.s, applied field: -20 kV, temperature: 25 ^{o}C, indirect UV detection at λ = 350 nm, Ref 200 nm.

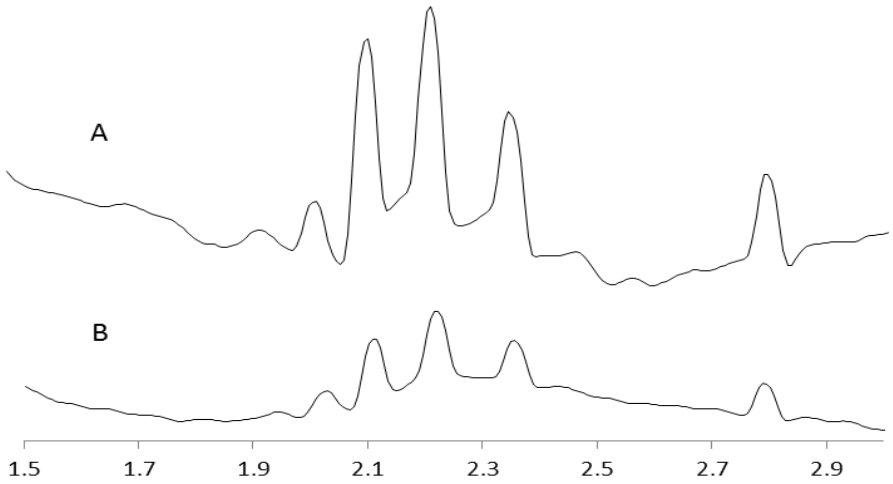

Figure A 9. Electropherograms of thiosalts showing the influence of FASS on detection sensitivity. A. Analysis with stacking 3s at 30 mbar of water followed by 5 s at 50 mbar of sample, B. Analysis without stacking. [thiosalts] = 0.2 µg/mL each.

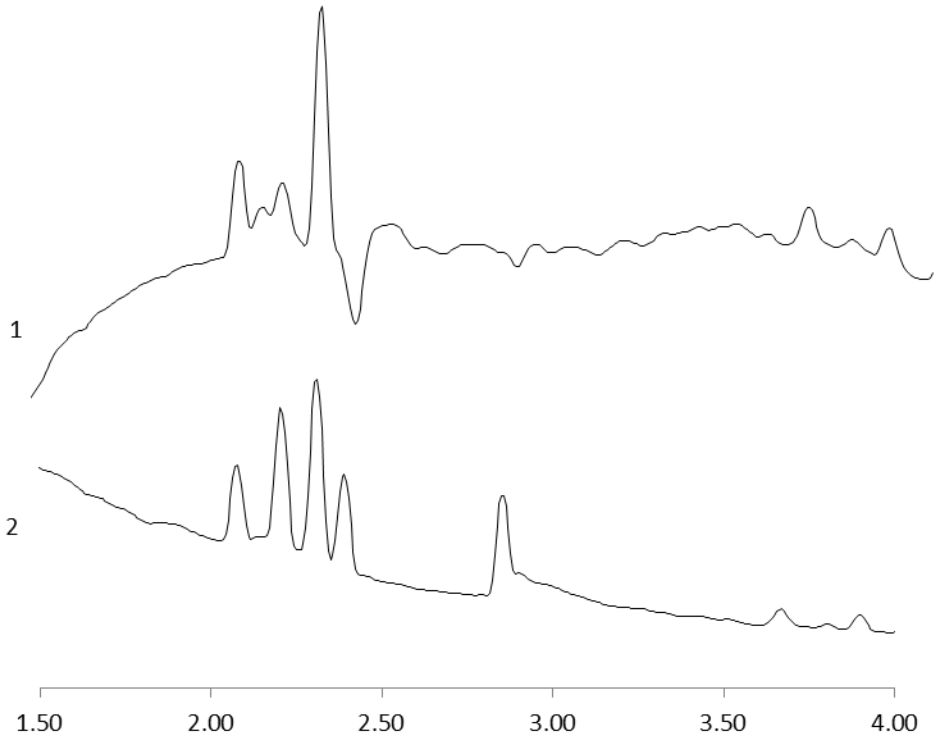

Figure A 10. Electropherograms of 1. Diluted (1:50) real sample from surface of thiosalts tailings pond, 2. Addition of 500 µL addition of thiosalt standard mixture 1 CZE conditions: injection: 250 mbar.s, applied field: -20 kV, temperature: 25 ^{o}C, indirect UV detection at λ = 350 nm, Ref 200 nm. BGE [PMA] = 2.00 mM, [HMOH] = 0.80 mM pH adjusted to with TEA.

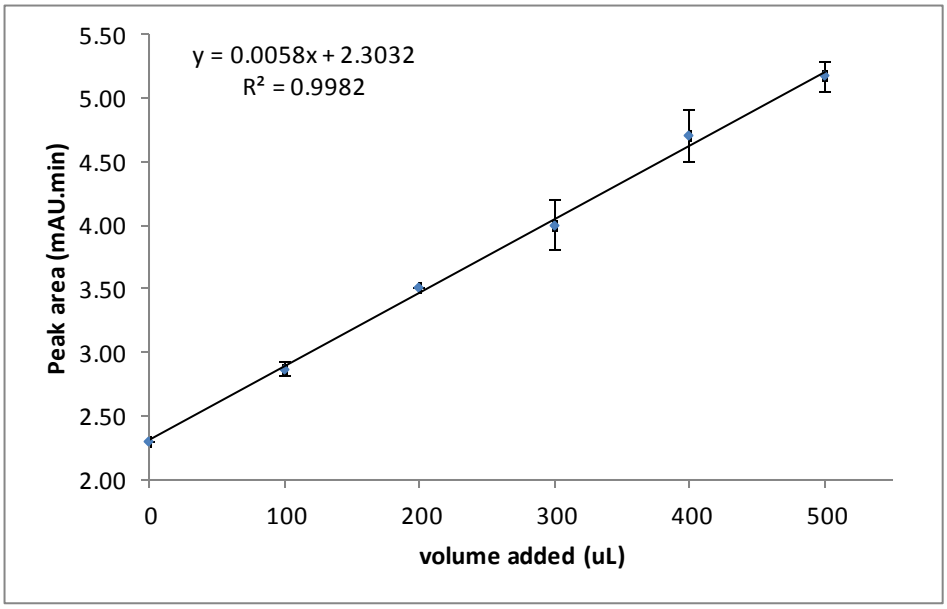

Figure A 11. Standard addition calibration curve showing addition of standard SO_4^{2-} to 1:50 diluted sample on the peak area of SO_4^{2-}

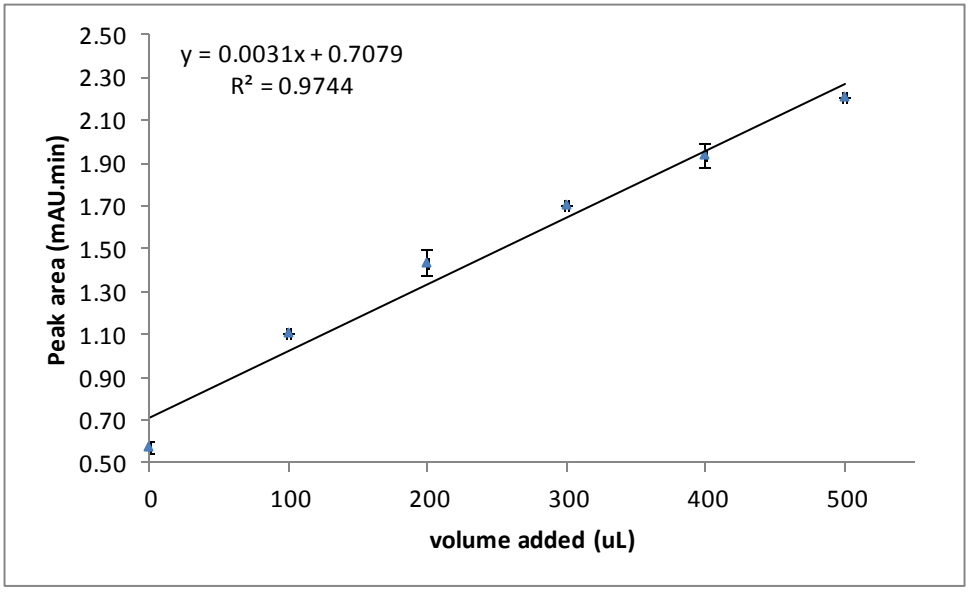

Figure A 12. Standard addition calibration curve showing addition of standard $S_2O_3^{2-}$ to 1:50 diluted sample on the peak area of $S_2O_3^{2-}$

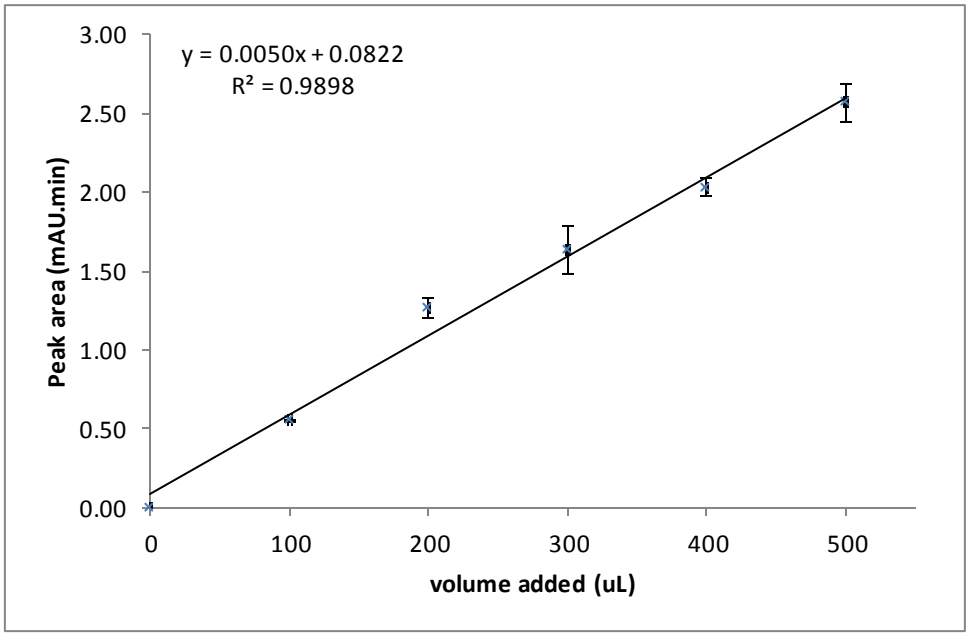

Figure A 13. Standard addition calibration curve showing addition of standard $S_3O_6^{2-}$ to 1:50 diluted sample on the peak area of $S_3O_6^{2-}$

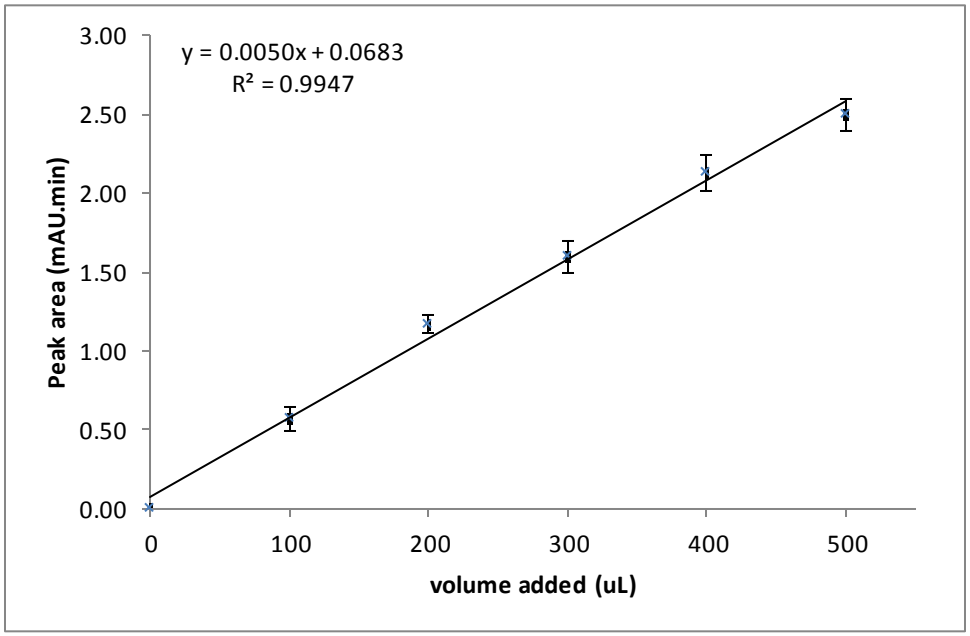

Figure A 14. Standard addition calibration curve showing addition of standard $S_4O_6^{2-}$ to 1:50 diluted sample on the peak area of $S_4O_6^{2-}$

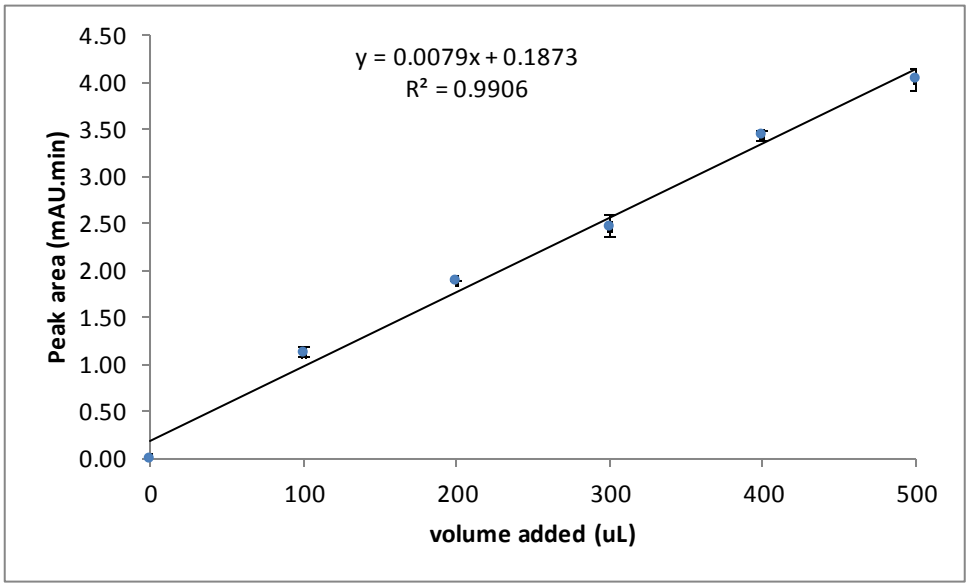

Figure A 15. Standard addition calibration curve showing addition of standard $S_5O_6^{2-}$ to 1:50 diluted sample on the peak area of $S_4O_6^{2-}$

Appendix B

Central composite response surface designs for optimization of capillary electrophoresis with indirect detection using a triethanolamine-buffered pyromellitic acid probe for the analysis of thiosalts mine tailings

In this section we present additional information on the central composite experimental design (CCD) factors, levels and results (Table B 1); calculations (Equation B-1 and B-2); surface plots of influence of influence of [PMA] and [HM^{2+}] on the resolution factor (R_s) (Figure B1 – B4); standard calibration curves for 5 thiosalt species (Figure B5 – B9); and standard addition calibration curves for 5 thiosalt species (Figure B10 – B14)

Table B 1. Central composite experimental design (CCD) of factors, levels and results of experiments

StdOrder	RunOrder	PtType	Blocks	[PMA]	[HM^{2+}]	Applied Field (-kV)	$R_{1,2}$	$R_{2,3}$	$R_{3,4}$	$R_{4,5}$	*i*	t (min)
10	1	1	2	5.00	1.00	30	1.37	3.70	1.74	10.40	19.1	3.03
11	2	0	2	3.00	0.60	24	2.78	3.22	1.52	10.59	10.2	3.87
12	3	0	2	3.00	0.60	24	2.80	3.23	1.51	10.31	10.3	3.86
7	4	1	2	5.00	0.20	18	1.92	5.34	1.38	14.54	15.4	4.26
8	5	1	2	1.00	1.00	18	2.89	1.36	2.42	11.46	3.0	4.76
9	6	1	2	1.00	0.20	30	0.00	3.61	1.12	8.46	5.4	2.97
2	7	1	1	5.00	1.00	18	1.64	5.11	2.34	15.75	11.4	5.16
3	8	1	1	5.00	0.20	30	0.93	4.38	1.22	12.24	19.8	3.33
6	9	0	1	3.00	0.60	24	2.83	3.25	1.51	11.17	10.2	3.86
1	10	1	1	1.00	0.20	18	4.61	1.63	1.17	14.87	3.5	4.99
5	11	0	1	3.00	0.60	24	2.79	3.27	1.49	11.30	10.2	3.85
4	12	1	1	1.00	1.00	30	2.74	1.42	1.99	8.71	5.5	2.84
17	13	-1	3	3.00	0.60	18	3.02	3.48	1.86	15.91	7.4	5.06
18	14	-1	3	3.00	0.60	30	2.49	2.73	1.40	9.32	12.7	3.01
16	15	-1	3	3.00	1.00	24	2.32	2.97	2.09	12.28	10.2	3.65
19	16	0	3	3.00	0.60	24	2.79	3.27	1.52	11.89	10.1	3.86
15	17	-1	3	3.00	0.20	24	3.04	3.58	1.06	14.33	10.5	4.07
14	18	-1	3	5.00	0.60	24	1.31	3.77	1.49	9.56	15.6	3.94
20	19	0	3	3.00	0.60	24	2.81	3.26	1.44	11.24	10.1	3.87
13	20	-1	3	1.00	0.60	24	3.36	1.39	1.62	10.75	4.5	3.65

$R_{1,2}$; $R_{2,3}$; $R_{3,4}$ and $R_{4,5}$ = peak resolution factors; *i* = system current; and t = migration time (min) of last analyte peak

Calculations:

The resolution factor (R_s) was calculated using the equation:

$$R_{1,2} = \frac{2\,(t_2 - t_1)}{w_1 + w_2} \qquad \text{B-1}$$

Where $R_{1,2}$ is the peak resolution between two adjacent peaks 1 and 2; t_1 is the migration time of peak 1 and t_2 is the migration time of peak 2.

Percent Difference (% Diff) between the predicted and experimental responses was calculated using the equation:

$$\%\ \text{Diff} = \frac{|T - E|}{\frac{1}{2}(T + E)} \qquad \text{B-2}$$

where T is the theoretically predicted response using the mathematical model and E is the experimental response.

The response surface plots of the influence of [PMA] and [HM^{2+}] on the peak resolution factors are presented below:

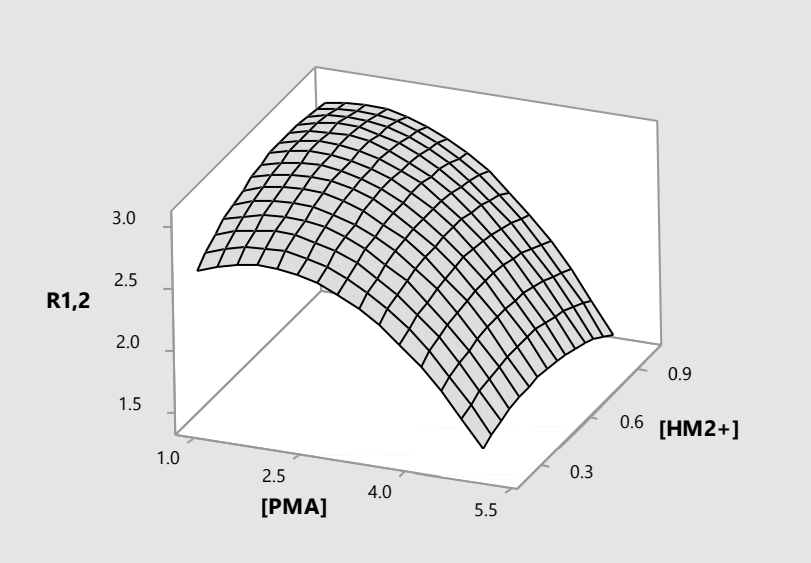

Figure B 16. Response surface plot of Resolutions $R_{1,2}$, vs [PMA] and [HM^{2+}]

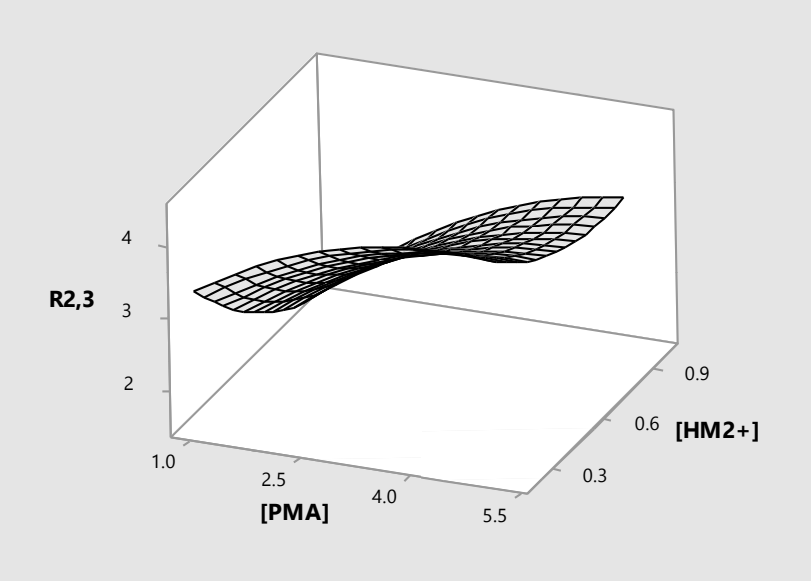

Figure B 2. Response surface plot of Resolutions $R_{2,3}$, vs [PMA] and [HM^{2+}]

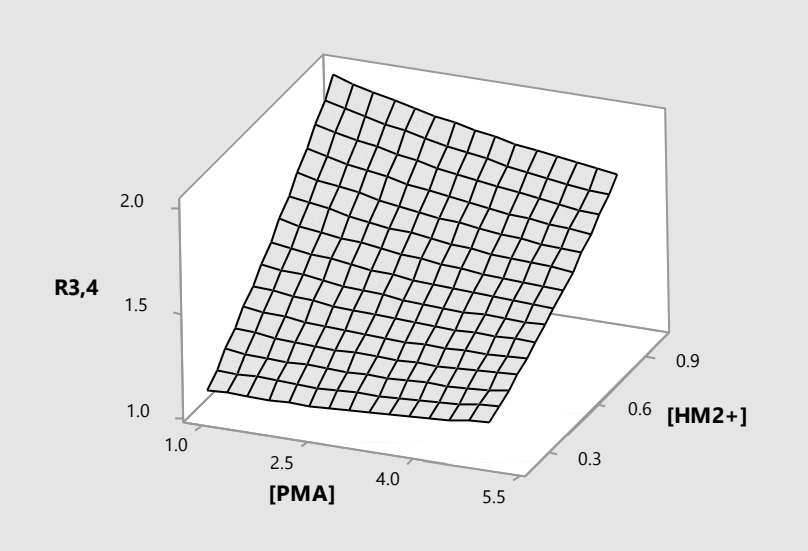

Figure B 17. Response surface plot of Resolutions $R_{2,3}$, vs [PMA] and [HM^{2+}]

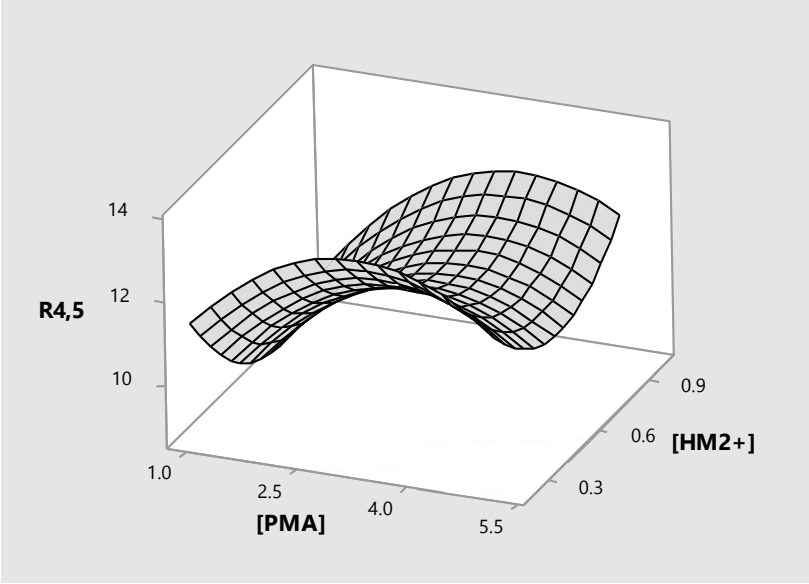

Figure B 18. Response surface plot of Resolutions $R_{2,3}$, vs [PMA] and [HM^{2+}]

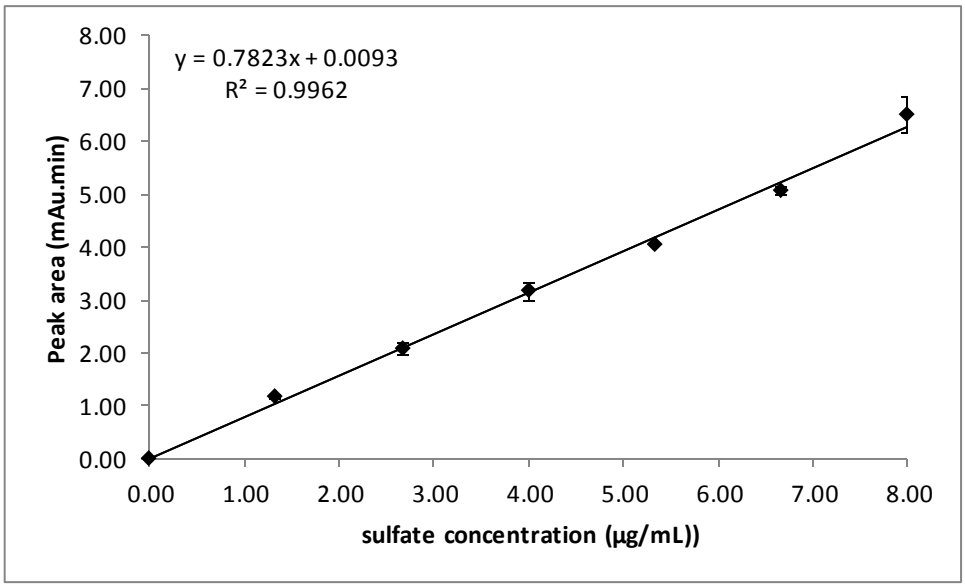

Figure B 19. External calibration curve for sulfate using the optimized PMA BGE system

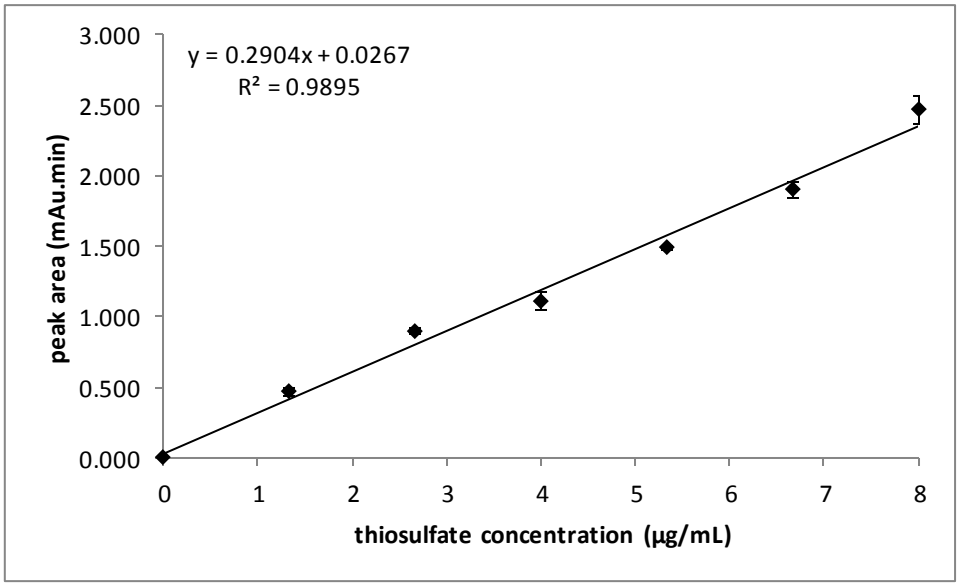

Figure B 20. External calibration curve for thiosulfate using the optimized PMA BGE system

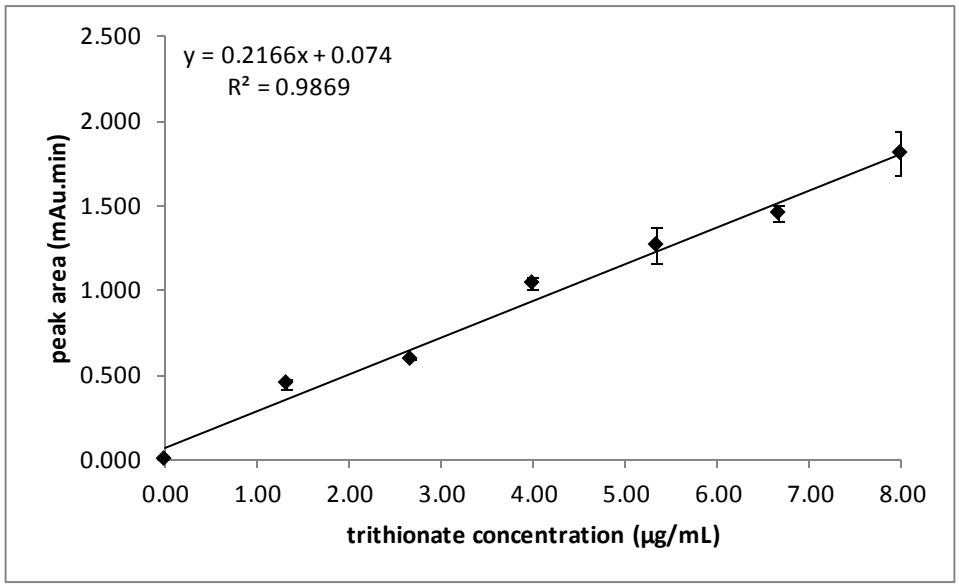

Figure B 21. External calibration curve for trithionate using the optimized PMA BGE system

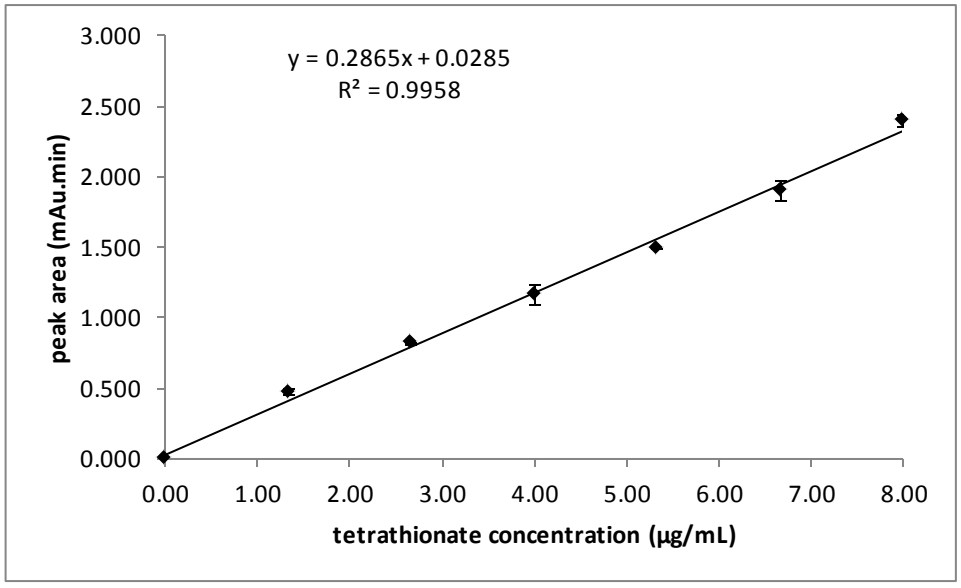

Figure B 22. External calibration curve for tetrathionate using the optimized PMA BGE system

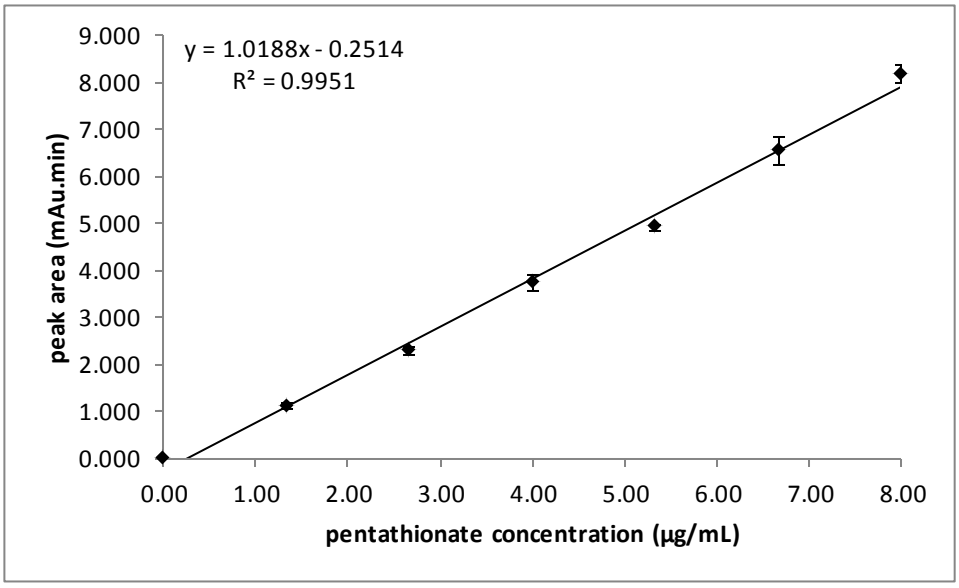

Figure B 23. External calibration curve for pentathionate using the optimized PMA BGE system

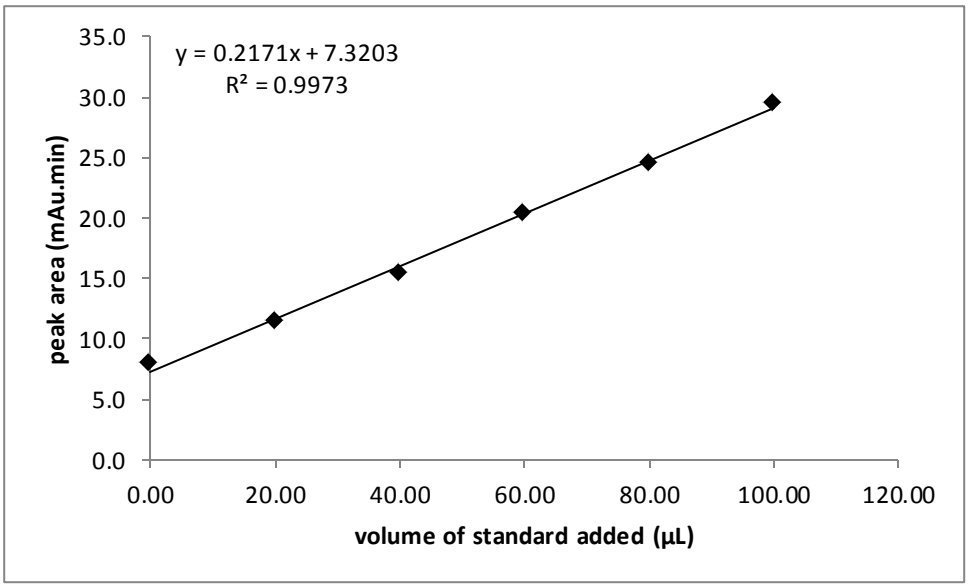

Figure B 24. Standard addition calibration curve for determination of sulfate using the optimized PMA BGE system

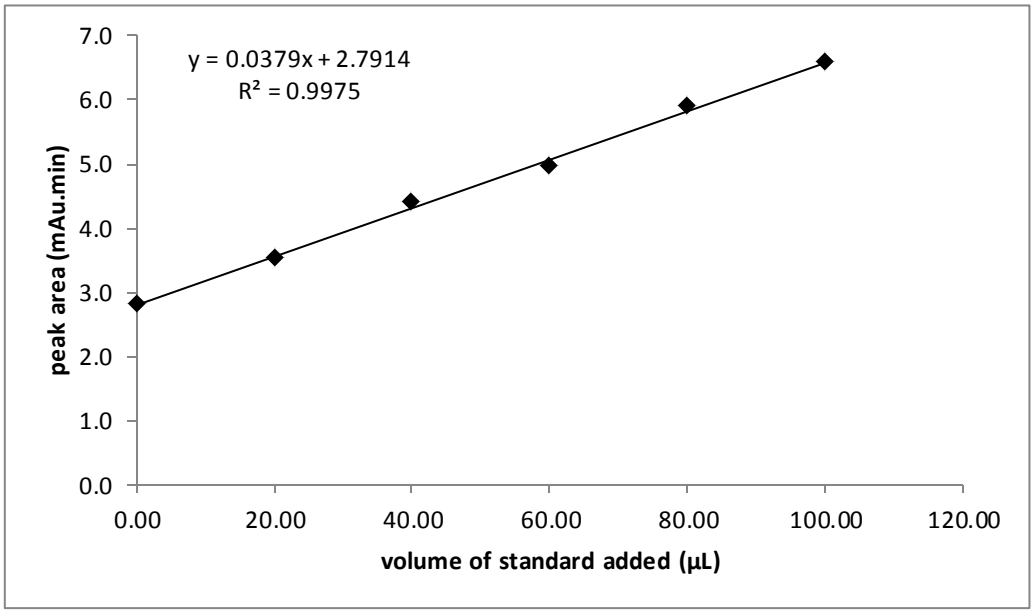

Figure B 25. Standard addition calibration curve for determination of thiosulfate using optimized PMA BGE system

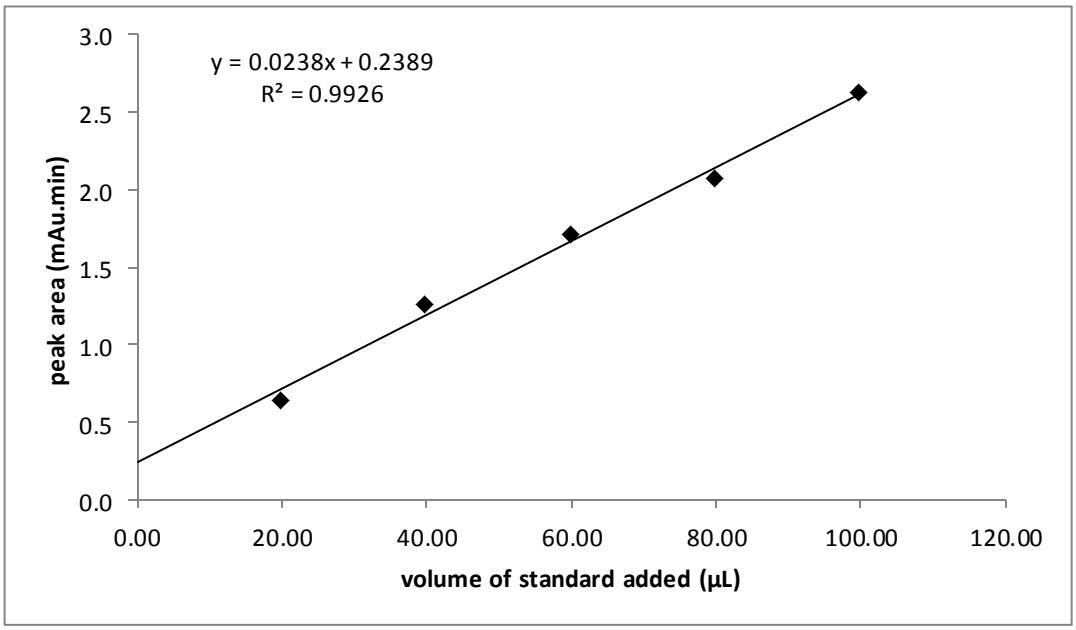

Figure B 262. Standard addition calibration curve for determination of trithionate using optimized PMA BGE system

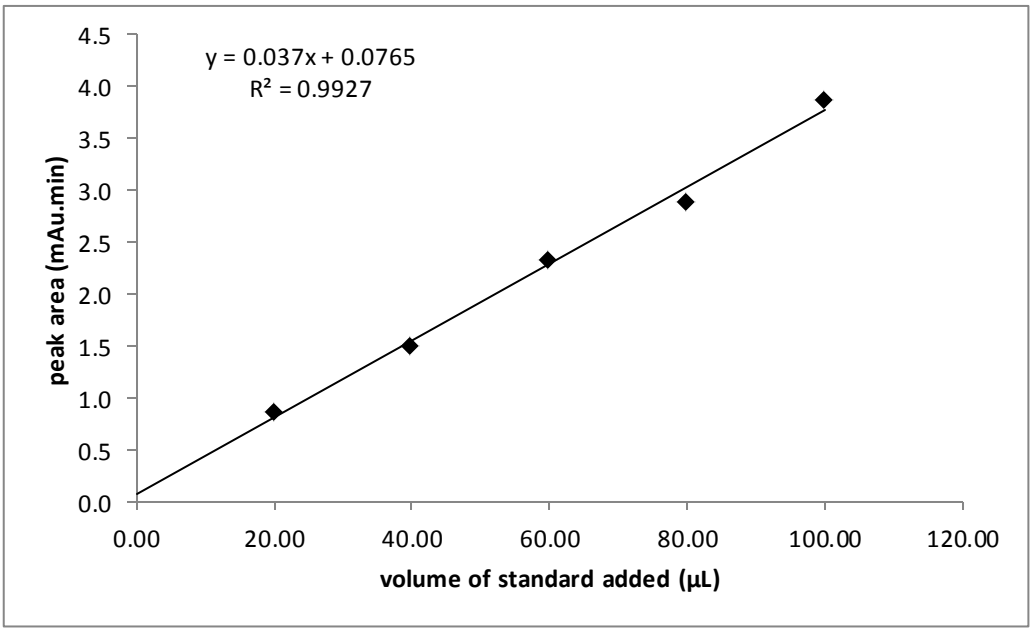

Figure B 27. Standard addition calibration curve for determination of tetrathionate using optimized PMA BGE system

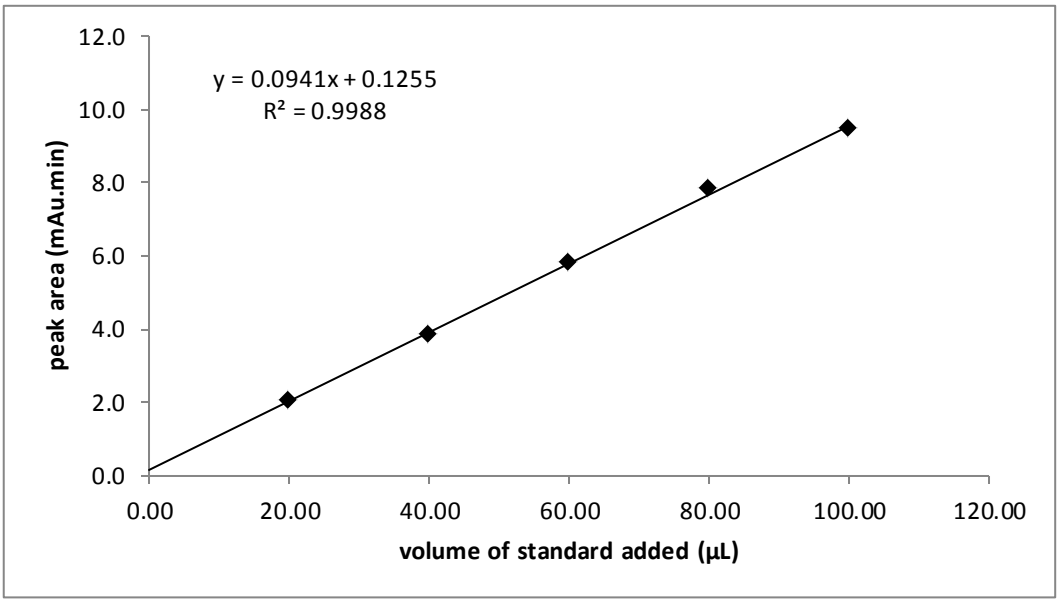

Figure B 28. Standard addition calibration curve for determination of tetrathionate using optimized PMA BGE system

Appendix C

Use of fractional factorial and Box-Behnken response surface designs for the screening and optimization of factors for capillary zone electrophoresis separation and indirect UV-vis detection of thiosalts

In this section we present additional information on the fractional factorial screening design (fFD) and Box-Behnken central composite experimental design (BBD) on the factors, levels and results; Pareto charts of the effects of the factors on the responses for the determination of the magnitude and statistical importance of the factors effects at 95% confidence level; calculations; surface plots of influence of influence of [TMA] and [HM^{2+}] on the resolution factor (R_s), peak symmetries and migration time of last migrating peak (t) Hold values for all surface plots are 4 s injection time (at 50 mbar) and applied field strength of -30 kV; and standard calibration curves for 5 thiosalt species.

Table C 1. Central composite experimental design (CCD) of factors, levels and results of experiments

RunOrder	CenterPt	[TMA]	[HMOH]	Inj time	Cass temp	App Field	Wavelength	$R_{1,2}$	$R_{2,3}$	$R_{3,4}$	$R_{4,5}$	t
1	1	2.00	1.50	2	20	30	254	1.68	2.68	2.81	7.77	2.91
2	0	3.50	1.00	6	22.5	25	227	1.54	2.77	1.36	4.87	3.46
3	1	2.00	0.50	10	20	30	254	1.79	1.68	0.00	4.83	3.08
4	1	2.00	0.50	2	25	20	254	3.51	2.31	1.18	12.73	4.36
5	1	5.00	1.50	10	25	30	254	2.26	1.92	0.00	6.08	2.70
6	1	2.00	1.50	10	25	20	254	1.10	1.69	1.89	5.68	4.00
7	1	5.00	1.50	10	20	30	200	2.54	1.98	0.00	6.55	2.93
8	1	5.00	1.50	2	25	20	200	1.02	4.73	2.58	7.22	4.12
9	1	5.00	0.50	10	25	20	200	1.35	4.00	1.05	10.57	4.68
10	1	5.00	0.50	10	20	20	254	1.17	5.19	0.98	10.70	5.08
11	1	5.00	0.50	2	20	30	200	1.48	5.04	1.20	11.79	3.33
12	1	2.00	1.50	2	25	30	200	1.38	1.99	2.06	5.29	2.67
13	1	2.00	0.50	2	20	20	200	3.45	2.86	1.01	11.80	4.70
14	1	5.00	1.50	2	20	20	254	4.40	2.58	0.00	7.22	4.47
15	1	2.00	0.50	10	25	30	200	1.75	1.23	0.00	5.42	2.91
16	1	5.00	0.50	2	25	30	254	1.57	4.17	1.18	11.00	3.10
17	1	2.00	1.50	10	20	20	200	1.07	2.27	1.99	5.32	4.35

R1,2; R2,3; R3,4 and R4,5 = peak resolution factors; *i* = system current; and t = migration time (min) of last analyte peak;

In Table S2 below: Sym1-5 = peak symmetries of peaks 1, 2, 3, 4 and 5 respectively

Table C 2. Results of BBD optimizing experiments

RunOrder	[TMA]	[HMOH]	Inj time	Field	$R_{1,2}$	$R_{2,3}$	$R_{3,4}$	$R_{4,5}$	t	Sym1	Sym2	Sym3	Sym4	Sym5
1	2.00	1.00	6	30	1.79	2.04	1.86	5.86	2.69	1.98	1.56	1.27	0.93	0.52
2	2.00	1.00	2	25	2.18	2.07	1.45	4.49	3.24	1.21	1.45	1.28	0.32	0.31
3	3.50	1.50	10	25	0.83	2.33	1.93	6.49	3.21	5.84	1.24	1.64	0.95	0.98
4	5.00	1.00	6	30	0.96	3.30	1.08	3.26	2.82	0.00	0.99	1.29	0.25	0.24
5	3.50	1.00	6	25	1.48	2.49	1.30	5.16	3.33	1.54	1.29	1.55	0.35	0.33
6	5.00	0.50	6	25	1.42	3.68	1.01	10.26	3.74	1.57	1.22	1.65	0.57	0.67
7	3.50	1.00	6	25	1.55	2.56	1.28	4.96	3.35	1.46	1.22	1.52	0.31	0.30
8	3.50	1.50	6	20	1.09	2.87	2.15	7.31	4.05	2.21	1.29	1.79	0.57	0.69
9	2.00	1.50	6	25	1.23	1.76	1.97	5.96	3.22	2.01	1.58	1.69	0.65	0.68
10	2.00	1.00	10	25	1.15	1.34	1.06	4.85	3.28	1.99	1.54	1.41	0.62	0.56
11	3.50	0.50	6	20	1.77	2.91	1.04	9.25	4.48	1.96	1.90	2.02	0.65	0.60
12	2.00	0.50	6	25	2.19	1.65	0.93	9.41	3.47	1.92	2.13	1.86	0.51	0.74
13	3.50	0.50	10	25	1.45	2.68	0.98	8.64	3.57	1.88	1.75	2.15	0.63	0.76
14	5.00	1.00	6	20	1.00	3.39	1.02	3.51	3.43	3.27	0.90	1.46	1.18	1.17
15	3.50	0.50	2	25	2.17	3.91	1.37	10.83	3.58	1.03	1.14	1.07	0.54	0.56
16	5.00	1.00	2	25	1.34	4.13	0.93	2.93	3.44	1.07	0.67	1.07	0.11	0.12
17	3.50	1.00	6	25	1.48	2.42	1.18	4.52	3.34	1.49	1.24	1.60	0.28	0.27
18	3.50	1.00	2	20	1.95	3.44	1.34	3.98	4.10	1.22	1.08	1.35	0.18	0.19
19	2.00	1.00	6	20	1.72	1.65	1.38	5.45	4.09	2.12	2.39	2.16	0.46	0.45
20	3.50	1.50	6	30	1.11	2.38	1.94	6.09	2.69	2.18	1.13	1.29	0.58	0.57
21	3.50	1.00	2	30	1.68	2.77	1.80	8.82	2.79	0.95	0.89	1.08	0.16	0.22
22	3.50	1.00	10	20	1.29	2.23	1.06	4.47	4.18	2.71	1.71	2.45	0.34	0.33
23	5.00	1.50	6	25	2.13	1.47	0.00	4.63	3.29	2.12	1.30	0.62	0.62	0.59
24	5.00	1.00	10	25	2.38	0.93	0.00	3.27	3.42	2.47	1.79	0.20	0.20	0.21
25	3.50	0.50	6	30	1.75	2.81	1.08	8.75	2.96	1.31	1.34	1.34	0.59	0.63
26	3.50	1.50	2	25	1.57	3.35	2.41	7.04	3.26	1.06	0.99	1.17	0.47	0.47
27	3.50	1.00	10	30	1.13	2.12	0.98	3.57	2.78	1.83	1.32	1.51	0.25	0.28

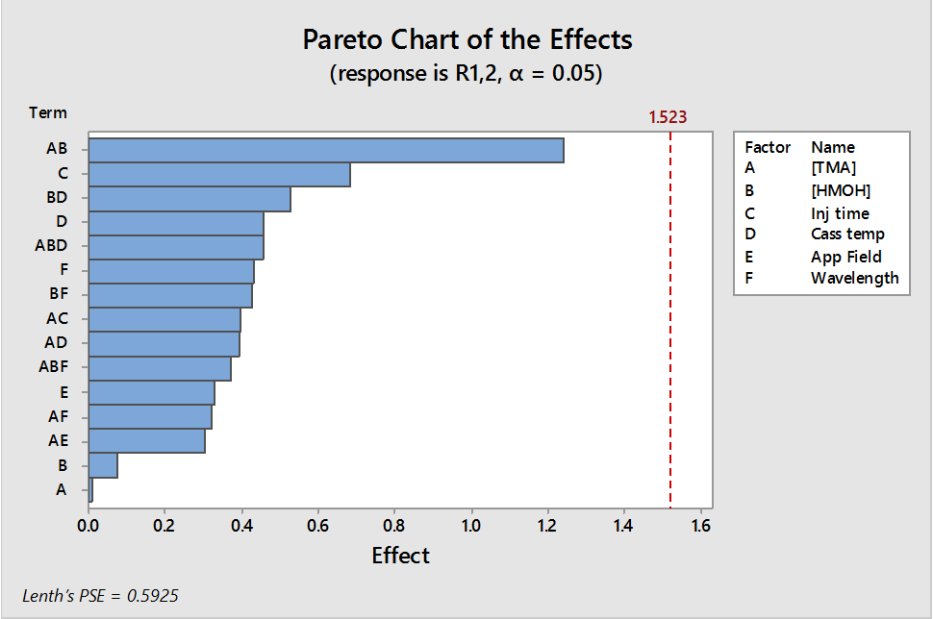

Figure C 29. Pareto Charts showing the effects of the 6 factors on peak resolution ($R_{1,2}$) response.

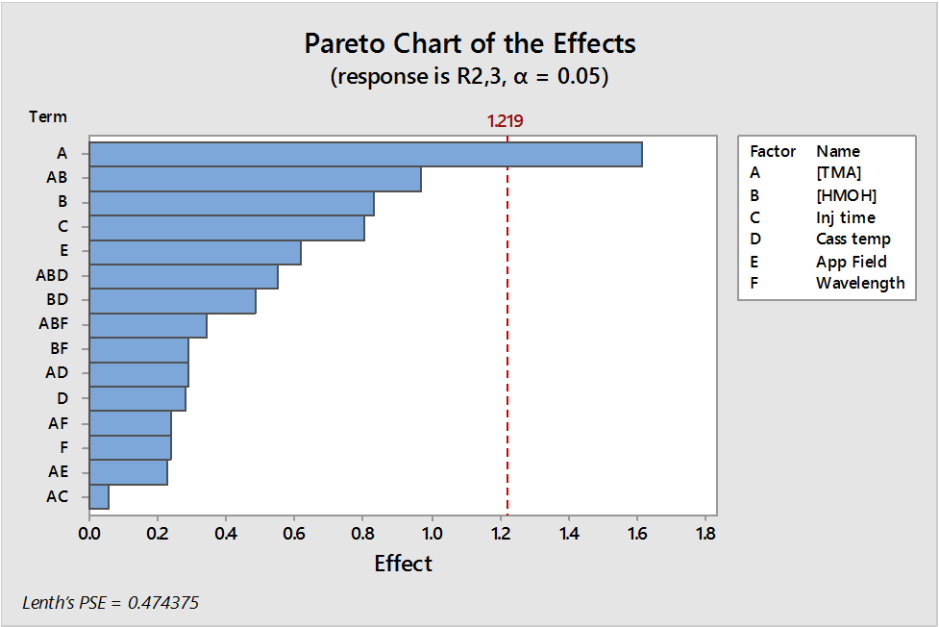

Figure C 30. Pareto Charts showing the effects of the 6 factors on peak resolution ($R_{2,3}$) response.

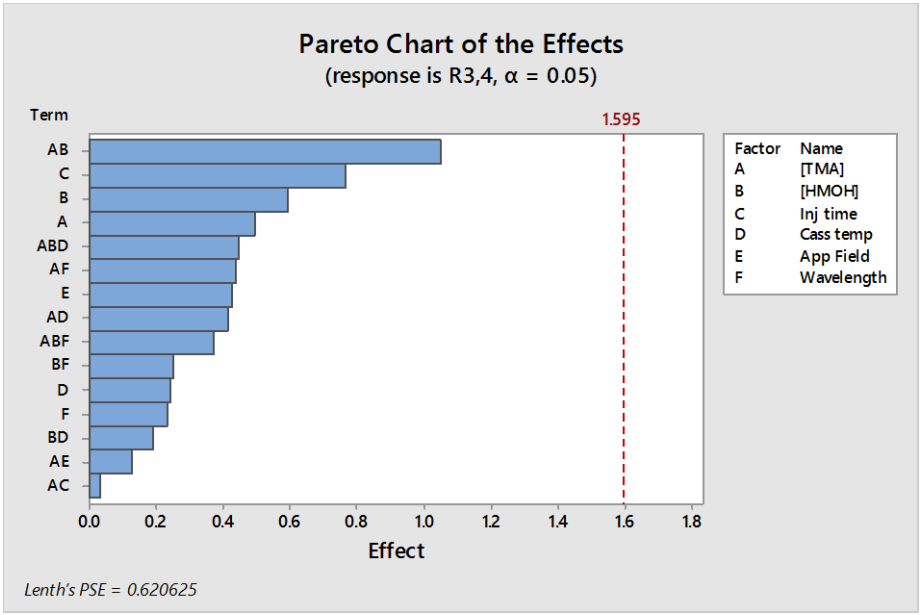

Figure C 31. Pareto Charts showing the effects of the 6 factors on peak resolution ($R_{3,4}$) response.

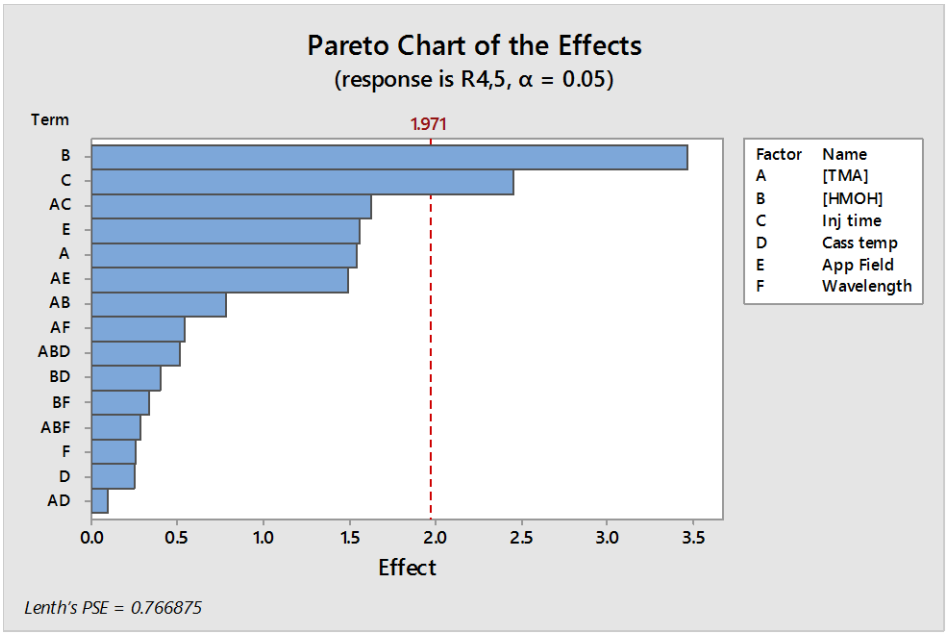

Figure C 32. Pareto Charts showing the effects of the 6 factors on peak resolution ($R_{4,5}$) response.

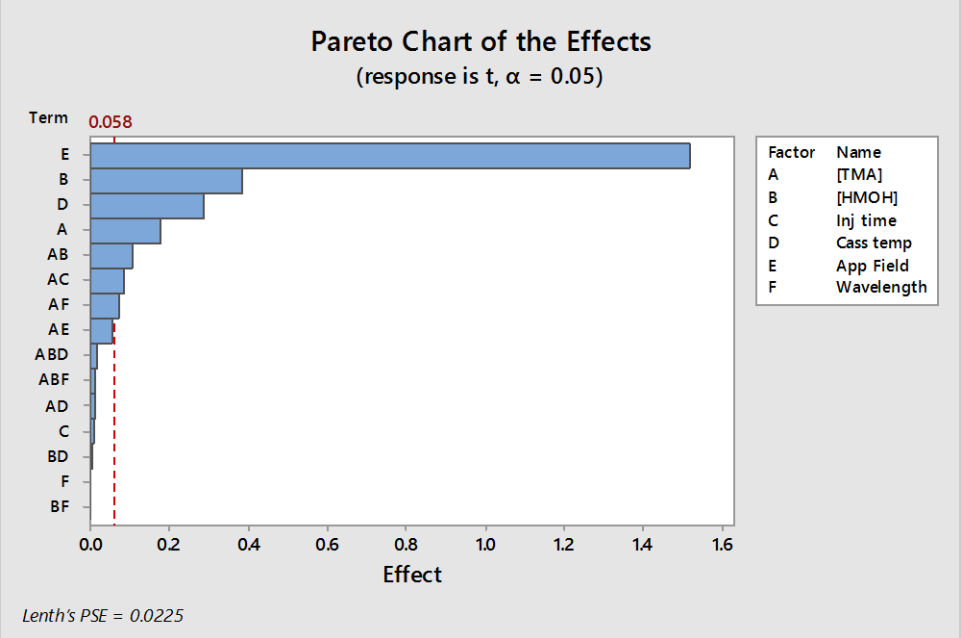

Figure C 33. Pareto Charts showing the effects of the 6 factors on migration time (t) of last migrating peak

Calculations:

The resolution factor (R_s) was calculated using the equation:

$$R_{1,2} = \frac{2\,(t_2 - t_1)}{w_1 + w_2} \qquad \text{C-1}$$

Where $R_{1,2}$ is the peak resolution between two adjacent peaks 1 and 2; t_1 is the migration time of peak 1 and t_2 is the migration time of peak 2.

Percent Difference (% Diff) between the predicted and experimental responses was calculation using the equation:

$$\% \text{ Diff} = \frac{|T-E|}{\frac{1}{2}(T+E)} \qquad \text{C-2}$$

where T is the theoretically predicted response using the mathematical model and E is the experimental response.

The response surface plots of the influence of [TMA] and [HM^{2+}] on the peak resolution factors are presented below:

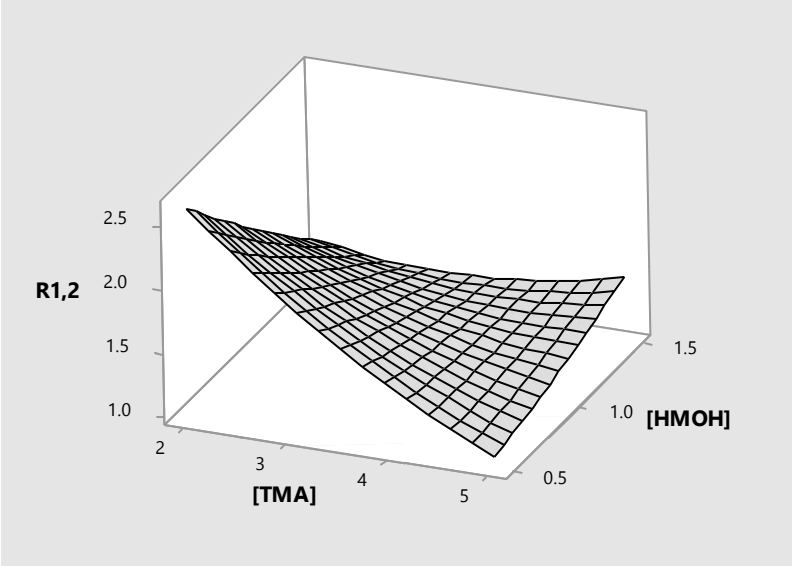

Figure C 34. Response surface plot of Resolutions $R_{1,2}$, vs [TMA] and [HM^{2+}]

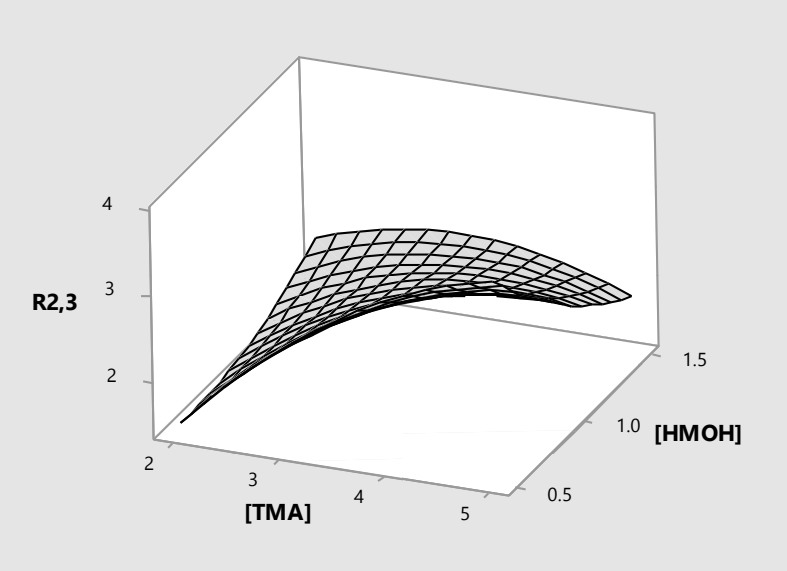

Figure C 35. Response surface plot of Resolutions $R_{2,3}$, vs [TMA] and [HM^{2+}]

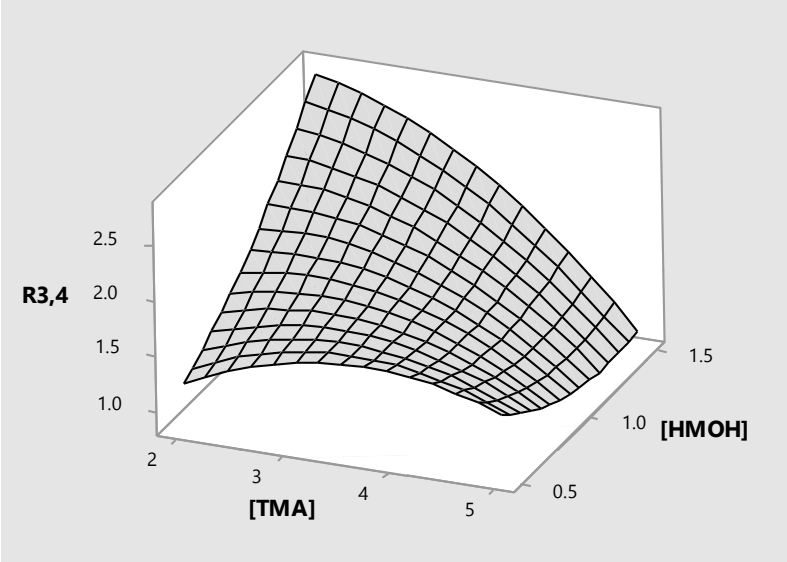

Figure C 36. Response surface plot of Resolutions $R_{3,4}$, vs [TMA] and [HM^{2+}]

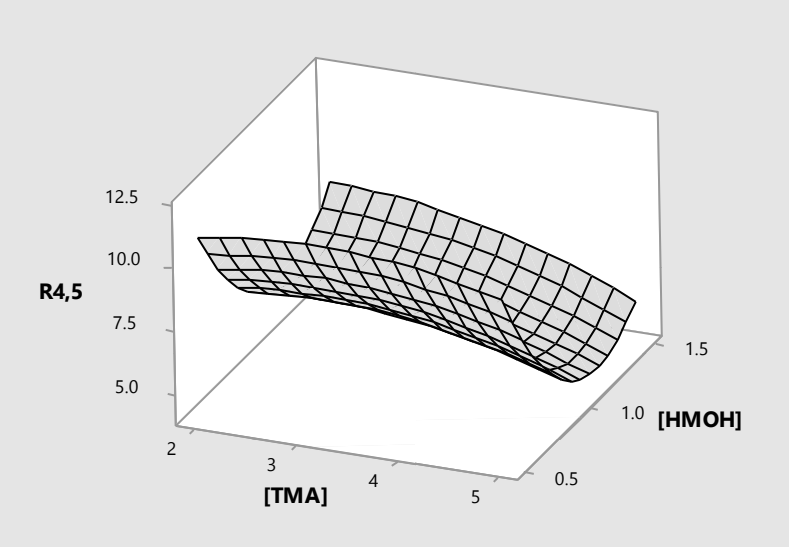

Figure C 37. Response surface plot of Resolutions $R_{4,5}$, vs [TMA] and [HM^{2+}]

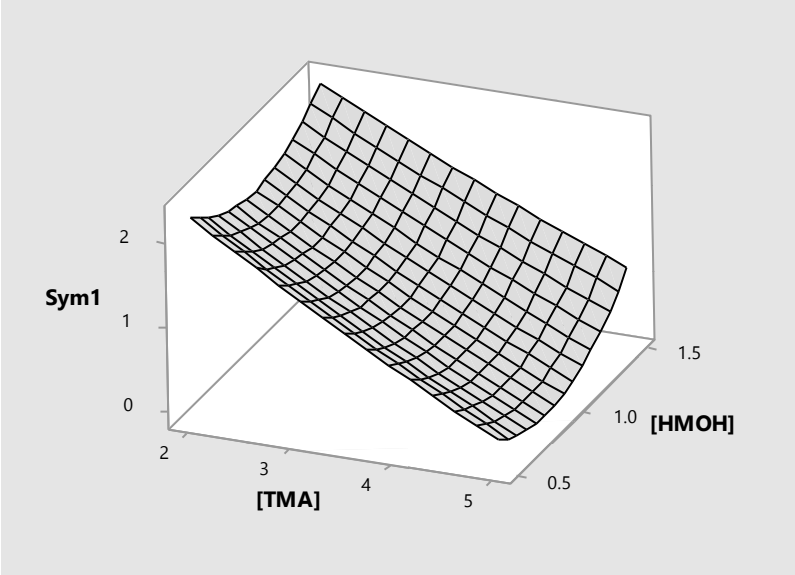

Figure C 38. Response surface plot of peak symmetry Sym1 vs [TMA] and [HM^{2+}]

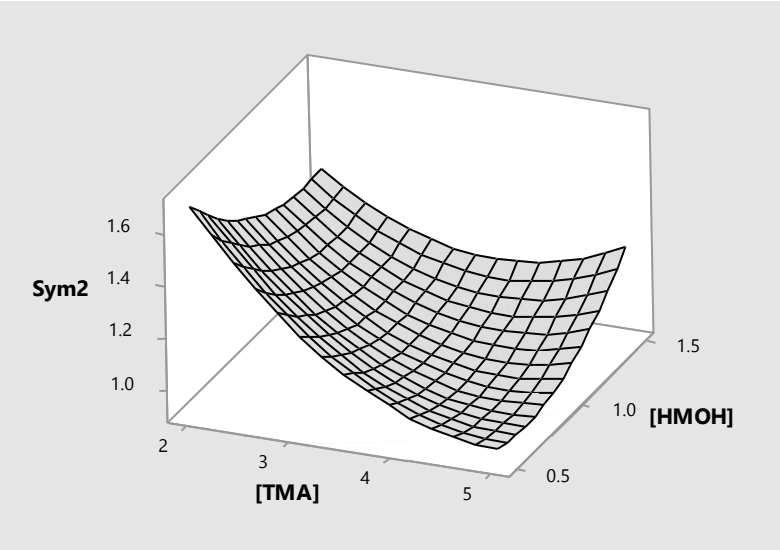

Figure C 39. Response surface plot of peak symmetry Sym2 vs [TMA] and [HM^{2+}]

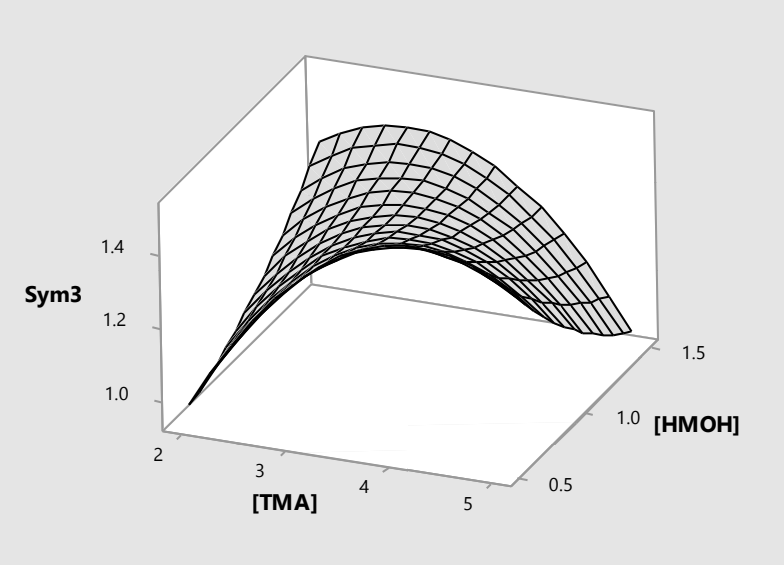

Figure C 40. Response surface plot of peak symmetry Sym3 vs [TMA] and [HM^{2+}]

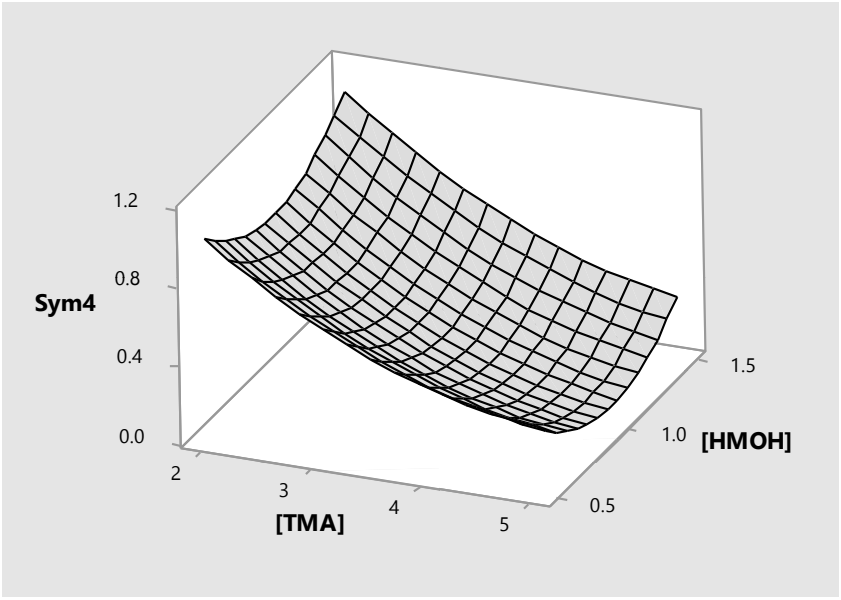

Figure C 41. Response surface plot of peak symmetry Sym4 vs [TMA] and [HM^{2+}]

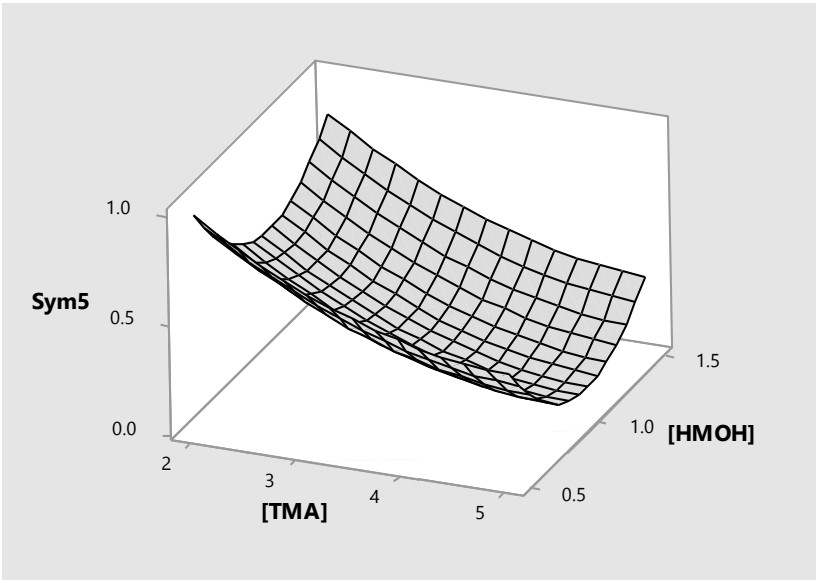

Figure C 42. Response surface plot of peak symmetry Sym5 vs [TMA] and [HM^{2+}]

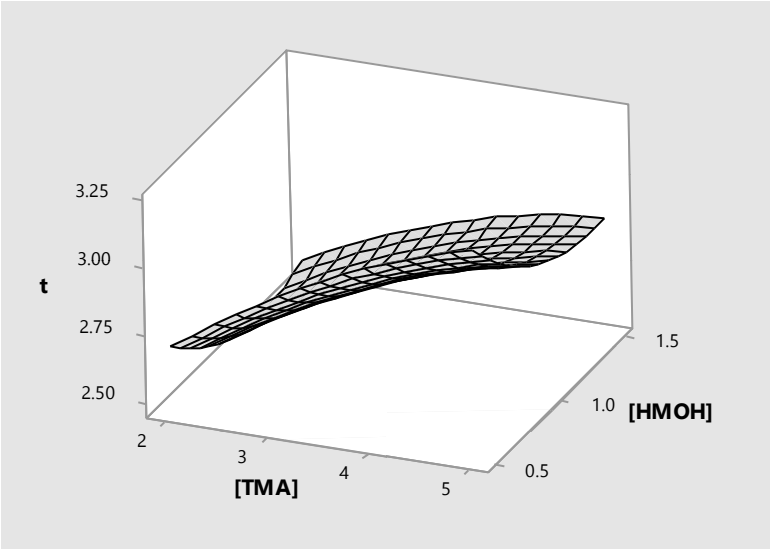

Figure C 43. Response surface plot of migration time of last migrating peak (*t)* vs [TMA] and [HM^{2+}]

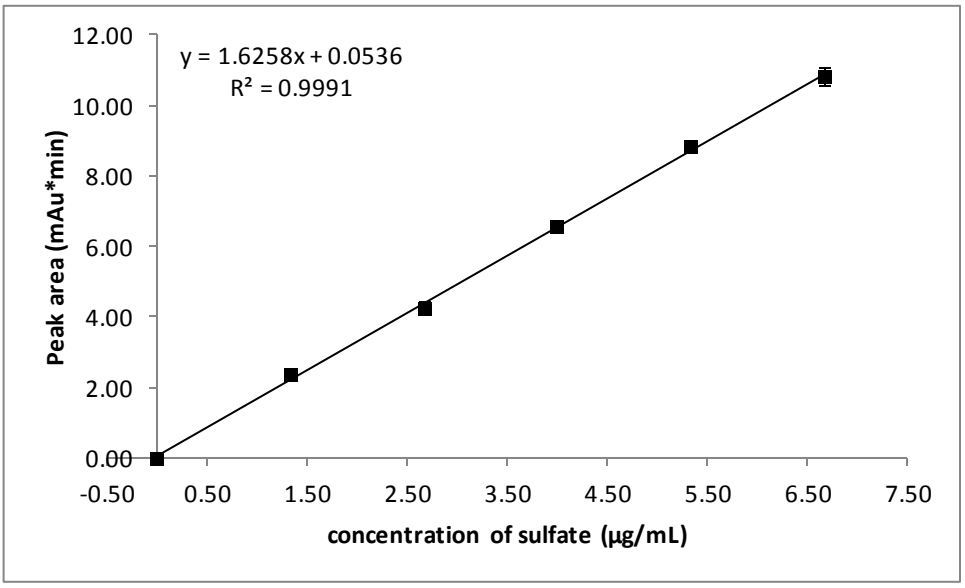

Figure C 44. Calibration curve for sulfate using optimized TMA BGE system

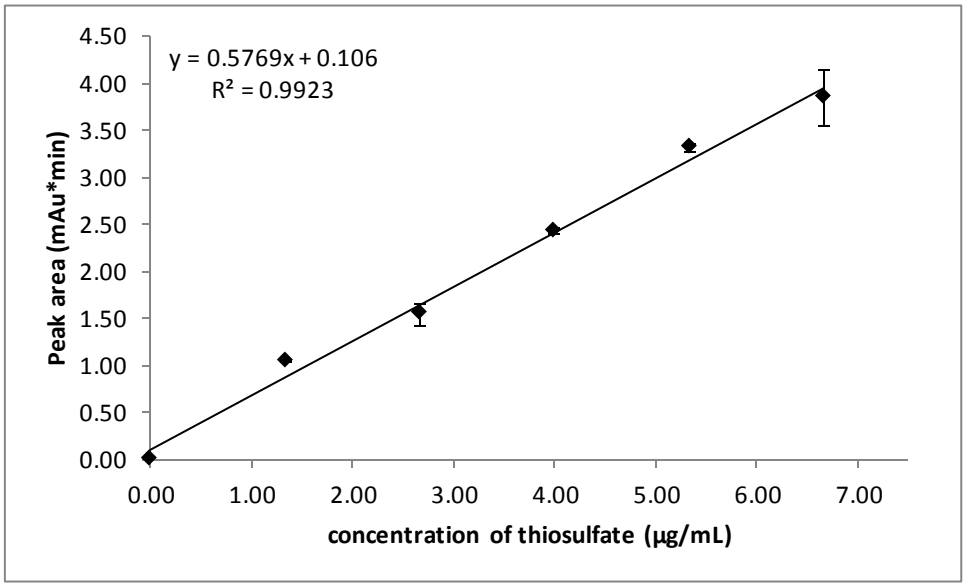

Figure C 45. Calibration curve for thiosulfate using optimized PMA BGE system

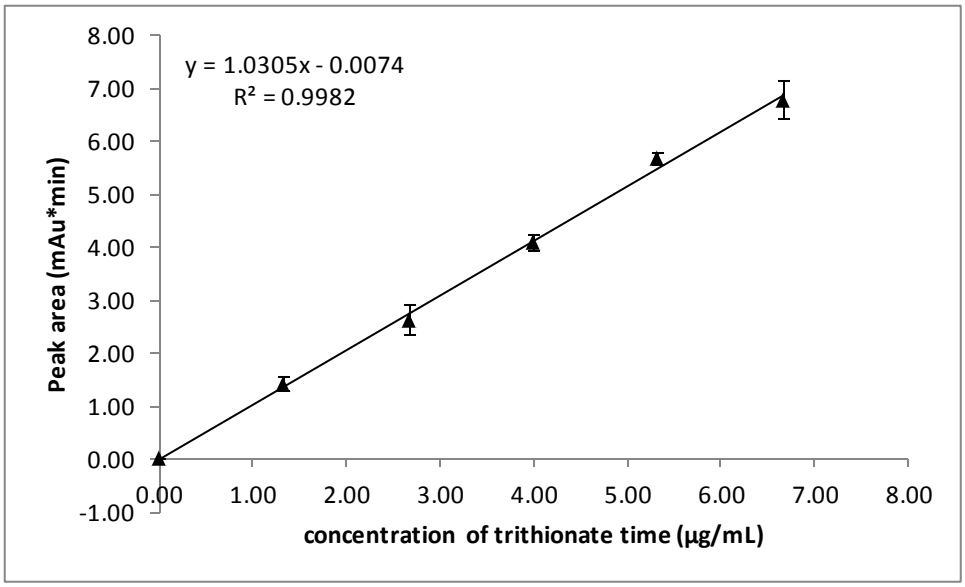

Figure C 46. Calibration curve for trithionate using optimized PMA BGE system

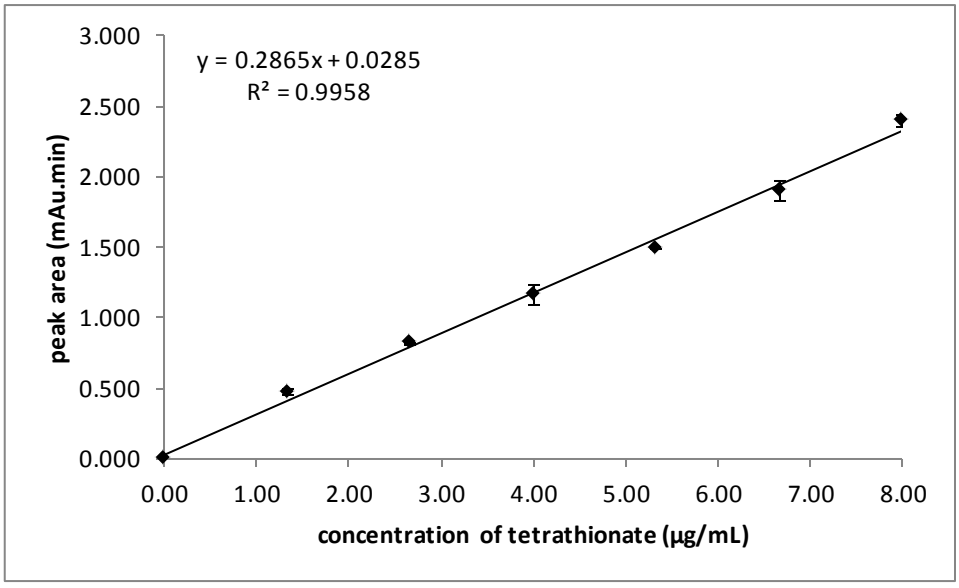

Figure C 47. Calibration curve for tetrathionate using optimized PMA BGE system

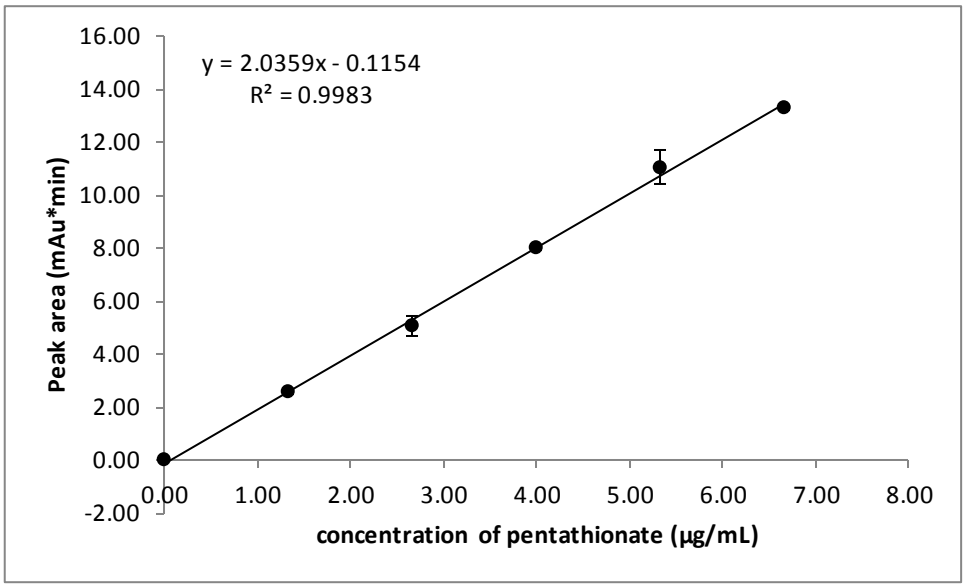

Figure C 48. Calibration curve for pentathionate using optimized PMA BGE system

Appendix D

Determination of association constants of tricationic-thiosalt ion-pairs using electrospray ionization time-of-flight mass spectrometry (ESI-TOF-MS)

In this section additional information is provided on the binding isotherms of the ion-pairing reagents (IP-L-Imid, IP-T-Imid and IP-T-Phos) with the thiosalt species (sulfate (SO_4^{2-}), thiosulfate ($S_2O_3^{2-}$), trithionate ($S_3O_6^{2-}$), and tetrathionate ($S_4O_6^{2-}$) showing the showing effect of $[IP]_0$ ratio on the signal count (*S*) of the $[IP*TS]^+$ ion-pair; quadratic model for the relationship between the signal ratio of $[IP]^{3+}$ and the ion-pairs $[IP.TS]^+$ and the initial concentrations of the ion pair reagent $[IP]_0$ and the thiosalt species $[TS]_{0;}$ optimization dashboard for optimizing the TOF-MS; and iterative approach to determining the association constants. The mass spectra of unimolar (10 μM) mixtures of the three ion-pair reagents and the four thiosalt species are also reported in this section.

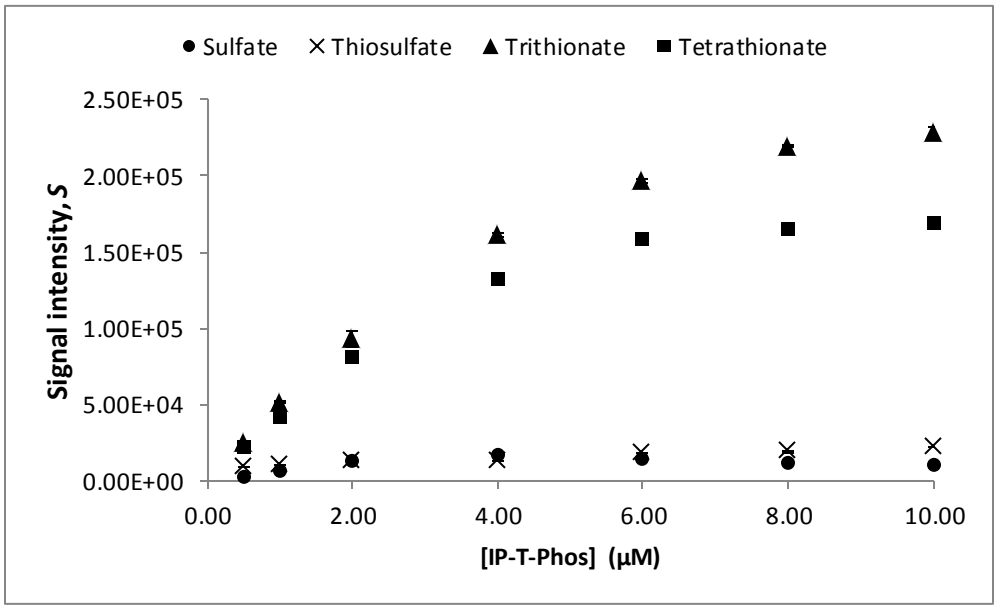

Figure D 1: Binding isotherm of IP-T-Imid with four thiosalt species showing effect of [IP-T-Phos] on the signal intensity (*S*) of the $[IP\text{-}T\text{-}Phos{:}SO_4]^+$, $[IP\text{-}T\text{-}Phos{:}S_2O_3]^+$, $[IP\text{-}T\text{-}Phos{:}S_3O_6]^+$ and $[IP\text{-}T\text{-}Phos{:}S_4O_6]^+$ ion-pairs

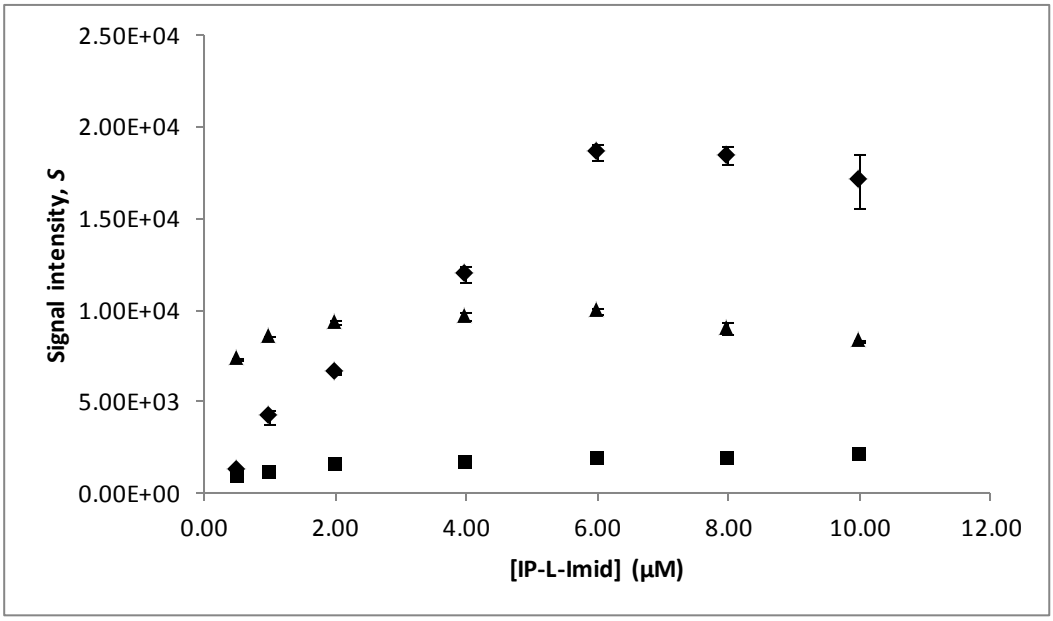

Figure D 49: Binding isotherm of IP-T-Imid with four thiosalt species showing effect of [IP-L-Imid] on the signal intensity (*S*) of the $[IP\text{-}L\text{-}Imid{:}SO_4]^+$, $[IP\text{-}L\text{-}Imid{:}S_2O_3]^+$, $[IP\text{-}L\text{-}Imid{:}S_3O_6]^+$ and $[IP\text{-}L\text{-}Imid{:}S_4O_6]^+$ ion-pairs

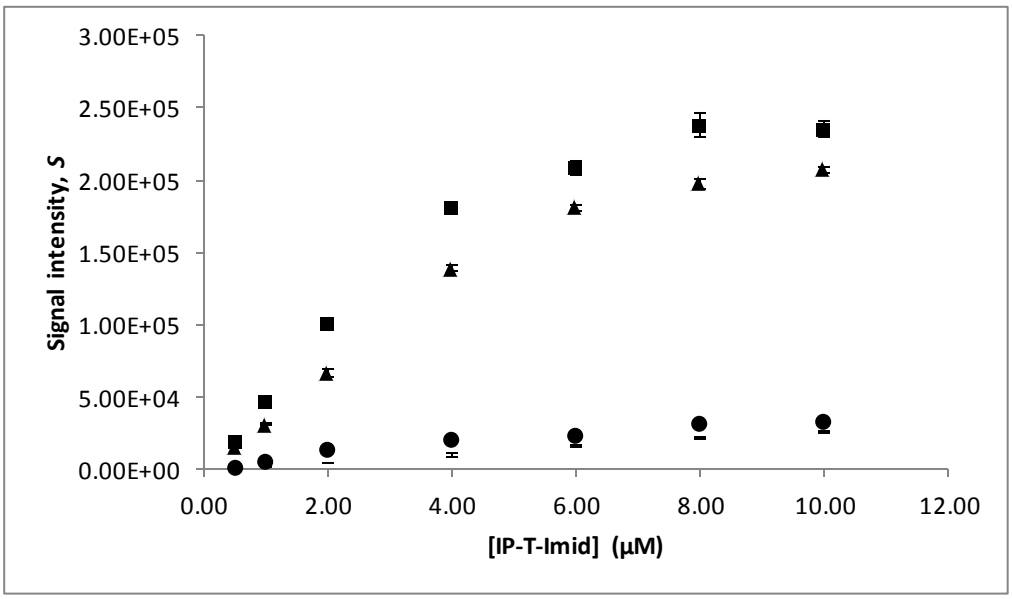

Figure D 3: Binding isotherm of IP-T-Imid with four thiosalt species showing effect of [IP-T-Imid] on the signal intensity (S) of the $[IP\text{-}T\text{-}Imid{:}SO_4]^+$, $[IP\text{-}T\text{-}Imid{:}S_2O_3]^+$, $[IP\text{-}T\text{-}Imid{:}S_3O_6]^+$ and $[IP\text{-}T\text{-}Imid{:}S_4O_6]^+$ ion-pairs

The model used for determination of association constant was based on the real root of the quadratic equation:

$$S_R = \frac{-(1+K_{assoc}[IP]_0-K_{assoc}[TS]_0)+\sqrt{(1+K_{assoc}[IP]_0-K_{assoc}[TS]_0)^2+4K_{assoc}[TS]_0}}{2} \qquad \text{(D-1)}$$

The following tables show the iterative approach to fitting the non-linear equation. The smallest residuals (tolerance) for convergence was found to vary from one system to the other.

In the optimization of TOF-MS for the analysis of gas phase ion-pairs, a Box-Behnken multivariate experimental design approach was utilized. Fifteen (15) experiments were performed and the optimal conditions modeled. The experimental values and the ones predicted by the model were very close with percentage difference ~ 20%. The dashboard of the interactions of the TOF-MS parameters and the optimum conditions (in red) are shown below:

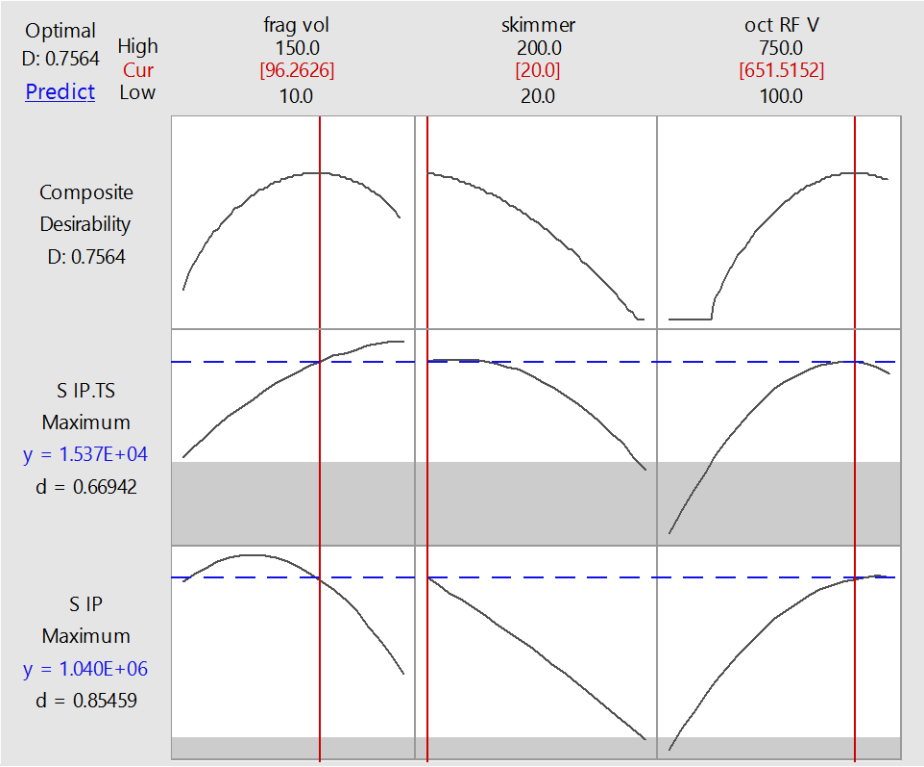

Figure D 4. Experimental design dashboard showing optimization of TOF MS for the analysis of trication – thiosalt ion-pairs in the positive mode ESI

Iteration for convergence (reducing residuals) approach for non-linear (quadratic) model fitting for determination of K_{assoc}

Table D1. IP-T-Phos: Tetrathionate Trial 1

TS_0 uM	IP_0 uM	TS_0 M	IP_0 M	S IP	S IP·TS	K	SR obs	SR cal +	obs-cal	(obs-cal)^2
2.00	0.50	0.000002	0.0000005	6.3580E+05	2.1925E+04	38150	0.034484	0.07497	-4.0485E-02	0.001639
2.00	1.00	0.000002	0.0000010	9.2135E+05	4.1493E+04	38150	0.045035	0.07368	-2.8647E-02	0.000821
2.00	2.00	0.000002	0.0000020	1.3615E+06	8.1848E+04	38150	0.060117	0.07123	-1.1110E-02	0.000123
2.00	4.00	0.000002	0.0000040	1.7387E+06	1.3314E+05	38150	0.076579	0.06675	9.8274E-03	0.000097
2.00	6.00	0.000002	0.0000060	1.9281E+06	1.6006E+05	38150	0.083011	0.06278	2.0232E-02	0.000409
2.00	8.00	0.000002	0.0000080	1.9919E+06	1.6600E+05	38150	0.083336	0.05923	2.4103E-02	0.000581
2.00	10.00	0.000002	0.0000100	2.0663E+06	1.6993E+05	38150	0.082238	0.05605	2.6187E-02	0.000686
								Σ	**0.000108**	**0.004356**

Table D2. IP-T-Phos: Tetrathionate Trial 2

TS_0 uM	IP_0 uM	TS_0 M	IP_0 M	S IP	S IP·TS	K	SR obs	SR cal +	obs-cal	(obs-cal)^2
2.00	0.50	0.000002	0.0000005	6.3390E+05	2.1481E+04	37850	0.033887	0.07439	-4.0503E-02	0.001640
2.00	1.00	0.000002	0.0000010	9.4855E+05	4.2946E+04	37850	0.045275	0.07312	-2.7846E-02	0.000775
2.00	2.00	0.000002	0.0000020	1.3586E+06	8.1089E+04	37850	0.059686	0.0707	-1.1015E-02	0.000121
2.00	4.00	0.000002	0.0000040	1.7373E+06	1.3244E+05	37850	0.076238	0.06629	9.9501E-03	0.000099
2.00	6.00	0.000002	0.0000060	1.9143E+06	1.5796E+05	37850	0.082520	0.06237	2.0152E-02	0.000406
2.00	8.00	0.000002	0.0000080	2.0145E+06	1.6394E+05	37850	0.081383	0.05887	2.2517E-02	0.000507
2.00	10.00	0.000002	0.0000100	2.0239E+06	1.6737E+05	37850	0.082695	0.05572	2.6972E-02	0.000728
								Σ	**0.000227**	**0.004277**

Table D 3. IP-T-Phos: Trithionate Trial 1

TS_0 uM	IP_0 uM	TS_0 M	IP_0 M	S IP	S IP·TS	K	SR obs	SR cal +	obs-cal	(obs-cal)^2
2.00	0.50	0.000002	0.0000005	6.1276E+05	2.4282E+04	49260	0.039627	0.09636	-5.6729E-02	0.003218
2.00	1.00	0.000002	0.0000010	9.5919E+05	5.1429E+04	49260	0.053618	0.09428	-4.0658E-02	0.001653
2.00	2.00	0.000002	0.0000020	1.3752E+06	9.6927E+04	49260	0.070483	0.09036	-1.9873E-02	0.000395
2.00	4.00	0.000002	0.0000040	1.7597E+06	1.6218E+05	49260	0.092162	0.08336	8.8036E-03	0.000078
2.00	6.00	0.000002	0.0000060	1.9322E+06	1.9610E+05	49260	0.101490	0.07731	2.4180E-02	0.000585
2.00	8.00	0.000002	0.0000080	2.0228E+06	2.1957E+05	49260	0.108549	0.07204	3.6510E-02	0.001333
2.00	10.00	0.000002	0.0000100	2.0081E+06	2.3137E+05	49260	0.115219	0.06741	4.7808E-02	0.002286
								Σ	**0.000043**	**0.009547**

Table D 4. IP-T-Phos: Trithionate Trial 2

TS_0 uM	IP_0 uM	TS_0 M	IP_0 M	S IP	S IP·TS	K	SR obs	SR cal +	obs-cal	(obs-cal)^2
2.00	0.50	0.000002	0.0000005	6.1230E+05	2.4322E+04	48870	0.039723	0.09561	-5.5885E-02	0.003123
2.00	1.00	0.000002	0.0000010	9.6195E+05	5.1765E+04	48870	0.053812	0.09356	-3.9747E-02	0.001580
2.00	2.00	0.000002	0.0000020	1.2864E+06	8.9149E+04	48870	0.069303	0.08969	-2.0392E-02	0.000416
2.00	4.00	0.000002	0.0000040	1.7497E+06	1.6077E+05	48870	0.091880	0.08279	9.0871E-03	0.000083
2.00	6.00	0.000002	0.0000060	1.9303E+06	1.9728E+05	48870	0.102201	0.07682	2.5380E-02	0.000644
2.00	8.00	0.000002	0.0000080	2.0172E+06	2.1874E+05	48870	0.108439	0.07161	3.6826E-02	0.001356
2.00	10.00	0.000002	0.0000100	2.0145E+06	2.2522E+05	48870	0.111800	0.06704	4.4762E-02	0.002004
								Σ	**0.000032**	**0.009205**

Table D 5. IP-T-Phos: Thiosulfate Trial 1

TS_0 uM	IP_0 uM	TS_0 M	IP_0 M	S IP	S IP·TS	K	SR obs	SR cal +	obs-cal	(obs-cal)^2
2.00	0.50	0.000002	0.0000005	5.8334E+05	8.8702E+03	5582	0.015206	0.01113	4.0725E-03	0.000017
2.00	1.00	0.000002	0.0000010	9.2781E+05	1.0417E+04	5582	0.011227	0.0111	1.2452E-04	0.000000
2.00	2.00	0.000002	0.0000020	1.4409E+06	1.2502E+04	5582	0.008676	0.01104	-2.3660E-03	0.000006
2.00	4.00	0.000002	0.0000040	1.6951E+06	1.2705E+04	5582	0.007495	0.01092	-3.4274E-03	0.000012
2.00	6.00	0.000002	0.0000060	1.8524E+06	1.8291E+04	5582	0.009874	0.01081	-9.3177E-04	0.000001
2.00	8.00	0.000002	0.0000080	1.8237E+06	1.9866E+04	5582	0.010894	0.01069	2.0195E-04	0.000000
2.00	10.00	0.000002	0.0000100	1.7103E+06	2.2076E+04	5582	0.012908	0.01058	2.3280E-03	0.000005
								Σ	**0.000002**	**0.000040**

Table D6. IP-T-Phos: Thiosulfate Trial 2

TS_0 uM	IP_0 uM	TS_0 M	IP_0 M	S IP	S IP·TS	K	SR obs	SR cal +	obs-cal	(obs-cal)^2
2.00	0.50	0.000002	0.0000005	5.7995E+05	8.7142E+03	5532	0.015026	0.01103	3.9919E-03	0.000016
2.00	1.00	0.000002	0.0000010	9.4728E+05	1.0153E+04	5532	0.010718	0.011	-2.8567E-04	0.000000
2.00	2.00	0.000002	0.0000020	1.3958E+06	1.2030E+04	5532	0.008618	0.01094	-2.3258E-03	0.000005
2.00	4.00	0.000002	0.0000040	1.6458E+06	1.2797E+04	5532	0.007776	0.01083	-3.0514E-03	0.000009
2.00	6.00	0.000002	0.0000060	1.7252E+06	1.7642E+04	5532	0.010226	0.01071	-4.8622E-04	0.000000
2.00	8.00	0.000002	0.0000080	1.8430E+06	1.8967E+04	5532	0.010291	0.0106	-3.0860E-04	0.000000
2.00	10.00	0.000002	0.0000100	1.6936E+06	2.1953E+04	5532	0.012962	0.01049	2.4722E-03	0.000006
								Σ	**0.000006**	**0.000037**

Table D 7. IP-T-Phos: Sulfate Trial 1

TS_0 uM	IP_0 uM	TS_0 M	IP_0 M	S IP	S IP·TS	K	SR obs	SR cal +	obs-cal	(obs-cal)^2
8.00	2.00	0.000008	0.0000020	1.2308E+06	2.4312E+03	732	0.001975	0.00585	-3.8723E-03	0.000015
8.00	4.00	0.000008	0.0000040	1.6985E+06	5.7975E+03	732	0.003413	0.00584	-2.4257E-03	0.000006
8.00	8.00	0.000008	0.0000080	1.8682E+06	1.2524E+04	732	0.006704	0.00582	8.8171E-04	0.000001
8.00	16.00	0.000008	0.0000160	1.8048E+06	1.6300E+04	732	0.009031	0.00579	3.2428E-03	0.000011
8.00	24.00	0.000008	0.0000240	1.8742E+06	1.4039E+04	732	0.007490	0.00576	1.7349E-03	0.000003
8.00	32.00	0.000008	0.0000320	1.7777E+06	1.1268E+04	732	0.006339	0.00572	6.1601E-04	0.000000
8.00	40.00	0.000008	0.0000400	1.7328E+06	9.6348E+03	732	0.005560	0.00569	-1.3017E-04	0.000000
								Σ	**0.000047**	**0.000036**

Table D 8. IP-T-Phos: Sulfate Trial 2

TS_0 uM	IP_0 uM	TS_0 M	IP_0 M	S IP	S IP·TS	K	SR obs	SR cal +	obs-cal	(obs-cal)^2
8.00	2.00	0.000008	0.0000020	1.2292E+06	2.9152E+03	769	0.002372	0.00614	-3.7710E-03	0.000014
8.00	4.00	0.000008	0.0000040	1.7064E+06	6.8025E+03	769	0.003987	0.00613	-2.1467E-03	0.000005
8.00	8.00	0.000008	0.0000080	1.8311E+06	1.2358E+04	769	0.006749	0.00611	6.3433E-04	0.000000
8.00	16.00	0.000008	0.0000160	1.8795E+06	1.6822E+04	769	0.008950	0.00608	2.8724E-03	0.000008
8.00	24.00	0.000008	0.0000240	1.8583E+06	1.4723E+04	769	0.007923	0.00604	1.8818E-03	0.000004
8.00	32.00	0.000008	0.0000320	1.7173E+06	1.1312E+04	769	0.006587	0.00601	5.8177E-04	0.000000
8.00	40.00	0.000008	0.0000400	1.7498E+06	1.0434E+04	769	0.005963	0.00597	-6.5719E-06	0.000000
								Σ	**0.000046**	**0.000031**

Table D 9. IP-L-Imid: Tetrathionate Trial 1

TS_0 uM	IP_0 uM	TS_0 M	IP_0 M	S IP	S IP·TS	K	SR obs	SR cal +	obs-cal	(obs-cal)^2
2.00	0.50	0.000002	0.0000005	2.1186E+04	4.5082E+03	141790	0.212790	0.26857	-5.5781E-02	0.003112
2.00	1.00	0.000002	0.0000010	2.2835E+04	5.1280E+03	141790	0.224567	0.25479	-3.0222E-02	0.000913
2.00	2.00	0.000002	0.0000020	2.6430E+04	6.3753E+03	141790	0.241212	0.23047	1.0747E-02	0.000115
2.00	4.00	0.000002	0.0000040	2.8180E+04	6.3249E+03	141790	0.224445	0.19216	3.2284E-02	0.001042
2.00	6.00	0.000002	0.0000060	2.8824E+04	5.2933E+03	141790	0.183641	0.16383	1.9815E-02	0.000393
2.00	8.00	0.000002	0.0000080	2.9234E+04	4.6500E+03	141790	0.159060	0.14229	1.6774E-02	0.000281
2.00	10.00	0.000002	0.0000100	2.9497E+04	3.8902E+03	141790	0.131884	0.12549	6.3960E-03	0.000041
								Σ	**0.00001255**	**0.00589753**

Table D 10. IP-L-Imid: Tetrathionate Trial 2

TS_0 uM	IP_0 uM	TS_0 M	IP_0 M	S IP	S IP·TS	K	SR obs	SR cal +	obs-cal	(obs-cal)^2
2.00	0.50	0.000002	0.0000005	2.0972E+04	4.6413E+03	147640	0.221307	0.27917	-5.7862E-02	0.003348
2.00	1.00	0.000002	0.0000010	2.3732E+04	5.6503E+03	147640	0.238088	0.26441	-2.6319E-02	0.000693
2.00	2.00	0.000002	0.0000020	2.5749E+04	6.3174E+03	147640	0.245347	0.23843	6.9159E-03	0.000048
2.00	4.00	0.000002	0.0000040	2.7515E+04	6.1317E+03	147640	0.222850	0.19777	2.5080E-02	0.000629
2.00	6.00	0.000002	0.0000060	2.8023E+04	5.4488E+03	147640	0.194445	0.16792	2.6527E-02	0.000704
2.00	8.00	0.000002	0.0000080	2.8926E+04	4.7382E+03	147640	0.163807	0.14537	1.8435E-02	0.000340
2.00	10.00	0.000002	0.0000100	2.8445E+04	3.8444E+03	147640	0.135152	0.12788	7.2702E-03	0.000053
								Σ	**0.00004759**	**0.00581394**

Table D 11. IP-L-Imid: Trithionate Trial 1

TS_0 uM	IP_0 uM	TS_0 M	IP_0 M	S IP	S IP·TS	K	SR obs	SR cal +	obs-cal	(obs-cal)^2
2.00	0.50	0.000002	0.0000005	1.7261E+04	7.3440E+03	357420	0.425479	0.64478	-2.1930E-01	0.048094
2.00	1.00	0.000002	0.0000010	1.9893E+04	8.5683E+03	357420	0.430725	0.58318	-1.5246E-01	0.023243
2.00	2.00	0.000002	0.0000020	2.2652E+04	9.3269E+03	357420	0.411747	0.48226	-7.0516E-02	0.004972
2.00	4.00	0.000002	0.0000040	2.4365E+04	9.4394E+03	357420	0.387410	0.34674	4.0667E-02	0.001654
2.00	6.00	0.000002	0.0000060	2.4935E+04	9.7838E+03	357420	0.392376	0.26525	1.2712E-01	0.016160
2.00	8.00	0.000002	0.0000080	2.6472E+04	9.2193E+03	357420	0.348265	0.21291	1.3535E-01	0.018320
2.00	10.00	0.000002	0.0000100	2.6125E+04	8.2629E+03	357420	0.316281	0.1771	1.3918E-01	0.019372
								Σ	0.00005231	0.13181579

Table D 12. IP-L-Imid: Trithionate Trial 2

TS_0 uM	IP_0 uM	TS_0 M	IP_0 M	S IP	S IP·TS	K	SR obs	SR cal +	obs-cal	(obs-cal)^2
2.00	0.50	0.000002	0.0000005	1.7420E+04	7.2309E+03	353720	0.415096	0.63852	-2.2342E-01	0.049918
2.00	1.00	0.000002	0.0000010	2.0141E+04	8.5349E+03	353720	0.423766	0.57789	-1.5413E-01	0.023755
2.00	2.00	0.000002	0.0000020	2.2760E+04	9.2159E+03	353720	0.404922	0.47849	-7.3567E-02	0.005412
2.00	4.00	0.000002	0.0000040	2.3954E+04	9.7768E+03	353720	0.408155	0.34473	6.3427E-02	0.004023
2.00	6.00	0.000002	0.0000060	2.5907E+04	1.0057E+04	353720	0.388185	0.26407	1.2411E-01	0.015404
2.00	8.00	0.000002	0.0000080	2.5817E+04	8.7804E+03	353720	0.340096	0.21216	1.2794E-01	0.016368
2.00	10.00	0.000002	0.0000100	2.6634E+04	8.3158E+03	353720	0.312230	0.17658	1.3565E-01	0.018401
								Σ	**0.00000975**	**0.13328056**

Table D 13. IP-L-Imid: Thiosulfate Trial 1

TS_0 uM	IP_0 uM	TS_0 M	IP_0 M	S IP	S IP·TS	K	SR obs	SR cal +	obs-cal	(obs-cal)^2
2.00	0.50	0.000002	0.0000005	1.8544E+04	9.0700E+02	36320	0.048911	0.07143	-2.2518E-02	0.000507
2.00	1.00	0.000002	0.0000010	2.0476E+04	1.0501E+03	36320	0.051285	0.07026	-1.8971E-02	0.000360
2.00	2.00	0.000002	0.0000020	2.3889E+04	1.5401E+03	36320	0.064469	0.06801	-3.5450E-03	0.000013
2.00	4.00	0.000002	0.0000040	2.5415E+04	1.6273E+03	36320	0.064030	0.06391	1.1748E-04	0.000000
2.00	6.00	0.000002	0.0000060	2.6582E+04	1.9535E+03	36320	0.073489	0.06026	1.3234E-02	0.000175
2.00	8.00	0.000002	0.0000080	2.7139E+04	1.9023E+03	36320	0.070096	0.05698	1.3119E-02	0.000172
2.00	10.00	0.000002	0.0000100	2.7936E+04	2.0295E+03	36320	0.072648	0.05402	1.8624E-02	0.000347
								Σ	0.00005987	0.00157364

Table D 14. IP-L-Imid: Thiosulfate Trial 2

TS_0 uM	IP_0 uM	TS_0 M	IP_0 M	S IP	S IP·TS	K	SR obs	SR cal +	obs-cal	(obs-cal)^2
2.00	0.50	0.000002	0.0000005	1.8494E+04	7.7963E+02	30898	0.042156	0.06091	-1.8753E-02	0.000352
2.00	1.00	0.000002	0.0000010	2.0360E+05	1.0379E+03	30898	0.005098	0.06005	-5.4948E-02	0.003019
2.00	2.00	0.000002	0.0000020	2.3436E+04	1.4589E+03	30898	0.062251	0.05839	3.8639E-03	0.000015
2.00	4.00	0.000002	0.0000040	2.5147E+04	1.6970E+03	30898	0.067485	0.05532	1.2167E-02	0.000148
2.00	6.00	0.000002	0.0000060	2.5874E+04	1.7403E+03	30898	0.067260	0.05254	1.4718E-02	0.000217
2.00	8.00	0.000002	0.0000080	2.6914E+04	1.8407E+03	30898	0.068391	0.05002	1.8370E-02	0.000337
2.00	10.00	0.000002	0.0000100	2.9095E+04	2.1039E+03	30898	0.072310	0.04772	2.4588E-02	0.000605
								Σ	**0.00000615**	**0.00469258**

Table D 15. IP-L-Imid: Sulfate Trial 1

TS_0 uM	IP_0 uM	TS_0 M	IP_0 M	S IP	S IP·TS	K	SR obs	SR cal +	obs-cal	(obs-cal)^2
8.00	2.00	0.000008	0.0000020	1.2941E+06	1.2114E+03	682	0.000936	0.00545	-4.5125E-03	0.000020
8.00	4.00	0.000008	0.0000040	1.6711E+06	3.8088E+03	682	0.002279	0.00544	-3.1620E-03	0.000010
8.00	8.00	0.000008	0.0000080	1.8915E+06	6.5742E+03	682	0.003476	0.00543	-1.9508E-03	0.000004
8.00	16.00	0.000008	0.0000160	2.0759E+06	1.1628E+04	682	0.005601	0.0054	2.0375E-04	0.000000
8.00	24.00	0.000008	0.0000240	2.1462E+06	1.8242E+04	682	0.008499	0.00537	3.1307E-03	0.000010
8.00	32.00	0.000008	0.0000320	2.1041E+06	1.8041E+04	682	0.008574	0.00534	3.2339E-03	0.000010
8.00	40.00	0.000008	0.0000400	2.1467E+06	1.8007E+04	682	0.008388	0.00531	3.0762E-03	0.000009
								Σ	**0.00001924**	**0.00006393**

Table D 16. IP-L-Imid: Sulfate Trial 2

TS_0 uM	IP_0 uM	TS_0 M	IP_0 M	S IP	S IP·TS	K	SR obs	SR cal +	obs-cal	(obs-cal)^2
8.00	2.00	0.000008	0.0000020	1.2544E+06	1.2474E+03	688	0.000994	0.0055	-4.5021E-03	0.000020
8.00	4.00	0.000008	0.0000040	1.6871E+06	4.4059E+03	688	0.002611	0.00549	-2.8775E-03	0.000008
8.00	8.00	0.000008	0.0000080	1.9197E+06	6.4610E+03	688	0.003366	0.00547	-2.1083E-03	0.000004
8.00	16.00	0.000008	0.0000160	2.0657E+06	1.2270E+04	688	0.005940	0.00544	4.9537E-04	0.000000
8.00	24.00	0.000008	0.0000240	2.1241E+06	1.8931E+04	688	0.008912	0.00542	3.4973E-03	0.000012
8.00	32.00	0.000008	0.0000320	2.1502E+06	1.8762E+04	688	0.008726	0.00539	3.3399E-03	0.000011
8.00	40.00	0.000008	0.0000400	2.1271E+06	1.5992E+04	688	0.007518	0.00536	2.1611E-03	0.000005
								Σ	**0.00000578**	**0.00006130**

Table D 17. IP-T-Imid: Tetrathionate Trial 1

TS_0 uM	IP_0 uM	TS_0 M	IP_0 M	S IP	S IP·TS	K	SR obs	SR cal +	obs-cal	(obs-cal)^2
2.00	0.50	0.000002	0.0000005	2.6327E+05	1.9479E+04	104406	0.073987	0.20011	-1.2612E-01	0.015906
2.00	1.00	0.000002	0.0000010	4.4979E+05	4.5935E+04	104406	0.102125	0.192	-8.9870E-02	0.008077
2.00	2.00	0.000002	0.0000020	7.1741E+05	1.0203E+05	104406	0.142221	0.17736	-3.5136E-02	0.001235
2.00	4.00	0.000002	0.0000040	9.9498E+05	1.8087E+05	104406	0.181783	0.1533	2.8483E-02	0.000811
2.00	6.00	0.000002	0.0000060	1.0480E+06	2.0560E+05	104406	0.196187	0.13453	6.1656E-02	0.003802
2.00	8.00	0.000002	0.0000080	1.2309E+06	2.4426E+05	104406	0.198436	0.11959	7.8843E-02	0.006216
2.00	10.00	0.000002	0.0000100	1.2605E+06	2.3906E+05	104406	0.189659	0.10748	8.2175E-02	0.006753
								Σ	**0.000032**	**0.042799**

Table D 18. IP-T-Imid: Tetrathionate Trial 2

TS_0 uM	IP_0 uM	TS_0 M	IP_0 M	S IP	S IP·TS	K	SR obs	SR cal +	obs-cal	(obs-cal)^2
2.00	0.50	0.000002	0.0000005	2.5164E+05	1.8582E+04	105100	0.073845	0.20139	-1.2755E-01	0.016268
2.00	1.00	0.000002	0.0000010	4.6552E+05	4.8586E+04	105100	0.104368	0.19318	-8.8815E-02	0.007888
2.00	2.00	0.000002	0.0000020	7.1390E+05	1.0132E+05	105100	0.141919	0.17838	-3.6461E-02	0.001329
2.00	4.00	0.000002	0.0000040	9.8138E+05	1.8345E+05	105100	0.186928	0.15407	3.2854E-02	0.001079
2.00	6.00	0.000002	0.0000060	1.0681E+06	2.1243E+05	105100	0.198897	0.13513	6.3767E-02	0.004066
2.00	8.00	0.000002	0.0000080	1.1793E+06	2.3202E+05	105100	0.196749	0.12007	7.6681E-02	0.005880
2.00	10.00	0.000002	0.0000100	1.2290E+06	2.3102E+05	105100	0.187978	0.10787	8.0110E-02	0.006418
								Σ	**0.000589**	**0.042929**

Table D 19. IP-T-Imid: Trithionate Trial 1

TS_0 uM	IP_0 uM	TS_0 M	IP_0 M	S IP	S IP·TS	K	SR obs	SR cal +	obs-cal	(obs-cal)^2
2.00	0.50	0.000002	0.0000005	2.7604E+05	1.5733E+04	72460	0.056998	0.14046	-8.3460E-02	0.006966
2.00	1.00	0.000002	0.0000010	4.6892E+05	3.1539E+04	72460	0.067260	0.13623	-6.8973E-02	0.004757
2.00	2.00	0.000002	0.0000020	7.2125E+05	6.5260E+04	72460	0.090482	0.12843	-3.7945E-02	0.001440
2.00	4.00	0.000002	0.0000040	1.0566E+06	1.3778E+05	72460	0.130401	0.11502	1.5380E-02	0.000237
2.00	6.00	0.000002	0.0000060	1.2034E+06	1.8230E+05	72460	0.151489	0.10397	4.7516E-02	0.002258
2.00	8.00	0.000002	0.0000080	1.2543E+06	1.9485E+05	72460	0.155349	0.09475	6.0600E-02	0.003672
2.00	10.00	0.000002	0.0000100	1.3386E+06	2.0599E+05	72460	0.153884	0.08695	6.6930E-02	0.004480
								Σ	**0.000047**	**0.023809**

Table D 20. IP-T-Imid: Trithionate Trial 2

TS_0 uM	IP_0 uM	TS_0 M	IP_0 M	S IP	S IP·TS	K	SR obs	SR cal +	obs-cal	(obs-cal)^2
2.00	0.50	0.000002	0.0000005	2.7464E+05	1.5791E+04	73630	0.057497	0.14266	-8.5166E-02	0.007253
2.00	1.00	0.000002	0.0000010	4.6327E+05	3.0596E+04	73630	0.066043	0.13831	-7.2270E-02	0.005223
2.00	2.00	0.000002	0.0000020	7.4412E+05	6.9092E+04	73630	0.092850	0.13029	-3.7435E-02	0.001401
2.00	4.00	0.000002	0.0000040	1.0522E+06	1.4081E+05	73630	0.133818	0.11652	1.7295E-02	0.000299
2.00	6.00	0.000002	0.0000060	1.1973E+06	1.7956E+05	73630	0.149967	0.10521	4.4761E-02	0.002004
2.00	8.00	0.000002	0.0000080	1.2767E+06	2.0016E+05	73630	0.156787	0.09578	6.1011E-02	0.003722
2.00	10.00	0.000002	0.0000100	1.3085E+06	2.0896E+05	73630	0.159698	0.08782	7.1879E-02	0.005167
								Σ	**0.000074**	**0.025069**

Table D 21. IP-T-Imid: Thiosulfate Trial 1

TS_0 uM	IP_0 uM	TS_0 M	IP_0 M	S IP	S IP·TS	K	SR obs	SR cal +	obs-cal	(obs-cal)^2
2.00	0.50	0.000002	0.0000005	2.6928E+05	5.5708E+02	5482	0.002069	0.01093	-8.8656E-03	0.000079
2.00	1.00	0.000002	0.0000010	4.7239E+05	1.8503E+03	5482	0.003917	0.0109	-6.9879E-03	0.000049
2.00	2.00	0.000002	0.0000020	7.2830E+05	4.3840E+03	5482	0.006019	0.01085	-4.8269E-03	0.000023
2.00	4.00	0.000002	0.0000040	1.0028E+06	1.0379E+04	5482	0.010350	0.01073	-3.8072E-04	0.000000
2.00	6.00	0.000002	0.0000060	1.1513E+06	1.5274E+04	5482	0.013267	0.01062	2.6486E-03	0.000007
2.00	8.00	0.000002	0.0000080	1.2309E+06	2.2410E+04	5482	0.018206	0.01051	7.6978E-03	0.000059
2.00	10.00	0.000002	0.0000100	1.2661E+06	2.6735E+04	5482	0.021115	0.0104	1.0716E-02	0.000115
								Σ	**0.000001**	**0.000332**

Table D 22. IP-T-Imid: Thiosulfate Trial 2

TS_0 uM	IP_0 uM	TS_0 M	IP_0 M	S IP	S IP·TS	K	SR obs	SR cal +	obs-cal	(obs-cal)^2
2.00	0.50	0.000002	0.0000005	2.6425E+05	5.2144E+02	5177	0.001973	0.01033	-8.3543E-03	0.000070
2.00	1.00	0.000002	0.0000010	4.7261E+05	1.7809E+03	5177	0.003768	0.0103	-6.5330E-03	0.000043
2.00	2.00	0.000002	0.0000020	7.1989E+05	4.1161E+03	5177	0.005718	0.01025	-4.5313E-03	0.000021
2.00	4.00	0.000002	0.0000040	1.0094E+06	8.4789E+03	5177	0.008400	0.01015	-1.7456E-03	0.000003
2.00	6.00	0.000002	0.0000060	1.1439E+06	1.6512E+04	5177	0.014435	0.01005	4.3895E-03	0.000019
2.00	8.00	0.000002	0.0000080	1.2659E+06	2.1338E+04	5177	0.016856	0.00995	6.9100E-03	0.000048
2.00	10.00	0.000002	0.0000100	1.2711E+06	2.5058E+04	5177	0.019715	0.00985	9.8656E-03	0.000097
								Σ	**0.000001**	**0.000300**

Table D 23. IP-T-Imid: Sulfate Trial 1

TS_0 uM	IP_0 uM	TS_0 M	IP_0 M	S IP	S IP·TS	K	SR obs	SR cal +	obs-cal	(obs-cal)^2
8.00	2.00	0.000008	0.0000020	6.0832E+05	2.4472E+03	1905	0.004023	0.01518	-1.1160E-02	0.000125
8.00	4.00	0.000008	0.0000040	8.6474E+05	5.5535E+03	1905	0.006422	0.01513	-8.7043E-03	0.000076
8.00	8.00	0.000008	0.0000080	1.1361E+06	1.3968E+04	1905	0.012295	0.01501	-2.7197E-03	0.000007
8.00	16.00	0.000008	0.0000160	1.3079E+06	2.0681E+04	1905	0.015812	0.0148	1.0168E-03	0.000001
8.00	24.00	0.000008	0.0000240	1.3797E+06	2.4504E+04	1905	0.017760	0.01458	3.1775E-03	0.000010
8.00	32.00	0.000008	0.0000320	1.3973E+06	3.2662E+04	1905	0.023375	0.01438	8.9990E-03	0.000081
8.00	40.00	0.000008	0.0000400	1.4474E+06	3.4184E+04	1905	0.023618	0.01417	9.4429E-03	0.000089
								Σ	**0.000052**	**0.000389**

Table D 24. IP-T-Imid: Sulfate Trial 2

TS_0 uM	IP_0 uM	TS_0 M	IP_0 M	S IP	S IP·TS	K	SR obs	SR cal +	obs-cal	(obs-cal)^2
8.00	2.00	0.000008	0.0000020	6.1063E+05	2.2970E+03	1872	0.003762	0.01492	-1.1159E-02	0.000125
8.00	4.00	0.000008	0.0000040	8.6115E+05	5.8669E+03	1872	0.006813	0.01487	-8.0535E-03	0.000065
8.00	8.00	0.000008	0.0000080	1.1333E+06	1.3016E+04	1872	0.011485	0.01476	-3.2734E-03	0.000011
8.00	16.00	0.000008	0.0000160	1.3289E+06	2.1335E+04	1872	0.016054	0.01455	1.5079E-03	0.000002
8.00	24.00	0.000008	0.0000240	1.3449E+06	2.4357E+04	1872	0.018111	0.01434	3.7706E-03	0.000014
8.00	32.00	0.000008	0.0000320	1.4335E+06	3.2947E+04	1872	0.022984	0.01414	8.8436E-03	0.000078
8.00	40.00	0.000008	0.0000400	1.4239E+06	3.1827E+04	1872	0.022352	0.01395	8.4056E-03	0.000071
								Σ	**0.000041**	**0.000365**

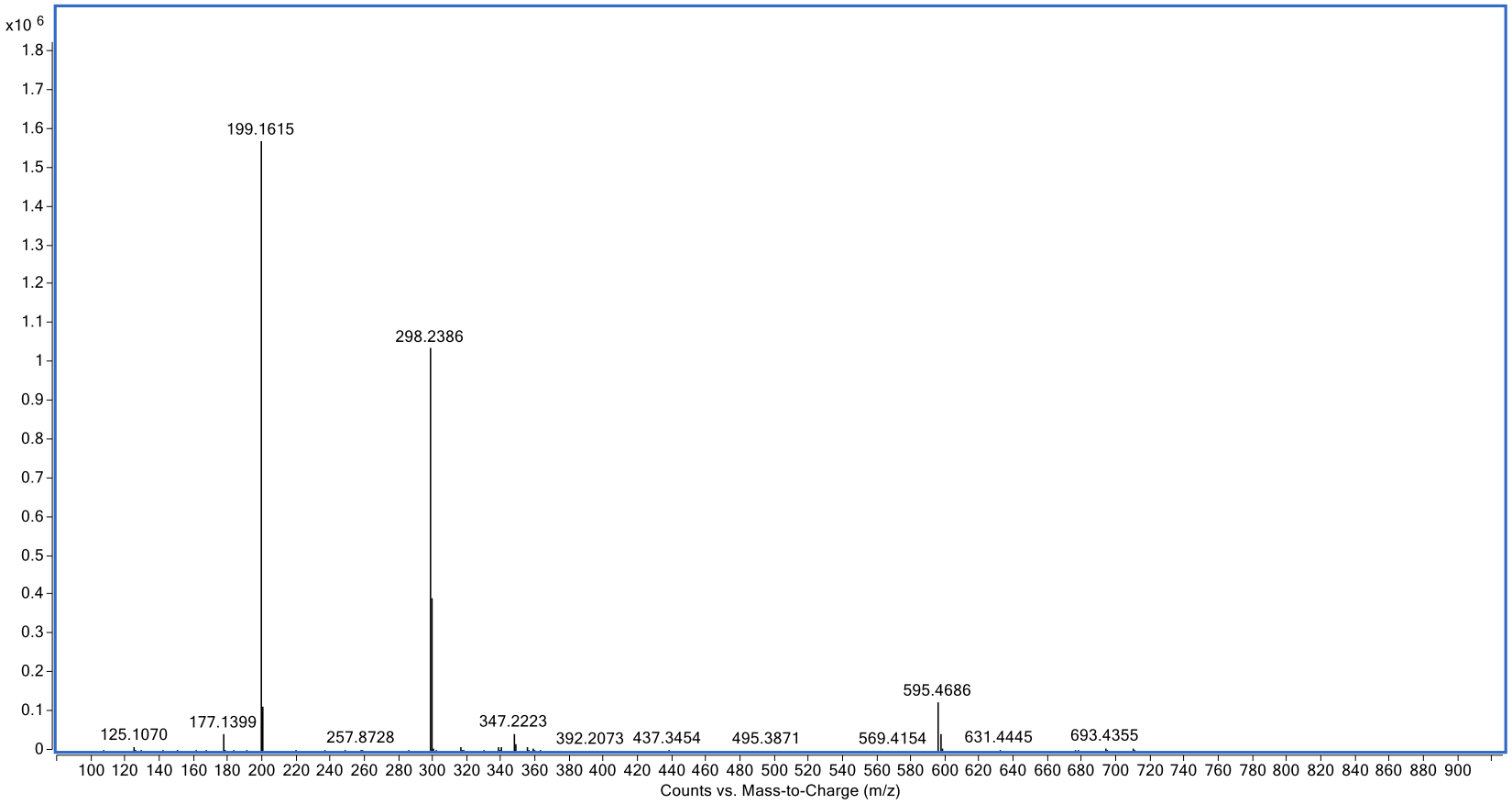

Figure D 5. FIA-ESI-TOF mass spectrum showing signals for equimolar (10 µM each) of IP-T-Phos and SO_4^{2-} showing $[IP\text{-}T\text{-}Phos{:}SO_4]^+$ (m/z 693) and that of $[IP\text{-}T\text{-}Phos^{3+}]$ alone (m/z 199)

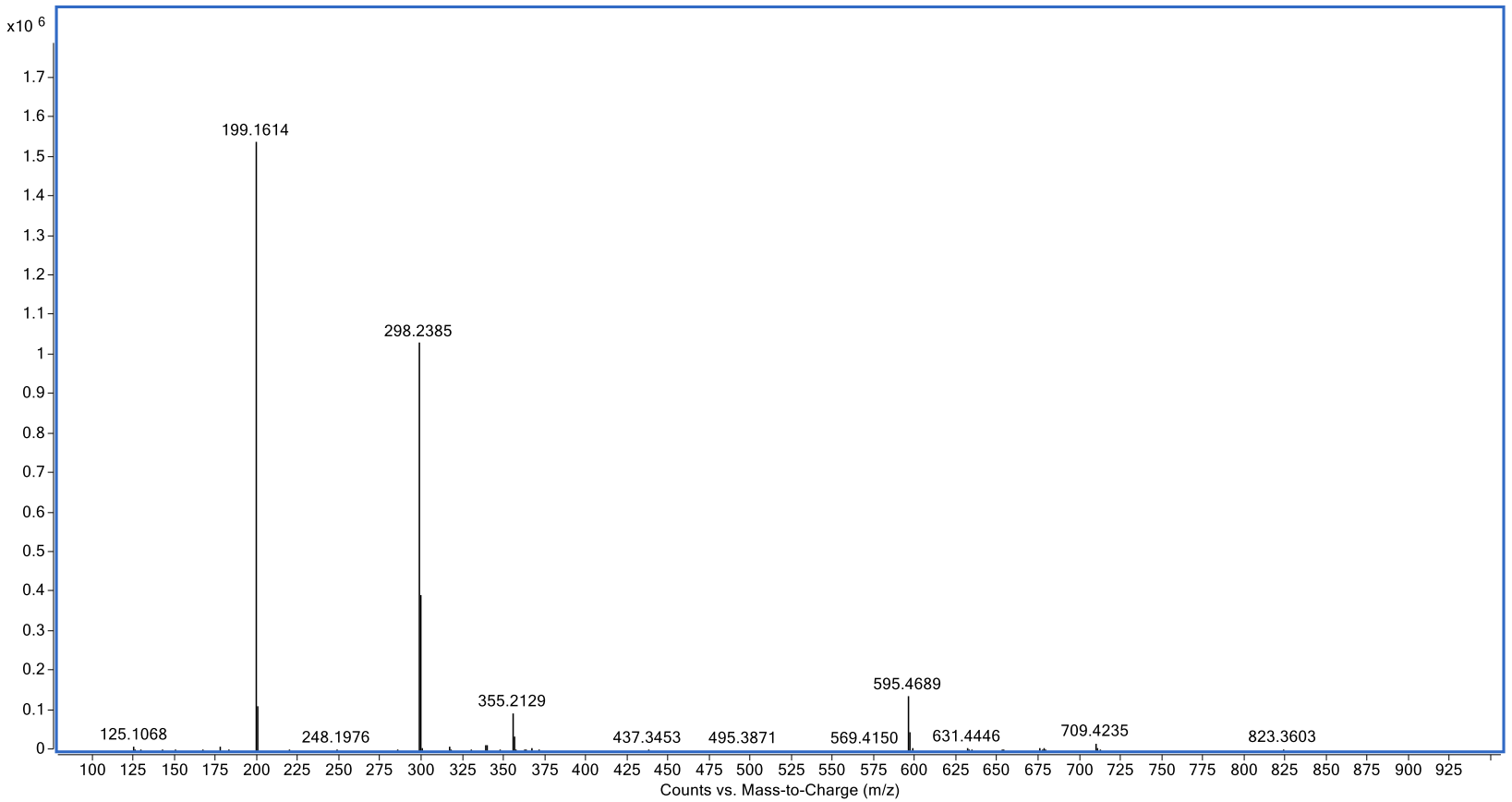

Figure D 6. FIA-ESI-TOF mass spectrum showing signals for equimolar (10 µM each) of IP-T-Phos and $S_2O_3^{2-}$ showing [IP-T-Phos:S_2O_3]$^+$ (m/z 709) and that of [IP-T-Phos^{3+}] alone (m/z 199)

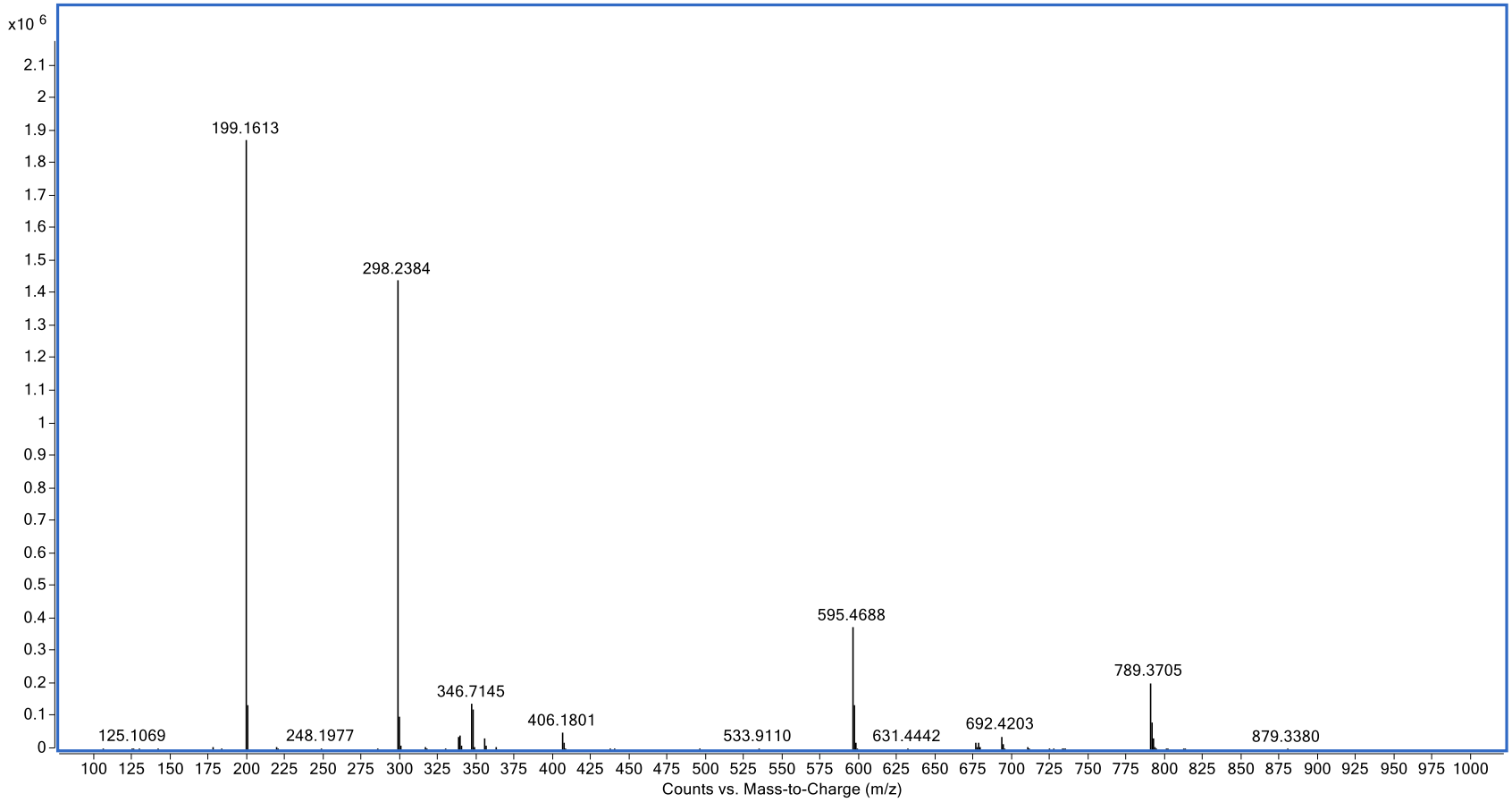

Figure D 7. FIA-ESI-TOF mass spectrum showing signals for equimolar (10 µM each) of IP-T-Phos and $S_3O_6^{2-}$ showing [IP-T-Phos:S_3O_6]$^+$ (m/z 789) and that of [IP-T-Phos^{3+}] alone (m/z 199)

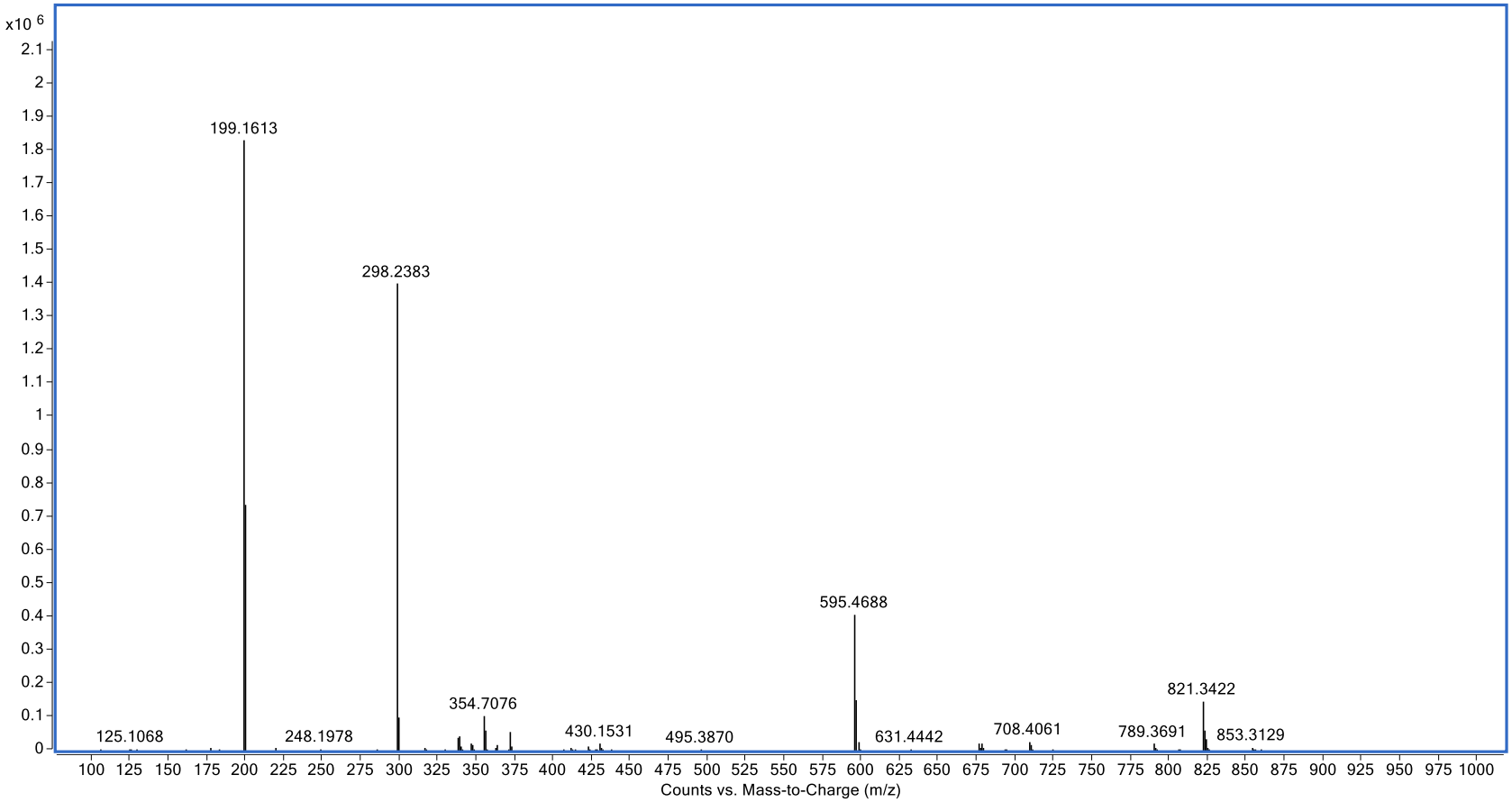

Figure D 8. FIA-ESI-TOF mass spectrum showing signals for equimolar (10 µM each) of IP-T-Phos and $S_4O_6^{2-}$ showing [IP-T-Phos:S_4O_6]$^+$ (m/z 821) and that of [IP-T-Phos^{3+}] alone (m/z 199)

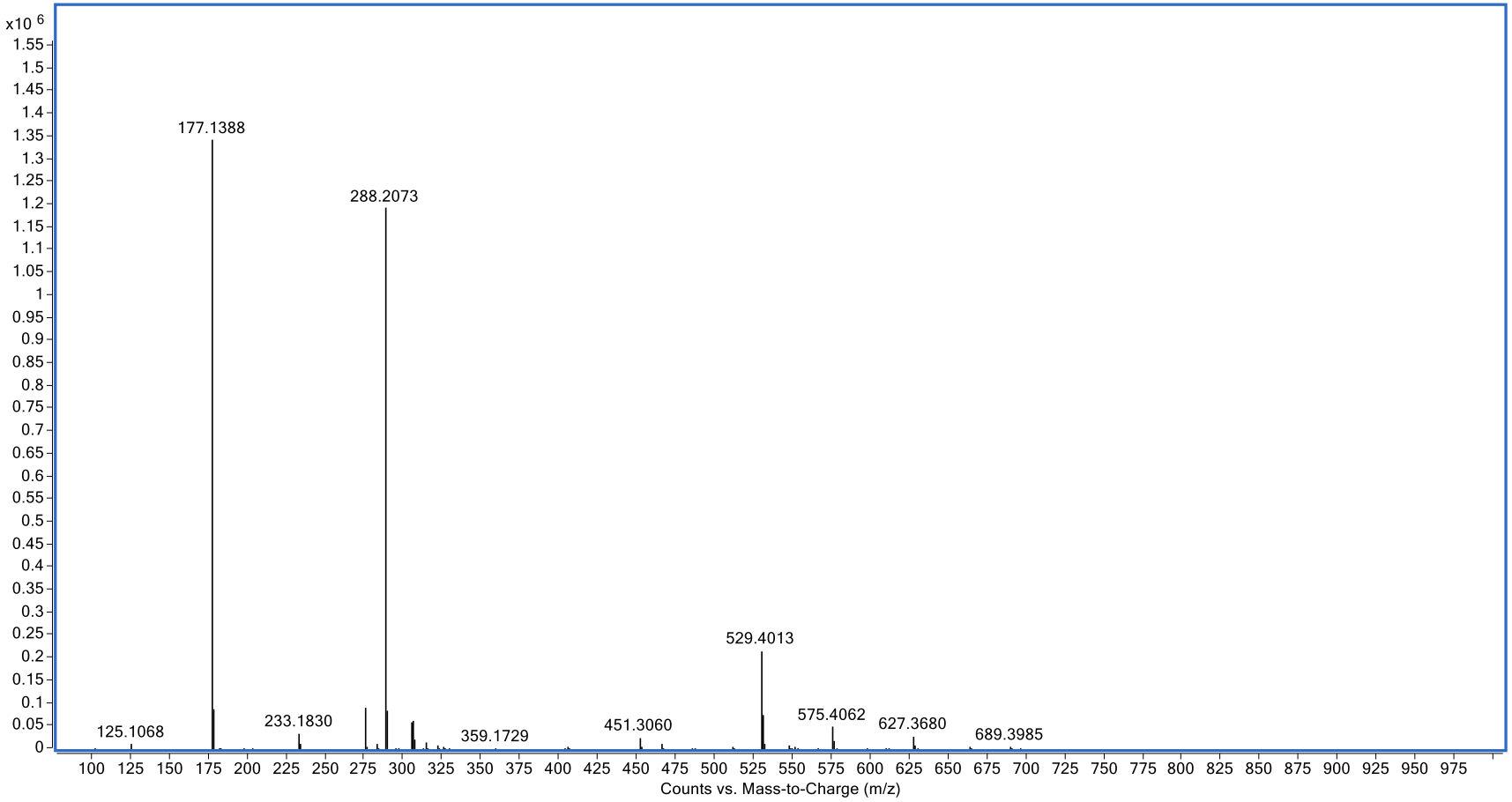

Figure D 9. FIA-ESI-TOF mass spectrum showing signals for equimolar (10 µM each) of IP-T-Imid and SO_4^{2-} showing $[IP\text{-}T\text{-}Imid:SO_4]^+$ (m/z 627) and that of $[IP\text{-}T\text{-}Imid^{3+}]$ alone (m/z 177)

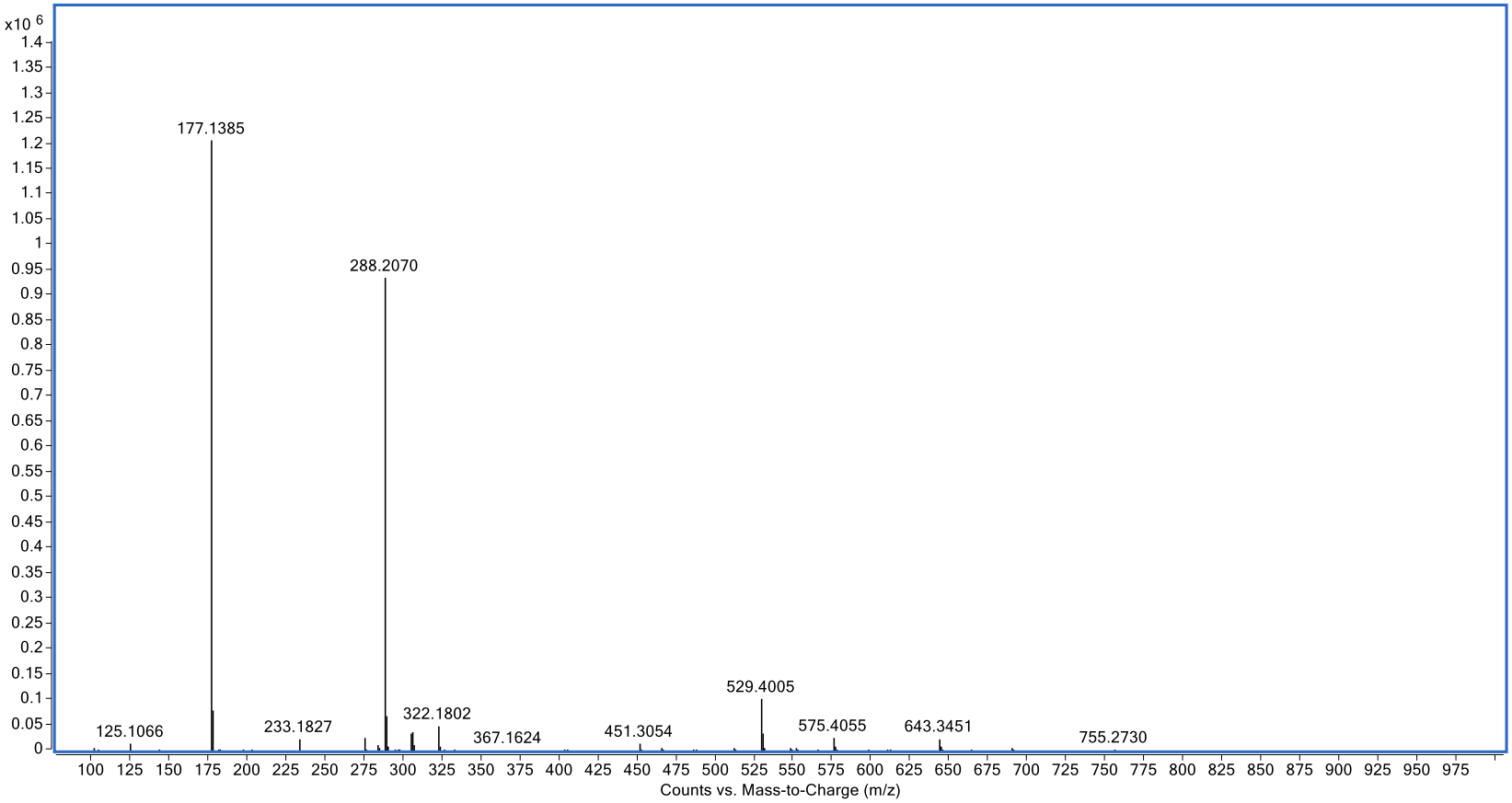

Figure D 10. FIA-ESI-TOF mass spectrum showing signals for equimolar (10 µM each) of IP-T-Imid and $S_2O_3^{2-}$ showing [IP-T-Imid:S_2O_3]$^+$ (m/z 643) and that of [IP-T-Imid^{3+}] alone (m/z 177)

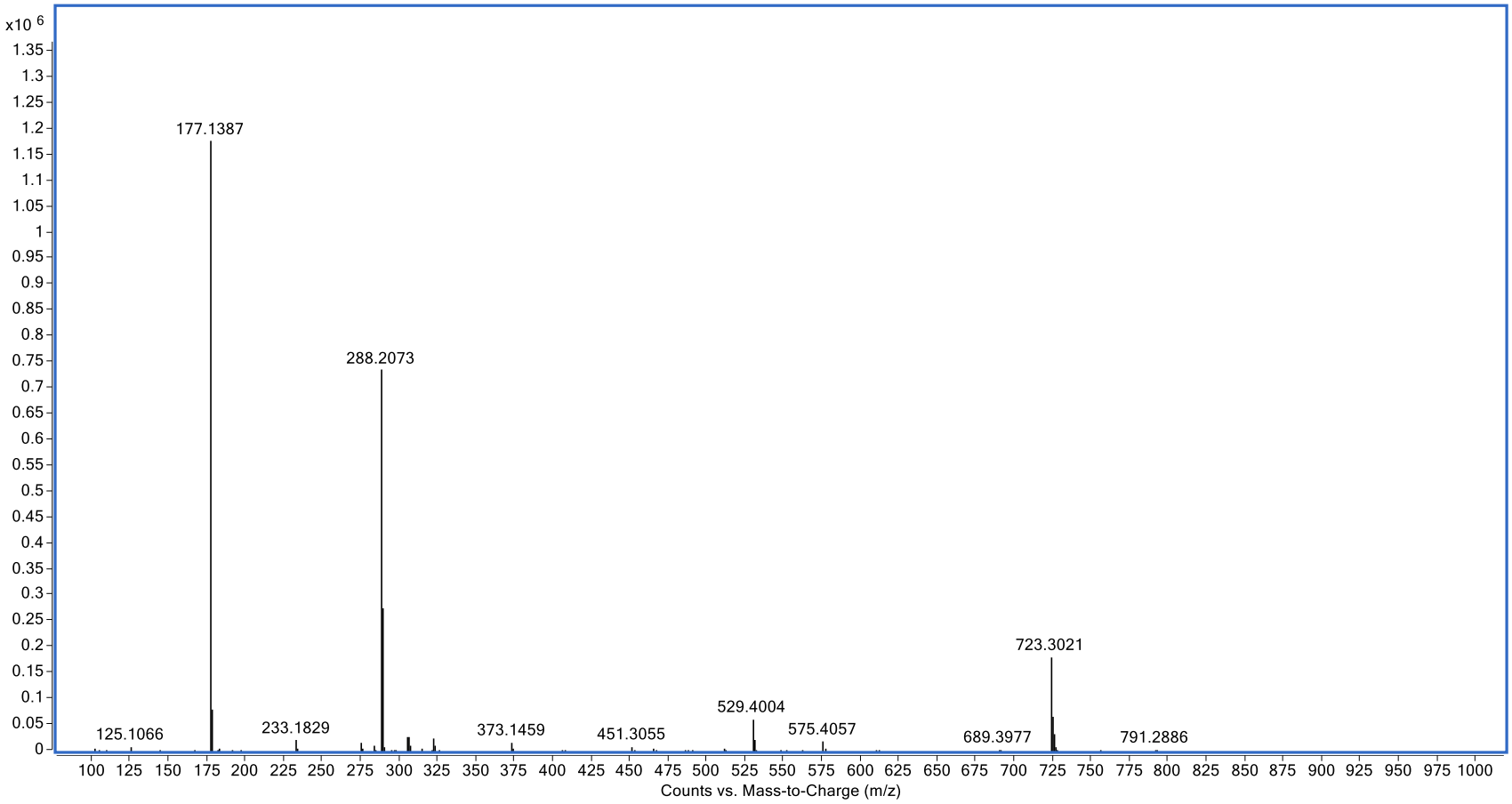

Figure D 11. FIA-ESI-TOF mass spectrum showing signals for equimolar (10 µM each) of IP-T-Imid and $S_3O_6^{2-}$ showing [IP-T-Imid:S_3O_6]$^+$ (m/z 723) and that of [IP-T-Imid^{3+}] alone (m/z 177)

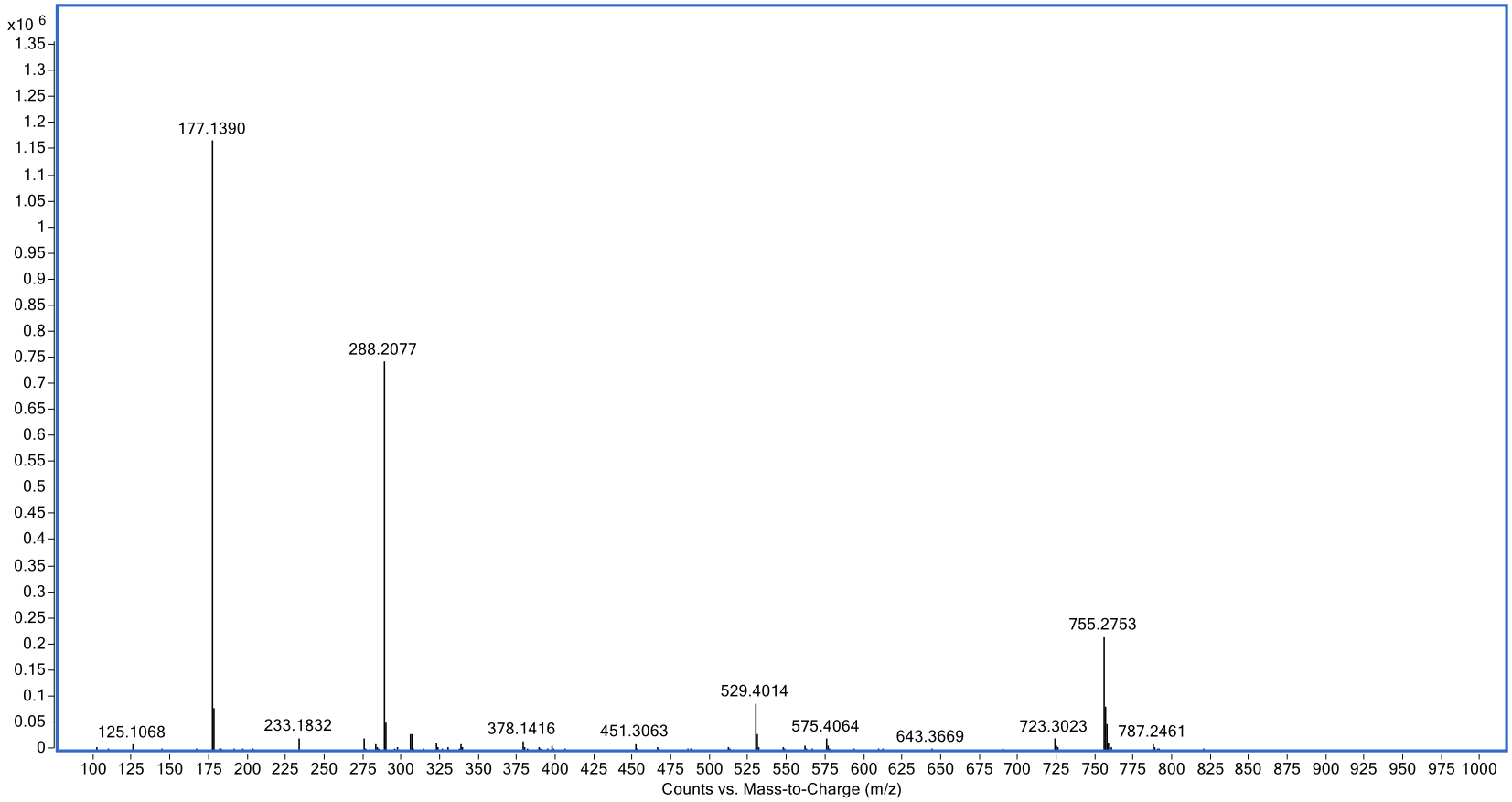

Figure D 12. FIA-ESI-TOF mass spectrum showing signals for equimolar (10 µM each) of IP-T-Imid and $S_4O_6^{2-}$ showing [IP-T-Imid:S_4O_6]$^+$ (m/z 755) and that of [IP-T-Imid^{3+}] alone (m/z 177)

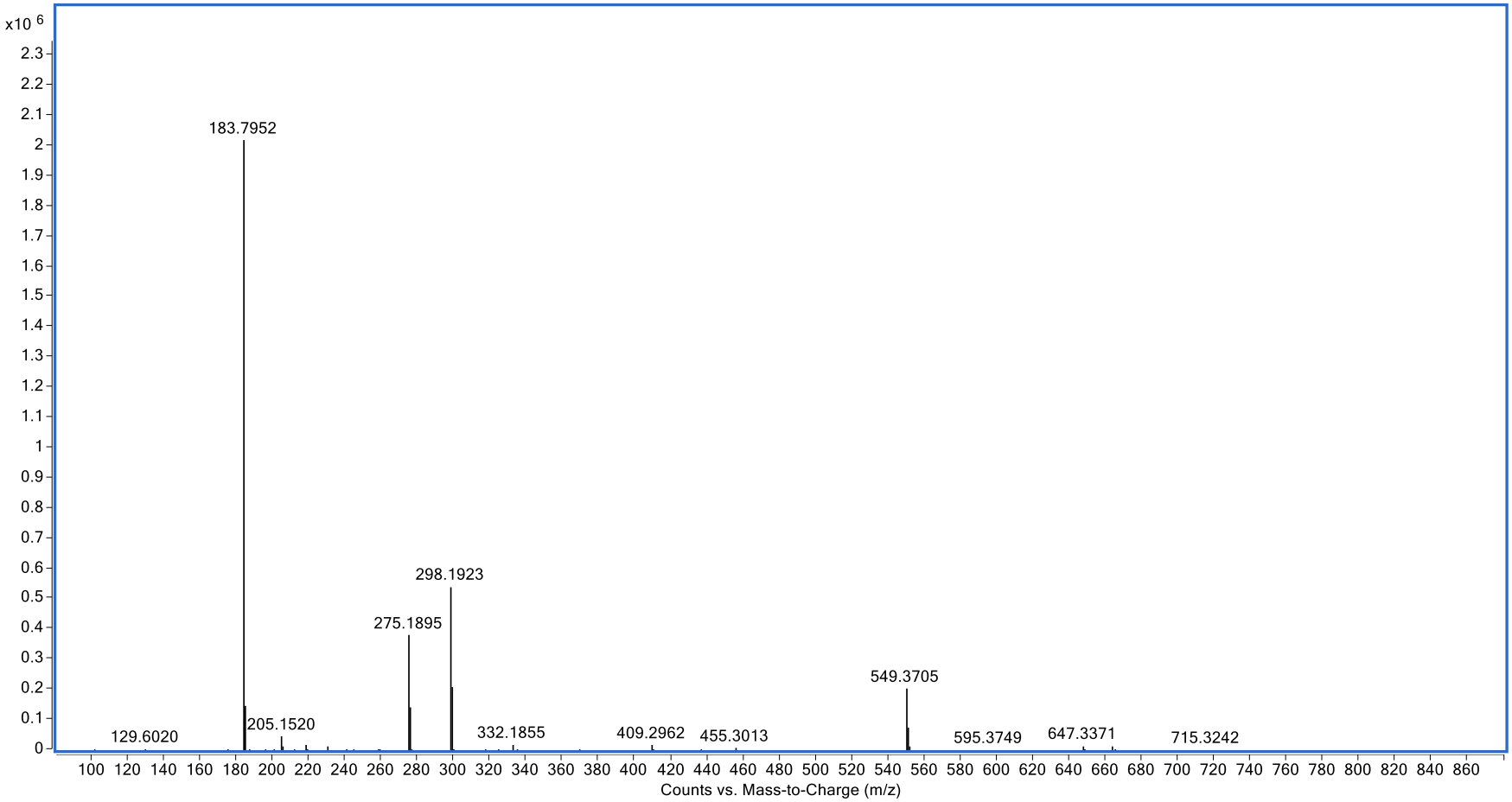

Figure D 13.. FIA-ESI-TOF mass spectrum showing signals for equimolar (10 µM each) of IP-L-Imid and SO_4^{2-} showing [IP-L-Imid:SO_4]$^+$ (m/z 647) and that of [IP-L-Imid^{3+}] alone (m/z 183)

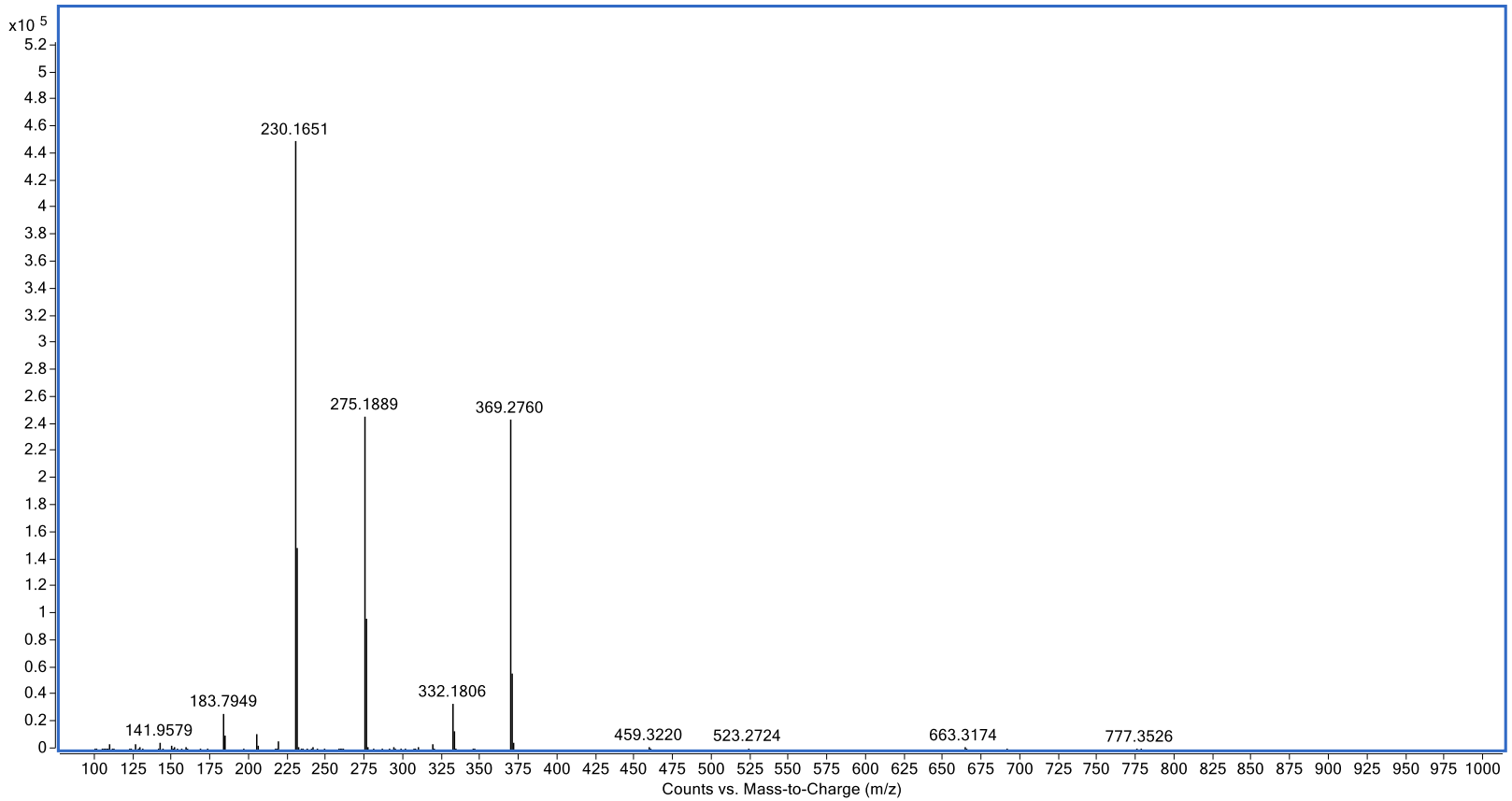

Figure D 14. FIA-ESI-TOF mass spectrum showing signals for equimolar (10 µM each) of IP-L-Imid and $S_2O_3^{2-}$ showing [IP-L-Imid:S_2O_3]$^+$ (m/z 663) and that of [IP-L-Imid^{3+}] alone (m/z 183)

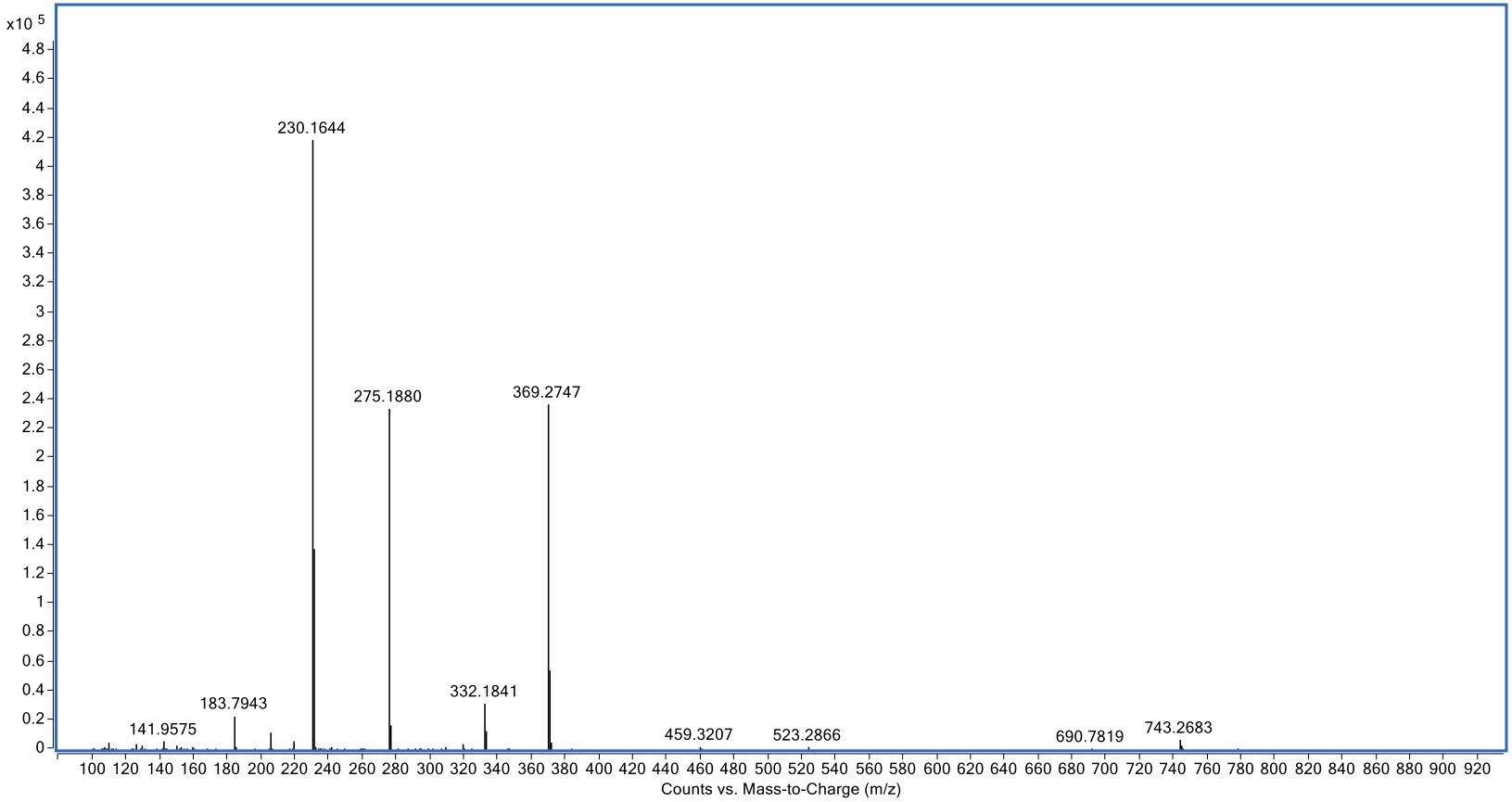

Figure D 15. FIA-ESI-TOF mass spectrum showing signals for equimolar (10 µM each) of IP-L-Imid and $S_3O_6^{2-}$ showing [IP-L-Imid:S_3O_6]$^+$ (m/z 743) and that of [IP-L-Imid^{3+}] alone (m/z 183)

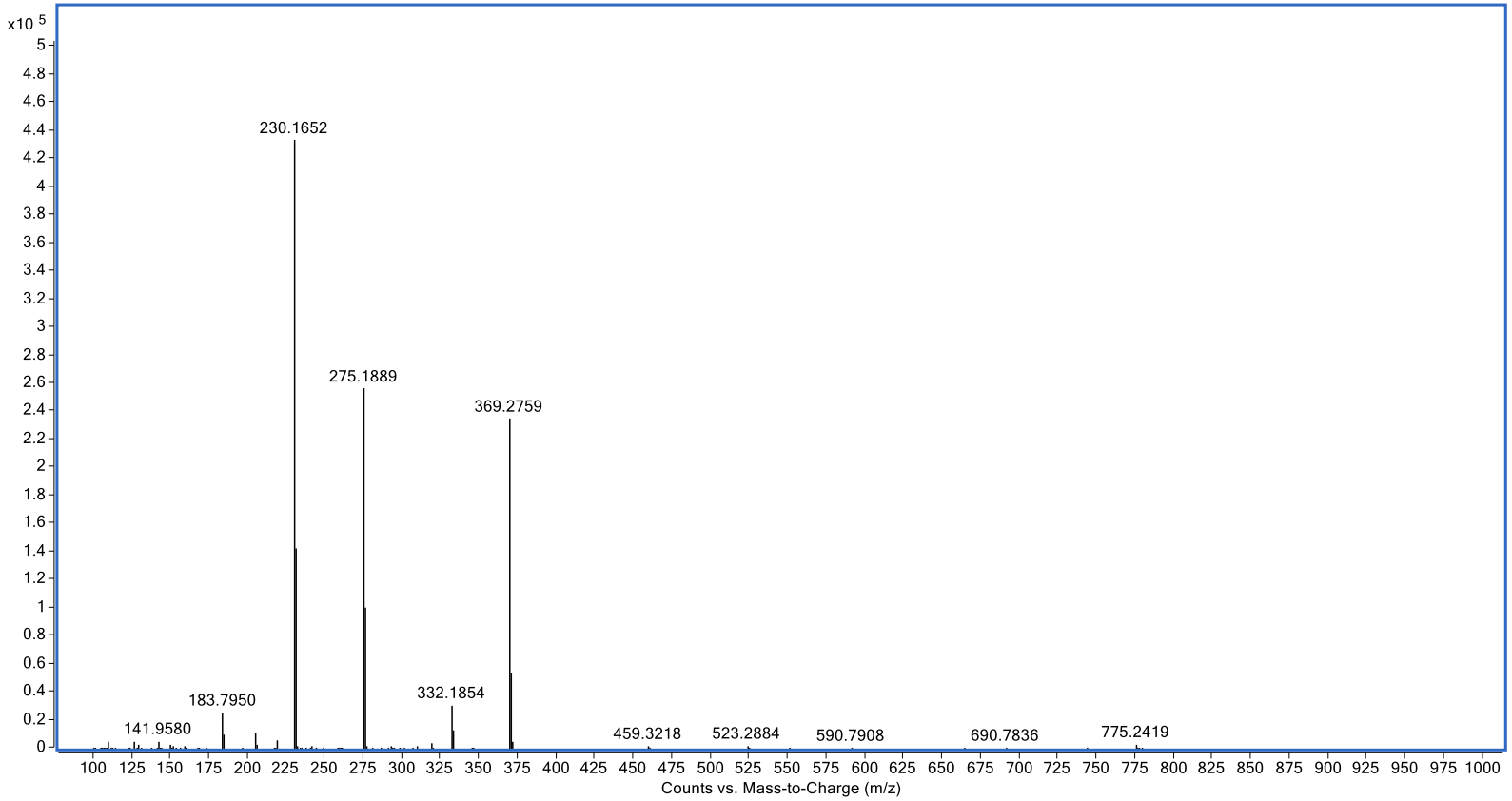

Figure D 16. FIA-ESI-TOF mass spectrum showing signals for equimolar (10 µM each) of IP-L-Imid and $S_4O_6^{2-}$ showing [IP-L-Imid:S_4O_6]$^+$ (m/z 775) and that of [IP-L-Imid^{3+}] alone (m/z 183)